DYNAMIC AND STATIC CHARACTERISTICS OF A ROCKER-PIVOT, TILTING-PAD BEARING WITH 50% AND 60% OFFSETS

A Thesis

by

CHRIS DAVID KULHANEK

Submitted to the Office of Graduate Studies of
Texas A&M University
in partial fulfillment of the requirements for the degree of

MASTER OF SCIENCE

December 2010

Major Subject: Mechanical Engineering

DYNAMIC AND STATIC CHARACTERISTICS OF A ROCKER-PIVOT, TILTING-PAD BEARING WITH 50% AND 60% OFFSETS

A Thesis

by

CHRIS DAVID KULHANEK

Submitted to the Office of Graduate Studies of
Texas A&M University
in partial fulfillment of the requirements for the degree of

MASTER OF SCIENCE

Approved by:

Chair of Committee,	Dara W. Childs
Committee Members,	Alan Palazzolo
	Lynn Beason
Department Head,	Dennis L. O'Neal

December 2010

Major Subject: Mechanical Engineering

ABSTRACT

Dynamic and Static Characteristics of a Rocker-Pivot, Tilting-Pad Bearing with 50% and 60% Offsets.

(December 2010)

Chris David Kulhanek, B.S., Texas A&M University

Chair of Advisory Committee: Dr. Dara W. Childs

Static performance and rotordynamic coefficients are provided for a rocker-pivot, tilting-pad journal bearing with 50 and 60% offset pads in a load-between-pad configuration. The bearing uses leading-edge-groove lubrication and has the following characteristics: 5-pads, 101.6 mm (4.0 in) nominal diameter, .0814 - .0837 mm (.0032 - .0033 in) radial bearing clearance, .25 to .27 preload, 60.325 mm (2.375 in) axial pad length. Operating conditions included loads from 0 to 3101 kPa (450 psi) and speeds from 7 to 16 krpm.

Dynamic tests were conducted over a range of frequencies to obtain complex dynamic stiffness coefficients as functions of excitation frequency. For most test conditions, the direct real dynamic stiffnesses were well fitted with a quadratic function with respect to frequency. This curve fit allowed for the stiffness frequency dependency to be captured by including an added mass matrix [M] to a conventional [K][C] model, producing a frequency independent [K][C][M] model. The direct imaginary dynamic stiffness coefficients increased linearly with frequency, producing frequency independent direct damping coefficients. Compared to the 50% offset, the 60% offset configuration's direct stiffness coefficients were larger at light unit loads. At high loads, the 50% offset configuration had a larger direct stiffness in the loaded direction. Negative direct added-mass coefficients were regularly obtained for both offsets, especially in the unloaded direction. Added-mass magnitudes were below 32 kg for all test cases. No appreciable difference was measured in direct damping coefficients for both pivot offset.

A bulk-flow Navier-Stokes CFD code provided rotordynamic coefficient predictions. The following stiffness and damping prediction trends were observed for both 50 and 60% offsets. The direct stiffness coefficients were modeled well at light loads and became increasingly over-predicted with increasing unit load. Stiffness orthotropy was measured at zero and light load conditions that was not predicted. Direct damping predictions in the loaded direction increased significantly with unit load while the experimental direct damping coefficients remained constant with load. The direct damping coefficients were reasonably modeled only at the highest test speed of 16 krpm. Experimental cross-coupled stiffness coefficients were larger than predicted for both offsets, but were of the same sign and considerably smaller than the direct coefficients.

DEDICATION

For my grandparents,
Walter and Bessie Kulhanek, Clearance and Beatrice Wasut
who showed me how to work hard

ACKNOWLEDGEMENTS

I sincerely express my thanks to Dr. Dara Childs for the great opportunity to work and learn at the Turbomachinery Lab. My path to graduate school began with the student worker position that he offered during my undergraduate degree. His supervision, guidance, and teaching have been invaluable during my time as his student and research assistant.

My research was made possible thanks to the funding of the Turbomachinery Research Consortium and the bearing donation from John Crane Orion. I thank Jim Ball from John Crane Orion for his technical assistance on the test bearing.

At the Turbo Lab, I have been able to work with, learn, and take advice from many exceptional individuals. I am thankful for the constant assistance provided by Eddie Denk. His experience and knowledge has aided my research throughout its entirety. I also thank Stephen Phillips for his technical expertise and advice concerning the test rig. My time at the Turbo Lab cannot be described without mentioning the help and companionship of Jason Wilkes. I sincerely appreciate his workmanship and his numerous improvements to the test rig. Also, I thank Robert Sheets for introducing me to the rig and aiding me at the beginning of my research.

Throughout my time at Texas A&M University, I am thankful to have studied under many skilled and talented professors. I especially thank Dr. Alan Palazzolo and Art Belmonte for being exceptional teachers in engineering and mathematics.

I thank my parents, David and Sally Kulhanek, for their unending support and guidance throughout my life. I also thank my sister, Kristy Kulhanek, for a great continuing friendship. I am very thankful of my fiancée, Jessica Honish for her love, support, and patience.

I give thanks to God for everything in my life, for he ultimately made all of this possible.

TABLE OF CONTENTS

LIST OF FIGURES

Page

Page

Page

LIST OF TABLES

NOMENCLATURE

$\boldsymbol{A_{ij}}$	Fourier transforms for the measured stator acceleration (e.g. A_{ij} is the acceleration in "j" direction, due to an excitation force in the "i" direction) [L/t^2]
C_{ij}	Direct and cross-coupled damping coefficients [F.t/L]
ΔC_{ij}	Uncertainty of direct and cross-coupled damping coefficients [F.t/L]
C_b	Radial bearing clearance [L]
C_p	Radial pad clearance [L]
c_p	Lubricant specific heat [F.L/(M.t)]
D	Bearing diameter [L]
$\boldsymbol{D_{ij}}$	Fourier transforms for the measured stator relative motion [L]
e_x e_y	Bearing equilibrium position in the *x* and *y* directions [L]
$\boldsymbol{F_{ij}}$	Fourier transforms for the measured stator force [F]
F_s	Static force applied by pneumatic loader [F]
f_{bx} f_{by}	Bearing reaction force component in the *x,y* direction respectively [F]
f_{x} f_{y}	Measured excitation force component in the *x,y* direction [F]
$\boldsymbol{H_{ij}}$	Direct and cross-coupled dynamic stiffnesses [F/L]
$\Delta\boldsymbol{H_{ij}}$	Uncertainty of direct and cross-coupled dynamic stiffnesses [F/L]
$\boldsymbol{J}$	Imaginary unit, $\sqrt{-1}$ [-]
K_{ij}	Direct and cross-coupled stiffness coefficients [F/L]
ΔK_{ij}	Uncertainty of direct and cross-coupled stiffness coefficients [F/L]
L	Pad axial length [L]
M_s	Mass of the stator [M]
M_{ij}	Direct and cross-coupled added-mass coefficients [M]
ΔM_{ij}	Uncertainty of added-mass coefficients [M]
N	Number of shakes [-]
n	Number of data points when applying a curve fit [-]
$\dot{Q}$	Bearing oil supply flow rate [L^3/t]
R_b	Bearing radius [L]
R_s	Shaft radius [L]

Re	Shear Reynolds number [-]
Re_s	Squeeze Reynolds number [-]
Re_*	Modified Shear Reynolds number [-]
r^2_{ij}	Square of the correlation coefficient [-]
S	Sommerfeld number [-]
S_{xx}	Uncertainty quantity for independent variable [-]
T_{in}	Oil inlet temperature [T]
T_{out}	Oil outlet temperature [T]
$\ddot{x}_s \quad \ddot{y}_s$	Absolute acceleration of the stator in the *x*,*y* direction [L/t^2]
$\Delta x \ \Delta y$	Relative motion between the rotor and the stator in the *x*,*y* directions [L]
ε_o	Eccentricity ratio [-]
θ	Bearing circumferential coordinate [-]
ϕ	Attitude angle measured from the load axis to the eccentricity vector [Angle]
Λ	Square of the excitation frequency, Ω^2 [(1/t)^2]
ρ	Lubricant density [M/L^3]
μ	Lubricant viscosity [F.t /L^2]
σ^2	Square mean error (SME) [-]
ω	Running speed of rotor [1/t]
Ω	Excitation frequency of stator [1/t]

Subscripts

k	Sample or shake number of a dynamic test
x,y	*x* and *y* orthogonal directions
i,j	*x*,*y*

Abbreviations

CFD	Computational Fluid Dynamics
DE, NDE	Drive end, non-drive end
LBP	Load-between-pad
LEG	Leading-edge groove

LOP	Load-on-pad
[K][C]	Dynamic bearing model with stiffness and damping matrices
[K][C][M]	Dynamic bearing model with stiffness, damping, and added-mass matrices
rpm	Revolutions per minute
TPJB	Tilting-pad journal bearings
TH	Theoretical predictions (Bulk-flow Navier Stokes unless otherwise specified)
NS	Bulf-flow Navier Stokes equations

INTRODUCTION

Tilting-pad journal bearings (TPJBs) are commonly used in rotating machines due to their substantial stability benefits over conventional, fixed-geometry journal bearings. Figure 1 below provides a general TPJB schematic. TPJBs are characterized by separate bearing segments or pads that can individually rotate about an axis parallel to the journal. These bearings typically have four to six tilting pads that are encased in a housing.

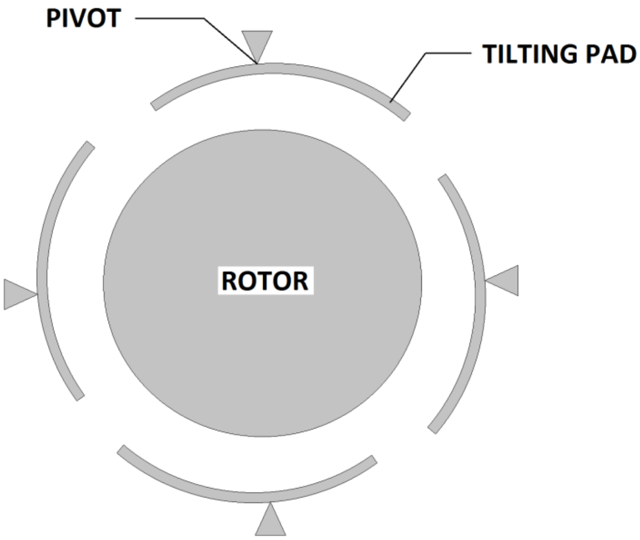

Figure 1. Schematic of a typical tilting-pad journal bearing.

A tilting pad provides support to a journal through hydrodynamic fluid film lubrication. As a shaft rotates, the viscous lubricant in a converging geometry creates fluid pressure between the pads and shaft. The fluid pressure profile provides a net force that provides lift and supports the shaft. Often, the fluid film forces acting between a bearing and rotor can be modeled with a linearized two degree-of-freedom system of springs and dampers, as shown below in Figure 2. The symbols K_{ij} and C_{ij} represent the stiffness and damping coefficients respectively.

This thesis follows the style and format of the ASME Journal of Engineering for Gas Turbines and Power.

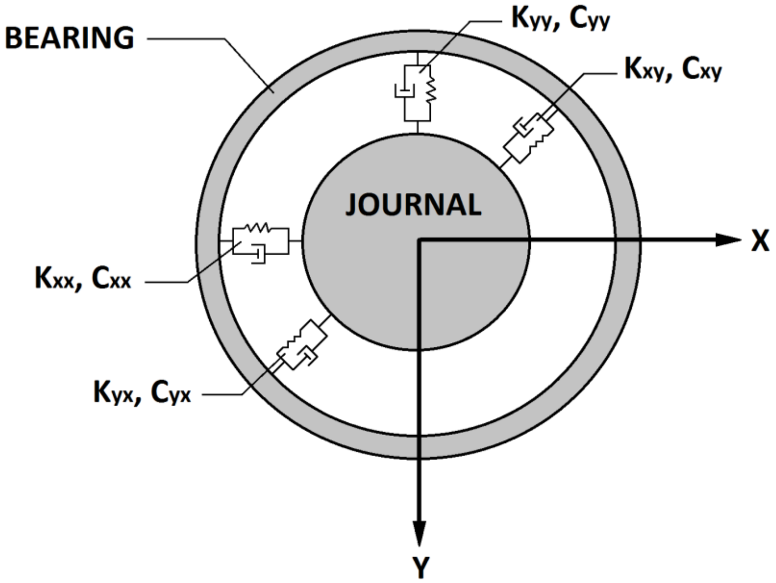

Figure 2. Linearized spring and damper model of a fluid film.

From the model presented above, the bearing reaction forces, f_{bx} and f_{by}, can be written in terms of the stiffness [K] and damping [C] matrices, as shown in Eq. (1).

$$-\begin{Bmatrix} f_{bx} \\ f_{by} \end{Bmatrix} = \begin{bmatrix} K_{xx} & K_{xy} \\ K_{yx} & K_{yy} \end{bmatrix} \begin{Bmatrix} \Delta x \\ \Delta y \end{Bmatrix} + \begin{bmatrix} C_{xx} & C_{xy} \\ C_{yx} & C_{yy} \end{bmatrix} \begin{Bmatrix} \Delta \dot{x} \\ \Delta \dot{y} \end{Bmatrix} \tag{1}$$

Each coefficient in the matrices is denoted by subscripts (xx,yy) or (xy,yx), representing the direct or cross-coupled coefficients, respectively. The variables Δx, Δy, and their time derivatives represent the relative displacements and velocities between the bearing and shaft in each orthogonal direction.

As a TPJB supports a rotor, no pad can support a moment and therefore rotates to an equilibrium position where the fluid film forces are equal on each side of the pivot. The net fluid film force of each pad is in the direction that that passes through each pivot and the shaft center [1]. Since all fluid film forces point to the journal center, forces from cross-coupled coefficients are practically eliminated. This feature causes tilting-pad bearings to be very stable when compared to conventional bearings that typically have substantial cross-coupling. This characteristic of titling-pad bearings is especially beneficial for high-speed, light-load applications where fixed-geometry bearings cause the rotor to become unstable.

TPJBs have small amounts of cross-coupled stiffness that can arise from pivot inertia, pivot friction, and manufacturing imperfections. In addition to the advantage of stability, TPJBs offer tolerance to misalignment. Just as the pads tilt to equalize fluid film pressure, this rotation allows the pads to adjust for radial misalignment of the shaft. Some tilting-pad-pivot designs allow the pad to rotate in more than one direction to also accommodate angular misalignment.

TPJBs can be defined by multiple geometric parameters that affect the bearing performance. These parameters are defined in Table 1 and shown in Figure 3.

Table 1. Definitions of tilting-pad bearing geometric parameters.

SYMBOL	*DEFINITION*
R_s	Shaft Radius
R_p	Pad Radius
R_b	Bearing Radius
θ_{pad}	Pad Arc Angle
θ_{pivot}	Pivot Arc Angle
L	Pad Axial Length
C_p	Radial Pad Clearance, $C_p = R_p - R_s$
C_b	Radial Bearing Clearance, $C_b = R_b - R_s$

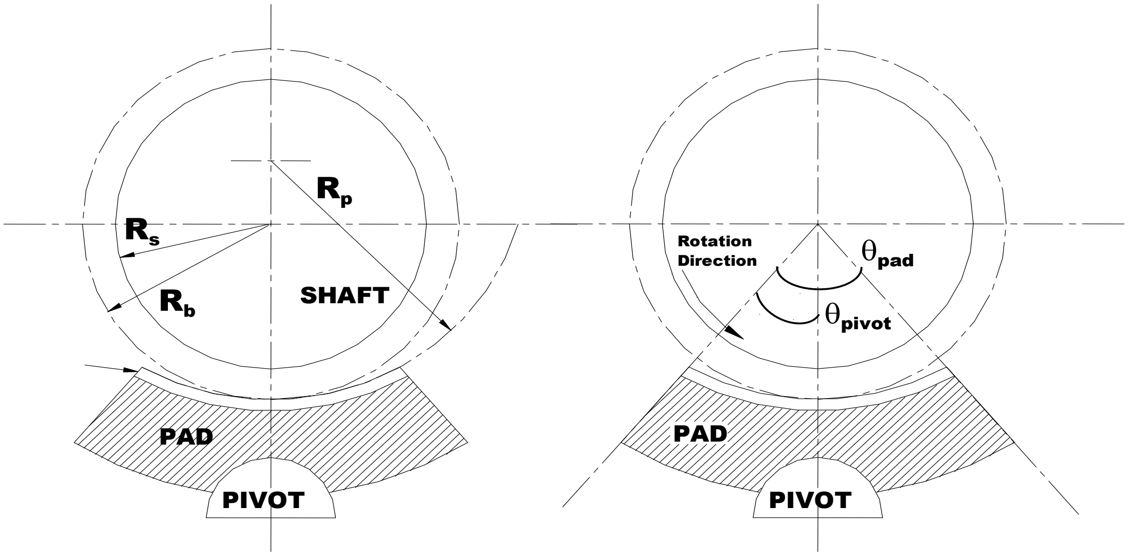

Figure 3. Tilting-pad bearing geometric parameters [2].

The geometric parameters given previously are used to define the three main bearing parameters that control the static and dynamic characteristics. These TPJB parameters include the pad pivot offset, pad preload, and the external loading configuration.

The pivot offset is the angular pivot location divided by the angular extent of the pad as given in Eq. (2).

$$PIVOT\ OFFSET = \frac{\theta_{pivot}}{\theta_{pad}} \tag{2}$$

The angular pivot location, θ_{pivot}, is measured from the leading edge of the pad. For a pad with a centered pivot, the offset is .5 or 50%. Increasing the offset helps ensure a converging oil wedge for proper operation. Many bearing designers believe that offsetting the pad pivot will increase the direct stiffness and load carrying capability of the bearing [3]. Pivot offsets from 50% to 60% are commonly seen in industrial applications.

The preload of a bearing quantifies the amount that the pad radius differs from the journal radius. Eq. (3) defines pad preload where C_b and C_p are given previously in Table 1.

$$M_p = 1 - \frac{C_b}{C_p} \tag{3}$$

A preload of zero means $C_b = C_p$, and a constant clearance exists across the pad. A positive preload helps ensure a converging fluid film, even in light or no-load conditions [3]. Increasing the preload is a common technique to alleviate pad flutter where unloaded pads vibrate due to an absence of fluid film forces [4]. Alternatively, lowering pad preload is predicted to increase the effective damping [3]. Negative preloads are generally avoided to prevent divergent oil films and pad flutter.

The static external load orientation with respect to the pads can either be load-on-pad (LOP) or load-between-pad (LBP). The LOP configuration is predicted to provide more stiffness asymmetry, specifically a larger stiffness in the loaded direction. LBP typically offers more symmetric rotordynamic coefficients and increases the bearing’s load carrying capacity.

A variety of pivot types exist for TPJBs, and most fall under one of the three main categories: rocker-pivot, spherical-seat, and flexure-pivot. Drawings of these pivot types are shown below in Figure 4. The rocker-pivot type generally uses cylinder or spherical-backed pads in a cylindrical housing. A spherical-seat pivot typically uses two spheres with similar radii between the pad and bearing housing. The flexible pivot, or flexure-pivot design employs a web that is machined between the pad and housing. Since the pad and housing are machined from the same piece, stack-up tolerances of the rocker and spherical designs are eliminated. The flexure design also adds a rotational stiffness to each pad that is not present in other tilting pad pivots.

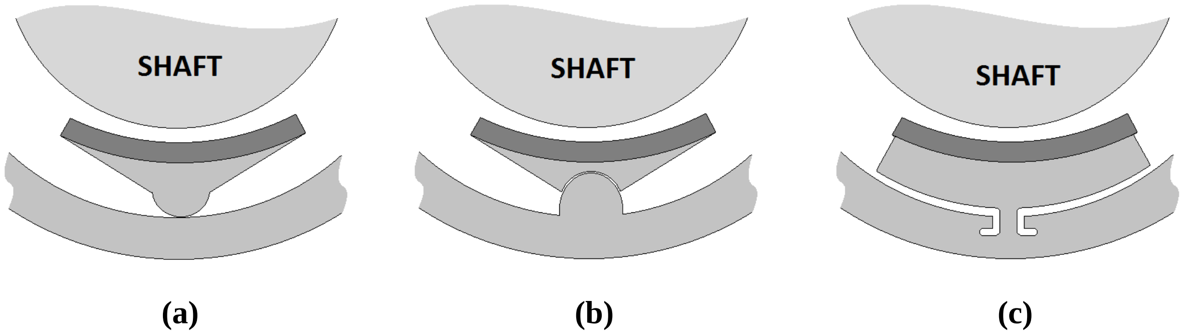

Figure 4. TPJB pivot types: (a) Rocker-pivot, (b) Spherical-seat, and (c) Flexure-pivot.

Pivot type can significantly influence bearing characteristics, especially the pivot support stiffness. Kirk and Ready [5] predicted that support stiffness can vary substantially with pivot type, impacting the equivalent stiffness observed at the bearing.

While the main function of a bearing is to provide support to a rotor system, a bearing's dynamic response significantly impacts the overall dynamics of the system. Specifically, bearing stiffness and damping characteristics impact critical speeds, unbalance response, and stability. For a TPJB, the fluid film at each pad contributes to the overall stiffness and damping characteristics. In 1964, Lund [1] presented the original technique of summing the contribution of each pad to obtain a combined stiffness and damping for two orthogonal directions that fits the model described previously in Eq. (1). The "Lund Pad Assembly Method" has long been the basis of predicting dynamic performance to tilting pad bearings [6]. Lund presented stiffness and damping design curves for multiple tilting pad bearing configurations. He made the first observation that neglecting pad inertia will yield zero cross-coupled stiffness coefficients. This realization clearly showed the stability benefits of tilting-pad bearings.

While implementing the Lund Pad Assembly Method, a pad vibration frequency must be assumed during coefficient reduction. Lund chose this frequency to be equal to the shaft running speed, or the synchronous frequency [1]. This frequency assumption was widespread among researchers and designers of the time [7]-[9]. Assuming synchronous frequency, Nicholas, Gunter, and Allaire [9] calculated pad dynamic data with a finite element method and determined bearing stiffness and damping design curves with the pad assembly method. Nicholas, Gunter, and Barrett [10] employed these design curves to show the effects of pad preload, pivot offset, and other TPJB properties on the stability of a centrifugal compressor. After observing these results, Nicholas [6] stated "Lund pointed out that it is mathematically incorrect to use a synchronous frequency for a stability calculation." Lund stated that TP bearing coefficients should be calculated with the rotor processing at the damped natural frequency. Lund's comments led to the ongoing debate of using synchronous versus non-synchronous (damped natural frequency) reduced TPJB coefficients for stability calculations. The resulting area of research has attempted to determine the frequency dependency of the dynamic response of tiling pad bearings.

In 1983, Parsell et al. [11] presented one of the earliest studies concerning frequency dependency of tilting pad bearing coefficients. The authors derived rotordynamic coefficients for a 5-pad bearing in LOP and LBP configurations. Their resulting stiffness coefficients decreased with increasing frequency while damping coefficients increased with frequency. This coefficient frequency dependency was reduced when pad preload was increased. Additional authors [12]-[14], have also provided theoretical results for the frequency dependency of rotordynamic coefficients.

Experimental data on TPJB coefficient frequency dependency is rather limited. One of the first studies was conducted by Ha and Yang [15] in 1999. They tested a 5-pad, 300 mm (11.8 in) diameter tilting pad bearing in LOP configuration. Test conditions included speeds up to 3600 rpm and static unit loads of 111 and 222 kPa (16 and 32 psi). Dynamic testing used single excitation frequencies, ranging from .5 to two-times running speed. The authors reported that the stiffness coefficients slightly decreased with increasing excitation frequency, while the damping coefficients slightly increased with excitation frequency. Even though excitation frequencies were limited to 60 Hz, and speeds were relatively low, their investigation was the earliest to cite measured frequency dependency of TPJBs.

In 2001, Wygant [16] tested a five-pad, 70mm (2.76 in) diameter, rocker-pivot, TPJB in LOP and LBP configurations. The bearing had an 81.3 µm (3.2 mil) clearance, *L/D*=.75, and 50 % offset pads. Testing was conducted at speeds to 2250 rpm and loads near 690 kPa (100 psi). While altering pad pre-load and pivot type, Wygant also examined the effect of excitation frequency on the dynamic coefficients. The bearing was excited with single frequency orbital excitations at .5, one, and two times ω, producing frequency dependent stiffness and damping coefficients. RMS Uncertainties for the synchronous direct damping coefficients are cited as C_{xx} (15.5%) and C_{yy} (14.66%). While significantly better uncertainties were found at .5 and two times ω, quantifying frequency dependency of the direct damping coefficients is difficult due to the limited excitation frequencies and uncertainties. The direct stiffness coefficients were found to decrease with increasing frequency, consistent with the results of Ha and Yang [15].

In 2004, Ikeda et al. [17] performed experimental testing on the dynamic and static characteristics of a 580 mm (22.8 in) diameter TPJB. The test bearing was a four-pad, direct lubricated rocker-pivot bearing with 60% offset pads and a C_b/R of .0013. Tests were conducted at speeds to 3600 rpm, loads to 2.9 MPa (420 psi), and excitation frequencies from 40 to 60 Hz. The study mainly involved optimizing static parameters, but non-dimensional stiffness and damping coefficients were provided versus Sommerfeld numbers. Experimental direct stiffness coefficients increased linearly with Sommerfeld number. Stiffness calculations from a Reynolds equation code agreed well with test results for low Sommerfeld numbers (approximately .2 to .3) but over-predicted stiffness coefficients at higher Sommerfeld numbers. The experimental direct damping coefficients remained relatively constant with respect to speed and load. Calculated damping coefficients were consistently higher than test results, and the difference increased with increasing Sommerfeld number. The authors attribute the discrepancy between experimental and predicted coefficients to the influence of fluid inertia in the test results and the simplification in their calculation. While these results did not speak directly to the frequency dependency issue, the dynamic coefficient trends are relevant because their test bearing is a larger version of the bearing tested in this thesis.

Additional investigations regarding the frequency dependency of TPJB rotordynamic coefficients have been carried out by Rodriguez and Childs [18], Al-Ghasem and Childs [19], and Hensley and Childs [20]. Rodriguez and Childs tested a four-pad, flexure-pivot, TP bearing with 50 % offset pads in a LOP configuration. The test bearing had 116.8 mm (4.6

in) nominal diameter, .19 mm (7.5 mil) C_b, and .25 preload. Test conditions included speeds from 6 to 16 krpm, and unit static loads to 1034 kPa (150 psi). Using the parameter identification procedure described by Childs and Hale [21], complex dynamic stiffness coefficients were obtained from a multi-frequency excitation including frequencies from 20 to 300 Hz in 20 Hz increments. The real dynamic stiffness coefficients were frequency dependent, and generally decreased with increasing frequency. The imaginary dynamic stiffness coefficients increased linearly with frequency, implying a constant, frequency-independent damping coefficient. If a conventional [K][C] model is used, the stiffness coefficients are frequency-dependent. By applying the [K][C][M] model shown below in Eq. (4), the frequency dependency of the stiffness was captured by an added-mass, or apparent mass matrix, [M].

$$-\begin{Bmatrix} f_{bx} \\ f_{by} \end{Bmatrix} = \begin{bmatrix} K_{xx} & K_{xy} \\ K_{yx} & K_{yy} \end{bmatrix} \begin{Bmatrix} \Delta x \\ \Delta y \end{Bmatrix} + \begin{bmatrix} C_{xx} & C_{xy} \\ C_{yx} & C_{yy} \end{bmatrix} \begin{Bmatrix} \Delta \dot{x} \\ \Delta \dot{y} \end{Bmatrix} + \begin{bmatrix} M_{xx} & M_{xy} \\ M_{yx} & M_{yy} \end{bmatrix} \begin{Bmatrix} \Delta \ddot{x} \\ \Delta \ddot{y} \end{Bmatrix} \tag{4}$$

The real dynamic stiffness coefficients were curve fitted as a quadratic function with respect to excitation frequency, yielding frequency-independent stiffness and added-mass coefficients. The largest added-mass coefficients observed were on the order of 40 kg. Summarizing, the rotordynamic coefficients from Rodriguez and Childs can be considered frequency-independent when applying a [K][C][M] model. Predictions from both a Reynolds equation as well as a Navier Stokes, bulk-flow code did an adequate job of predicting the dynamic response for excitations frequencies up to running speed. Al-Ghasem and Childs [19] tested the same bearing in a LBP configuration with similar loads and obtained very similar results. Hensley and Childs [20] also tested this flexure-pivot bearing in LBP configuration, but for higher loads ranging from 1 to 2.2 MPa (150 to 320 psi). They were also able to account for the observed coefficient frequency dependency by applying a [K][C][M] model.

In 2006, Dmochowski [22] performed an experimental and theoretical investigation of the dynamic coefficients of a rocker-pivot TP bearing. He tested a five-pad bearing with a 98 mm (3.858 in) diameter, .3 preload, and an unspecified offset. Tests and predictions were conducted at ω = 9 krpm with unit loads of 460 and 1160 kPa (67 and 168 psi). Two bearing configurations were considered, including a LBP case with a .4 *L/D* and a LOP case with an *L/D* of 1. Dynamic testing included a multi-frequency excitation range up to 300 Hz in 10 Hz increments. Although the measured dynamic results showed some scatter, the direct dynamic stiffness coefficients exhibited trends that could be fit with a [K][C][M] model. That is, the direct real dynamic stiffness coefficients generally fit a quadratic curve with respect to frequency, yielding frequency-independent stiffness and added-mass coefficients. The direct imaginary coefficients generally increased linearly with frequency, providing a frequency-independent damping coefficient. Test results were modeled quite well by his code that accounted for thermal effects, turbulent flows, and *pad-support flexibility*. Not all available bearing codes account for pad-support flexibility when calculating rotordynamic coefficients. Dmochowski concluded that the frequency dependency of TPJB stiffness and damping properties is influenced by pad inertia and pivot flexibility.

In 2007, Carter and Childs [23,24] tested 5-pad rocker-pivot TP bearing in LBP and LOP configuration. The pads had a 60% pivot offset and were direct lubricated with leading-edge-groove (LEG) technology. The bearing assembly included a half-flooded design where one end seal was used to prevent axial leakage in one direction. The bearing had a .1575 mm (.0031 in) C_b, .28 pad preload, and 101.6 mm (4 in) *D*. Dynamic and static tests were performed at ω = 4 to 13 krpm with unit static loads from 345 kPa to 3101 kPa. A multi-frequency excitation, similar to Rodriguez [18], was used to obtain dynamic stiffness coefficients. For the majority of the test conditions, the real part of the dynamic stiffnesses could be approximated as quadratic functions of excitation frequency. This allowed for the frequency dependency of the stiffness coefficients to be captured with an added-mass term, producing a frequency-independent [K][C][M] model, agreeing with the results of the flexure-pivot bearing, Refs. [18-20]. The direct damping terms showed no frequency dependency and changed very little with respect to speed and load. Experimental results were compared with predictions from a Navier Stokes bulk-flow CFD analysis. Direct stiffness coefficients were slightly over predicted while damping was over predicted substantially in the loaded direction.

Childs and Harris [25] provide dynamic measurements and predictions for a 101.6 mm (4 in) diameter, 4-pad, ball-in-socket, tilting-pad bearing. The test bearing had an approximate 95.3μm (3.75 mil) radial bearing clearance and a mean loaded pad preload of

.37. Using a multi-frequency excitation, similar to Rodriguez [18], dynamic stiffness coefficients were obtained for speeds to 12 krpm and loads to 1896 kPa (275 psi). Rotordynamic coefficients were determined from curve fitting the complex dynamic stiffness coefficients with respect to frequency. A frequency-independent, [K][C][M] model did a good job at fitting the measurements, agreeing with the results for other bearing configurations, [18-20]. Results were reasonably predicted with a Navier Stokes bulk-flow code after pivot-support stiffness was accounted for by adding a spring in series with the model results.

Carter and Childs' [23] results led some researchers to state that a rocker-pivot TPJB with a 50% pivot offset is more likely to exhibit frequency dependency. This belief is consistent with some predictions, e.g., Schmeid, et al. [26]. These authors present a dynamic model for TPJBs that includes the pad inertias and pad rotational angles. Predictions for dynamic coefficients are made by solving the Reynolds Equation for the perturbed equilibrium position. Stiffness and damping coefficients are presented as functions of excitation frequency for three bearing configurations that alter pad number and pivot offset. All bearings have a 125 mm diameter, .2 preload, and LBP configuration. Simulations were for ω = 6000 rpm and a static load of 500 kPa (73 psi). The four-pad bearing with 55% offset yields rotordynamic coefficients that are highly frequency-dependent, and cannot be modeled with added mass terms. The direct stiffness coefficients decrease while direct damping coefficients increase in sub-synchronous range. The coefficients of the five-pad bearing with 55% offset exhibit a smaller amount of frequency dependency, which the authors accredit to the shorter pad arc. The four-pad bearing with 60% offset provides stiffness and damping coefficients that are frequency-independent.

Most recently, Delgado et al. [27] implemented a bearing test rig with a similar design to that of Texas A&M Turbomachinery lab designed by Kaul [28]. This new test rig uses the same "floating" bearing design to measure the dynamic response of fluid film bearings. They compared rotordynamic coefficients of a rocker-pivot TPJB obtained from three different excitation methods, including single frequency, pseudo random multi-frequency, and dual orbital excitations. Results show that all three methods show good agreement for the bearing and conditions tested.

In addition, Delgado et al. [29] performed a series of tests on multiple rocker-pivot, tilting-pad bearing configurations. They tested a five-pad bearing with .16 preload in LOP configuration and a four-pad bearing with .3 preload in LBP configuration. Both bearings were tested with 50 and 60 % pivot offset pads. The test bearings were directly lubricated and had a nominal 110 mm (in) diameter. Testing was performed at 7.5, 10, and 15 krpm with a static unit load of 300 kPa. Dynamic stiffness coefficients for the test bearings were obtained from multi-frequency excitation. The direct rotordynamic coefficients were identified from curve fitting the complex dynamic stiffnesses and showed to be frequency independent when considering an added-mass term. Applying a [K][C][M] model yields frequency-independent coefficients for all bearing configurations and conditions tested. Experimental results were modeled with a predictive code and showed discrepancies within 50% for the direct stiffness coefficients and within 30% for the direct damping coefficients at high speed and light load condition.

This thesis provides measured and predicted static and dynamic characteristics of a 5-pad rocker-pivot tilting-pad bearing with 50 and 60 % pad offsets. The main focus of this work is the frequency dependency of the rotordynamic coefficients while observing the effect of pivot offset. The test bearing consists of the same bearing housing as used by Carter, with similar clearances and preload, but includes 50% pivot offset pads. A multi-frequency excitation is applied to the test bearing on the test apparatus described by Kaul [28], while the static and dynamic response, including rotordynamic coefficients, is observed. Tests are conducted in LBP configuration at speeds at and above those tested by Carter.

While Delgado et al. [29] tested a variety of titling-pad bearing configurations and conditions, tests were limited to unit loads of 300 kPa. TPJBs often see much higher loads, on the order of 3413 kPa (495 psi) or more, due to the gear forces in high speed gearboxes and integrally geared compressors [30]. Tests results in this thesis include static loads from zero to 3101 kPa (450 psi). Additionally, Reynolds numbers are comparable to Carter's [24] and Delgado et al.'s [29]. Direct comparisons with Carter's results [24] are not practical because: (1) Carter's bearing used a half flooded configuration that included only one axial end seal. Research on tiling pad bearing cooling techniques has shown that an evacuated configuration (no end seals) can substantially lower pad temperatures [30]. (2) Carter's instrumentation arrangement included proximity probes that were located opposite of the dynamic shaker attachment points on the housing. This configuration was confirmed to be inferior to the new configuration of locating the probes near the shakers. This instrumentation improvement is discussed fully in the Instrumentation section.

The static and dynamic results in this thesis are compared to theoretical predictions from XLTFPBrg, a bearing code that is part of the XLTRC^2 Rotordynamics Software Suite. This code can predict static and dynamic behavior of rigid-pad, flexure-pad, and tilting-pad bearings. The program uses either a CFD algorithm to solve bulk-flow Navier Stokes (NS) equations or a Reynolds-equation solver to calculate bearing stiffness and damping coefficients. Unless stated otherwise, all predictions shown were found using the bulk-flow NS analysis.

TEST RIG DESCRIPTION

Testing Apparatus

The oil bearing test rig at Texas A&M Turbomachinery Laboratory is used to measure static and dynamic performance of high speed journal bearings. Figure 5 depicts the test rig main section view. This rig uses a *floating* test bearing design, similar to that used by Glienicke [31] to test journal bearings. Kaul [28] presents a detailed account of the design and features of the test rig and facility at the Turbomachinery Lab. The following summary accounts for its main features.

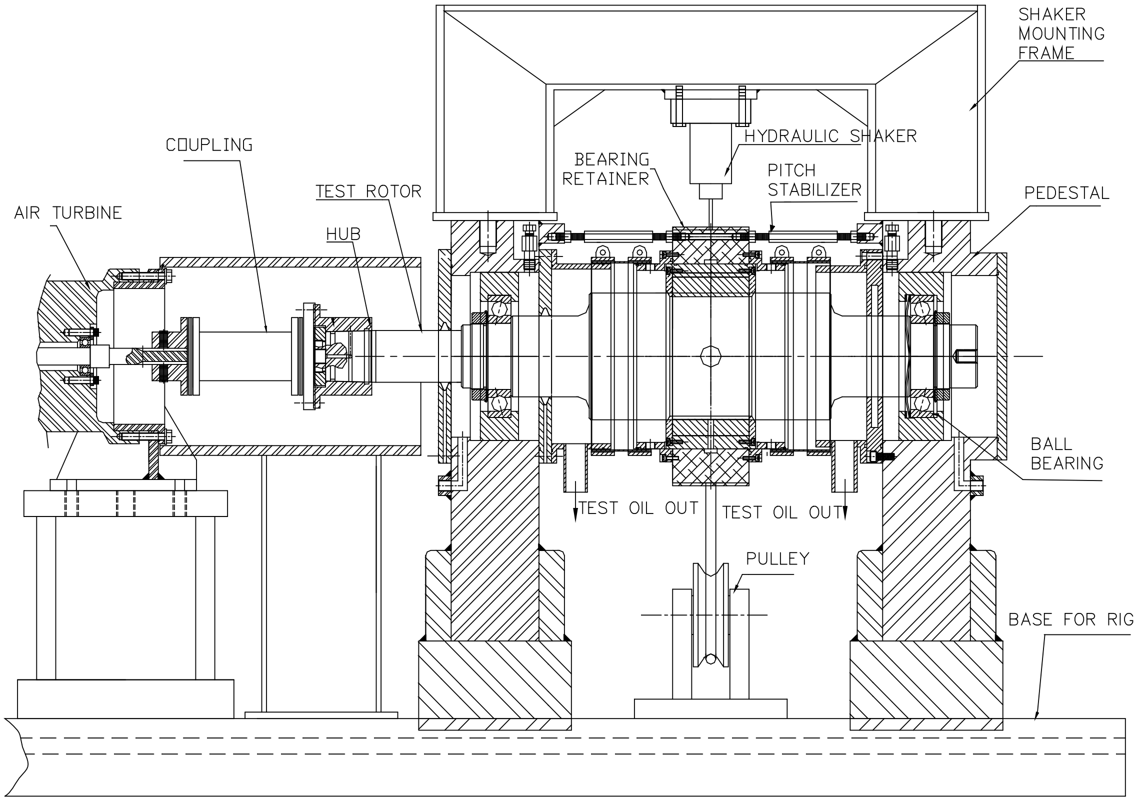

Figure 5. Test rig main section.

The rig consists of a steel base that supports the main test section and the air turbine drive motor. Connected to the shaft by a flexible disc coupling, the air turbine can produce 65 kW and has a maximum running speed of 17,000 rpm. The 4140 steel rotor is machined to a diameter of 101.59 mm (3.9995 in) at the test section and is supported on the pedestals with hybrid-ceramic, angular contact ball bearings spaced approximately 457 mm (18 in) apart. Lubrication for the ball bearings is provided by an oil mist lubrication system. Pressurized air seals separate the oil outlet chambers from the ball bearing locations.

A split designed stator section holds the test bearing and all associated instrumentation, including non-contacting eddy current motion probes, accelerometers, thermocouples and pressure transducers. A pneumatic loader and two hydraulic shakers apply the static and dynamic loads to the stator section. Angular alignment between the rotor and test bearing is provided by an arrangement of six pitch stabilizers. The oil is supplied to the bearing through a port located in the bottom of the stator housing and exits through the side caps and collection chambers.

ISO VG32 turbine oil is delivered to the test bearing by an oil supply system and has the properties given below in Eqs. (5) through (7), where *T* is the oil temperature in Kelvin.

$$\rho = -0.6616T + 1064 \qquad \left[kg/m^3\right] \tag{5}$$

$$\mu = -0.045336\, e^{-0.030069(T-294.2611)} \qquad \left[Pa-s\right] \tag{6}$$

$$c_p = 3.6273T + 811.75 \qquad \left[J/kg-K\right] \tag{7}$$

The oil system can deliver a maximum volumetric flow of 75 liters per minute and a maximum pressure of 82.7 bars. A heat exchanger and a set of pneumatically controlled valves allow for temperature control of the oil being delivered to the test section.

Loading Configuration

The loading of the test bearing consists of two orthogonal dynamic forces and a unit static load. Hydraulic shakers provide dynamic loads in the *x* and *y* directions while a static loader operates in the *y* direction only. A schematic of stator-shaker arrangement is shown in Figure 6, as observed from the non-drive end of the test rig.

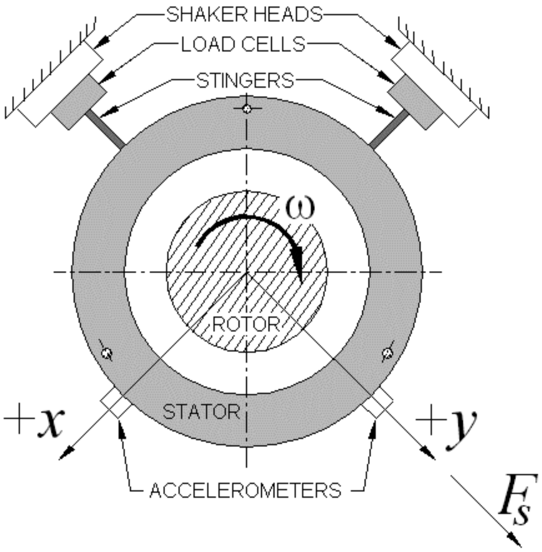

Figure 6. Stator-shaker arrangement and coordinate system.

The shaker heads are attached to the stator section by beam elements called stingers. The stingers isolate the test structure from the dynamics of the shakers' structure. The loads applied to the stator are measured by load cells located between the stingers and shakers. The *x*-shaker can excite the stator section with dynamic loads up to 4450 N in both tension and compression. The *y*-shaker can produce dynamic loads up to 4450 N in tension and 11125 N in compression. Both shakers can produce excitation frequencies up to 1000 Hz.

The pneumatic loader provides a static tensile load to the stator in the *y* direction. This static force is denoted as F_s in Figure 6. The test rig and static loading arrangement as viewed from the non-drive end is given below in Figure 7.

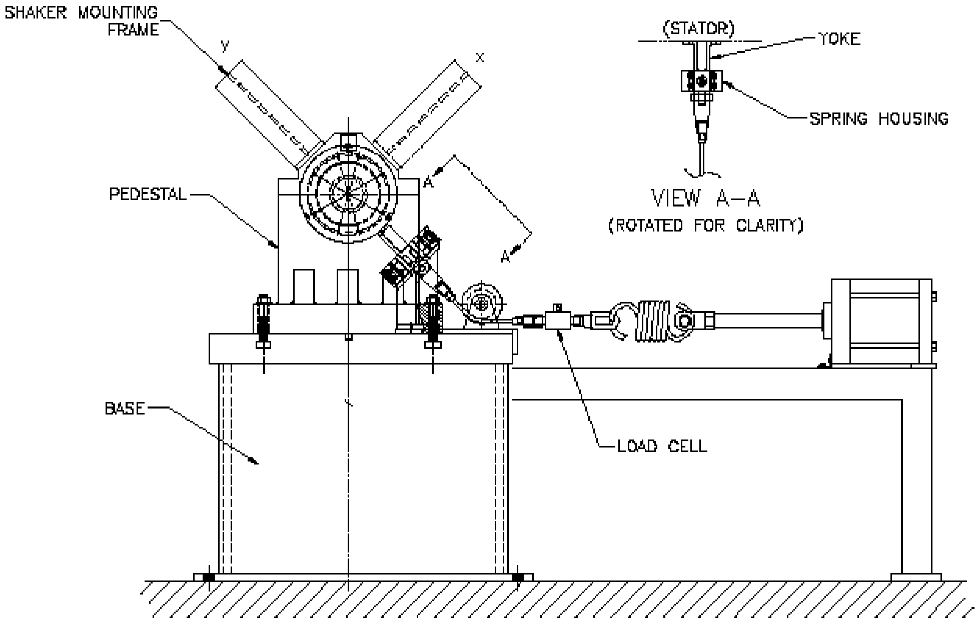

Figure 7. Static loader arrangement.

The pneumatic cylinder can produce a maximum load of 22000 N (5000 lb_f). This loader is attached to the stator assembly through a yoke, cable, and spring system. This cable and spring assembly ensures the load is constant and applied in one direction. The static force is measured with a load cell attached in series with the cable and spring arrangement.

Instrumentation

Figure 6 shows the stator assembly, which is comprised of the test bearing, housing, end-caps, and instrumentation. The figure also details the location of all the measurement probes in the end caps and the housing, as well as the location of the measurement planes. Note that the turbine side and non-turbine side refer to the drive end, DE, and the non-drive end, NDE, respectively.

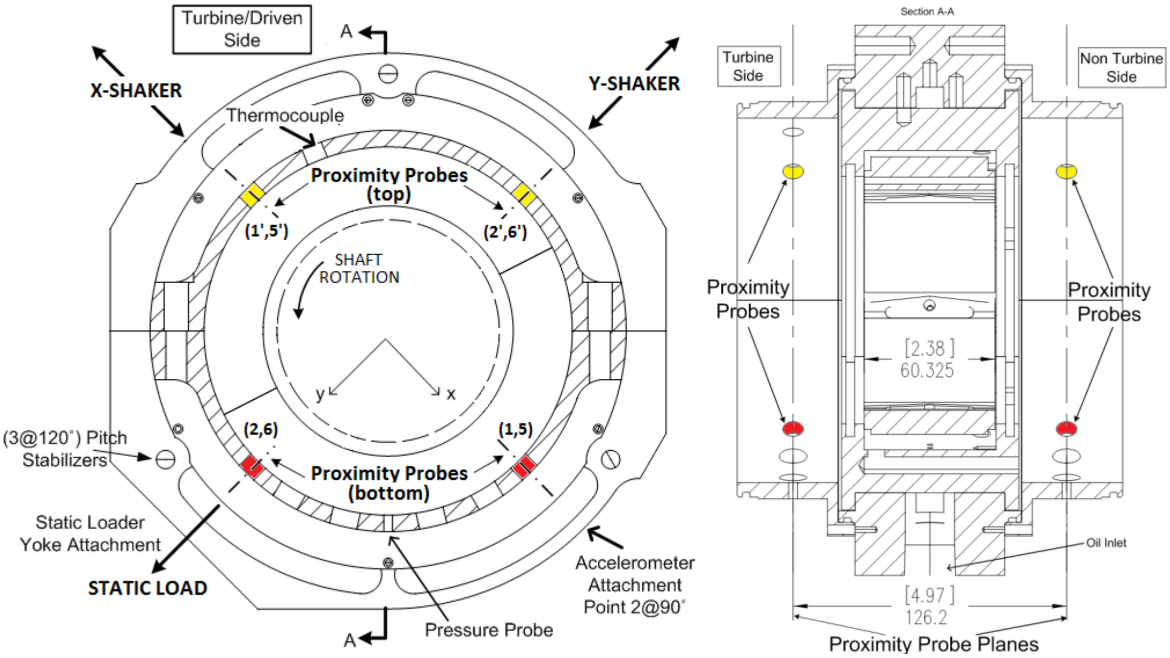

Figure 8. Bearing stator configuration and instrumentation.

Four proximity probes, located in the stator end caps, record the relative motion of the stator with respect to the rotor for each direction of excitation. Two proximity probes are placed in a plane at the NDE and two at a parallel plane at the DE. Measurement of the stator position in two parallel planes allows monitoring of the stator's pitch and provides an average bearing position.

For previous testing, including the work by Carter and Childs [23], the proximity probes were located at the bottom of the end-caps at the locations designated by (2,6) and (1,5) in Figure 8. This configuration places the probes opposite the shakers where the *y* direction probes are near the static load attachment. Prior to the current work, pivot or backup-structure stiffness measurements were taken by applying a static load to the test bearing at zero speed and measuring the displacement. This backup-structure stiffness measurement changed considerably whether the load was applied via the *y*-shaker or the static loader. Specifically, loading the stator with the shaker produced less displacement than the static loader, and hence a larger backup-structure stiffness measurement. It was concluded that flexibility in the stator was causing this discrepancy.

Since flexibility was observed in the stator, the top-mounted position, designated by (2',6') and (1',5') in Figure 8, was determined to be the most accurate probe location. This orientation is superior because it places the proximity probes near the stinger-shaker attachment points. This shortens the load path between the probes and the points of the excitation forces. Also, this configuration is better because it puts the motion probes near the loaded pads. This minimizes the influence of the stator stretch on the measured displacement during static loading.

This proximity probe change had a measurable effect on the static eccentricity data and the dynamic stiffness functions. Static and dynamic results comparing top and bottom probe locations are provided in Appendix F. All the static and dynamic data presented in this thesis was obtained with the proximity probes located at the top locations, except where stated otherwise.

Piezoelectric accelerometers measure the stator absolute acceleration in both the x and y directions. Temperature probes are located in the oil-inlet chamber as well as the downstream end caps. Static pressure probes measure the oil pressure at the inlet and both of the outlet locations. The oil flow-rate is measured with a turbine flow-meter upstream of the test bearing. In-pad thermocouples provide pad metal temperatures just below the babit surface. A summary of the measured quantities and associated instrumentation is provided below in Table 2.

Table 2. Measured parameters and associated instrumentation.

CATEGORY	*QUANTITY MEASURED*	*INSTRUMENTATION*
DYNAMIC	Dynamic Force	Load Cells
	Relative Stator to Rotor Motion	Eddie Current motion Probes
	Absolute Stator Acceleration	Accelerometers
STATIC	Rotor Speed	Tachometer
	Static Load	Load Cell
	Oil Flow-rate	Flowmeter
	Oil Pressure (inlet and exit)	Pressure Probes
	Temperatures (inlet, exit, and pad)	Thermocouples

Test Bearing

The test bearing is a 5-pad, rocker-pivot, titling-pad bearing. This bearing was manufactured by the Orion Corporation, now John Crane Orion, and uses the same split-design bearing shell as tested by Carter [23]. The bearing assembly includes two different pad sets in order to obtain pivot offsets of 50 and 60%. Figure 9 provides a graphical comparison of the 50 and 60% offset pads of the test bearing.

(a) **(b)**

Figure 9. Test bearing pad with a pivot offset of (a) 60% and (b) 50%.

All pads are directly lubricated by a leading-edge groove, or LEG, that is machined into the pad, as shown below in Figure 10. Note that the pivot offset discussed previously does not include the LEG portion of the pads. The LEG technology initiated with the work of Ball and Byrne [32] for the Orion Corporation. This wedge-shaped groove is designed to provide the leading edge of a pad with cool lubricant and prevent hot oil carry-over from the previous pad. The LEG pad design is also called the “Advantage” because it offers the possibility of cooler pad temperatures.

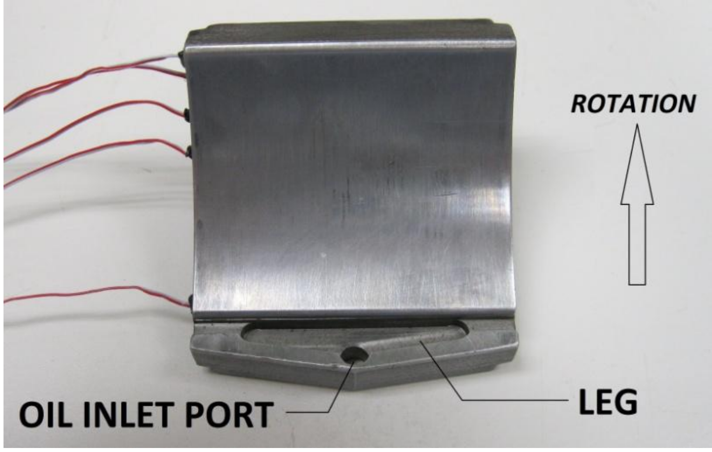

Figure 10. Tilting pad with leading edge groove.

The test bearing uses a flooded configuration where floating end seals prevent axial leakage out of the bearing. This design requires the majority of the oil from each pad to exit through ports in the bearing shell rather than the axial clearances. These ports direct the exiting oil from each pad into axial flow from the side of the bearing shell. The oil exit ports and end seals of the test bearing are shown below in Figure 11. Note that the drilled holes in the top end seal are for the passing of pad thermocouple wires.

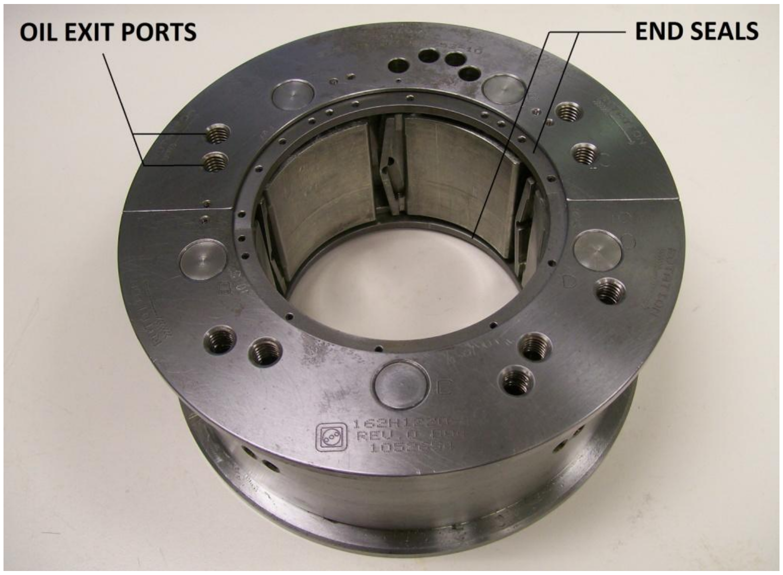

Figure 11. Oil exit ports and end seals of the test bearing.

A summary of the test bearing geometry, loading style, and lubricant type are presented below in Table 3. These parameters are constant for both the 50 and 60% offset configurations.

Table 3. Test bearing parameters that are constant for both offsets.

Number of Pads	5
Configuration	LBP
Pad Arc Angle, θ	57.87°
Rotor Diameter	101.587 mm (3.9995 in)
Pad Axial Length	60.325 mm (2.375 in)
Radial Pad Clearance, C_p	.112 mm (.0044 in)
Pad Mass	.44 kg (.96 lbm)
Lubricant Type	ISO VG 32

The measured bearing clearance, C_b, and preload, M_p change a small amount with pivot offset as seen below in Table 4. This discrepancy occurs because different sets of pads are used to obtain the different pivot offsets. The bearing clearances provided are the average measured clearances taken for each bearing assembly, described later in the Static Results.

Table 4. Test bearing clearances and preloads.

PARAMETER	***50% OFFSET***	***60% OFFSET***
Radial Bearing Clearance, C_b	.0814 mm (.0032 in)	.0837 mm (.0033 in)
Measured Preload, M_p	0.27	0.25

EXPERIMENTAL PROCEDURE

Testing Procedure Overview

At the beginning of a test series, a cold-clearance measurement is made. This clearance measurement is used to estimate the average bearing clearance and to provide a clearance boundary for centering the bearing for the zero load condition.

The general testing procedure includes achieving steady state operating conditions and data acquisition. This requires operating the test rig near a set of nominal test conditions, including rotor speed, bearing static load, and oil inlet temperature. During a test, the bearing stator is excited using the hydraulic shakers with a pre-specified pseudo-random dynamic excitation waveform in two orthogonal directions, i.e., x and y directions. Static data, such as temperatures and pressures, are taken automatically before and after the x and y direction dynamic shakes, allowing for an average of steady state conditions for the dynamic tests.

The dynamic waveform consists of frequencies from 20 to 320 Hz in approximately 20 Hz increments. The actual excitation frequencies are slightly offset from the nominal values in order to avoid noise from 60 Hz and its multiples. The maximum amplitude of the dynamic force is approximately 250 lbs. Dynamic data taken during testing includes the relative motion at the DE and NDE, the dynamic load, and absolute acceleration of the bearing stator. These data are captured in the time domain and later transformed to the frequency domain via Fast Fourier Transform and reduced with the procedure described in the Parameter Identification Model.

Testing Conditions

The test conditions refer to the controlled variables: rotor running speed, static load on the bearing, oil flow-rate, and oil inlet temperature. These conditions include four running speeds varying from 7000 to 16000 rpm and six static unit loads from 0 kPa to 3101 kPa (450 psi). The oil flow-rate is maintained constant for each running speed. Table 5 presents a matrix of the nominal test conditions for load, speed, and flow-rate.

Table 5. Matrix of nominal test conditions.

Static Load kPa (*psi*)	**Speed [RPM],** *Flow-rate [gpm]*			
	7000, *5.5*	**10000**, *5.5*	**13000**, *8.0*	**16000**, *10*
0 (*0*)	✓	✓	✓	✓
345 (*50*)	✓	✓	✓	✓
1034 (*150*)	✓	✓	✓	✓
1723 (*250*)	✓	✓	✓	✓
2413 (*350*)	✓	✓	✓	✓
3101 (*450*)	✓	✓	✓	✓

The above cases are the ideal test conditions while the actual measured test conditions, including inlet and exit temperatures, pressures, and other static measurements are reported in Appendix A. These measured conditions were used for any necessary calculations, e.g. Reynolds Number. All of the reported dynamic data are organized with respect to nominal speed and load.

Table 6 presents the nominal and measured average oil inlet temperatures for all the tests. Both the 50 and 60 percent offset pads were tested at a nominal inlet temperature of 43.3°C (110°F). Uncertainty of the oil inlet temperatures was less than 0.5 °C.

Table 6. Matrix of nominal and measured oil inlet temperatures.

Test Bearing Offset	**Inlet Temperature, °C (*°F*)**		
	Nominal	**Measured**	**Uncertainty**
50%	43.3 (*110*)	43.7 (*110.6*)	0.4 (*0.7*)
60%	43.3 (*110*)	43.9 (*111.0*)	0.3 (*0.5*)

Static Characteristics

Static performance characteristics for TPJBs typically include the bearing clearance, eccentricities, attitude angles, pad temperatures, power loss estimations, and static stiffness coefficients. These parameters are defined and explained in the following section while test results and predictions are provided in the Static Results section.

A clearance measurement involves a slow rotating clearance test taken at a given temperature. “Cold” clearances refer to measurements taken at room temperature without the influence of operating temperatures. The hydraulic shakers used for dynamic testing are used to move the bearing in contact with the rotor with a rotating force at approximately .2 Hz. Continuous position data from the proximity probes is taken during this process. This position data yields a pentagon clearance for a five-pad bearing. The radius of a circle fit provides an average radial bearing clearance. The reported bearing clearance for a given bearing configuration is averaged from clearance data taken from three clearance tests. Figure 12 shows a clearance fit plotted with a measured clearance for a specific clearance test. Note that the average bearing clearance is used throughout this thesis.

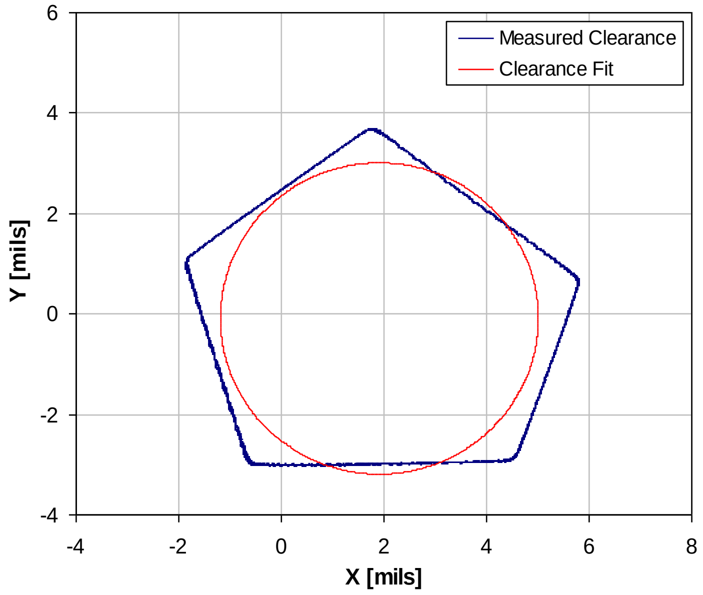

Figure 12. Example of a measured and an average fitted bearing clearance.

The position of the bearing at steady operating conditions may be described using the static eccentricity ratio ε_o and the attitude angle, ϕ. Eccentricity provides the distance between the bearing center and the shaft center as a ratio with respect to the bearing clearance. An eccentricity near zero indicates the shaft is nearly centered in the bearing while an eccentricity of one suggests contact between the bearing and shaft. Eccentricity is defined in the *x*, *y* directions, and as a magnitude in Eqs. (8) and (9).

$$\varepsilon_{io} = \frac{e_{io}}{C_b}, \quad i = x, y \tag{8}$$

$$\varepsilon_o = \sqrt{\varepsilon_{xo}^2 + \varepsilon_{yo}^2} \tag{9}$$

Attitude angle quantifies how much the relative displacement of the bearing and shaft deviates from the loaded axis, i.e. the amount of cross-coupling. Attitude angles near zero, indicate minimal cross-coupling effects between the *x* and *y* directions. The attitude angle is provided below in Eq. (10).

$$\phi = \tan^{-1}\left(\frac{\varepsilon_{xo}}{\varepsilon_{yo}}\right) \tag{10}$$

Figure 13 provides a generic locus plot and a physical interpretation of eccentricity and attitude angle. This represents the test rig coordinate system viewed from the DE with the static load in the *y* direction.

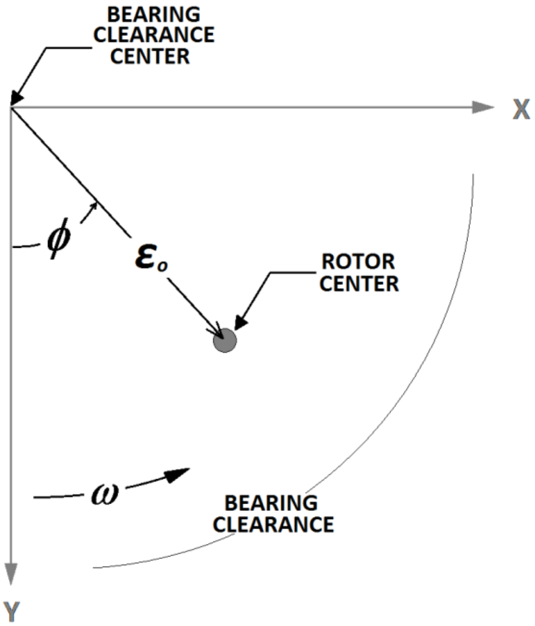

Figure 13. Eccentricity and attitude angle coordinate system.

The power loss values presented in this thesis are estimations from an energy balance assuming adiabatic conditions. From this assumption, the power loss from shearing the fluid is equal to the energy transfer from the fluid, specifically, the heat transferred as shown in Eq. (11).

$$P_{LOSS} = \dot{Q}\left\{\left(T\rho c_p\right)_{out} - \left(T\rho c_p\right)_{in}\right\} \tag{11}$$

In this equation, $\dot{Q}$ represents the average oil flow-rate, while T, ρ, and c_p represent the temperature, density, and specific heat of the oil at the inlet and outlet of the bearing. These parameters are measured or calculated as described previously.

Static stiffness is defined as the slope of the static load versus eccentricity plot for a given steady state condition, as shown below in Eq. (12). For the measured test data, this is approximated by the change in static force ΔF_s over the change in eccentricity Δe_y evaluated at a steady state condition. This value offers a base to compare the dynamic measured stiffness values in the loaded direction, K_{yy}.

$$K_{STATIC} = \left(\frac{\partial F_s}{\partial e_y}\right)_{SS} \approx \left(\frac{\Delta F_s}{\Delta e_y}\right)_{SS} \tag{12}$$

Dynamic Characteristics

Parameter Identification Model

Rotordynamic coefficients are extracted from the measured dynamic data through the parameter identification model described by Childs and Hale [21] and Rouvas and Childs [33]. To start, the equation of motion for the stator mass M_s can be written by applying Newtons's Second Law in the x and y directions, as shown in Eq. (13).

$$M_s\begin{bmatrix}\ddot{x}_s \\ \ddot{y}_s\end{bmatrix} = \begin{bmatrix}f_x \\ f_y\end{bmatrix} - \begin{bmatrix}f_{bx} \\ f_{by}\end{bmatrix} \tag{13}$$

In Eq. (13), $\ddot{x}_s$ and $\ddot{y}_s$ are the absolute stator accelerations, f_x and f_y are the excitation forces, and f_{bx} and f_{by} are the bearing reaction forces. Applying a [K][C][M] model, the bearing reaction forces are written in terms of the rotordynamic coefficients through previously given Eq. (2). The model is rewritten below for clarity.

$$-\begin{bmatrix} f_{bx} \\ f_{by} \end{bmatrix} = \begin{bmatrix} K_{xx} & K_{xy} \\ K_{yx} & K_{yy} \end{bmatrix} \begin{bmatrix} \Delta x \\ \Delta y \end{bmatrix} + \begin{bmatrix} C_{xx} & C_{xy} \\ C_{yx} & C_{yy} \end{bmatrix} \begin{bmatrix} \Delta \dot{x} \\ \Delta \dot{y} \end{bmatrix} + \begin{bmatrix} M_{xx} & M_{xy} \\ M_{yx} & M_{yy} \end{bmatrix} \begin{bmatrix} \Delta \ddot{x} \\ \Delta \ddot{y} \end{bmatrix} \tag{2}$$

Substituting Eq. (2) into Eq. (13) and rearranging yields Eq. (14). The left side terms as well as the Δx and Δy terms are measured directly via instrumentation.

$$\begin{bmatrix} f_x - M_s \ddot{x}_s \\ f_y - M_s \ddot{y}_s \end{bmatrix} = -\begin{bmatrix} K_{xx} & K_{xy} \\ K_{yx} & K_{yy} \end{bmatrix} \begin{bmatrix} \Delta x \\ \Delta y \end{bmatrix} - \begin{bmatrix} C_{xx} & C_{xy} \\ C_{yx} & C_{yy} \end{bmatrix} \begin{bmatrix} \Delta \dot{x} \\ \Delta \dot{y} \end{bmatrix} - \begin{bmatrix} M_{xx} & M_{xy} \\ M_{yx} & M_{yy} \end{bmatrix} \begin{bmatrix} \Delta \ddot{x} \\ \Delta \ddot{y} \end{bmatrix} \tag{14}$$

Extracting rotordynamic coefficients occurs in the frequency domain and requires performing a fast Fourier transform (FFT) on Eq. (14), yielding:

$$\begin{bmatrix} \boldsymbol{F_x} - M_s \boldsymbol{A_x} \\ \boldsymbol{F_y} - M_s \boldsymbol{A_y} \end{bmatrix} = -\begin{bmatrix} \boldsymbol{H_{xx}} & \boldsymbol{H_{xy}} \\ \boldsymbol{H_{yx}} & \boldsymbol{H_{yy}} \end{bmatrix} \begin{bmatrix} \boldsymbol{D_x} \\ \boldsymbol{D_y} \end{bmatrix} \tag{15}$$

The parameters $\boldsymbol{F_i}$, $\boldsymbol{A_i}$, and $\boldsymbol{D_i}$ are the Fourier transforms of the excitation force, absolute stator acceleration, and the relative stator to rotor motion for the x and y directions. $\boldsymbol{H_{ij}}$ is the complex dynamic stiffness that relates a force in the “i” direction in response to a motion in the “j” direction. These dynamic stiffness functions are written in terms of the rotordynamic coefficients, shown below in Eq. (16).

$$\boldsymbol{H_{ij}} = K_{ij} - \Omega^2 M_{ij} + \boldsymbol{j}(\Omega C_{ij}) \tag{16}$$

Taking the real and imaginary components of the dynamic stiffness yields:

$$\mathrm{Re}(\boldsymbol{H_{ij}}) = K_{ij} - \Omega^2 M_{ij} \tag{17}$$

$$\mathrm{Im}(\boldsymbol{H_{ij}}) = \Omega C_{ij} \tag{18}$$

Eq. (17) shows that the stiffness and added mass coefficients can be estimated by curve fitting the Re($\boldsymbol{H_{ij}}$) with a quadratic function of Ω. Estimates for the damping coefficients are obtained from the slope of the Im($\boldsymbol{H_{ij}}$) with respect to Ω.

Eq. (15) provides two equations for the four unknowns $\boldsymbol{H_{xx}}$, $\boldsymbol{H_{xy}}$, $\boldsymbol{H_{yx}}$, and $\boldsymbol{H_{yy}}$. Four equations are obtained by shaking the stator in the *x* and *y* directions while measuring the response in both directions, as shown in Eq. (19).

$$\begin{bmatrix} \boldsymbol{F_{xx}} - M_s\boldsymbol{A_{xx}} & \boldsymbol{F_{xy}} - M_s\boldsymbol{A_{xy}} \\ \boldsymbol{F_{yx}} - M_s\boldsymbol{A_{yx}} & \boldsymbol{F_{yy}} - M_s\boldsymbol{A_{yy}} \end{bmatrix} = -\begin{bmatrix} \boldsymbol{H_{xx}} & \boldsymbol{H_{xy}} \\ \boldsymbol{H_{yx}} & \boldsymbol{H_{yy}} \end{bmatrix}\begin{bmatrix} \boldsymbol{D_{xx}} & \boldsymbol{D_{xy}} \\ \boldsymbol{D_{yx}} & \boldsymbol{D_{yy}} \end{bmatrix} \tag{19}$$

Frequency-dependent dynamic stiffnesses ($\boldsymbol{H_{xx}}$, $\boldsymbol{H_{xy}}$, $\boldsymbol{H_{yx}}$, and $\boldsymbol{H_{yy}}$) for a single shake are obtained from 32 repeated excitations that are averaged in the frequency domain. For each experimental condition, 10 consecutive shakes are conducted in the *x* and *y* directions. This provides a total of 320 waveforms applied in each direction at each steady state test condition.

Theory of Baseline Dynamic Stiffness

The dynamic stiffness functions measured during a test accounts for the stiffness and damping of the bearing's fluid film, as well as any stiffness and damping from the pitch stabilizers, instrumentation, hoses, etc. To account for the dynamic stiffness of all the stator attachments, a baseline or *dry* dynamic test is performed at zero speed before any lubricating oil enters the bearing. We want to measure the dynamic stiffness of the stator attachments alone, without the effect of fluid inertia or dynamics. The baseline test involves the same excitations as those used during bearing testing with the exception of smaller excitation force amplitudes. Subtracting the baseline results from the dynamic stiffness measured during testing yields the dynamic stiffness of the fluid film only. Dynamic stiffness functions are typically an order of magnitude lower for the baseline test than for the fluid film.

Changing pads to obtain a different pivot offset for the test bearing required disassembly of the bearing stator, including all attachments. Even though the reassembly process is identical as possible for any bearing, a new baseline test is required because of the differences in the forces of the stator attachments. The pitch stabilizers and hoses provide slightly different amounts of stiffness and damping for each assembly. To account for any discrepancy from reassembly, separate baseline tests were conducted for the 50 and 60% offsets.

Curve Fitting and Uncertainty Analysis

The following outlines the curve fitting procedure used to estimate rotordynamic coefficients from the measured complex dynamic stiffneses. The test data used in this section was taken with the 50% pivot offset at high speed and lowest load case.

Recall that 10 individual shakes are conducted in each orthogonal direction for a given test condition. An average dynamic stiffness $\boldsymbol{H}_{\boldsymbol{ij}}$ at each excitation frequency for each test condition is obtained from Eq. (20) with N is the number of shakes and $(\boldsymbol{h}_{\boldsymbol{ij}})_k$ is the dynamic stiffness of each individual shake.

$$\boldsymbol{H}_{\boldsymbol{ij}} = \frac{1}{N}\sum_{k=1}^{N}\left(\boldsymbol{h}_{\boldsymbol{ij}}\right)_k \tag{20}$$

Eq. (20) is used to obtain average dynamic stiffness at each excitation frequency for the baseline test and during bearing testing. The uncertainty of the each dynamic stiffness data point is defined as two times the standard deviation as shown in Eq. (21).

$$\Delta\boldsymbol{H}_{\boldsymbol{ij}} = 2\sigma_{\boldsymbol{H}_{ij}} = 2\sqrt{\frac{\sum_{k=1}^{N}\left(\left(\boldsymbol{h}_{\boldsymbol{ij}}\right)_k - \boldsymbol{H}_{\boldsymbol{ij}}\right)^2}{N-1}} \tag{21}$$

The above equation is used to calculate uncertainties for the baseline dynamic stiffness and the test dynamic stiffness.

The dynamic stiffness of the fluid film is found by subtracting the baseline data from that obtained during testing, shown below in Eq. (22). Unless stated otherwise, $\boldsymbol{H_{ij}}$ denotes the dynamic stiffness of the fluid film only throughout this thesis.

$$\boldsymbol{H_{ij}} = \boldsymbol{H_{ij,TEST}} - \boldsymbol{H_{ij,BASE}} \tag{22}$$

In Eq. (22), the test and baseline dynamic stiffnesses are calculated from Eq. (20). The uncertainty of the fluid film dynamic stiffness depends on the uncertainty of the baseline and test dynamic stiffness, as shown in Eq. (23).

$$\Delta\boldsymbol{H_{ij}} = \sqrt{\left(\Delta\boldsymbol{H_{ij,TEST}}\right)^2 + \left(\Delta\boldsymbol{H_{ij,BASE}}\right)^2} \tag{23}$$

The uncertainty of the test and baseline dynamic stiffnesses in Eq. (23) are calculated as previously described with Eq. (21). The uncertainty of the dynamic stiffness $\Delta\boldsymbol{H_{ij}}$ quantifies the repeatability of the shake tests. These uncertainties are presented as error bars in the dynamic stiffness plots.

As shown previously in Eq. (17), the frequency independent stiffness K_{ij} and added-mass M_{ij} coefficients are related to the real part of the dynamic stiffness $\boldsymbol{H_{ij}}$ through a quadratic function of excitation frequency Ω. K_{ij} represents the zero-frequency intercept and M_{ij} denotes the curvature of Re($\boldsymbol{H_{ij}}$) with respect to Ω. By setting $\Omega^2 = \Lambda$, the Re($\boldsymbol{H_{ij}}$) becomes a linear function of Λ where K_{ij} is the intercept and M_{ij} is the negated slope, as shown below in Eq. (24).

$$\mathrm{Re}(\boldsymbol{H_{ij}}) = K_{ij} - \Lambda M_{ij} = K_{ij} + \Lambda\left(-M_{ij}\right) \tag{24}$$

K_{ij} and M_{ij} are determined from a least squares linear regression in the form of Eq. (25) that is applied to Re($\boldsymbol{H_{ij}}$) versus Λ data. Here, x and y represent the independent and dependent variables respectively.

$$y = mx + b \tag{25}$$

The *y*-intercept *m* and slope *b* of the linear regression Eq. (25) are given below in Eqs. (26) and (27).

$$m = \frac{n\sum_{k=1}^{n} x_k y_k - \sum_{k=1}^{n} x_k \sum_{k=1}^{n} y_k}{n\sum_{k=1}^{n} x_k^2 - \left(\sum_{k=1}^{n} x_k\right)^2} \tag{26}$$

$$b = \left(\frac{1}{n}\sum_{k=1}^{n} x_k\right) - m\left(\frac{1}{n}\sum_{k=1}^{n} y_k\right) \tag{27}$$

In the above equations, x_k and y_k represent the data points that are fitted and *n* is the number of data point pairs.

When applying this regression of the Re($\boldsymbol{H_{ij}}$) versus Λ data, the intercept *b* is equal to the stiffness coefficient K_{ij}, while the slope *m* is equal to the opposite sign of the added mass coefficient M_{ij}. This linear regression is used to estimate both direct and cross-coupled stiffness and added mass coefficients. Figure 14 provides an example of using linear regression to obtain K_{xx} and M_{xx} from the Re($\boldsymbol{H_{xx}}$) data obtained with the 50% offset at 16 krpm and zero load. Note the dynamic stiffness error bars represent the repeatability between shake tests that was described previously.

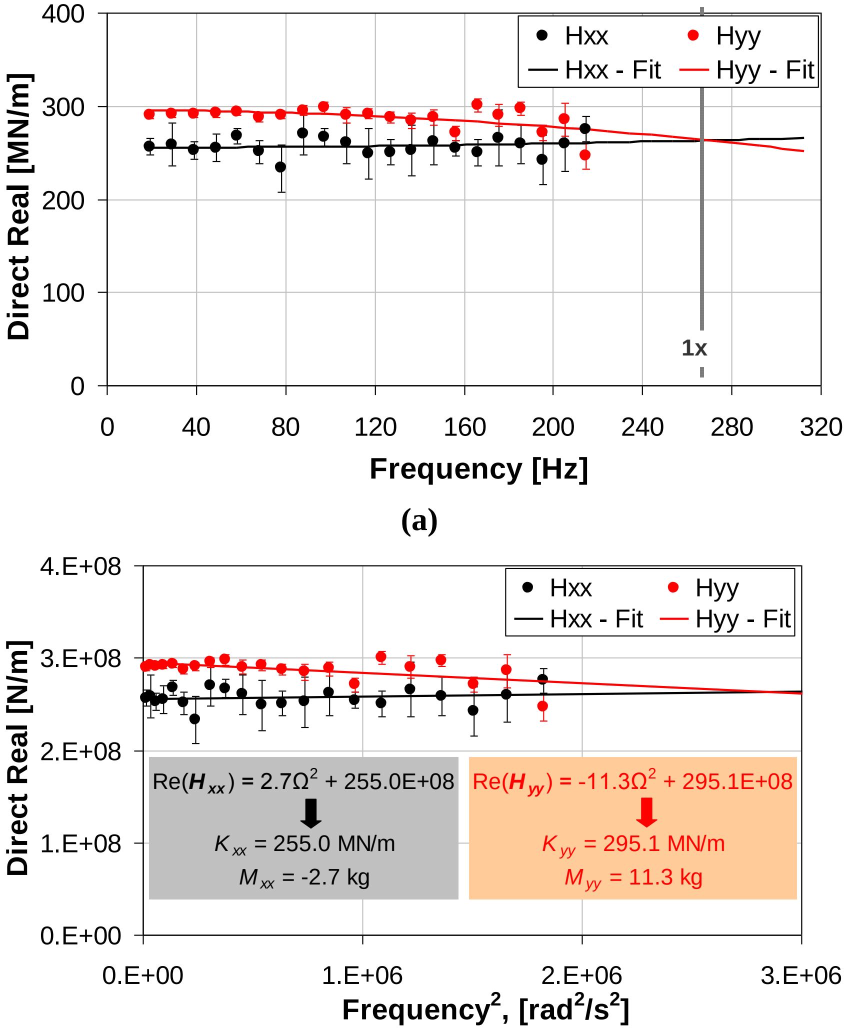

(a)

(b)

Figure 14. The direct real part of the dynamic stiffness for the 50% offset at 16 krpm and zero load plotted versus: (a) frequency, (b) frequency squared.

Figure 14 (a) shows the quadratic nature of Re($\boldsymbol{H}_{xx}$) when plotted versus Ω. As seen in Figure 14 (b), the regression provides the estimates for the direct stiffness coefficients, K_{xx} = 255.0 MN/m and K_{yy} = 295.1 MN/m. Additionally, the slopes from this regression provide the direct added-mass coefficients, M_{xx} = -2.7 kg and M_{yy} = 11.3 kg. The Re($\boldsymbol{H}_{xx}$) increases slightly with respect to Ω, producing a small negative M_{xx} while M_{yy} is positive because Re($\boldsymbol{H}_{yy}$) decreased with increasing Ω.

If the real part of the dynamic stiffness $\boldsymbol{H}_{ij}$ did not fit a quadratic function with excitation frequency, an added-mass coefficient could not be used to capture the frequency dependency of the stiffness. Therefore, frequency-dependent stiffness coefficients $K_{ij}(\Omega)$ would have to be reported.

The frequency independent damping coefficient C_{ij} is related to the imaginary part of the dynamic stiffness $\boldsymbol{H}_{ij}$ through a linear function of excitation frequency Ω, as shown previously in Eq. (18). By applying a least squares linear regression described above in Eq. (25), C_{ij} is equal to the slope *m* given in Eq. (26). The intercept *b* of the linear regression has no physical meaning and is therefore not reported. As before, this damping approximation can be applied to direct or cross-coupled coefficients.

Figure 15 provides an example of using linear regression obtain C_{xx} from the Im($\boldsymbol{H}_{xx}$) obtained with the 50% offset at 16 krpm and zero load.

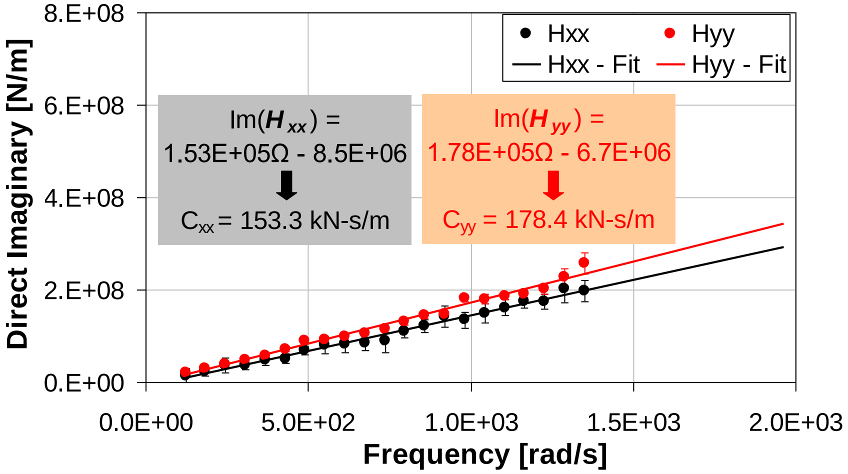

Figure 15. Fitting the imaginary part of the dynamic stiffness.

As seen in Figure 15, the linear regression produces a direct damping estimates of C_{xx} = 153.3 kN-s/m and C_{yy} = 178.4 kN-s/m. If the imaginary part of the dynamic stiffness $\boldsymbol{H}_{ij}$ was not a linear function with respect to excitation frequency, frequency-dependent damping coefficients $C_{ij}(\Omega)$ would be reported. $C_{ij}(\Omega)$ is equal to the derivative or slope of the Im($\boldsymbol{H}_{ij}$) for a given Ω.

The uncertainties of the stiffness, damping and added-mass coefficients are determined by the correlation of the linear regressions with the dynamic stiffness data. Note that the uncertainty of the rotordyanmic coefficients is different than the uncertainty of the dynamic stiffness.

The final coefficient uncertainty equations are functions of the mean square error (MSE), and the quantity S_{xx}, given below in Eqs. (28) and (29) respectively.

$$\hat{\sigma}^2 = \frac{\sum_{k=1}^{n} \left(y_k - \hat{y}_k \right)^2}{n-2} \tag{28}$$

$$S_{xx} = \sum_{k=1}^{N} \left(x_k^2 - \overline{x}_k^2 \right) \tag{29}$$

In Eq. (28), $\hat{y}_k$ represents the dependent variable fit data. As before, x and y represent the independent and dependent variables respectively. The uncertainties of the slope m and intercept b are calculated using Eqs. (30) and (31).

$$\Delta m = t \sqrt{\frac{\hat{\sigma}^2}{S_{xx}}} \tag{30}$$

$$\Delta b = t \sqrt{\hat{\sigma}^2 \left(\frac{1}{n} + \frac{\overline{x}^2}{S_{xx}} \right)} \tag{31}$$

The statistical variable t is a function of the confidence interval and number of fitted data points n. For a large number of data points and a 95% confidence interval, $t = 1.96$.

Since the stiffness coefficients were determined from the intercept of a linear regression, Eq. (31) is used to calculate the associated uncertainties. Added-mass and damping coefficients are the slopes of linear regressions and require Eq. (30) to calculate the respective uncertainties.

A summary of the rotordynamic coefficients and uncertainties for the 50% offset bearing at 16 krpm and zero load are provided below in Table 7.

Table 7. Experimental rotordynamic coefficients for the 50% offset at 16 krpm and zero load.

Units	Coefficient	Value	Uncert.	% Uncert.
MN/m	*Kxx*	255.0	6.6	2.6
	Kxy	-1.4	2.5	175.3
	Kyx	72.9	7.5	10.3
	Kyy	295.1	6.8	2.3
kN-s/m	*Cxx*	153.3	7.6	5.0
	Cxy	45.0	3.5	7.8
	Cyx	6.4	11.7	183.0
	Cyy	178.4	9.8	5.5
MN/m	*Mxx*	-2.7	7.5	275.7
	Mxy	-1.0	2.9	284.3
	Myx	15.4	8.5	55.6
	Myy	11.3	7.7	68.4

These coefficient uncertainties presented in Table 7 are representative of the majority of the test results. Note that large percent uncertainties occur where the coefficient values are small, such as for the cross-coupled coefficients.

Predictions: XLTPFBrg

All predictions given in this thesis were obtained from XLTFPBrg, a bearing code developed by Dr. San Andres [34] at the Texas A&M Turbomachinery Laboratory that is part of the XLTRC^2 Rotordynamics Suite. This program predicts the static and dynamic response, including 2x2 stiffness and damping matrices, of tilting-pad, flexure-pivot, and fixed-arc bearings. The user can choose to apply a CFD algorithm to solve bulk-flow Navier Stokes equations or a Reynolds Equation solver. The code also uses a thermo-hydrodynamic model to account for heat transfer and temperature conditions. This program does not account for pivot-support flexibility or backup-structure stiffness. The following offers a brief discussion on the solution methods, major assumptions, and input/output parameters of XLTFPBrg.

Fluid Inertia

Fluid film lubrication is governed by the Navier Stokes equations that include the continuity equation and three momentum equations: circumferential, axial, and cross-film. By assuming fluid inertia effects are negligible, the convective and temporal acceleration terms can be ignored. This yields the Reynolds equation of classical lubrication theory, a 2nd order partial differential equation that is much simpler to solve. Since XLTFPBrg has the option to use a Reynolds equation solution, it is important to determine if neglecting fluid inertia is valid. Reynolds numbers denotes the ratio of fluid inertia to viscous shear forces and can give insight as to whether fluid-inertia effects should be accounted for. The shear Reynolds number for a journal bearing is

$$Re = \frac{\rho C_b R_s \omega}{\mu} . \tag{32}$$

The modified shear Reynolds number Re_* for a journal bearing is defined in Eq. (33).

$$Re_* = Re\left(C_b \big/ R_s \right) \tag{33}$$

The squeeze Reynolds number Re_s represents the ratio between temporal fluid inertia forces due to transient motions and viscous-shear forces and is given in Eq. (34).

$$Re_s = \frac{\rho C_b^2 \omega^*}{\mu} \tag{34}$$

In Eq. (34), ω^* represents the maximum excitation frequency, which is on the order of 320 Hz for the given tests.

Reynolds numbers and modified Reynolds numbers for the test bearing are provided below in Table 8 and Table 9 respectively. These Reynolds numbers were calculated using Eq. (32) where ρ and μ for the oil were obtained by applying Eqs. (5) and (6) with the measured oil outlet temperatures. The outlet temperature provides an approximation of an average bearing temperature.

Table 8. Maximum Reynolds numbers for each nominal rotor speed.

Rotor Speed [rpm]	**7000**	**10000**	**13000**	**16000**
50% Offset Max. *Re* Numbers	187	309	408	553
60% Offset Max. *Re* Numbers	168	287	392	559

Table 9. Maximum modified and squeeze Reynolds numbers for each nominal rotor speed.

Rotor Speed [rpm]	7000	10000	13000	16000
50% Offset Max. Re_*	0.30	0.49	0.65	0.88
60% Offset Max. Re_*	0.28	0.47	0.65	0.92
50% Offset Max. Re_s	0.82	0.95	0.96	1.06
60% Offset Max. Re_s	0.76	0.91	0.95	1.11

Generally, fluid inertia effects can be considered important when $Re_* > 1$ and $Re_s > 1$ [35]. FromTable 9, all of the Re_* and Re_s for the test bearing meet this criteria except at 16 krpm, where Re_s values are slightly above 1. This suggests that fluid inertia can be ignored for the majority of the test conditions. In contrast, Reinhardt and Lund [36] reported that bearings with Reynolds numbers as low as 10^2 can have inertial effects where the Reynolds Equation may not be adequate.

Since the assumption to neglect fluid inertia may be debated, predictions were conducted at all test conditions using both the bulk-flow NS analysis and Reynolds equation. The static predictions did not change with solution the solution method. Overall, rotordynamic coefficient predictions only changed at higher excitation frequencies when ignoring fluid inertia, similar to the work of Rodriguez [37]. All predictions given in this thesis were calculated using the code's bulk-flow NS option.

Code Parameters and Options

XLTFPBrg uses a Microsoft Excel interface for the input parameters and outputting results. Figure 16 provides the input and output screen for XLTFPBrg.

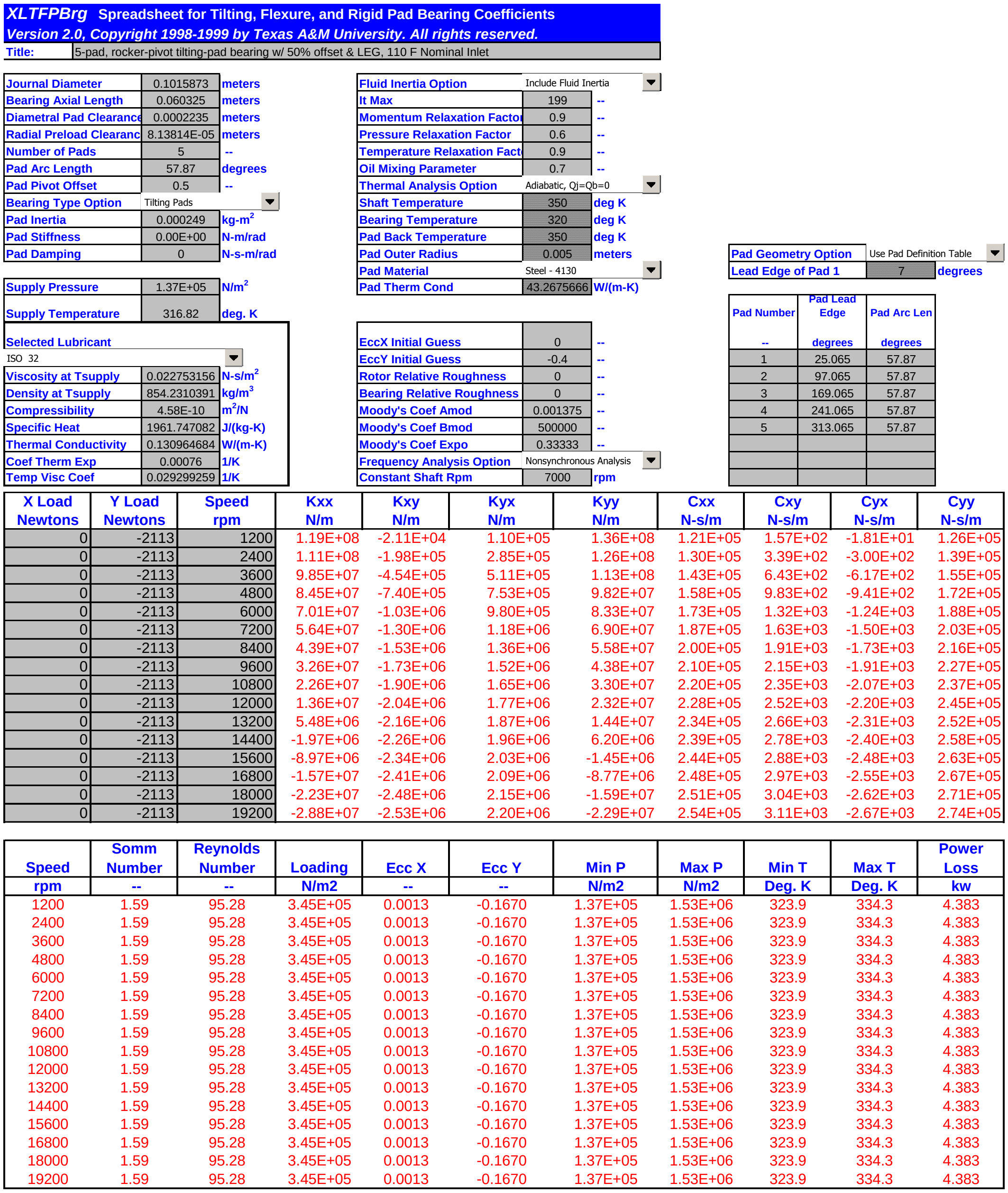

XLTFPBrg Spreadsheet for Tilting, Flexure, and Rigid Pad Bearing Coefficients

Version 2.0, Copyright 1998-1999 by Texas A&M University. All rights reserved.

Title: 5-pad, rocker-pivot tilting-pad bearing w/ 50% offset & LEG, 110 F Nominal Inlet

Journal Diameter	0.1015873	meters
Bearing Axial Length	0.060325	meters
Diametral Pad Clearance	0.0002235	meters
Radial Preload Clearanc	8.13814E-05	meters
Number of Pads	5	--
Pad Arc Length	57.87	degrees
Pad Pivot Offset	0.5	--
Bearing Type Option	Tilting Pads	
Pad Inertia	0.000249	kg-m^2
Pad Stiffness	0.00E+00	N-m/rad
Pad Damping	0	N-s-m/rad
Supply Pressure	1.37E+05	N/m^2
Supply Temperature	316.82	deg. K
Selected Lubricant	ISO 32	
Viscosity at Tsupply	0.022753156	N-s/m^2
Density at Tsupply	854.2310391	kg/m^3
Compressibility	4.58E-10	m^2/N
Specific Heat	1961.747082	J/(kg-K)
Thermal Conductivity	0.130964684	W/(m-K)
Coef Therm Exp	0.00076	1/K
Temp Visc Coef	0.029299259	1/K

Fluid Inertia Option	Include Fluid Inertia	
It Max	199	--
Momentum Relaxation Factor	0.9	--
Pressure Relaxation Factor	0.6	--
Temperature Relaxation Fact	0.9	--
Oil Mixing Parameter	0.7	--
Thermal Analysis Option	Adiabatic, Qj=Qb=0	
Shaft Temperature	350	deg K
Bearing Temperature	320	deg K
Pad Back Temperature	350	deg K
Pad Outer Radius	0.005	meters
Pad Material	Steel - 4130	
Pad Therm Cond	43.2675666	W/(m-K)
EccX Initial Guess	0	--
EccY Initial Guess	-0.4	--
Rotor Relative Roughness	0	--
Bearing Relative Roughness	0	--
Moody's Coef Amod	0.001375	--
Moody's Coef Bmod	500000	--
Moody's Coef Expo	0.33333	--
Frequency Analysis Option	Nonsynchronous Analysis	
Constant Shaft Rpm	7000	rpm

Pad Geometry Option	Use Pad Definition Table	
Lead Edge of Pad 1	7	degrees

Pad Number --	Pad Lead Edge degrees	Pad Arc Len degrees
1	25.065	57.87
2	97.065	57.87
3	169.065	57.87
4	241.065	57.87
5	313.065	57.87

X Load Newtons	Y Load Newtons	Speed rpm	Kxx N/m	Kxy N/m	Kyx N/m	Kyy N/m	Cxx N-s/m	Cxy N-s/m	Cyx N-s/m	Cyy N-s/m
0	-2113	1200	1.19E+08	-2.11E+04	1.10E+05	1.36E+08	1.21E+05	1.57E+02	-1.81E+01	1.26E+05
0	-2113	2400	1.11E+08	-1.98E+05	2.85E+05	1.26E+08	1.30E+05	3.39E+02	-3.00E+02	1.39E+05
0	-2113	3600	9.85E+07	-4.54E+05	5.11E+05	1.13E+08	1.43E+05	6.43E+02	-6.17E+02	1.55E+05
0	-2113	4800	8.45E+07	-7.40E+05	7.53E+05	9.82E+07	1.58E+05	9.83E+02	-9.41E+02	1.72E+05
0	-2113	6000	7.01E+07	-1.03E+06	9.80E+05	8.33E+07	1.73E+05	1.32E+03	-1.24E+03	1.88E+05
0	-2113	7200	5.64E+07	-1.30E+06	1.18E+06	6.90E+07	1.87E+05	1.63E+03	-1.50E+03	2.03E+05
0	-2113	8400	4.39E+07	-1.53E+06	1.36E+06	5.58E+07	2.00E+05	1.91E+03	-1.73E+03	2.16E+05
0	-2113	9600	3.26E+07	-1.73E+06	1.52E+06	4.38E+07	2.10E+05	2.15E+03	-1.91E+03	2.27E+05
0	-2113	10800	2.26E+07	-1.90E+06	1.65E+06	3.30E+07	2.20E+05	2.35E+03	-2.07E+03	2.37E+05
0	-2113	12000	1.36E+07	-2.04E+06	1.77E+06	2.32E+07	2.28E+05	2.52E+03	-2.20E+03	2.45E+05
0	-2113	13200	5.48E+06	-2.16E+06	1.87E+06	1.44E+07	2.34E+05	2.66E+03	-2.31E+03	2.52E+05
0	-2113	14400	-1.97E+06	-2.26E+06	1.96E+06	6.20E+06	2.39E+05	2.78E+03	-2.40E+03	2.58E+05
0	-2113	15600	-8.97E+06	-2.34E+06	2.03E+06	-1.45E+06	2.44E+05	2.88E+03	-2.48E+03	2.63E+05
0	-2113	16800	-1.57E+07	-2.41E+06	2.09E+06	-8.77E+06	2.48E+05	2.97E+03	-2.55E+03	2.67E+05
0	-2113	18000	-2.23E+07	-2.48E+06	2.15E+06	-1.59E+07	2.51E+05	3.04E+03	-2.62E+03	2.71E+05
0	-2113	19200	-2.88E+07	-2.53E+06	2.20E+06	-2.29E+07	2.54E+05	3.11E+03	-2.67E+03	2.74E+05

Speed rpm	Somm Number --	Reynolds Number --	Loading N/m2	Ecc X --	Ecc Y --	Min P N/m2	Max P N/m2	Min T Deg. K	Max T Deg. K	Power Loss kw
1200	1.59	95.28	3.45E+05	0.0013	-0.1670	1.37E+05	1.53E+06	323.9	334.3	4.383
2400	1.59	95.28	3.45E+05	0.0013	-0.1670	1.37E+05	1.53E+06	323.9	334.3	4.383
3600	1.59	95.28	3.45E+05	0.0013	-0.1670	1.37E+05	1.53E+06	323.9	334.3	4.383
4800	1.59	95.28	3.45E+05	0.0013	-0.1670	1.37E+05	1.53E+06	323.9	334.3	4.383
6000	1.59	95.28	3.45E+05	0.0013	-0.1670	1.37E+05	1.53E+06	323.9	334.3	4.383
7200	1.59	95.28	3.45E+05	0.0013	-0.1670	1.37E+05	1.53E+06	323.9	334.3	4.383
8400	1.59	95.28	3.45E+05	0.0013	-0.1670	1.37E+05	1.53E+06	323.9	334.3	4.383
9600	1.59	95.28	3.45E+05	0.0013	-0.1670	1.37E+05	1.53E+06	323.9	334.3	4.383
10800	1.59	95.28	3.45E+05	0.0013	-0.1670	1.37E+05	1.53E+06	323.9	334.3	4.383
12000	1.59	95.28	3.45E+05	0.0013	-0.1670	1.37E+05	1.53E+06	323.9	334.3	4.383
13200	1.59	95.28	3.45E+05	0.0013	-0.1670	1.37E+05	1.53E+06	323.9	334.3	4.383
14400	1.59	95.28	3.45E+05	0.0013	-0.1670	1.37E+05	1.53E+06	323.9	334.3	4.383
15600	1.59	95.28	3.45E+05	0.0013	-0.1670	1.37E+05	1.53E+06	323.9	334.3	4.383
16800	1.59	95.28	3.45E+05	0.0013	-0.1670	1.37E+05	1.53E+06	323.9	334.3	4.383
18000	1.59	95.28	3.45E+05	0.0013	-0.1670	1.37E+05	1.53E+06	323.9	334.3	4.383
19200	1.59	95.28	3.45E+05	0.0013	-0.1670	1.37E+05	1.53E+06	323.9	334.3	4.383

Figure 16. XLTFPBrg input and output screen.

As seen above, the input parameters include bearing geometry and operating conditions. Note the average bearing clearance was used since the code only allows for one bearing clearance. Where possible, the measured test conditions were used, including the oil inlet pressure and temperature. The lubricant properties are calculated automatically from the lubricant type and inlet temperature. The main analysis options are listed and discussed below.

(1) Fluid Inertia Option: The code can account for fluid inertia by using a bulk-flow NS analysis, or ignore fluid inertia by applying a Reynolds equation. As discussed previously, predictions were obtained using both options, showing discrepancies only at higher excitation frequencies. All results presented in this thesis were obtained from a bulk-flow NS analysis.

(2) Frequency Analysis Option: This option determines what processional or excitation frequency is used. The synchronous analysis predicts data only at running speed while the non-synchronous option allows for the input of a range of excitation frequencies. The multi-frequency option was used to obtain predictions over the test frequency range (0 - 320 Hz).

(3) Thermal Analysis Option: The code offers a variety of temperature options including adiabatic and isothermal models. Since neither assumption occurs during operation, both options were applied and compared to test data. Other thermal analysis options required knowledge of temperatures that could not be measured and were not considered. Appendix F compares the isothermal and adiabatic analysis options. The rotordynamic coefficients predicted with the adiabatic option agreed much better with measured data, and therefore all predictions were made with the adiabatic option.

The output is presented in tabular form as seen in the lower half of Figure 16. The output provides stiffness and damping coefficients as well as static parameters. Since the code only produces stiffness and damping coefficients, added-mass terms are obtained by curve fitting the stiffness coefficients as described previously.

Post Processing

The coordinate system of XLTFPBrg is different from the coordinates on the test rig, as seen below in Figure 17.

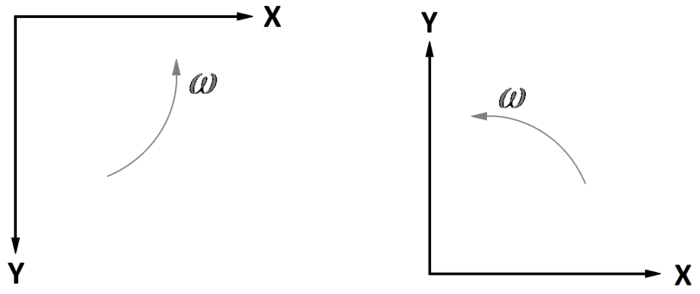

(a) **(b)**

Figure 17. Coordinate systems of: (a) test rig NDE, (b) XLTFPBrg.

Comparing predicted and experimental rotordynamic coefficients requires a single coordinate system. Using a coordinate transformation described by Al-Ghasem [2], the predicted coefficients are expressed in terms of the test rig coordinates, as seen in Eq. (35).

$$\begin{bmatrix} K_{xx} & K_{xy} \\ K_{yx} & K_{yy} \end{bmatrix} = \begin{bmatrix} \tilde{K}_{xx} & -\tilde{K}_{xy} \\ -\tilde{K}_{yx} & \tilde{K}_{yy} \end{bmatrix}, \quad \begin{bmatrix} C_{xx} & C_{xy} \\ C_{yx} & C_{yy} \end{bmatrix} = \begin{bmatrix} \tilde{C}_{xx} & -\tilde{C}_{xy} \\ -\tilde{C}_{yx} & \tilde{C}_{yy} \end{bmatrix} \tag{35}$$

In Eq. (35), the left-hand matrices represent the predicted coefficients in the test rig coordinate system while $\tilde{K}_{xx}$, $\tilde{K}_{xy}$, $\tilde{K}_{yx}$, $\tilde{K}_{yy}$, $\tilde{C}_{xx}$, $\tilde{C}_{xy}$, $\tilde{C}_{yx}$, and $\tilde{C}_{yy}$ represent the rotordynamic coefficients from XLTFPBrg. Note the direct coefficients remain unchanged and the cross-coupled coefficients change only by sign.

STATIC RESULTS

Clearance

Measured and fitted cold clearance plots for both 50 and 60% offset bearing configurations are provided below in Figure 18. The reported bearing clearance is the average cold clearance from six individual clearance measurements. The bearing clearances have been given previously in Table 4. Both bearing configurations have very similar clearances, but the 60% bearing clearance exhibits more non-symmetry.

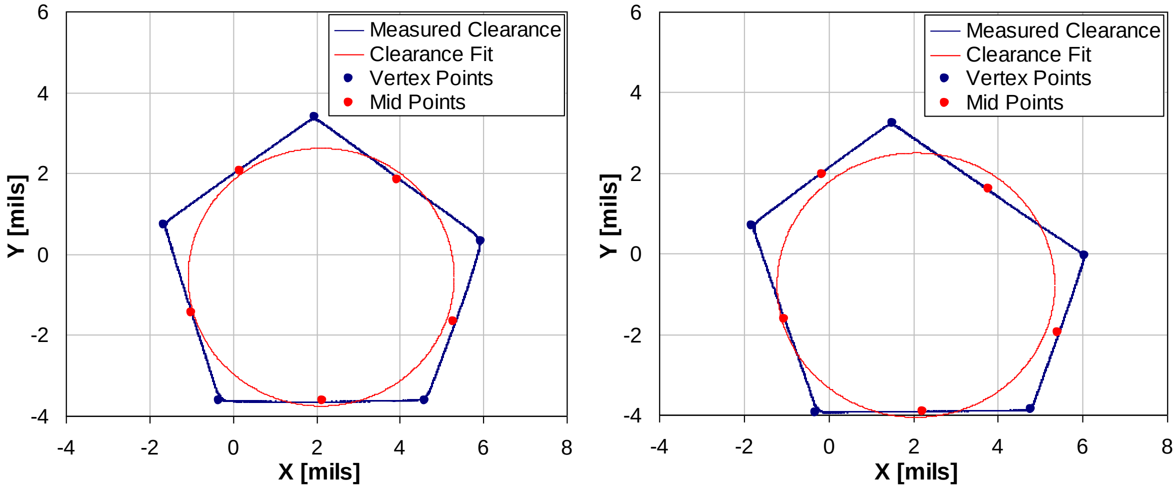

(a) (b)

Figure 18. Measured and fitted cold clearance plots for (a) 50% offset, (b) 60% offset.

Eccentricity and Attitude Angle

The following section provides measured and predicted loci plots organized by test speeds for each bearing offset. Each data point on a loci plot represents a static unit load condition. The data point near the origin represents the zero load case while the farthest displaced point represents the 3101 kPa load case.

Figure 19 provides the loci plots for the 50% offset. For low speeds, the eccentricity is predicted well at light unit loads but significantly over predicted at high loads. At higher speeds, eccentricity predictions match better with experimental data. Overall, the predictions correlate better with test results with increasing speed. As seen by the deviation from the loaded *y* axis in the above plots, unpredicted cross-coupling becomes more significant at higher running speeds.

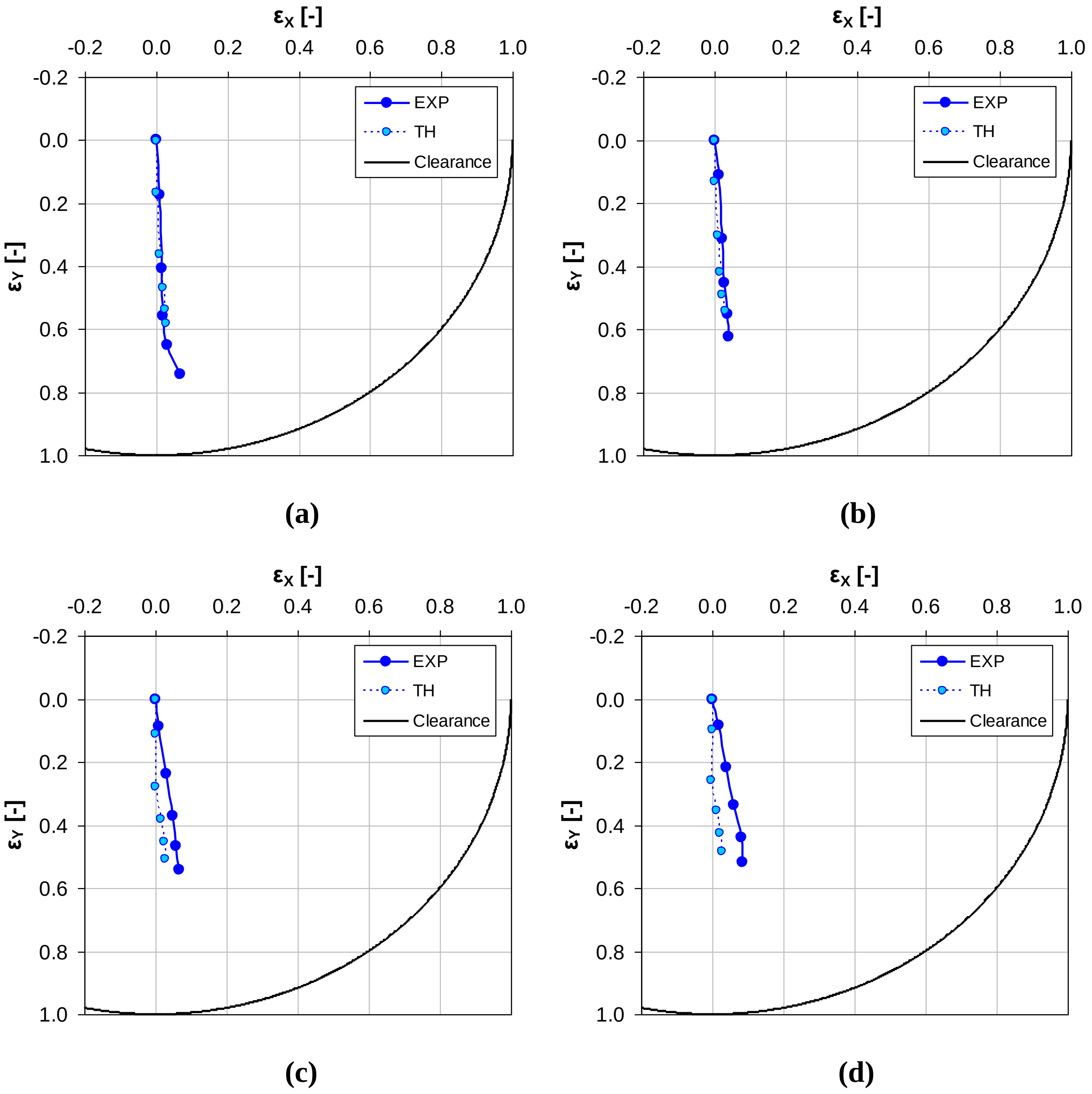

(a) (b) (c) (d)

Figure 19. 50% offset bearing loci at (a) 7 krpm, (b) 10 krpm, (c) 13 krpm, and (d) 16 krpm.

The 60% offset loci plots are presented in Figure 20. The same general trends between experimental results and theory for the 50% offset configuration also apply for the 60% offset. Generally, the predictions for the 60% offset show lower correlation between test data and predictions than the 50% offset.

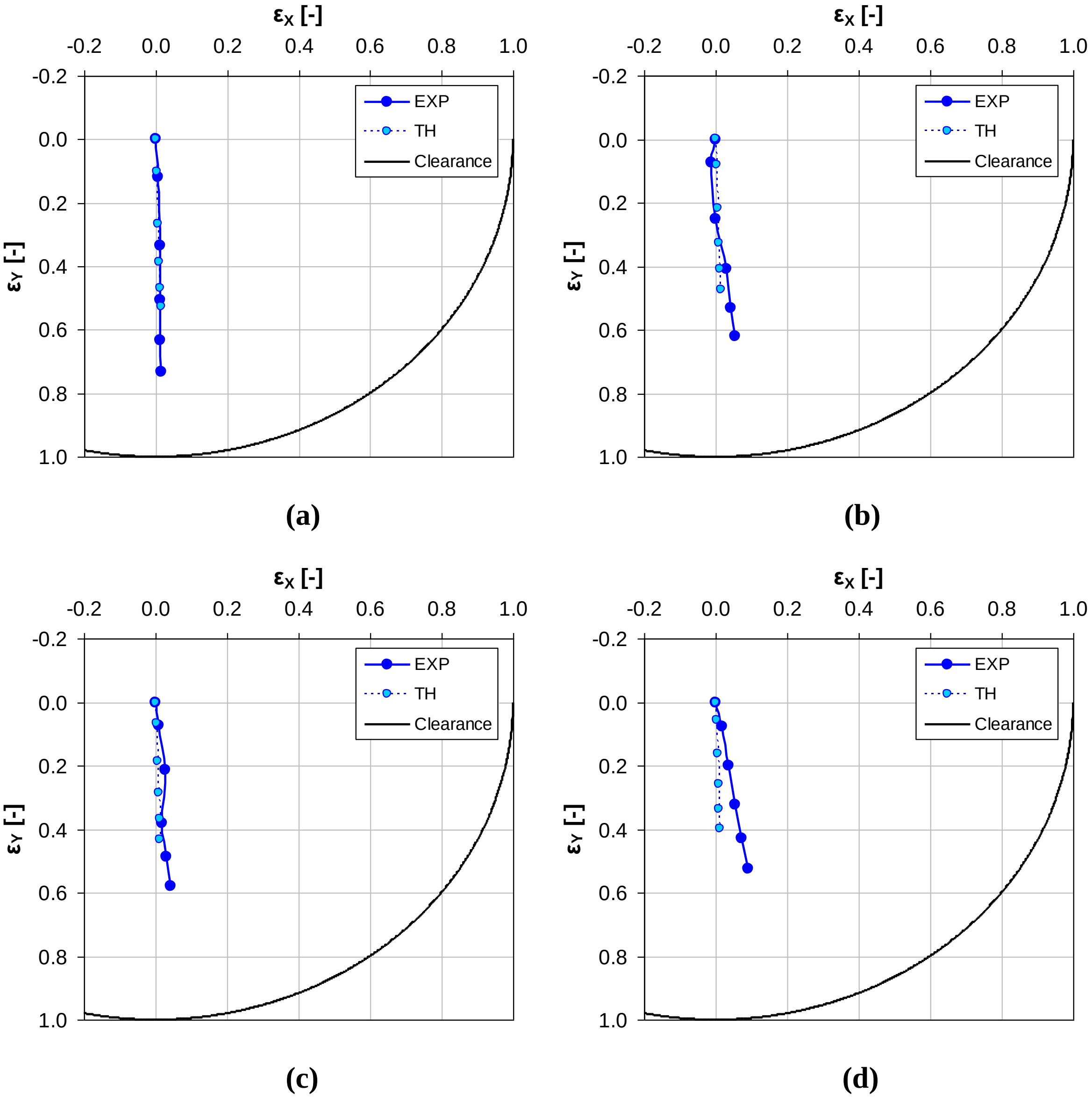

(a) (b)

(c) (d)

Figure 20. 60% offset bearing loci at (a) 7 krpm, (b) 10 krpm, (c) 13 krpm, and (d) 16 krpm.

The 50 and 60% offset have comparable loci plots, as seen below in Figure 21. These results show that the pivot offset has a small effect on the eccentricity or attitude angle.

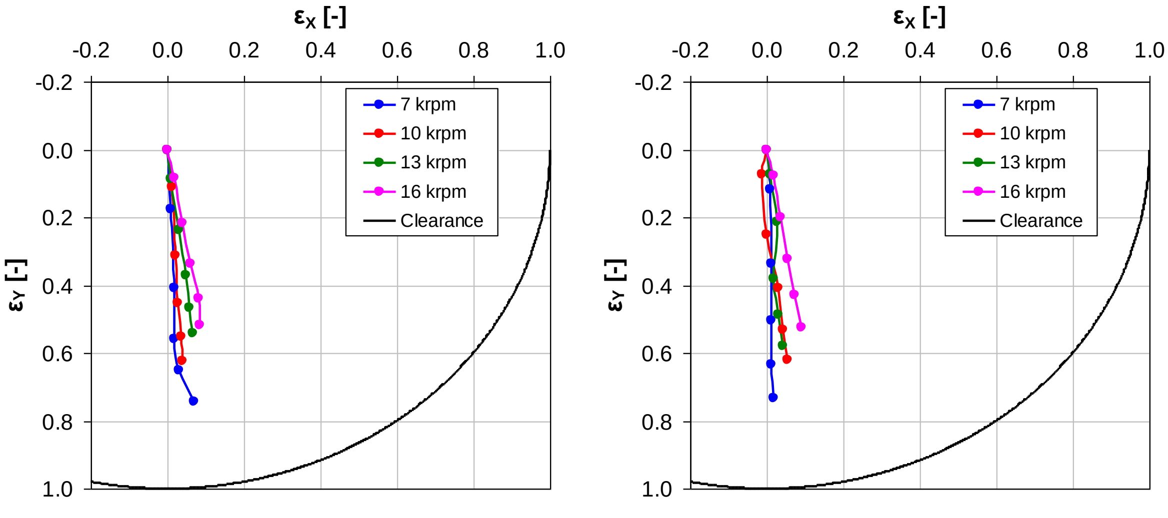

(a) **(b)**

Figure 21. Combined loci plots for (a) 50% offset, (b) 60% offset.

The measured and predicted attitude angles for the 50 and 60% offsets are presented below in Figure 22. The measured attitude angle increases with ω and becomes constant at higher unit loads while the predicted attitude angle is nearly zero for both offsets. Attitude angle predictions agree more with measurements for the lower speeds. The maximum attitude angle for both offsets occurs at the light load condition at 16 krpm. For higher loaded conditions, the maximum observed attitude angle is about 10°.

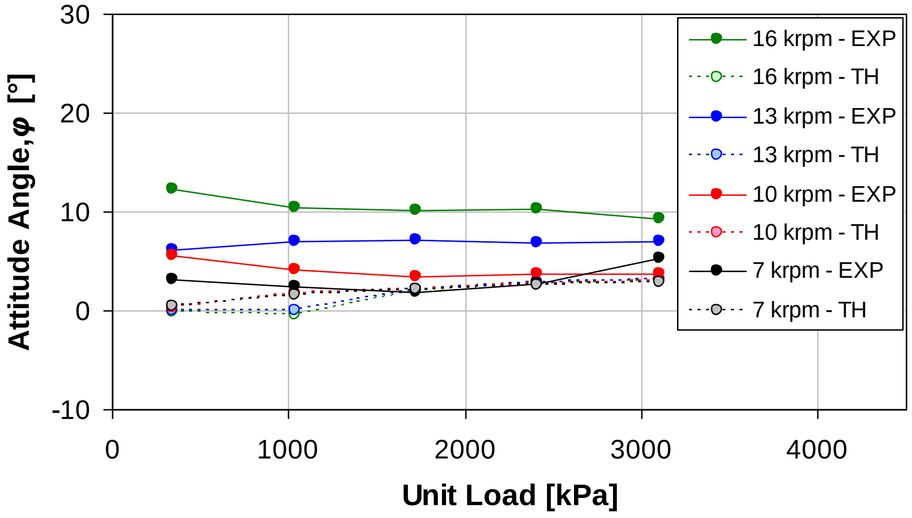

(a)

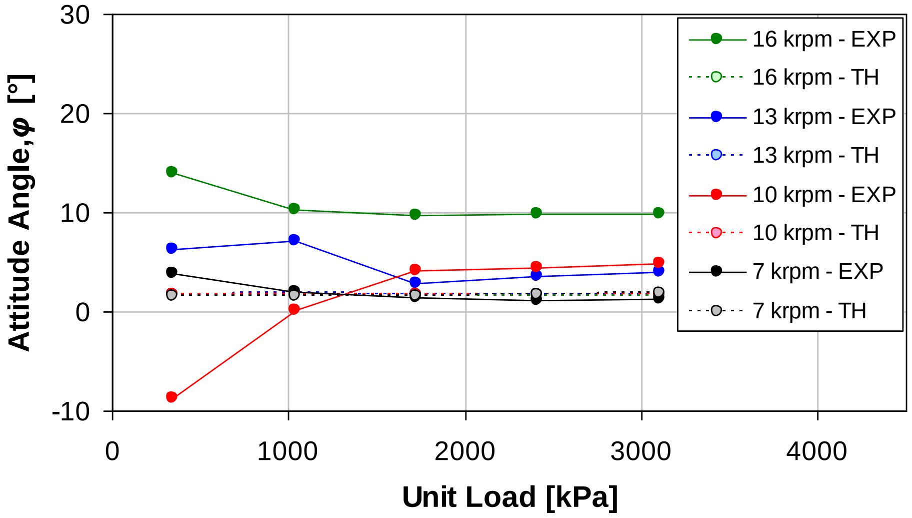

(b)

Figure 22. Measured and predicted attitude angle for (a) 50% offset, (b) 60% offset.

Pad Metal Temperatures

Pad metal temperatures are measured with thermocouples that are embedded in the pads just below the surface of the pad. These measurements provide an idea of the temperatures at the pad contact surface. The 60% offset pads were not embedded with thermocouples, and therefore pad temperatures are only reported for the 50% offset pads. Figure 23 shows the circumferential locations for each of the 20 thermocouples. The thermocouples at 56°, 128°, and 200° are located on a larger radius. All thermocouples are centered axially along the pad length. The loaded pads are identified as pad 1 and pad 2. All pad temperature data are given in Appendix C.

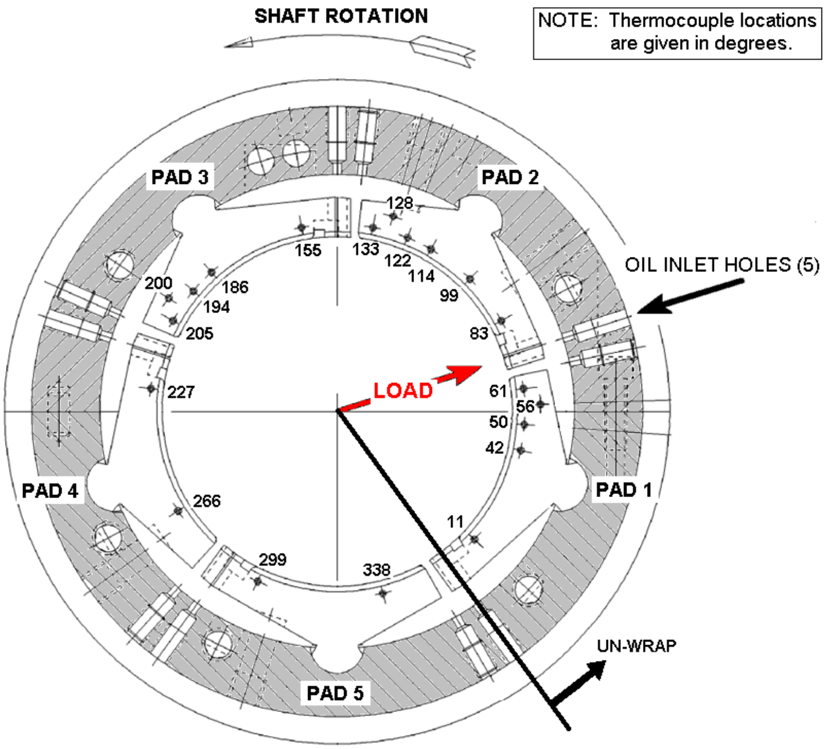

Figure 23. 50% offset pad thermocouple diagram.

Pad temperatures at 16 krpm for the various unit loads are provided below in Figure 24. This profile shows that the temperatures of loaded pads, 1 and 2, increase with increasing unit load while the unloaded pad 4 temperature decreases. Pads 3 and 5 provide support mainly in the unloaded direction, and have temperatures that show negligible change with unit load. For most of the pads, the highest measured temperature occurs near the trailing edge, with the exception of pad 2 where the maximum temperature occurs approximately 75% along pad 2. The trends observed in Figure 24 are representative of all other test speeds.

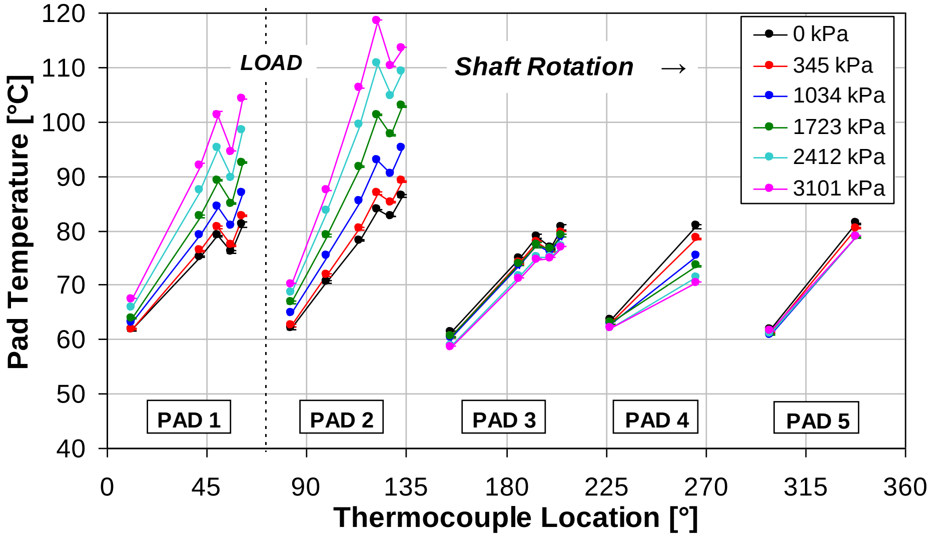

Figure 24. Pad metal temperatures for 50% offset bearing at 16 krpm.

Figure 25 presents pad temperatures for the full load condition of 3101 kPa at the different test speeds. The loaded pads experience higher temperatures, but all pad temperatures increase with speed, regardless of location. Similar to Figure 24 above, the maximum temperature occurs approximately 75% along pad 2. This trend is also seen for the other unit loads tested.

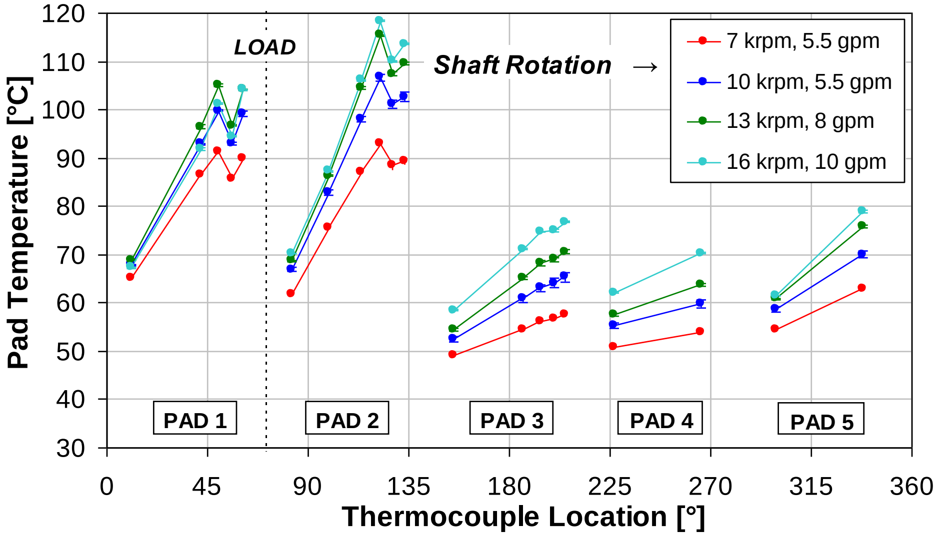

Figure 25. Pad metal temperatures for 50% offset bearing at 3101 kPa.

The overall maximum pad temperatures are compared with the predicted maximum bearing temperature in Figure 26. The maximum pad temperatures were measured at the 122° location, approximately 75% along the circumferential length of pad 2. The maximum temperature is consistently under predicted by about 15 to 20 °C. The trend of increasing temperature with respect to increasing load and speed is modeled well.

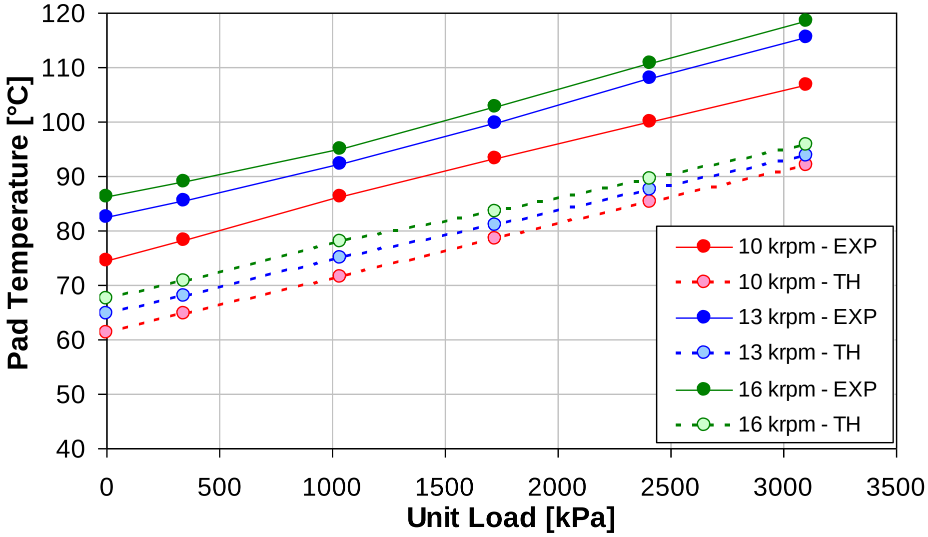

Figure 26. Predicted and measured maximum bearing temperatures for 50% offset.

Estimated Power Loss

Figure 27 provides the predicted and estimated power loss for both the 50 and 60% offsets. Generally, the power loss predictions are considerably lower than the power loss estimated from the measurements. The powerloss is modeled well only at 10 krpm for the 60% offset. The code predicts that power loss increases with increasing ω but is mostly independent from unit load, agreeing with measurements.

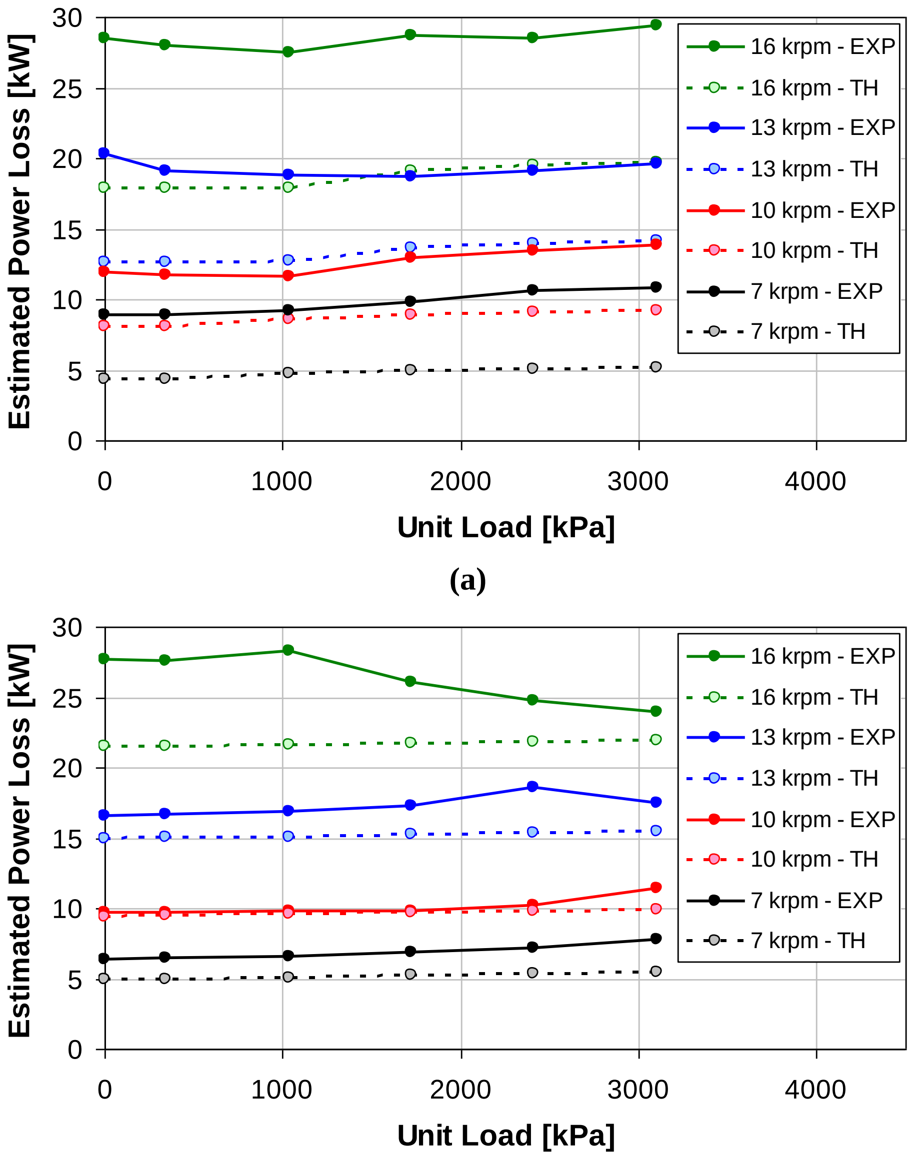

(a)

(b)

Figure 27. Estimated and predicted power loss for (a) 50% offset, (b) 60% offset.

Figure 28 compares the experimentally estimated power loss of the 50 and 60% offsets. Aside from 16 krpm, the 50% pivot offset had larger power losses than the 60% offset. This trend agrees with the results of Adolfo et al. [29] who observed higher pad temperatures with a 50% offset than a 60% offset.

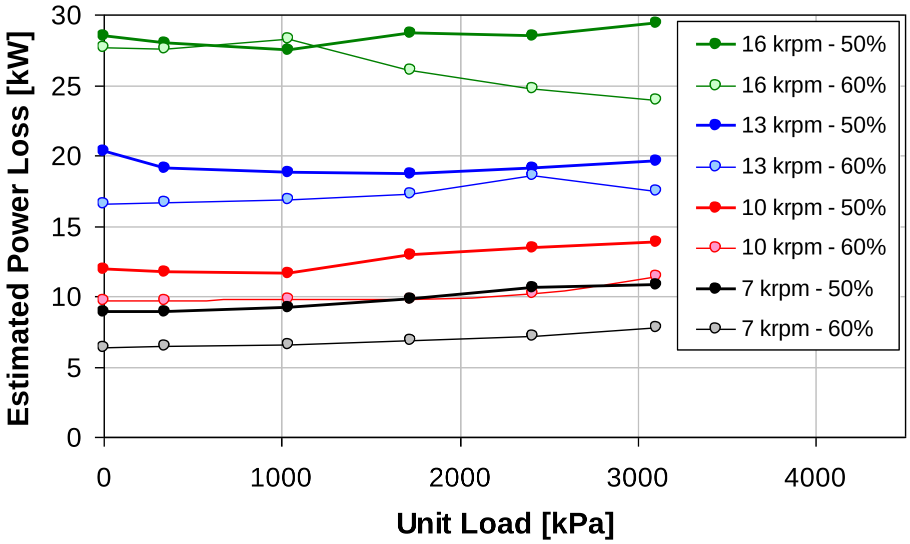

Figure 28. Estimated (experimental) power loss for 50 and 60% offset bearings.

DYNAMIC RESULTS

Baseline Dynamic Stiffness

Recall that separate baseline tests were conducted for both pivot offsets since bearing disassembly was required. Figures 29 and 30 present the baseline dynamic stiffness for the 50 and 60% pivot offsets. The baseline results were subtracted from the test dynamic stiffness to obtain the dynamic response of the fluid-film only.

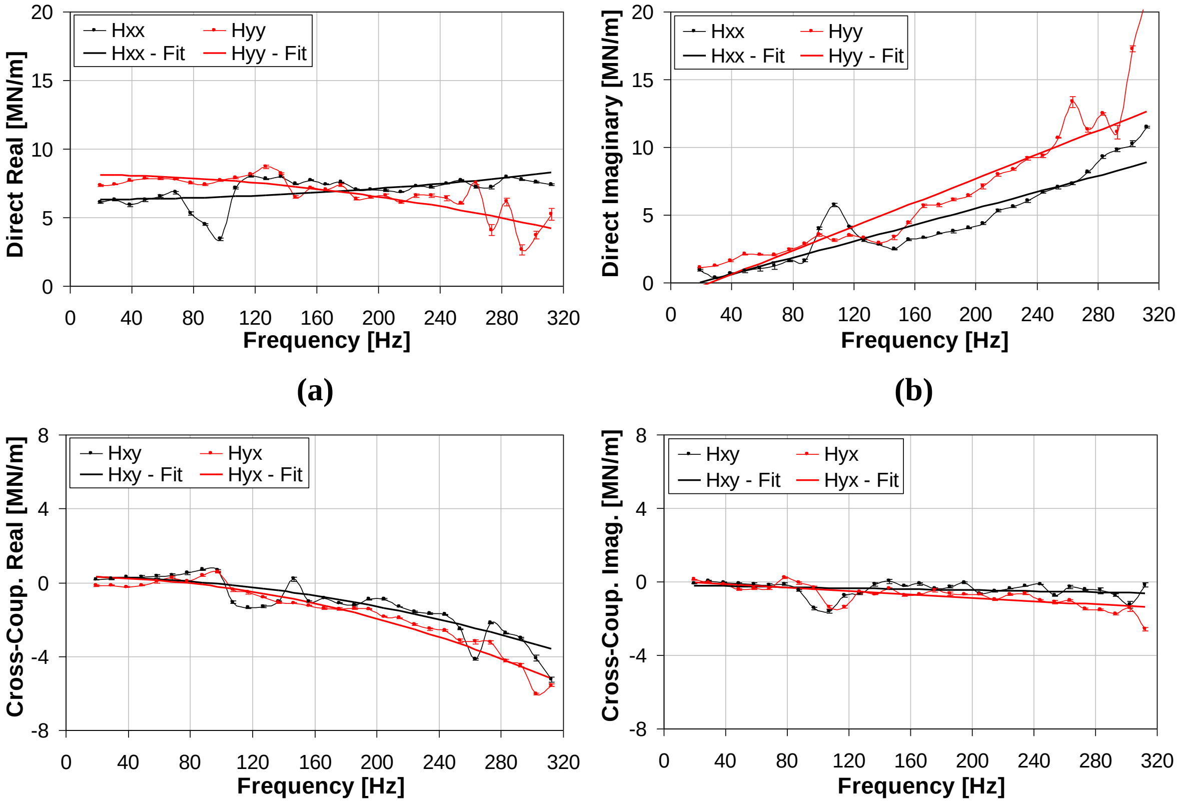

(a) (b)

(c) (d)

Figure 29. 50% offset baseline dynamic stiffness for: (a) direct real, (b) direct imaginary, (c) cross-coupled real, (d) cross-coupled imaginary.

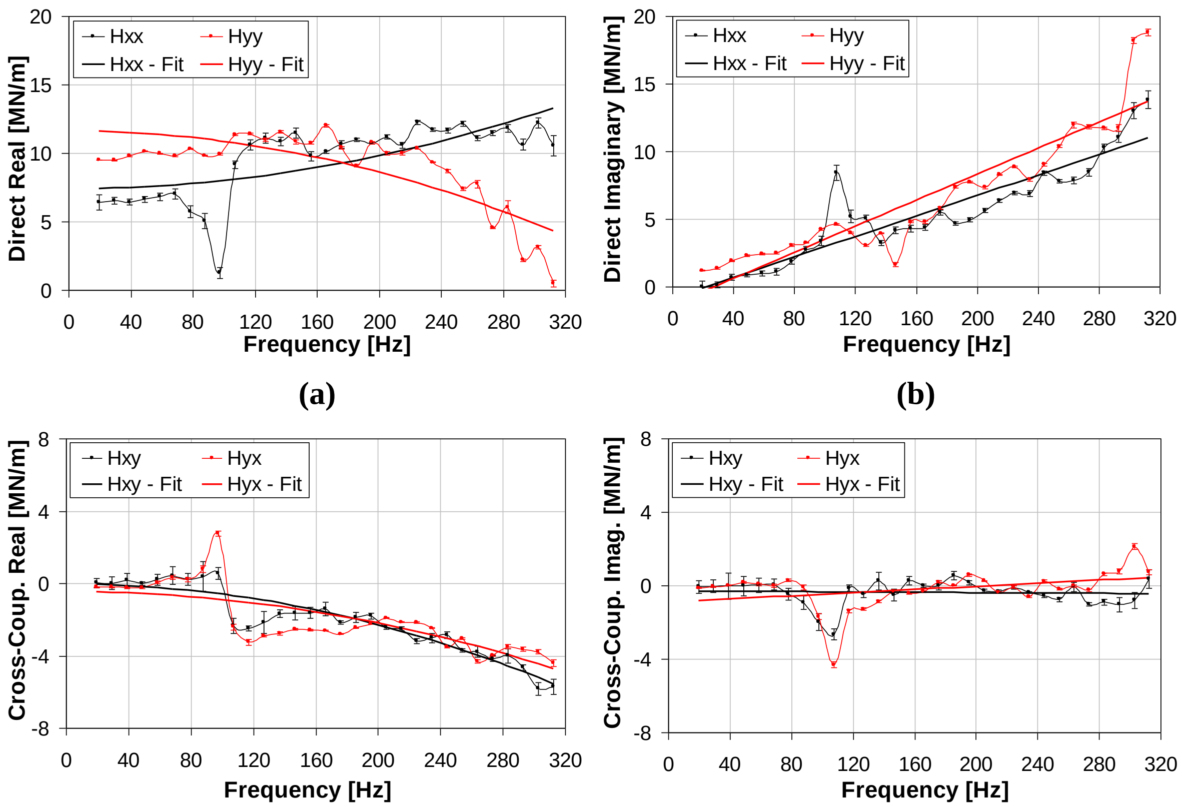

(a) (b)

(c) (d)

Figure 30. 60% offset baseline dynamic stiffness for: (a) direct real, (b) direct imaginary, (c) cross-coupled real, (d) cross-coupled imaginary.

Test Bearing Dynamic Stiffness

The following sections provide measured and predicted dynamic stiffness data for the test bearing at the lowest rotor speed and unit load and at the maximum speed and load. These conditions include a rotor speed of 7 krpm with no static load and speed of 16 kpm with a unit load 3101 kPa (450 psi). Experimental and theoretical data are presented for the 50% and 60% offset, followed by a comparison between the offsets.

The experimental dynamic stiffness coefficients presented here represent the bearing fluid film only. The baseline dynamic stiffness data has already been accounted for. All dynamic stiffness predictions were calculated using the NS bulk-flow analysis in XLTFPBrg.

Appendix E presents dynamic stiffness numerical data used to determine rotordynamic coefficients for all tested speeds and loads. Rotordynamic coefficients and uncertainty values for all test conditions are provided in Appendix D.

50% Offset Dynamic Stiffness

Figure 31 presents the experimental and predicted dynamic stiffness functions for the 50% offset at the lowest speed and no load condition.

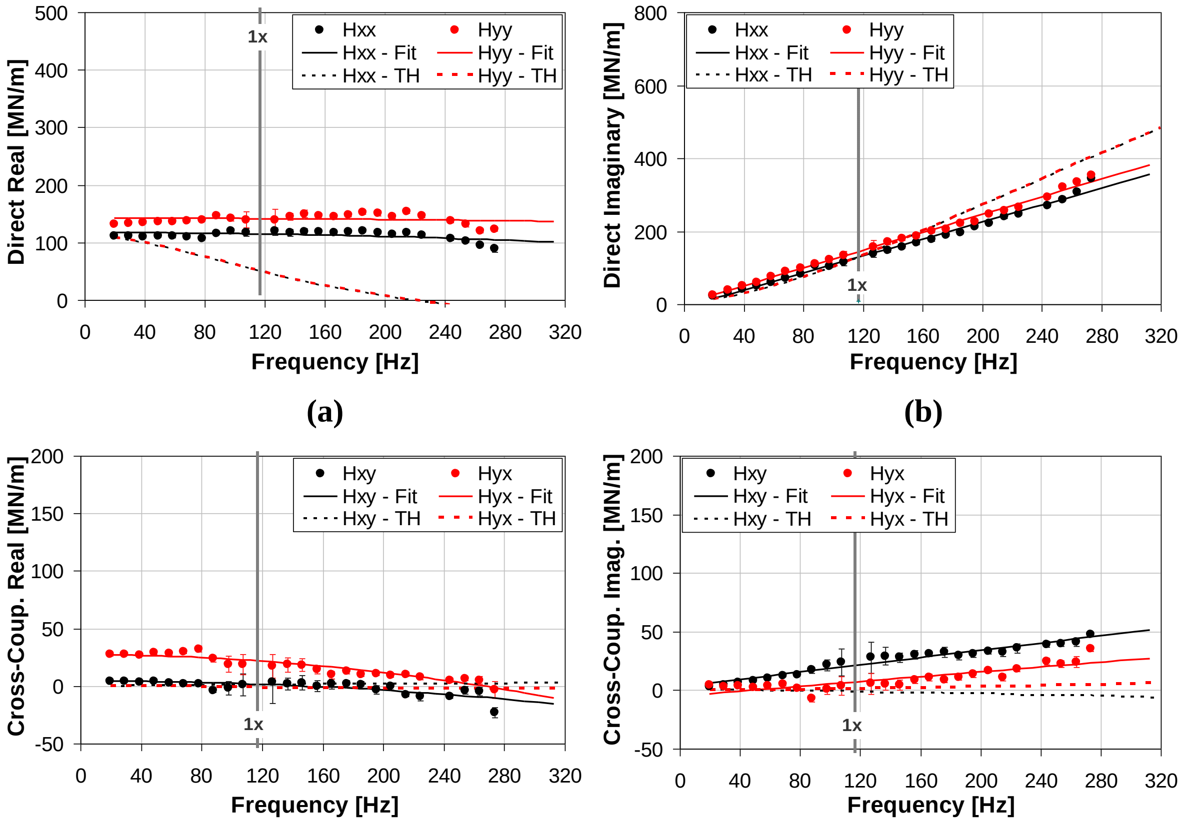

(a) (b)

(c) (d)

Figure 31. 50% offset dynamic stiffness at 7 krpm and zero unit load for: (a) direct real, (b) direct imaginary, (c) cross-coupled real, (d) cross-coupled imaginary.

The direct real dynamic stiffness functions are shown above in Figure 31 (a). The measured dynamic stiffnesses show a slight dependence on Ω. The curve fits show that the direct added-mass coefficients are quite small for both excitation directions, and that K_{yy} is larger than K_{xx}. The predicted low-frequency dynamic stiffness matches well, but the measured stiffness orthotropy is not predicted. Additionally, the measured frequency-dependency is not predicted well at all. The experimental Re($\boldsymbol{H}_{xx}$) and Re($\boldsymbol{H}_{yy}$) are relatively constant when compared to the predictions which show significant decrease with increasing Ω.

Figure 31 (b) provides the direct imaginary dynamic stiffness functions. These dynamic stiffnesses increase linearly with increasing frequency, providing frequency-independent direct damping coefficients. The data shows there is no considerable difference between C_{xx} and C_{yy}. The predictions match well below running speed, but the code predicts an increase in damping at super-synchrounous frequencies that is not measured.

The cross-coupled real dynamic stiffnesses are given in Figure 31 (c). The theory predicts cross-coupled terms that are approximately zero, and agrees well for the Re($\boldsymbol{H}_{xy}$). The Re($\boldsymbol{H}_{yx}$) is larger and matches with predictions only at higher excitation frequencies. The experimental Re($\boldsymbol{H}_{xy}$) and Re($\boldsymbol{H}_{yx}$) decrease with increasing frequency and show that positive cross-coupled mass coefficients can account for the frequency dependency.

In Figure 31 (d), the cross-coupled imaginary dynamic stiffness shows that cross-coupled damping coefficients exist where C_{xy} is larger than C_{yx} and both coefficients are positive, suggesting positive, real damping. Both Im($\boldsymbol{H}_{xy}$) and Im($\boldsymbol{H}_{yx}$) increase linearly with increasing Ω, showing that the cross-coupled damping coefficients are frequency independent. Additionally, both cross-coupled damping coefficients are of the same sign but considerably smaller than the direct damping coefficients estimated in Figure 31 (c).

The measured and theoretical dynamic stiffnesses for the 50% offset are given in Figure 32 for the highest speed and largest unit load case.

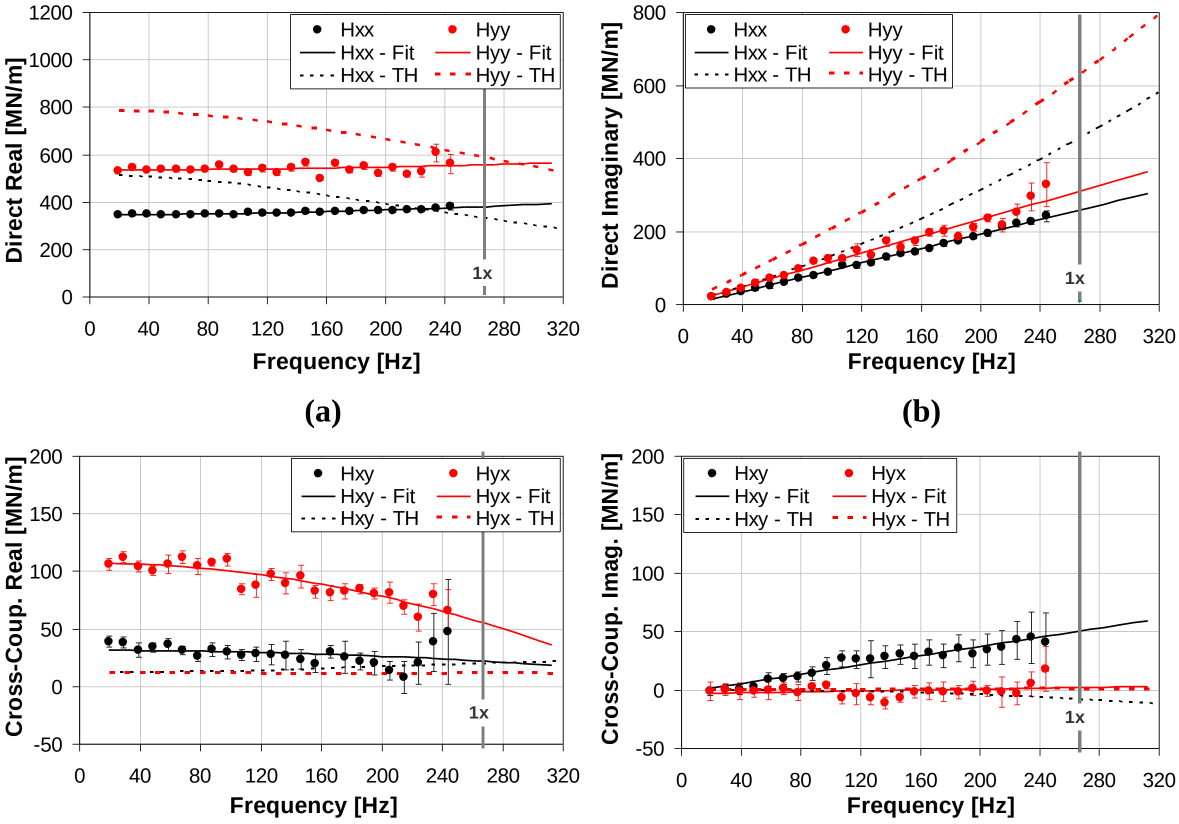

(a) (b)

(c) (d)

Figure 32. 50% offset dynamic stiffness at 16 krpm and 3101 kPa for: (a) direct real, (b) direct imaginary, (c) cross-coupled real, (d) cross-coupled imaginary.

The real part of the direct dynamic stiffness is provided above in Figure 32 (a). The experimental Re($\boldsymbol{H}_{xx}$) and Re($\boldsymbol{H}_{yy}$) show a slight increase with Ω and are well fit with slight quadratic curve. The data shows that direct stiffness is larger for the loaded direction while the direct added-mass coefficients are both slightly negative. The low frequency direct stiffnesses are over predicted for both Re($\boldsymbol{H}_{xx}$) and Re($\boldsymbol{H}_{yy}$). Furthermore, the predicted curves decrease substantially with increasing Ω. This predicted frequency-dependency is not modeled well with an added-mass term and does not correlate with the measured data.

Figure 32 (b) provides the direct imaginary dynamic stiffness and shows that the experimental data is fit well, providing frequency-independent damping coefficients where C_{yy} is slightly larger than C_{xx}. The code predicts the Im($\boldsymbol{H_{xx}}$) and Im($\boldsymbol{H_{yy}}$) to increase with Ω in a manner that produces increasing direct damping coefficients with increasing Ω. This results in the direct damping coefficients becoming more over predicted with increasing frequency. Additionally, the code predicts asymmetry between C_{xx} and C_{yy} that is not measured.

The imaginary part of the cross-coupled damping dynamic stiffness is given above in Figure 32 (c). The measured data shows that indirect stiffness coefficients exist where K_{yx} is larger than K_{xy}, and both coefficients are positive. These cross-coupled stiffness coefficients can be considered are frequency independent when applying positive cross-coupled added-mass coefficients. The predicted Re($\boldsymbol{H_{yx}}$) and Re($\boldsymbol{H_{xy}}$) curves are approximately equal and are smaller than the experimental results.

Figure 32 (d) plots the indirect imaginary dynamic stiffness. The experimental data shows a linear relationship with Ω, producing frequency-independent C_{xy} and C_{yx} which are of the same sign. Predictions are approximately zero for both coefficients, which agrees well only for C_{yx}.

60% Offset Dynamic Stiffness

The predicted and measured dynamic stiffness functions for the 60% offset are plotted in Figure 33 for the lowest speed, zero unit load case.

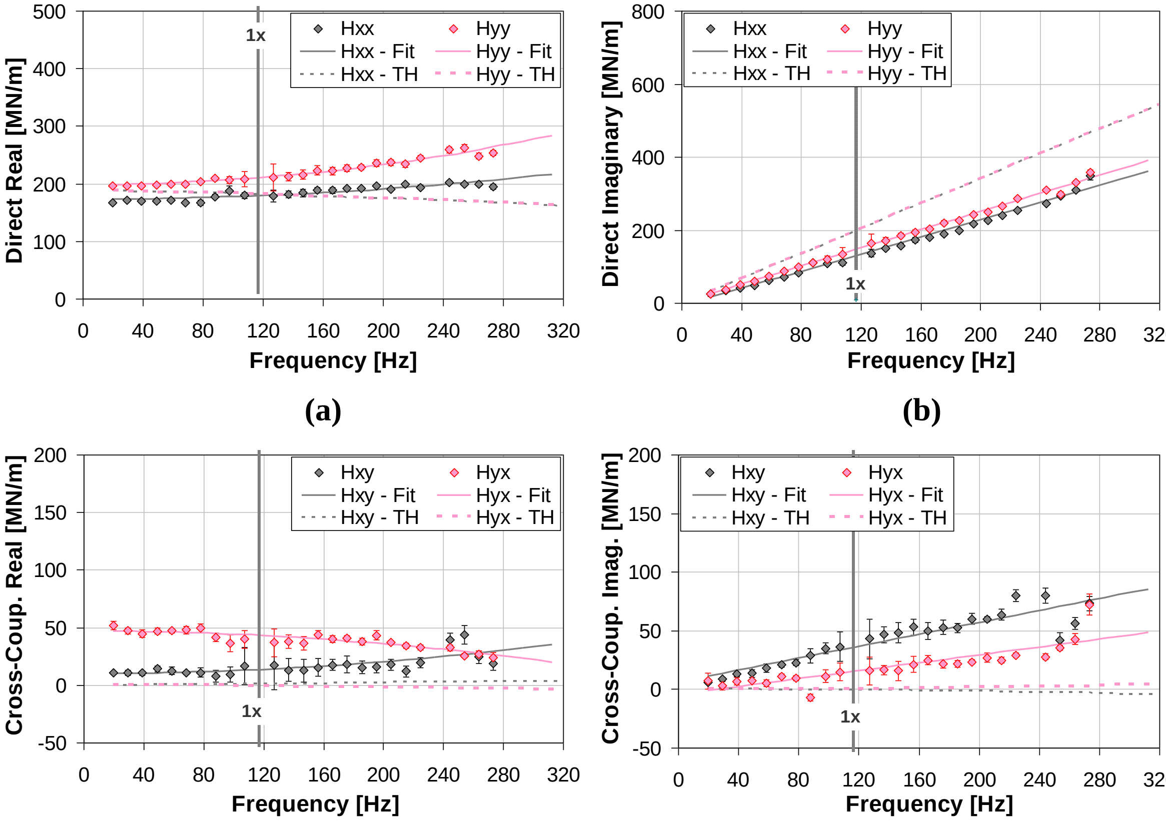

(a) (b)

(c) (d)

Figure 33. 60% offset dynamic stiffness at 7 krpm and zero unit load for: (a) direct real, (b) direct imaginary, (c) cross-coupled real, (d) cross-coupled imaginary.

Figure 33 (a) provides the direct real part of the dynamic stiffness. Both Re($\boldsymbol{H}_{xx}$) and Re($\boldsymbol{H}_{yy}$) increase with Ω and are fit well with the quadratic curves. The predicted dynamic stiffnesses match well at low frequencies, showing that the direct stiffness coefficients are well predicted. The code does not predict the stiffness asymmetry seen here for the zero unit load case. Additionally, the predicted stiffnesses decrease with increasing Ω while the test data increases. Therefore, the direct mass coefficients are predicted to be positive while the test results produce negative direct mass terms.

The direct imaginary dynamic stiffness is shown above in Figure 33 (b). The predicted and measured data increases linearly with increasing Ω, producing frequency-independent direct damping coefficients. The predicted Im($\boldsymbol{H}_{xx}$) and Im($\boldsymbol{H}_{yy}$) have larger slopes than the measurements, showing that C_{xx} and C_{yy} are both over predicted. The code predicts the same direct damping for both x and y directions, which agrees with the test results.

Figure 33 (c) presents the cross-coupled real dynamic stiffness and shows that measureable cross-coupling exists in comparison to the near zero predictions. The Re($\boldsymbol{H}_{xy}$) and Re($\boldsymbol{H}_{yx}$) data shows that K_{yx} is considerably larger than K_{xy}, but both coefficients are positive. The regression fits have opposite curvatures and therefore produce cross-coupled added-mass coefficients that have opposite signs, implying a negative impact on rotordynamic stability.

The imaginary part of the cross-coupled dynamic stiffness is given in Figure 33 (d). Both Im($\boldsymbol{H}_{xy}$) and Im($\boldsymbol{H}_{yx}$) increase linearly with Ω and produce positive, frequency independent cross-coupled damping coefficients that have the same sign. These plots show that the experimental C_{xy} is larger than C_{yx}, but both coefficients are considerable larger than the approximate zero predictions.

Figure 34 presents the experimental and theoretical dynamic stiffness functions for the 60% offset at the full speed and large load condition.

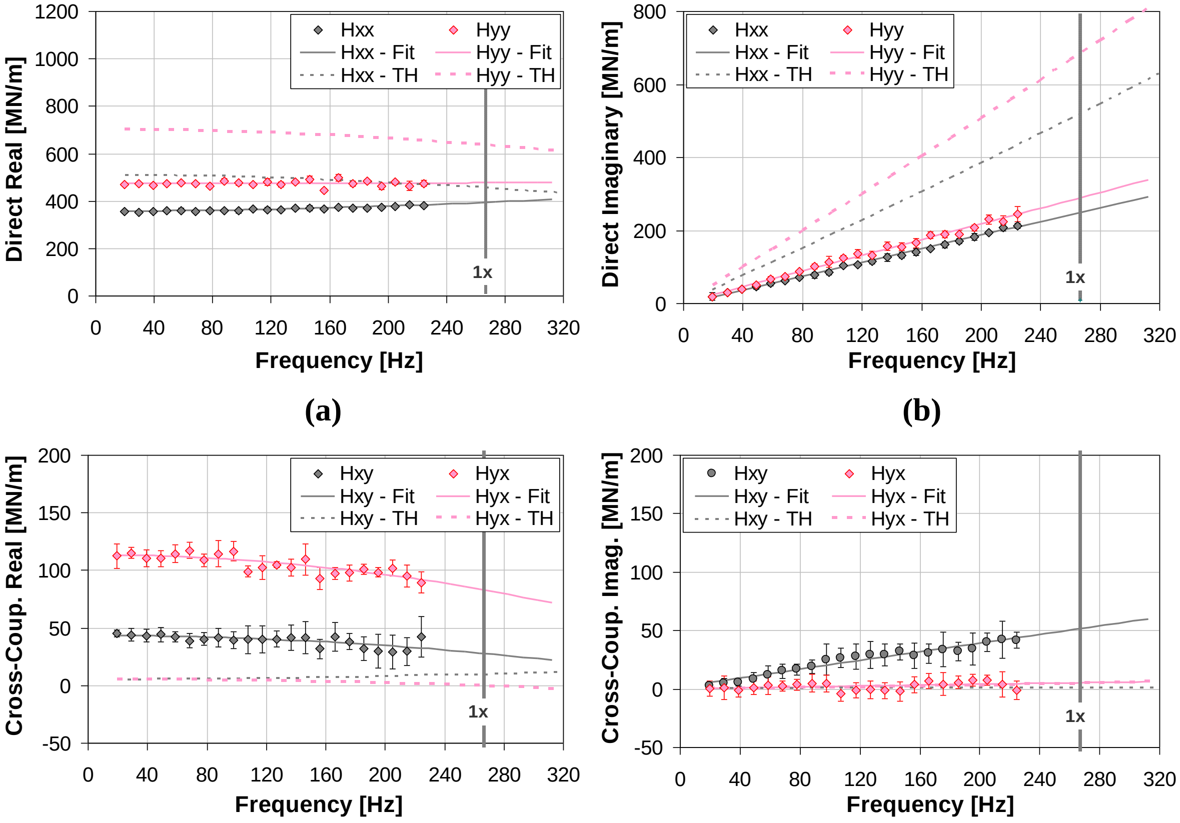

(a) (b)

(c) (d)

Figure 34. 60% offset dynamic stiffness at 16 krpm and 3101 kPa for: (a) direct real, (b) direct imaginary, (c) cross-coupled real, (d) cross-coupled imaginary.

The direct real part of the dynamic stiffness is provided in Figure 34 (a). The data are fit well with slight quadratic curves, allowing for negative added-mass coefficients to account for the frequency dependency. In addition, the plot shows that K_{yy} is about 25% larger than K_{xx}. Overall, Re($\boldsymbol{H}_{xx}$) and Re($\boldsymbol{H}_{yy}$) are over predicted with a downward curvature that is opposite of what is measured. Therefore, the direct stiffness coefficients are over predicted and the direct added-mass coefficients are negative versus a prediction of positive.

Figure 34 (b) provides the direct imaginary dynamic stiffness. Im($\boldsymbol{H}_{xx}$) and Im($\boldsymbol{H}_{yy}$) increase linearly with increasing Ω and provide frequency-independent direct damping coefficients. The code predicts both functions to increase linearly with Ω, but over-predicts the magnitude of the slope. As a result, the direct damping is over predicted, more so for the loaded direction.

The cross-coupled real dynamic stiffness functions are given above in Figure 34 (c). This plot shows that cross-coupling exists where K_{yx} is larger than K_{xy}, and both cross-coupled stiffness coefficients require added-mass terms to be frequency independent. These cross-coupled added mass coefficients are both positive, showing no impact on stability. In contrast to experimental results, the code predicts negligible cross-coupled stiffness and added-mass coefficients.

Figure 34 (d) plots the imaginary part of the cross-coupled dynamic stiffness functions. The experimental Im($\boldsymbol{H}_{xy}$) agrees well with the near zero predictions while the Im($\boldsymbol{H}_{yx}$) shows that a constant C_{xy} exists that is larger than predictions. Both cross-coupled damping coefficients are of the same sign and are considerable less than the direct damping terms.

50 and 60% Offset Dynamic Stiffness Comparison

Figure 35 provides the measured dynamic stiffness coefficients and curve fits used to determine rotordynamic coefficients for 50 and 60% offsets at the lowest speed and zero unit load condition.

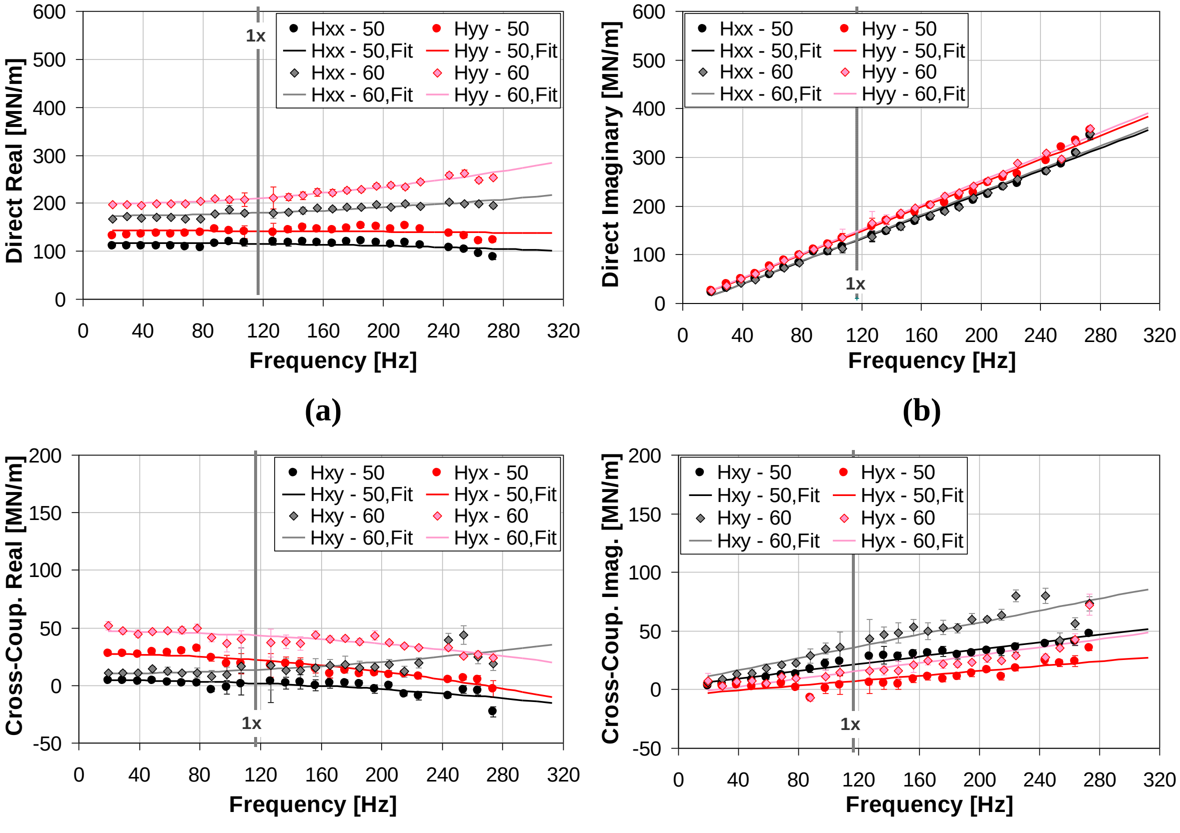

(a) **(b)**

(c) **(d)**

Figure 35. 50 and 60% offset measured dynamic stiffness at 7 krpm and zero unit load for: (a) direct real, (b) direct imaginary, (c) cross-coupled real, (d) cross-coupled imaginary.

Figure 35 (a) compares the direct real dynamic stiffness functions and shows that the 60% offset bearing is considerably stiffer in both orthogonal directions. In addition, the 60% offset direct real dynamic stiffness data has an upward curvature with increasing frequency while the 50% offset values are almost constant with frequency. This demonstrates that the direct added-mass coefficients will be negative and larger in magnitude for the 60% offset.

The direct imaginary dynamic stiffness functions shown in Figure 35 (b) are almost the same for the 50 and 60% offset, meaning the direct damping coefficients at this test condition are almost identical for both offsets. For both offsets, the Im($\boldsymbol{H}_{xx}$) and Im($\boldsymbol{H}_{yy}$) increase linearly with increasing Ω, allowing for frequency independent direct damping coefficients.

The real parts of the cross-coupled dynamic stiffnesses are plotted in Figure 35 (c). The zero frequency intercepts for Re($\boldsymbol{H}_{xy}$) and Re($\boldsymbol{H}_{yx}$) are larger for the 60% offset, showing that the 60% offset will have larger cross-coupled stiffness coefficients. Re($\boldsymbol{H}_{xy}$) and Re($\boldsymbol{H}_{yx}$) for the 50% offset decrease with increasing Ω, allowing for positive cross-coupled mass coefficients to capture the frequency dependency. For the 60% offset, the functions have opposite curvatures and will therefore give M_{xy} and M_{yx} of opposite signs, implying a negative impact on stability.

Figure 35 (d) shows that the cross-coupled imaginary dynamic stiffness functions show a linear dependence with Ω for both pivot offsets. The Im($\boldsymbol{H}_{xy}$) and Im($\boldsymbol{H}_{yx}$) functions have larger slopes for the 60% offset, meaning the cross-coupled damping coefficients are larger for the 60% offset configuration. For both pivot offsets, the C_{xy} and C_{yx} have the same sign, indicating real cross-coupled damping.

The measured dynamic stiffness functions and coefficient curve fits for both offsets at the full speed and full load condition are plotted in Figure 36.

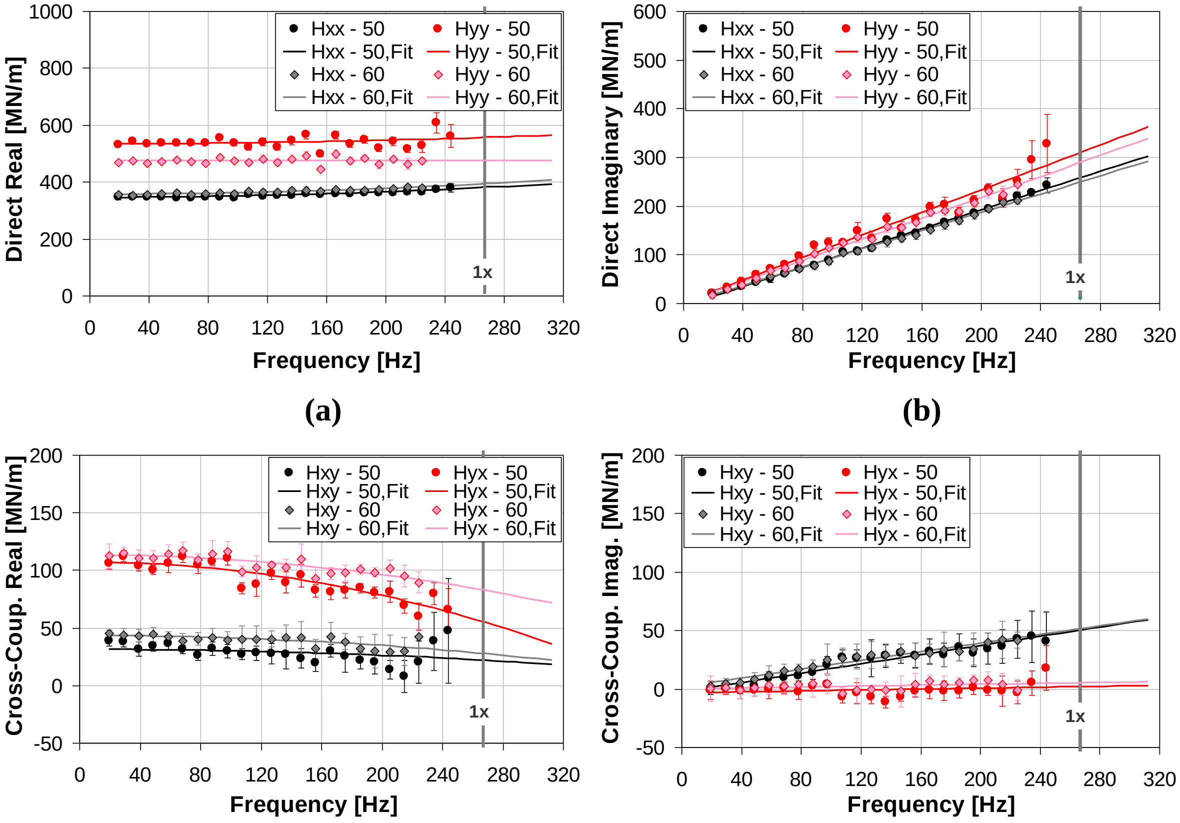

(a) **(b)**

(c) **(d)**

Figure 36. 50 and 60% offset measured dynamic stiffness at 16 krpm and 3101 kPa for: (a) direct real, (b) direct imaginary, (c) cross-coupled real, (d) cross-coupled imaginary.

Re($\boldsymbol{H}_{xx}$) and Re($\boldsymbol{H}_{yy}$) are provided in Figure 36 (a) and show a slight increase with increasing Ω. Curve fitting produces negative added-mass coefficients for both pivot offsets. Re($\boldsymbol{H}_{yy}$) is constantly larger for the 60% offset at all test frequencies, suggesting the 60% offset will have a larger K_{yy}, but similar M_{yy} when compared to the 50% offset. Re($\boldsymbol{H}_{xx}$) shows negligible change between pivot offsets and therefore negligible difference in K_{xx} and M_{xx} between offsets.

Figure 36 (b) presents the imaginary part of the direct dynamic stiffness functions. For both offsets and directions, the Im($\boldsymbol{H}_{xx}$) and Im($\boldsymbol{H}_{yy}$) increase linearly with increasing frequency, providing frequency independent direct damping coefficients. The plots show that the direct damping does not change between 50 and 60% pivot offset.

Re($\boldsymbol{H}_{xy}$) and Re($\boldsymbol{H}_{yx}$) are provided in Figure 36 (c). These plots indicate that cross-coupled stiffness and added-mass coefficients are quite comparable with respect to pivot offset. The low-frequency dynamic stiffness values show that the indirect stiffness coefficients are slightly larger for the 60% pivot offset, but all coefficients are positive. These cross-coupled added-mass coefficients suggest no impact on stability because of the same signs.

Figure 36 (d) shows that the indirect imaginary dynamic stiffness functions are practically the same for either offset. The Im($\boldsymbol{H}_{xy}$) increases linearly with increasing Ω allowing for a positive frequency independent C_{xy} for each offset. The Im($\boldsymbol{H}_{yx}$) is about zero for all test frequencies and both offsets, suggesting insignificant values for C_{yx}.

Stiffness Coefficients

All experimental stiffness coefficients are estimated from the least squares regression of the real part of the dynamic stiffness. When the *predicted* stiffness versus frequency was not fit well with a quadratic curve, the low-frequency predicted stiffness is reported. This predicted frequency dependency, such as that shown previously in Figure 31 (a), occurred for the majority of test cases for the 50% offset. Fitting these predictions with a quadratic curve produced very low r^2 values, indicating a poor fit.

Experimental and predicted stiffness coefficients are plotted for each offset, followed by a comparison of experimental results between 50 and 60% offsets.

50% Offset Stiffness

Figure 37 presents the experimental and predicted direct stiffness coefficients for the 50% pivot offset.

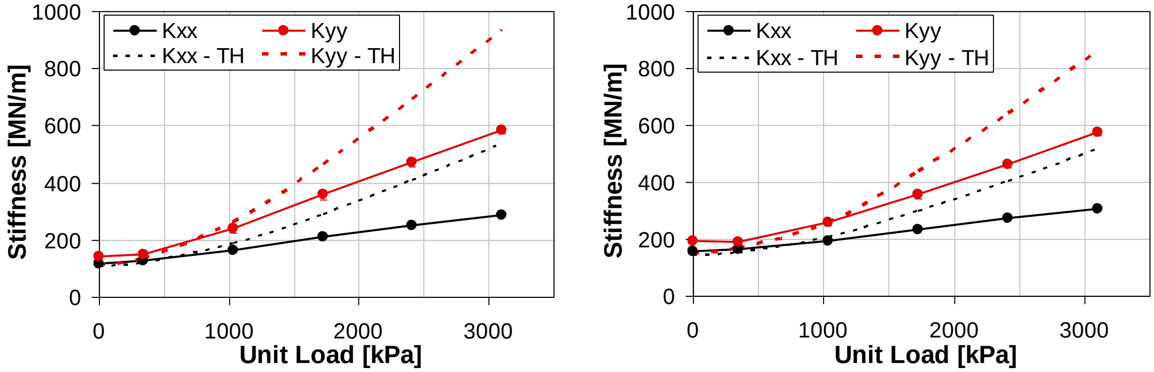

(a) 7 krpm **(b) 10 krpm**

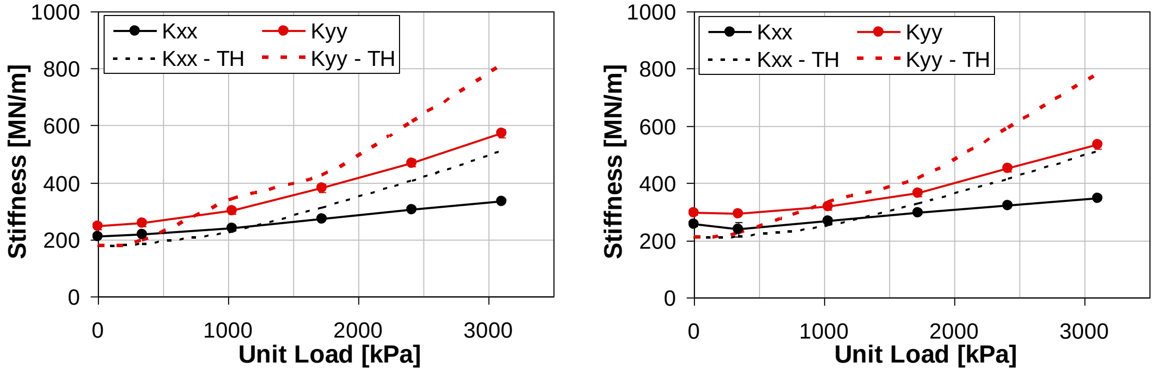

(c) 13 krpm **(d) 16 krpm**

Figure 37. 50% offset direct stiffness coefficients at: (a) 7 krpm, (b) 10 krpm, (c) 13 krpm, (d) 16 krpm.

As seen above, experimental K_{xx} and K_{yy} values increase with static unit load with K_{yy} increasing more than K_{xx}. For a constant unit load, K_{xx} increases with increasing rotor speed. K_{yy} becomes larger with increasing rotor speed for light unit loads, but decreases with increasing speed at high loads. Over the tested conditions, K_{yy} shows a larger dependency with respect to unit load than to rotor speed. For all speeds, both direct stiffness coefficients are predicted well at light unit loads and become increasingly over predicted with increasing unit load. In addition, measured stiffness asymmetry at light static loads is not predicted by the code.

The theoretical and experimental cross-coupled stiffness coefficients for the 50% pivot offset are presented below in Figure 38.

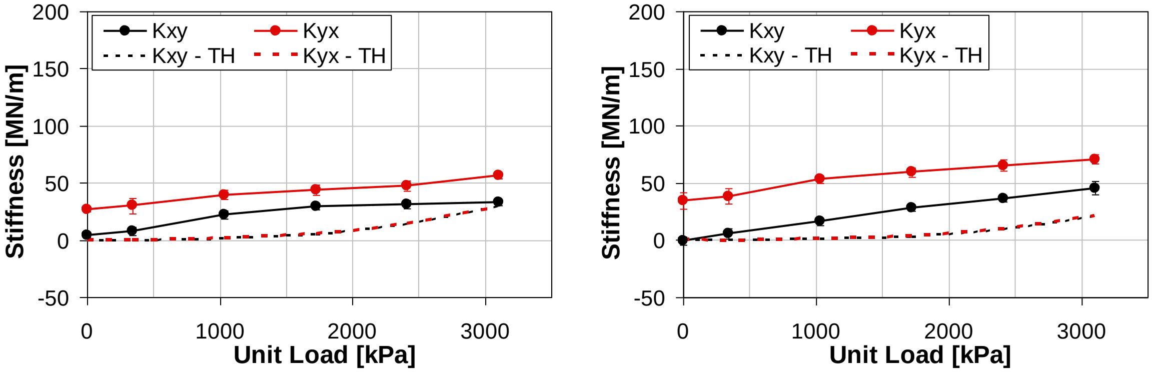

(a) 7 krpm **(b) 10 krpm**

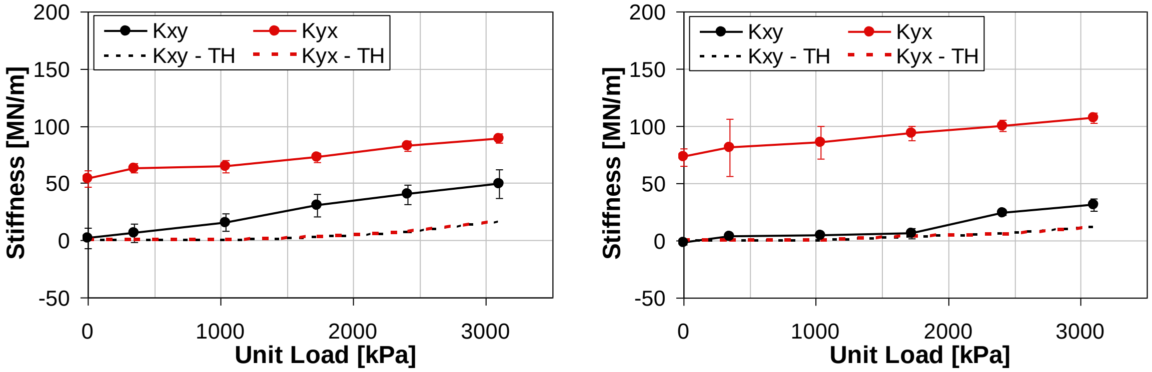

(c) 13 krpm **(d) 16 krpm**

Figure 38. 50% offset cross-coupled stiffness coefficients at: (a) 7 krpm, (b) 10 krpm, (c) 13 krpm, (d) 16 krpm.

Figure 38 shows significant experimental cross-coupled stiffness coefficients were obtained where K_{yx} is consistently larger than K_{xy}. Additionally, K_{yx} increases with both unit load and rotor speed while K_{xy} increases consistently with only unit load. Both coefficients are always positive and thus do not promote instability. This measured cross-coupling agrees with the measured trends of the loci plots and attitude angle. Predictions for both coefficients are near zero at light loads and show a small increase at higher static loads. K_{yx} is considerably under predicted for all conditions while K_{xy} is modeled well only at light static loads and at the full load case at 7 krpm. For all test conditions, K_{xy} and K_{yx} are significantly smaller than the direct coefficients described earlier in Figure 37. The most significant cross-coupling occurs at 16 krpm as seen in Figure 38 (d).

60% Offset Stiffness

Figure 39 below provides the direct stiffness coefficients for the 60% offset obtained from experiment and theory.

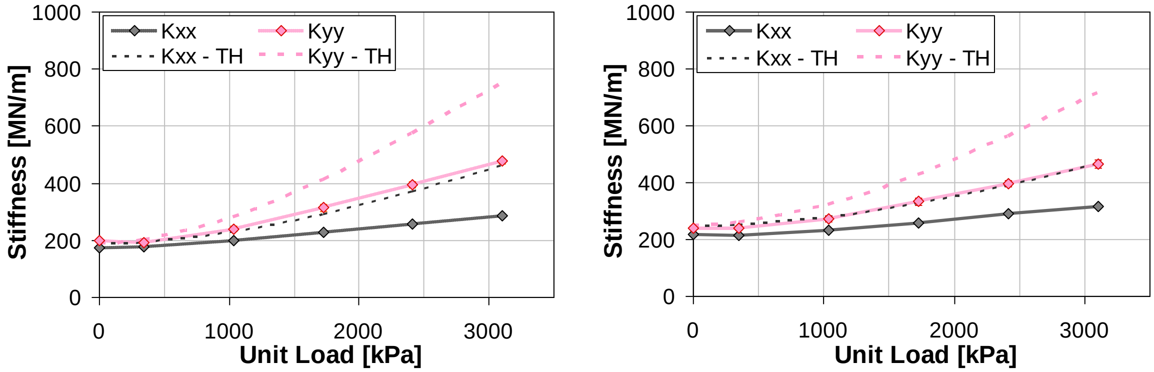

(a) 7 krpm **(b) 10 krpm**

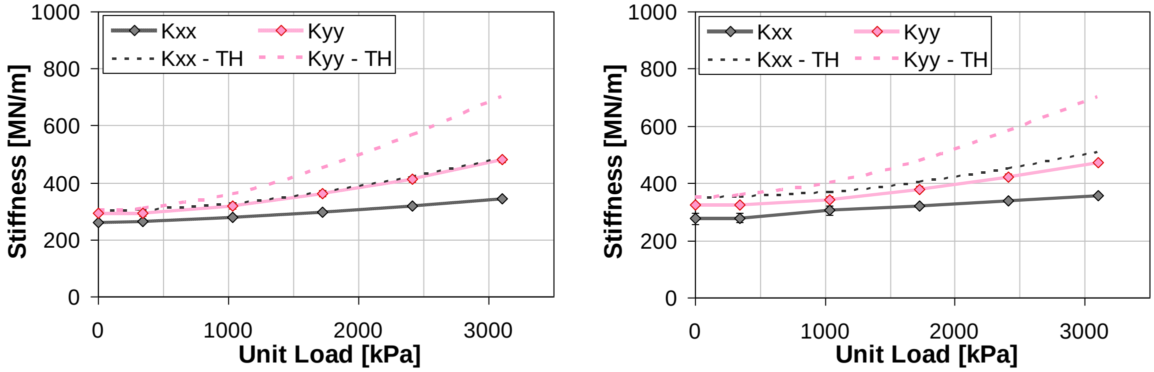

(c) 13 krpm **(d) 16 krpm**

Figure 39. 60% offset direct stiffness coefficients at: (a) 7 krpm, (b) 10 krpm, (c) 13 krpm, (d) 16 krpm.

Figure 39 shows the experimental K_{xx} and K_{yy} increasing with static unit load, more so for the loaded direction, for all rotor speeds. K_{xx} increases with increasing rotor speed for all unit loads while K_{yy} becomes larger with increasing speed for only light loads. At high static loads, K_{yy} is independent of rotor speed. Similar to the 50% pivot offset, the 60% direct stiffness coefficients are predicted well at light unit loads and become increasingly over predicted with increasing unit load for all speeds. Coincidentally, the K_{xx} predictions match well with the K_{yy} test data through all load conditions. Also, the code does not predict the measured stiffness asymmetry at light static loads.

The theoretical and experimental cross-coupled stiffness coefficients for the 60% pivot offset are given below in Figure 40.

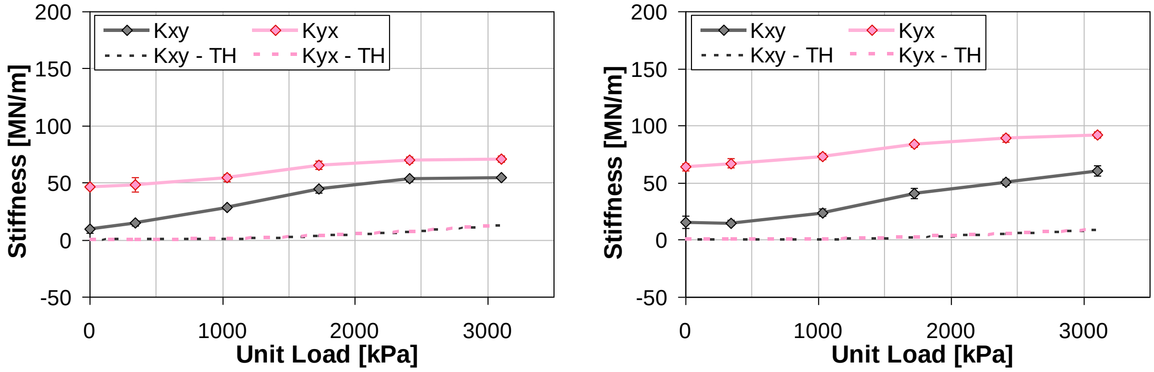

(a) 7 krpm **(b) 10 krpm**

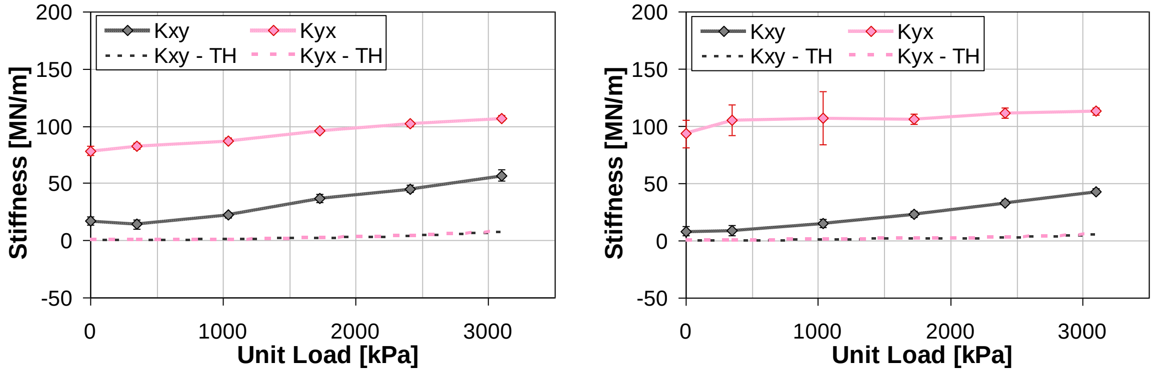

(c) 13 krpm **(d) 16 krpm**

Figure 40. 60% offset cross-coupled stiffness coefficients at: (a) 7 krpm, (b) 10 krpm, (c) 13 krpm, (d) 16 krpm.

The above figure shows that considerable cross-coupled stiffness coefficients were obtained for all test conditions in contrast to the near zero predictions for all conditions. The smallest discrepancy between predictions and test data occurs for K_{xy} at zero and light loads. K_{yx} is always larger than K_{xy}, and both coefficients tend to increase with unit load. Additionally, K_{yx} increases with increasing rotor speed while K_{xy} shows a small dependency on speed. Both coefficients always have the same sign, similar to the 50% offset bearing. The experimental results shown above agree with the trends of the loci plots and attitude angles of Figures 20 and 22 that suggest cross-coupling exists. Both cross-coupled stiffness coefficients are much smaller than the direct coefficients shown previously in Figure 39.

50 and 60% Offset Stiffness Comparison

Figure 41 compares the experimental direct stiffness coefficients of the 50 and 60% pivot offsets.

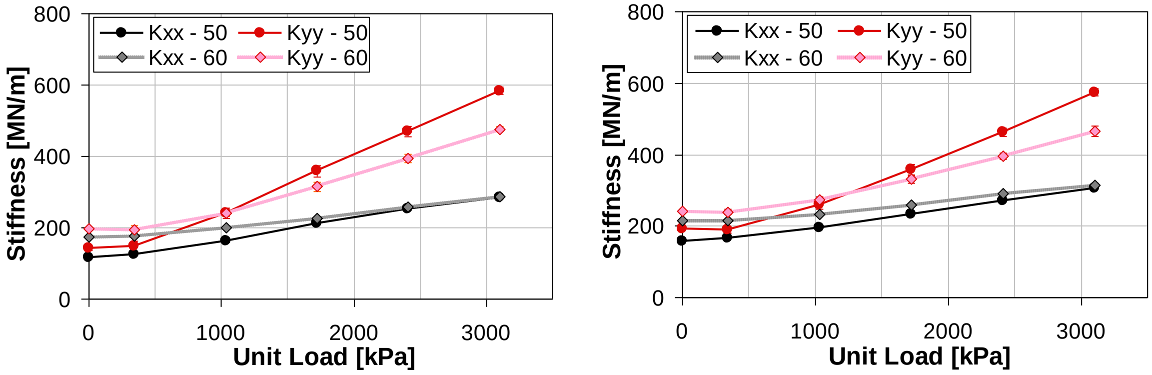

(a) 7 krpm **(b) 10 krpm**

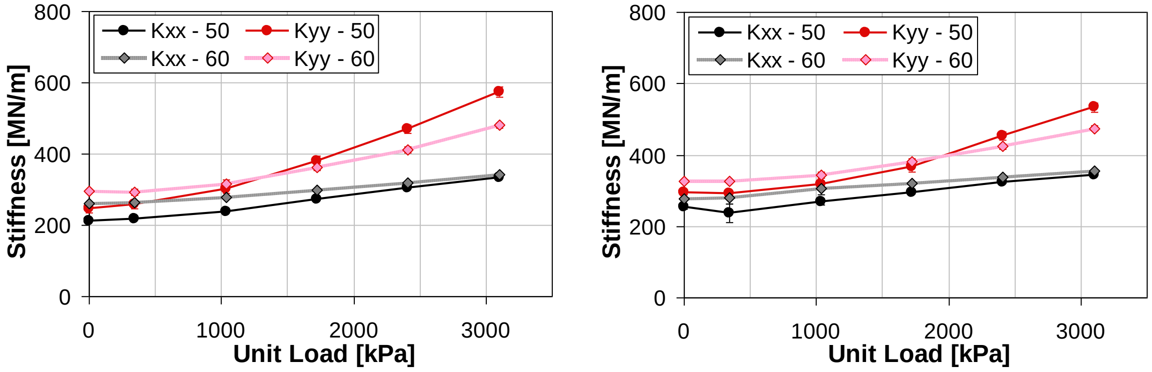

(c) 13 krpm **(d) 16 krpm**

Figure 41. 50 and 60% offset direct stiffness coefficients at: (a) 7 krpm, (b) 10 krpm, (c) 13 krpm, (d) 16 krpm.

As shown above, the direct stiffness coefficients are different between offsets for most test conditions. At zero unit loads, K_{yy} for the 60% offset is measurably higher than for the 50% offset. This difference in K_{yy} becomes reversed with increasing unit load to where the 50% offset K_{yy} is larger than the 60% offset at high unit loads. K_{xx} is larger for the 60% offset at zero unit load, but K_{xx} for both pivot offsets approach the same value with increasing unit load. At the full load case of 3101 kPa, no measureable difference in K_{xx} exists between offsets. These discussed trends of K_{yy} and K_{xx} comparing pivot offsets are seen across all test speeds.

The experimental cross-coupled stiffness coefficients are shown below in Figure 42 for the 50 and 60% pivots offsets.

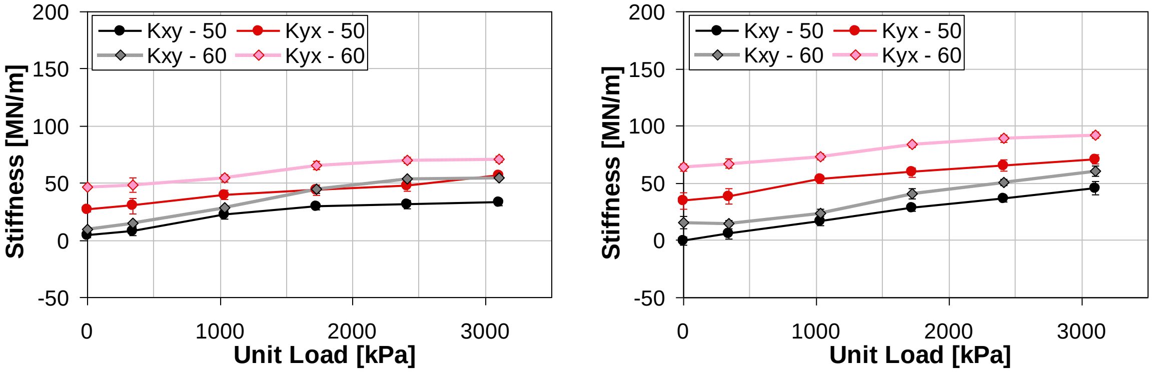

(a) 7 krpm **(b) 10 krpm**

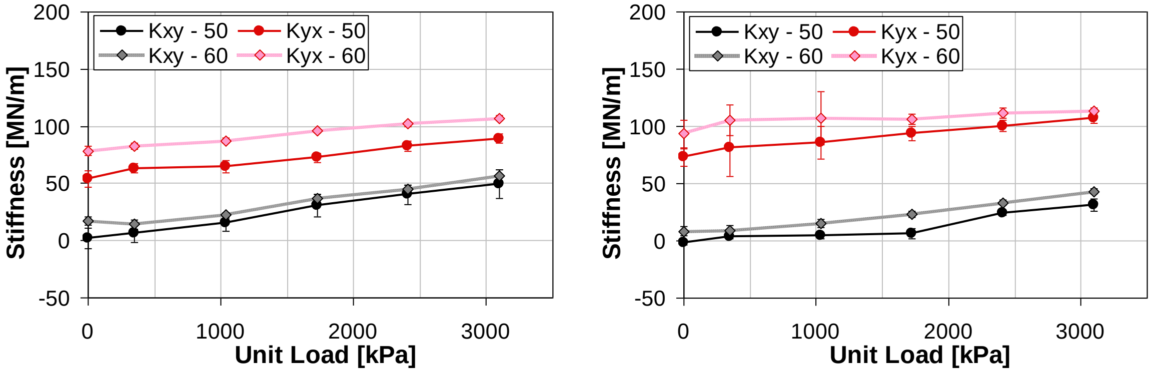

(c) 13 krpm **(d) 16 krpm**

Figure 42. 50 and 60% offset cross-coupled stiffness coefficients at: (a) 7 krpm, (b) 10 krpm, (c) 13 krpm, (d) 16 krpm.

The above figure shows that the cross-coupled stiffness coefficients for the 60% offset are slightly larger than the coefficients of the 50% offset. For both offsets, K_{yx} is always larger than K_{xy} and both coefficients have the same sign.

Damping Coefficients

The experimental damping coefficients are estimated as the slope from the linear regression of the imaginary dynamic stiffness. Note the *predicted* direct damping coefficients showed some frequency-dependency for most test cases of the 50% offset, and therefore the predicted direct damping coefficients were obtained at synchronous frequency.

50% Offset Damping

Figure 43 presents the experimental and predicted direct damping coefficients for the 50% pivot offset.

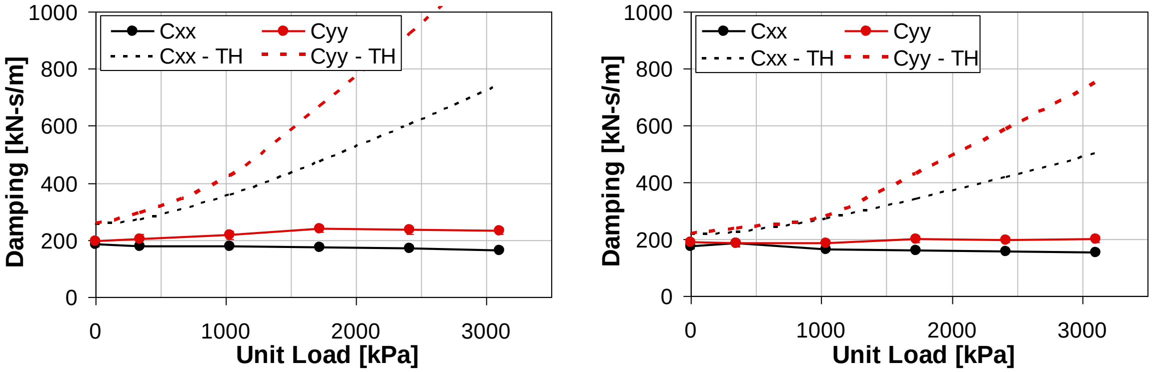

(a) 7 krpm **(b) 10 krpm**

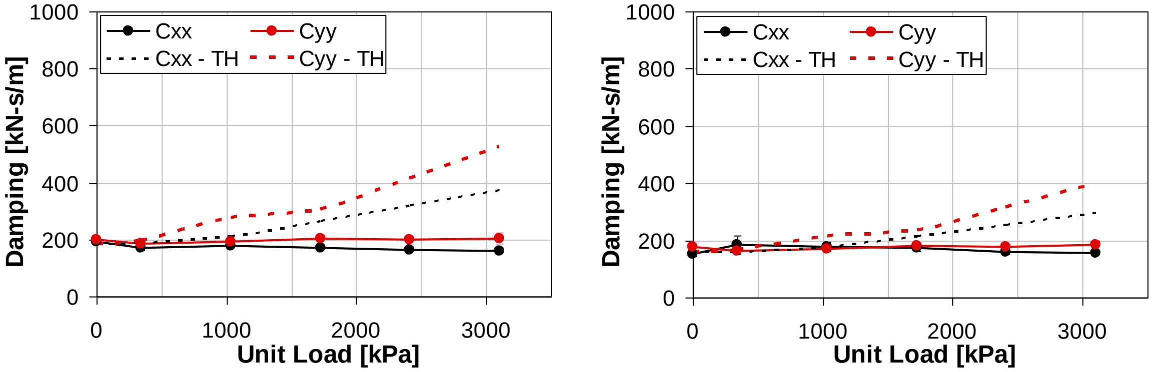

(c) 13 krpm **(d) 16 krpm**

Figure 43. 50% offset direct damping coefficients at: (a) 7 krpm, (b) 10 krpm, (c) 13 krpm, (d) 16 krpm.

As seen above, both direct damping coefficients from the experiment are largely independent of unit load. C_{xx} is also constant with respect to rotor speed while C_{yy} shows a small decrease with increasing speed. In contrast to almost constant experimental results, predictions for both direct damping coefficients increase considerably with unit load, with C_{yy} predicted to be larger than C_{xx}. Both coefficients are predicted well only at light loads for all test speeds. Correlation between experiment and theory improves considerably with increasing rotor speed. Considering all test speeds, the damping predictions match the data best at 16 krpm, but both coefficients are still substantially over predicted at high loads.

The theoretical and experimental cross-coupled damping coefficients for the 50% pivot offset are presented below in Figure 44.

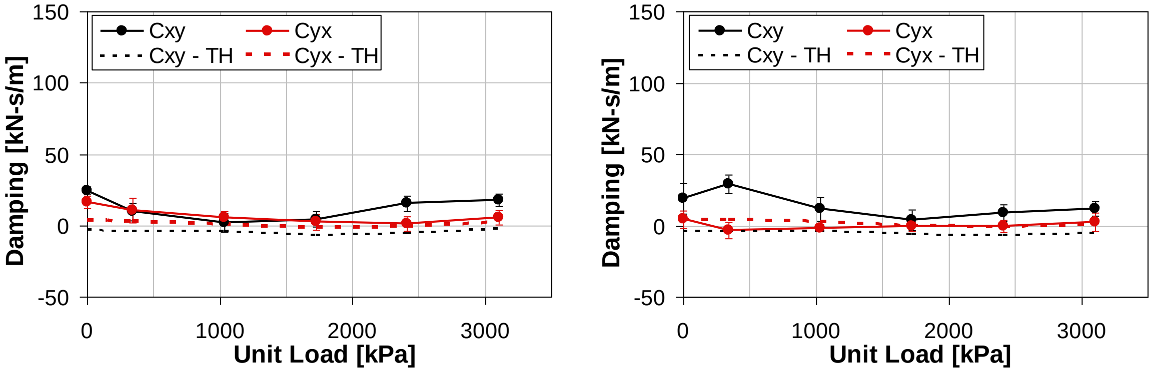

(a) 7 krpm **(b) 10 krpm**

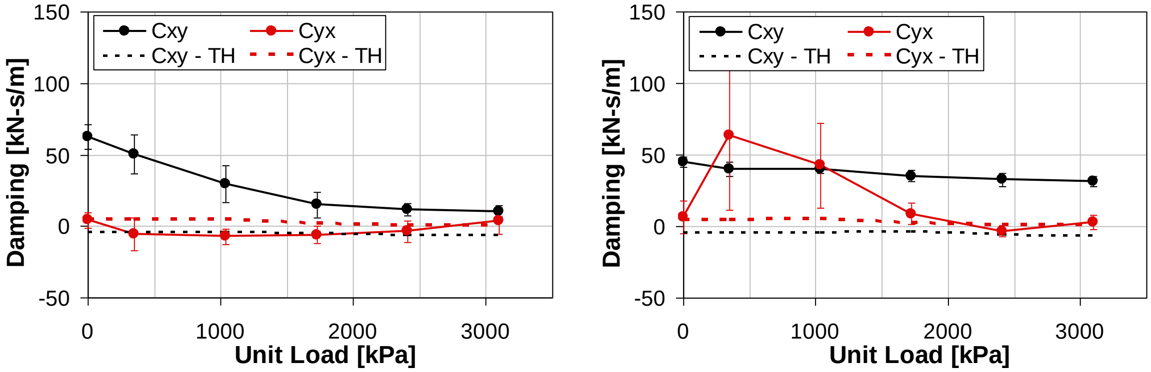

(c) 13 krpm **(d) 16 krpm**

Figure 44. 50% offset cross-coupled damping coefficients at: (a) 7 krpm, (b) 10 krpm, (c) 13 krpm, (d) 16 krpm.

The figure above shows that adequate experimental cross-coupled damping coefficients were obtained for most test conditions. C_{yx} is near zero for the majority of test conditions, matching well with predictions. Larger C_{yx} values were obtained for two load cases of 16 krpm, but these results have large uncertainties as seen above in Figure 44 (d). C_{xy} is small and matches well with predictions at 7 and 10 krpm, while C_{xy} at higher speeds is considerably larger. For all test conditions, both cross-coupled damping coefficients were dramatically smaller than the direct coefficients presented above in Figure 43.

60% Offset Damping

Figure 45 below provides the experimental and predicted direct damping coefficients for the 60% pivot offset.

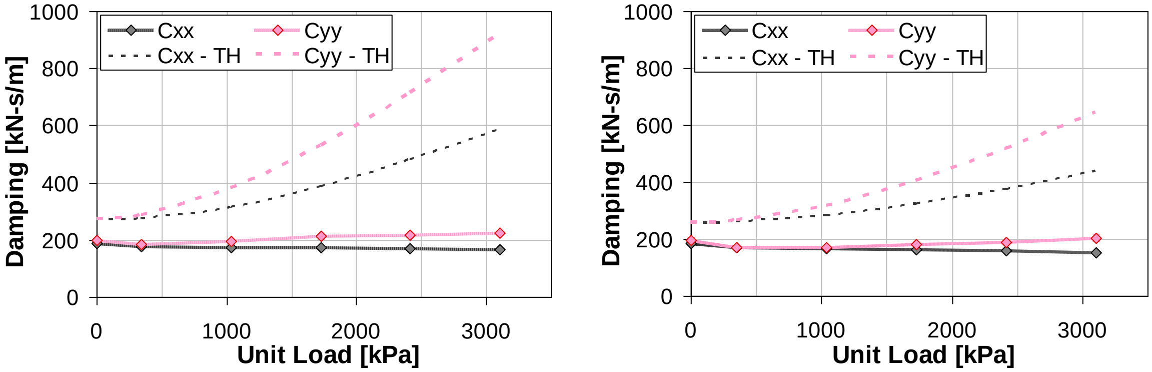

(a) 7 krpm **(b) 10 krpm**

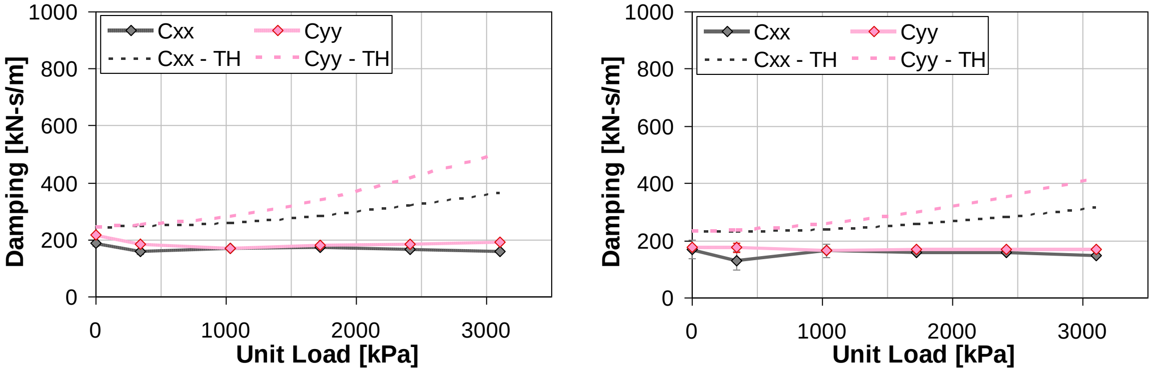

(c) 13 krpm **(d) 16 krpm**

Figure 45. 60% offset direct damping coefficients at: (a) 7 krpm, (b) 10 krpm, (c) 13 krpm, (d) 16 krpm.

As seen above, the direct damping coefficients obtained from experiment are constant with unit load and show a minimal change with rotor speed. In contrast, predictions for C_{xx} and C_{yy} increase significantly with increasing unit load and decrease with increasing speed. This over prediction trend is quite similar to that of the 50% offset shown previously in Figure 43. For all rotor speeds, the code predicts C_{yy} to become increasingly larger than C_{xx}. Across all test speeds, direct damping predictions best match the data at light unit loads, but both coefficients are still over predicted. The best agreement between predictions and test data occurs at 16 krpm, but both coefficients are still over predicted at higher loads.

The experimental and predicted cross-coupled damping coefficients are provided below in Figure 46 for the 60% offset.

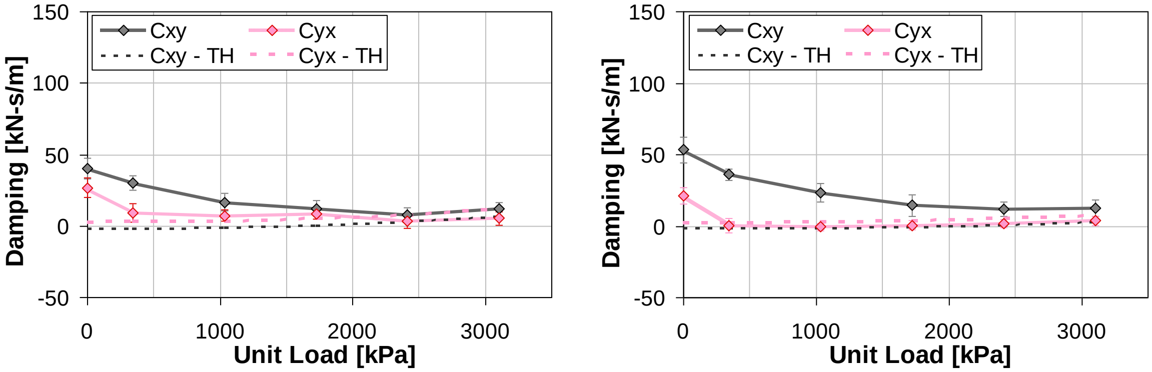

(a) 7 krpm **(b) 10 krpm**

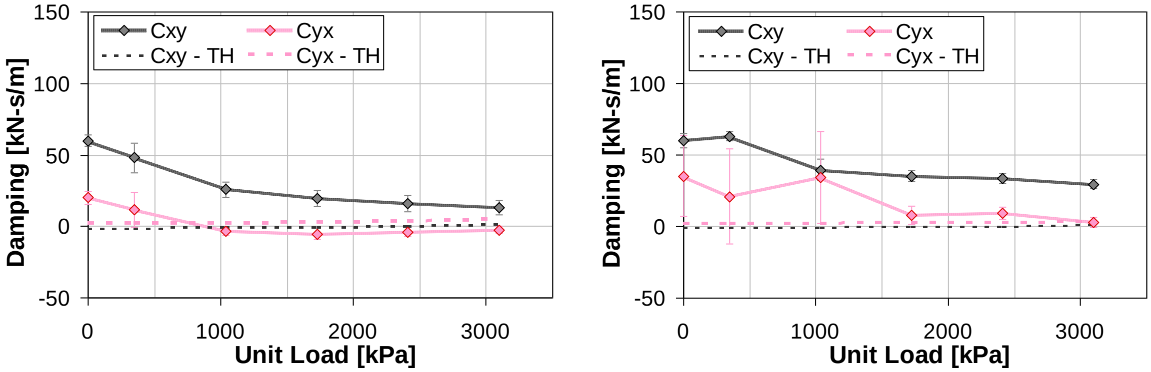

(c) 13 krpm **(d) 16 krpm**

Figure 46. 60% offset cross-coupled damping coefficients at: (a) 7 krpm, (b) 10 krpm, (c) 13 krpm, (d) 16 krpm.

Figure 46 shows that adequate experimental cross-coupled damping coefficients were obtained for most test conditions. C_{yx} is near zero for most test conditions, matching well with predictions. When C_{yx} does have a considerable magnitude, it has the same sign as C_{xy}. Large C_{yx} values were obtained for the light load cases of 16 krpm, but these results have large uncertainties as seen in Figure 46 (d). C_{xy} matches better with predictions low speeds, but is considerably under predicted at higher speeds. For all test conditions, both indirect damping coefficients were smaller than the direct coefficients presented above in Figure 45.

50 and 60% Offset Damping Comparison

Figure 47 compares the experimental direct damping coefficients of the 50 and 60% pivot offsets.

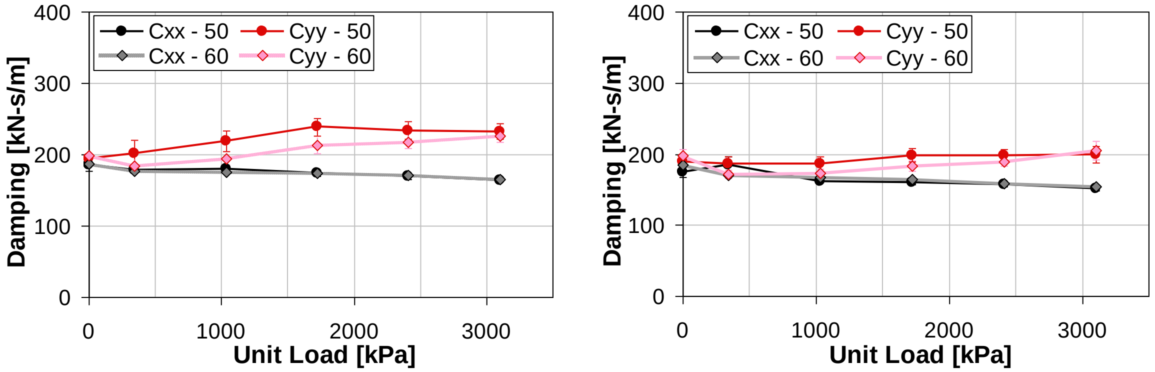

(a) 7 krpm **(b) 10 krpm**

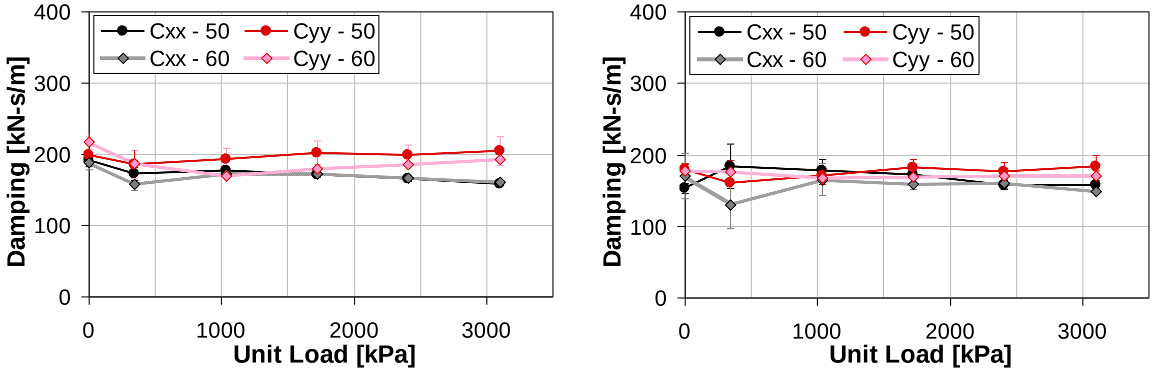

(c) 13 krpm **(d) 16 krpm**

Figure 47. 50 and 60% offset direct damping coefficients at: (a) 7 krpm, (b) 10 krpm, (c) 13 krpm, (d) 16 krpm.

As seen above, no appreciable difference arises in direct damping between 50 and 60% offsets for most test conditions. Regardless of offset, the direct damping coefficients show a small dependency on unit load or running speed. For the 7 krpm case shown in Figure 47, C_{yy} shows a slight increase while C_{xx} decreases with increasing unit load for both pivot offsets. C_{yy} decreases with increasing speed and becomes comparable to C_{xx} at 16 krpm.

The experimental cross-coupled added-mass coefficients for the 50 and 60% offsets are compared below in Figure 48.

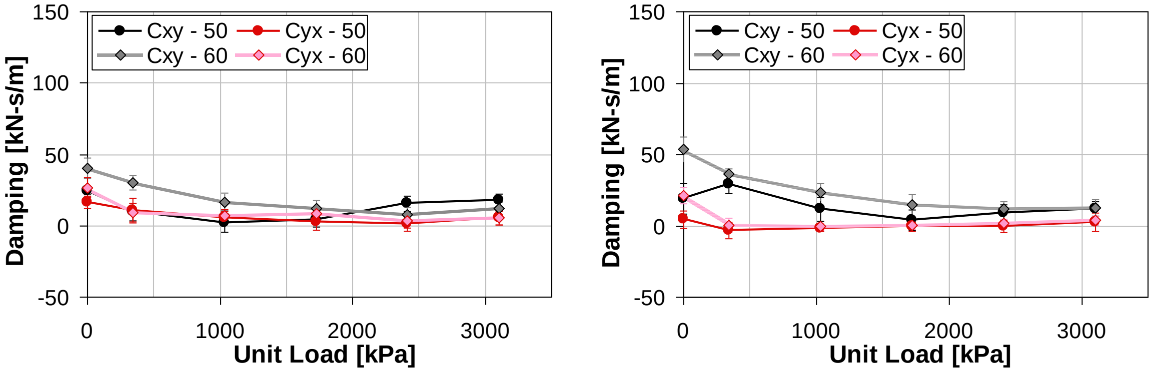

(a) 7 krpm

(b) 10 krpm

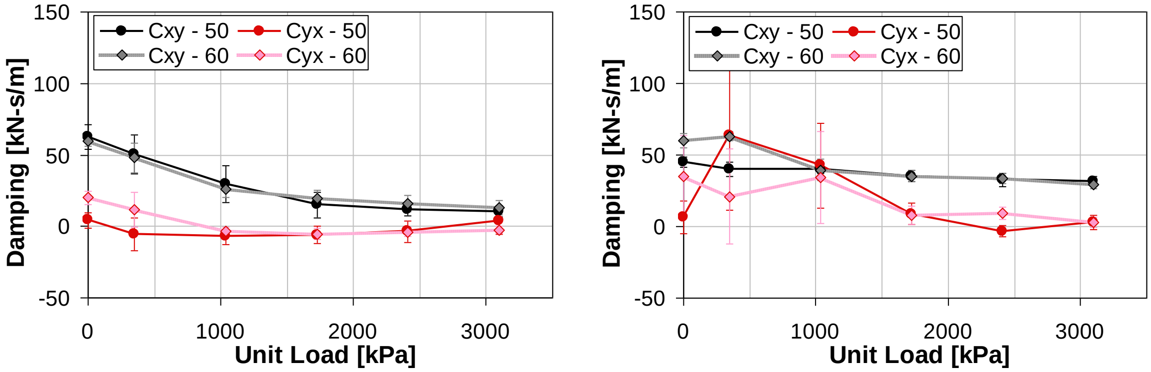

(c) 13 krpm

(d) 16 krpm

Figure 48. 50 and 60% offset cross-coupled damping coefficients at: (a) 7 krpm, (b) 10 krpm, (c) 13 krpm, (d) 16 krpm.

As with the direct coefficients, the cross-coupled damping coefficients do not show a significant difference between pivot offsets. Both offsets show C_{xy} to be consistently larger than C_{yx} for the higher test speeds and that C_{yx} is usually near zero for most speeds and loads.

Added-Mass Coefficients

All added-mass coefficients are estimated from the slope of the least squares regression of the real part of the dynamic stiffness. Experimental and predicted added-mass coefficients are plotted for each pivot offset, followed by a comparison of experimental results between 50 and 60% offsets.

50% Offset Added Mass

The experimental added mass coefficients for the 50% pivot offset are given below in Figure 49. As mentioned earlier, direct added mass predictions are not provided for the 50% offset because the theoretical direct stiffnesses fit the quadratic curve of a [K][C][M] model poorly.

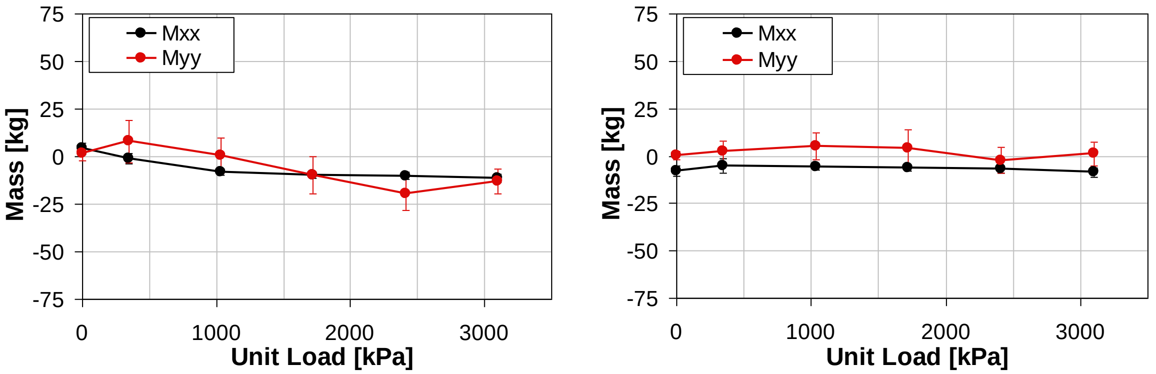

(a) 7 krpm **(b) 10 krpm**

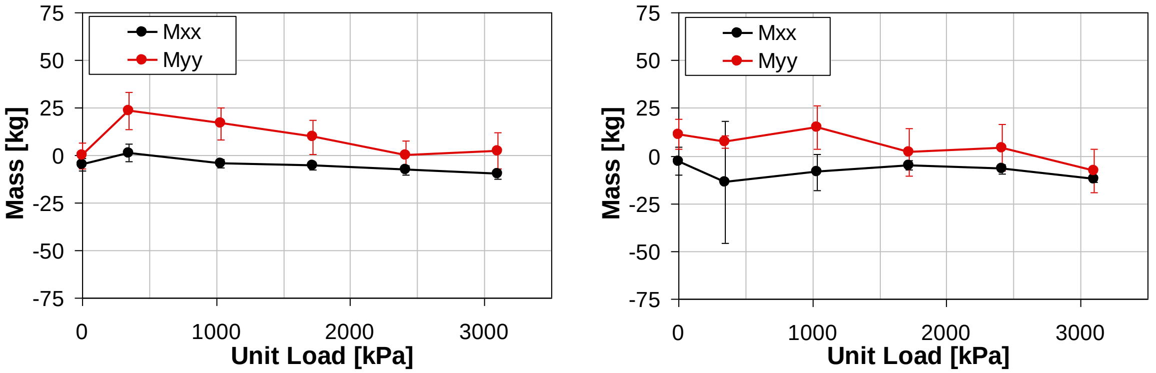

(c) 13 krpm **(d) 16 krpm**

Figure 49. 50% offset direct mass coefficients at: (a) 7 krpm, (b) 10 krpm, (c) 13 krpm, (d) 16 krpm.

The figure above shows the unloaded direction added mass, M_{xx}, is always negative, with the largest magnitude approaching 15 kg. Alternatively, M_{yy} coefficients are negative and positive, with the largest value near 25 kg. Over the majority of the test conditions, M_{yy} is consistently more positive (or less negative) than M_{xx}.

Figure 50 provides experimental and theoretical cross-coupled added-mass coefficients for the 50% pivot offset.

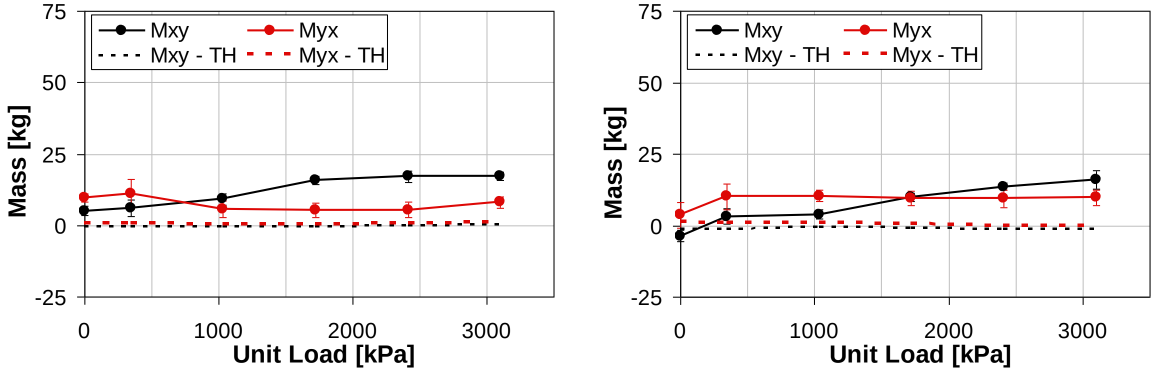

(a) 7 krpm **(b) 10 krpm**

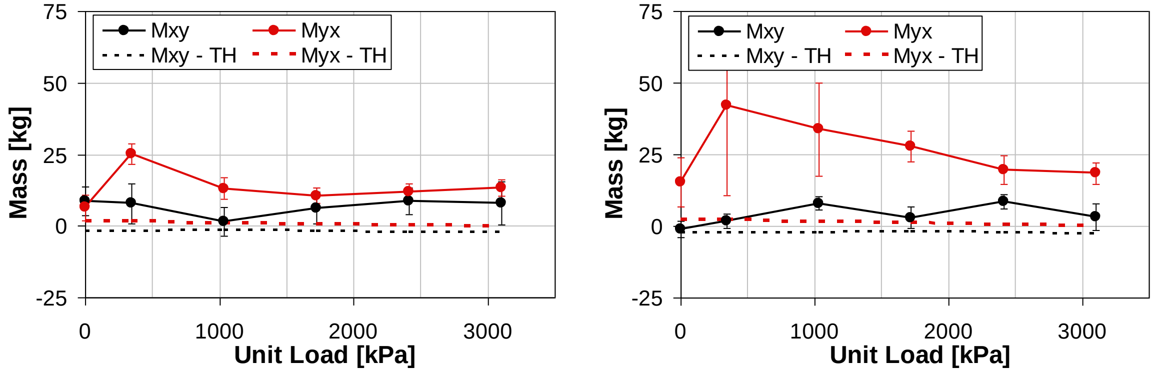

(c) 13 krpm **(d) 16 krpm**

Figure 50. 50% offset cross-coupled mass coefficients at: (a) 7 krpm, (b) 10 krpm, (c) 13 krpm, (d) 16 krpm.

As seen above, M_{xy} and M_{yx} are positive for the majority of the test cases and larger than the near-zero predictions. Generally, the coefficients are both the same sign, showing no effect on stability. Excluding 16 krpm, both coefficients are less than 25 kg. As seen in Figure 50 (d), larger M_{yx} values are obtained at 16 krpm but have very large uncertainties.

60% Offset Added Mass

The experimental and predicted added-mass coefficients are given below in Figure 51 for the 60% pivot offset.

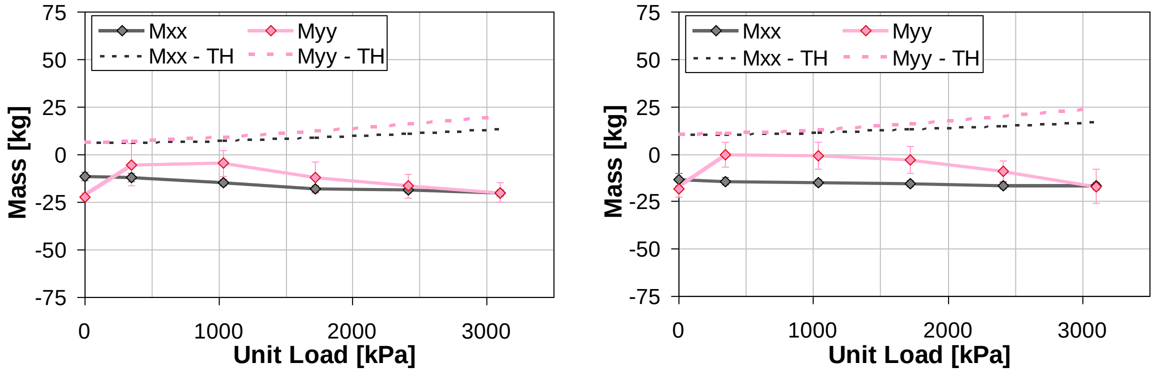

(a) 7 krpm **(b) 10 krpm**

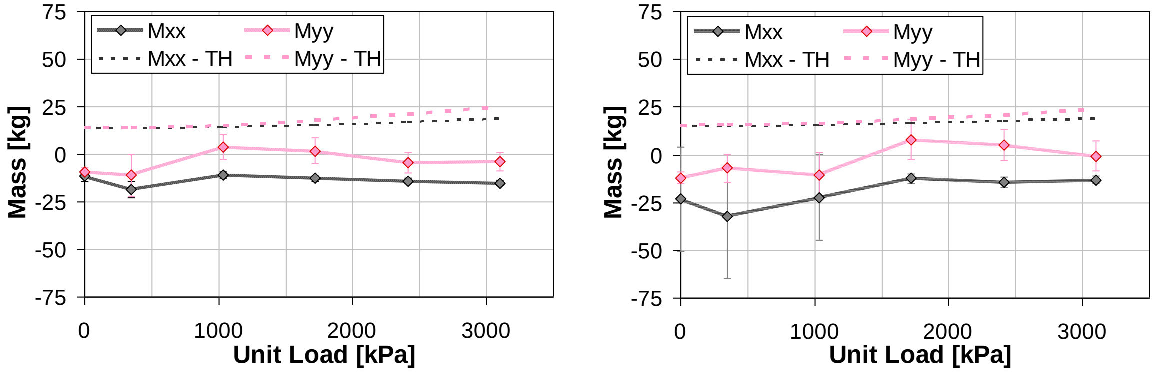

(c) 13 krpm **(d) 16 krpm**

Figure 51. 60% offset direct mass coefficients at: (a) 7 krpm, (b) 10 krpm, (c) 13 krpm, (d) 16 krpm.

Figure 51 shows that both experimental M_{xx} and M_{yy} are usually negative or approximately zero. In contrast, the code predicts positive added-mass coefficients that approach 25 kg. The experimental M_{xx} is always negative and has a similar magnitude as the predicted value. M_{yy} is usually negative or near zero, lower in magnitude than M_{xx}.

Figure 52 provides experimental and theoretical M_{xy} and M_{yx} coefficients for the 50% pivot offset.

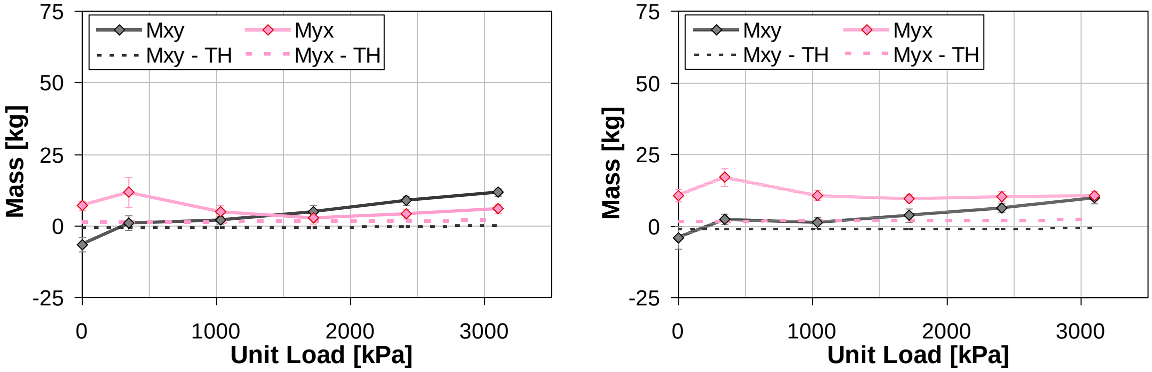

(a) 7 krpm **(b) 10 krpm**

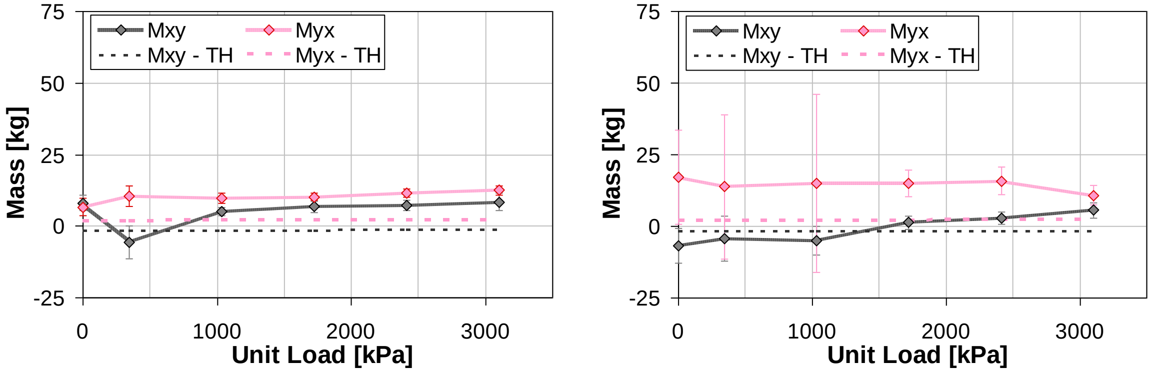

(c) 13 krpm **(d) 16 krpm**

Figure 52. 60% offset cross-coupled mass coefficients at: (a) 7 krpm, (b) 10 krpm, (c) 13 krpm, (d) 16 krpm.

In contrast to the direct added-mass coefficients which are mostly negative, the cross-coupled coefficients shown above are negative and positive. For the higher loaded test cases, M_{xy} and M_{yx} are both positive. At light loads, the coefficients have opposite signs where M_{xy} is negative and M_{yx} is positive, implying an impact on stability. The predictions are about zero for all test conditions while the experimental coefficients reach values near 20 kg. Aside from 7 krpm case, M_{yx} is usually larger than M_{xy}.

50 and 60% Offset Added Mass Comparison

M_{xx} and M_{yy} coefficients for the 50 and 60% pivot offsets are compared below in Figure 53.

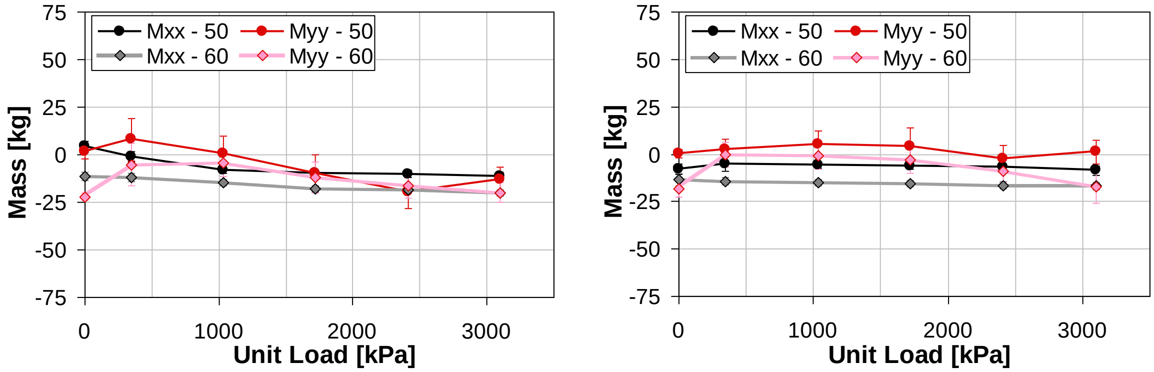

(a) 7 krpm **(b) 10 krpm**

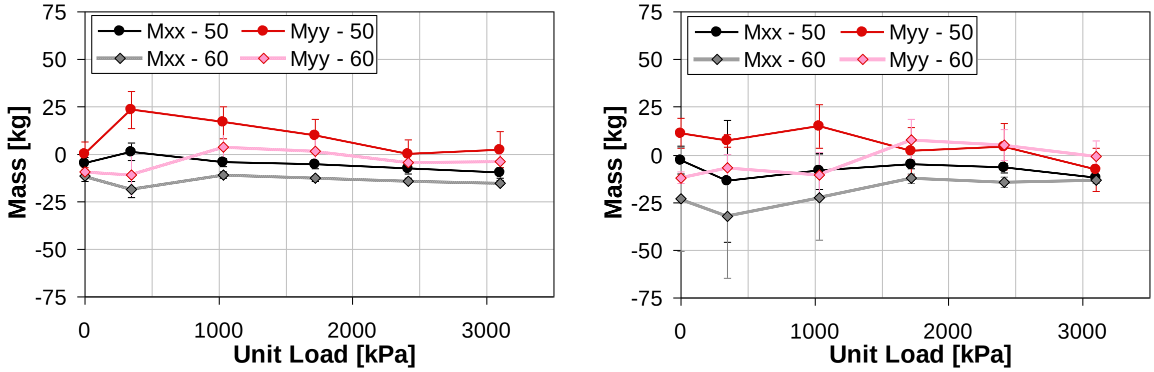

(c) 13 krpm **(d) 16 krpm**

Figure 53. 50 and 60% offset direct mass coefficients at: (a) 7 krpm, (b) 10 krpm, (c) 13 krpm, (d) 16 krpm.

For the given test conditions, M_{xx} and M_{yy} are slightly more positive (or less negative) for the 50% offset than for the 60%. For both offsets, M_{yy} is more positive than M_{xx}. From these observations, the largest positive added-mass coefficients are usually the 60% offset M_{yy} while the most negative added-mass term is typically M_{xx} of the 50% offset.

Figure 54 provides the experimental M_{xy} and M_{yx} values for the 50 and 60% pivot offsets.

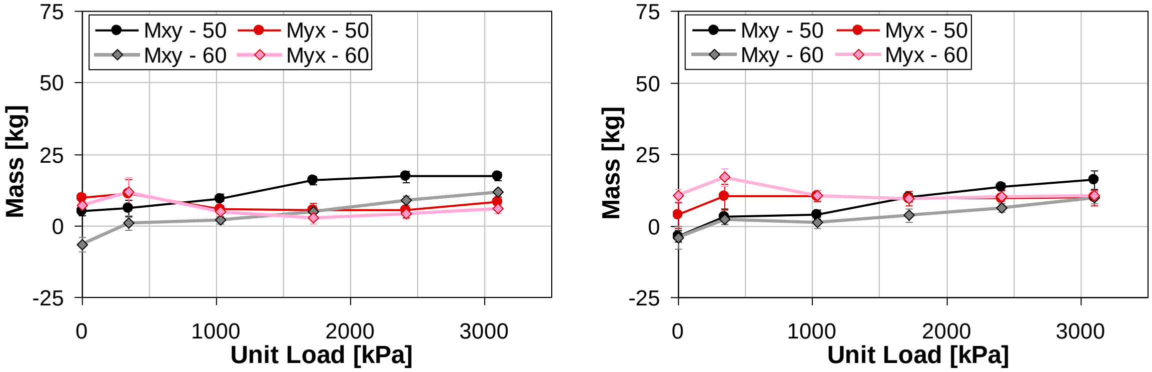

(a) 7 krpm **(b) 10 krpm**

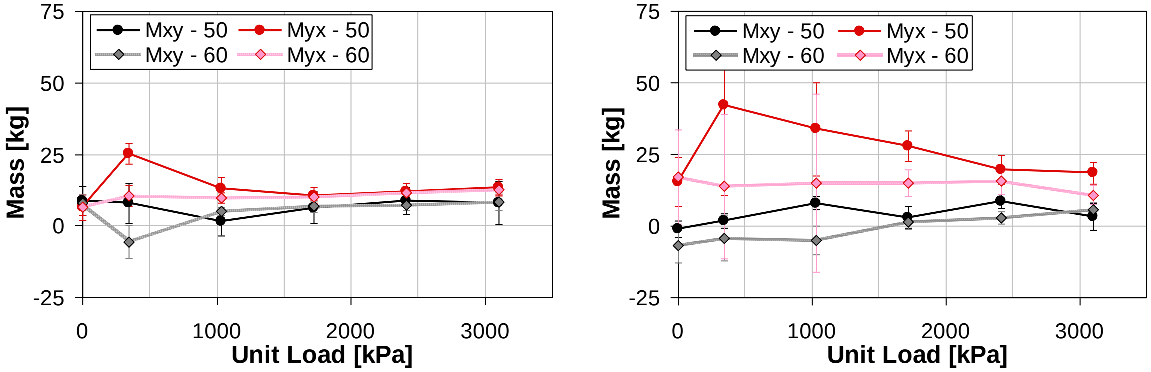

(c) 13 krpm **(d) 16 krpm**

Figure 54. 50 and 60% offset cross-coupled mass coefficients at: (a) 7 krpm, (b) 10 krpm, (c) 13 krpm, (d) 16 krpm.

The above figure shows that M_{xy} and M_{yx} are comparable for both pivot offsets. Over most test conditions, M_{xy} and M_{yx} are mostly positive and are typically less than 25 kg for both the 50 and 60% offset. Additionally, M_{xy} and M_{yx} usually have the same sign, showing no impact on stability.

Static Versus Dynamic Stiffness

The static stiffness, K_s, provides a stiffness value in the loaded direction that is derived from the static load and eccentricity. K_s provides a benchmark to compare the stiffness coefficient K_{yy} that was obtained from a dynamic test. Ideally, these coefficients should be the same. Figure 55 compares the dynamic and static stiffness coefficients for the 50% offset bearing.

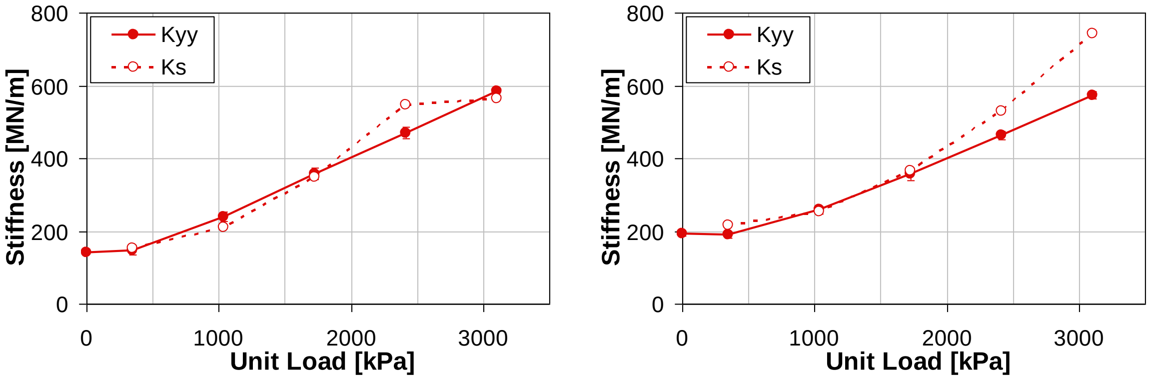

(a) 7 krpm **(b) 10 krpm**

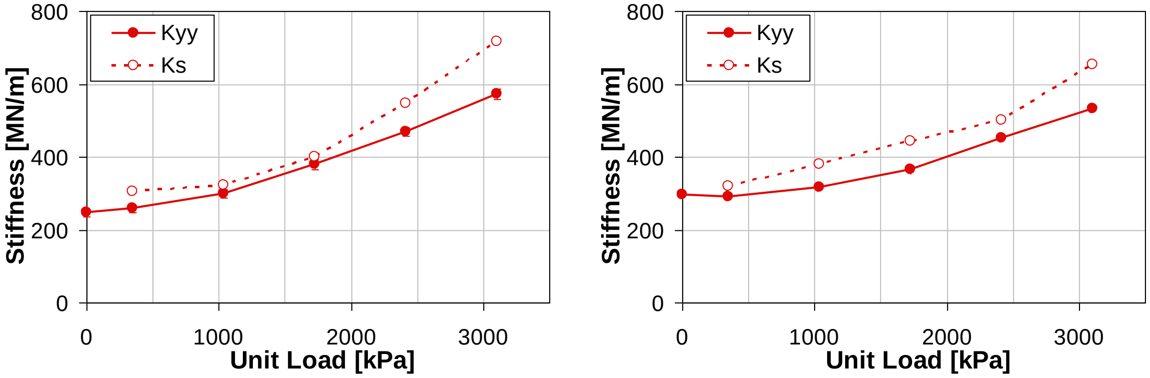

(c) 13 krpm **(d) 16 krpm**

Figure 55. 50% offset static and dynamic stiffness coefficients at: (a) 7 krpm, (b) 10 krpm, (c) 13 krpm, (d) 16 krpm.

As seen above in Figure 55 (a), K_{yy} and K_s agree very well at 7 krpm. At higher rotor speeds, the coefficients agree well at light unit loads, but diverge at high loads with K_s becoming larger than K_{yy}.

The static and dynamic stiffness coefficients for the 60% pivot offset are given below in Figure 56.

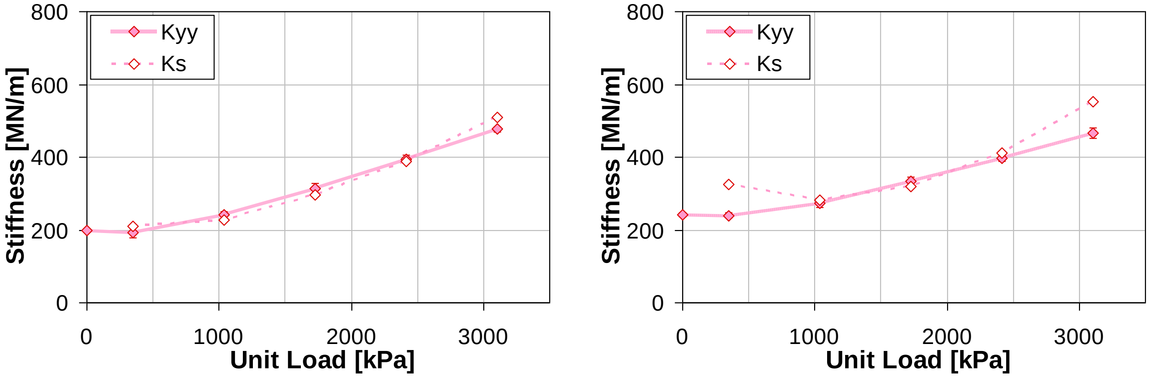

(a) 7 krpm **(b) 10 krpm**

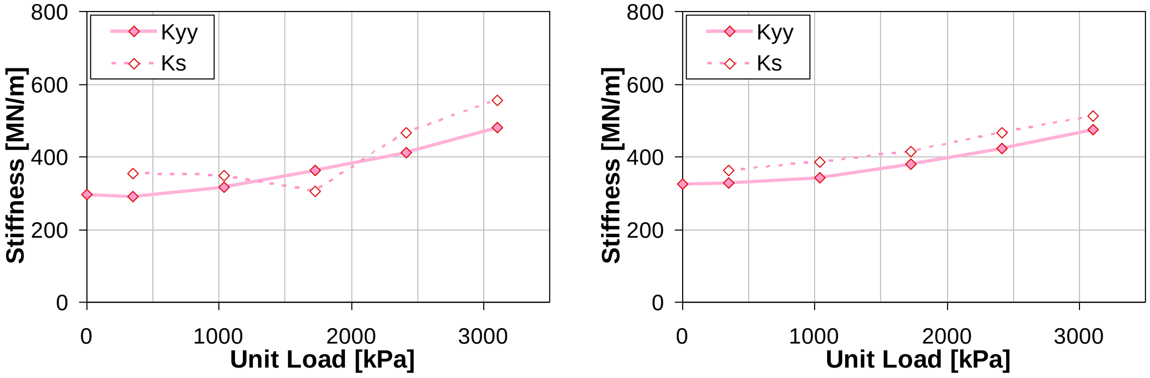

(c) 13 krpm **(d) 16 krpm**

Figure 56. 60% offset static and dynamic stiffness coefficients at: (a) 7 krpm, (b) 10 krpm, (c) 13 krpm, (d) 16 krpm.

Figure 56 shows that K_s matches well with K_{yy} at 7 krpm, and shows some divergence at higher speeds and loads. These 60% offset results are similar to those for the 50% offset presented earlier.

Multiple factors can contribute to the discrepancies between static and dynamic stiffness coefficients, including the thermal expansion or distortion of the bearing stator and rotor. Recall that the proximity probes are attached to the stator that holds the test bearing. During testing, the stator assembly and the shaft can experience some expansion because of the elevated temperatures. This could impact the steady state eccentricity measurements, and thus impact the static stiffness measurement.

Currently, there is no accurate method to quantify the impact of elevated temperatures. While thermal effects can impact motion measurements between test conditions, these effects do not impact the relative motion measurements that are taken at each steady-state condition, i.e., when dynamic testing dynamic stiffness. Hence, K_{yy} is the more accurate measurement of the direct stiffness coefficient for the loaded direction.

SUMMARY AND DISCUSSION

The static and dynamic characteristics are presented for a 5-pad, rocker-pivot tilting-pad journal bearing with 50 and 60% pivot offsets in LBP configuration. Tests were conducted using a floating bearing test rig at multiple speed and load conditions. Experimental data were compared to predictions from a bulk flow NS bearing code.

Static Characteristics

The static results presented for the test bearing included the measured clearance, eccentricity, attitude angle, pad temperatures, and estimated power loss. Measured bearing clearances showed that the actual clearances for both pivot offsets had non-symmetry, more so for the 60% pivot offset.

The measured eccentricity loci plots showed that cross-coupled stiffness exists for both pivot offsets, with negligible difference between offsets. Static eccentricities were modeled well with light unit loads and become over predicted at higher loads. Attitude angles increased with increasing ω, approaching 10° at 16 krpm. Predicted attitude angles agreed best at low rotor speeds.

Pad temperatures were only recorded for the 50% offset and show that the loaded pads consistently have the highest temperatures. For increasing ω, all pad temperatures increase approximately the same amount. As unit load increases, the temperatures of the loaded pads increase while the unloaded pad temperatures decrease. Furthermore, the maximum pad temperatures occurred approximately 75% along the second loaded pad. The maximum bearing temperature was under predicted by about 15 to 20 °C for most test cases.

Power losses were under predicted for both offsets at most test conditions. The experimental power loss estimations increased with increasing ω and showed a negligible dependence on unit load. Additionally, the 50% offset bearing generally had larger experimental power losses than the 60% offset. This trend agrees with the temperature results of Delgado et al. [29]. They measured higher bearing temperatures for 50% offset than for a 60% offset.

Dynamic Characteristics

Rotordynamic coefficients including stiffness, damping, and added-mass coefficients were determined from measured complex dynamic stiffnesses. For both offsets, the direct and cross-coupled real parts of the dynamic stiffness exhibited frequency dependency that could be accounted for with added-mass coefficients. This resulted in frequency independent stiffness and added-mass coefficients. The imaginary parts of the measured dynamic stiffness increased linearly with increasing Ω for both offsets, allowing for frequency-independent damping coefficients. Overall, the frequency dependency of the test bearing was well modeled with the [K][C][M] model for all test conditions and for both pivot offsets.

For many test conditions, the direct dynamic stiffnesses showed an increase with increasing frequency that could be accounted for with negative added-mass coefficients. This "hardening" effect is indicative of a spring in series with spring-damper combination as shown below in Figure 57.

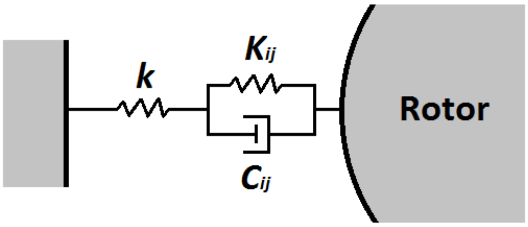

Figure 57. Spring in series with a fluid film model.

Here, the damper-spring combination represents the fluid film stiffness and damping while the single spring represents the pivot-support stiffness of the bearing. This system can be described in terms of an equivalent stiffness and damping coefficients. The Taylor expansion of the equivalent stiffness indicates that stiffness will increase with increasing excitation frequency. The measured Re($\boldsymbol{H}_{xx}$) and Re($\boldsymbol{H}_{yy}$) of the test bearings often followed this trend, suggesting that pivot stiffness could be important. Additionally, the expansion of equivalent damping shows a damping decrease or fall off with increasing frequency. The experimental damping from the test bearings did not indicate any frequency dependency and thus does not support pivot-support stiffness.

Direct stiffness coefficients for both pivot offsets were predicted well at light loads but became increasingly over predicted with increasing load. Unpredicted stiffness orthotropy existed for each pivot offset at zero unit loads. At low static loads, the direct stiffness coefficients were larger for the 60% offset configuration than for the 50% offset. For large loads, K_{xx} was about the same for each offset while K_{yy} was larger for the 50% offset. Experimental cross-coupled stiffness coefficients were positive and considerably smaller than the direct stiffness coefficients for both offsets. Predicted cross-coupled stiffness coefficients were approximately zero.

The direct damping coefficients obtained from testing were mostly constant with respect to unit load and slight dependency with ω. The experimental direct damping coefficients are relatively constant compared to the predictions which increased substantially with increasing unit load. The code predicted the 50% offset bearing to have frequency-dependent direct damping coefficients, while 60% offset predictions were frequency-independent. The direct damping coefficients were predicted best for light loads and at the highest test speed. Experimental cross-coupled damping coefficients were obtained for each pivot offset and were considerably smaller than the direct damping. C_{xy} and C_{yx} were positive for both pivot offsets, implying real and positive damping. Experimental direct and cross-coupled damping coefficients did not show an appreciable change with respect to the tested pivot offsets.

Added-mass coefficients for both offsets were able to capture the frequency dependency of the measured dynamic stiffness at all test conditions. For both pivot offsets, M_{xx} was consistently negative and M_{yy} was usually more positive. Direct added-mass *predictions* were not reported for 50% offset because the theoretical direct stiffnesses showed a frequency dependency that could not be captured by an added mass term. For the 60% offset, predicted direct added-mass coefficients were always positive while experimental coefficients were much smaller and negative. Comparing offsets, both direct added-mass coefficients were more positive (less negative) for the 50% offset. The cross-coupled added-mass coefficients obtained from testing were positive for both pivot offsets while the predictions were approximately zero. M_{xy} and M_{yx} were generally the same sign for both offsets, indicating no impact on stability. The largest added-mass magnitudes approached values near 32 kg.

Although the 60% offset bearing in this thesis is almost identical to that tested by Carter [24], the dynamic stiffnesses and rotordynamic coefficients showed differences that are credited to the updated motion probe location used for the current testing. The direct stiffness and damping coefficients presented in this thesis were typically 10 to 25% lower than those presented by Carter. The new probe setup also produced M_{xx} and M_{yy} values that were negative and small in magnitude compared to Carter's M_{xx} and M_{yy} values. K_{xy} and K_{yx} obtained in this thesis were typically both positive while Carter's K_{xy} and K_{yx} values had opposite signs. Additionally, the current test setup allows for meaningful estimates for C_{xy} and C_{yx}. All of these discussed differences with Carter's data agreed with the dynamic tests given in Appendix F that compares motion probe locations.

Overall, the dynamic stiffnesses and rotordynamic coefficients in this thesis agreed with the test results of Delgado et al. [29]. At light unit loading, the direct stiffness coefficients in this thesis were considerably larger for the 60% offset than the 50% offset, comparable to Delgado et al.. Additionally, Delgado et al. did not observe an appreciable difference in direct damping for different pivot offsets, similar to the direct damping presented in this thesis. Delgado et al. obtained positive and negative direct added-mass coefficients with the largest magnitude approaching 23 kg, comparable to the values given in this thesis.

REFERENCES

[1] Lund, J.W., 1964, "Spring and Damping Coefficients for the Tilting-Pad Journal Bearing," ASLE Trans., **7** (3), pp. 342-352.

[2] Al-Ghasem, A., 2004, "Measurement of Rotordynamic Coefficients for High Speed Flexure-Pivot Tilting-Pad Bearing (Load Between Pad) Configuration," M.S. thesis, Texas A&M University, College Station, TX.

[3] Nicholas, J.C., 1994, "Tilt Pad Bearing Design," *Proceedings of the 23rd Turbomachinery Symposium*, Houston, TX, pp. 179-194.

[4] Hargreaves, D. and Fillon, M., 2007, "Analysis of Tilting Pad Journal Bearing to Avoid Pad Fluttering," Tribology International, **40**, pp. 607-612.

[5] Kirk, R. G. and Reedy, S.W., 1988, "Evaluation of Pivot Stiffness for Typical Tilting-Pad Journal Bearing Designs," ASME Journal of Vibration, Acoustics, and Reliability in Design, **110**, pp. 165-171.

[6] Nicholas, J.C., 2003, "Lund's Tilting Pad Journal Bearing Assembly Method," ASME J. Vib. Accoust., **125** (4), pp. 448-454.

[7] Shapiro, W., and Colsher, R., 1977, "Dynamic Characteristics of Fluid Film Bearings," *Proceedings of the 6th Turbomachinery Symposium*, Houston, TX, pp. 39-53.

[8] Jones, G. J., and Martin, F.A., 1979, "Geometry Effects of Tilting-Pad Journal Bearings," ASLE Trans., **22** (3), pp. 227-244.

[9] Nicholas, J. C., Gunter, E.J., and Allaire, P.E., 1979, "Stiffness and Damping Coefficients for the Five Pad Tilting Pad Bearing," ASLE Trans., **22** (2), pp. 112-124.

[10] Nicholas, J. C., Gunter, E.J., and Barrett, L.E., 1978, "The Influence of Tilting Pad Bearing Characteristics on the Stability of High Speed Rotor-Bearing Systems," *Topics in Fluid Film Bearing and Rotor Bearings System Design and Optimization*, ASME Publication, pp. 55-78.

[11] Parsell, J.K., Allaire, P.E., Barrett, L.E., 1983, "Frequency Effects in Tilting-Pad Journal Bearing Dynamic Coefficients," ASLE Trans., **26**, pp. 222-227.

[12] Barrett, L. E., Allaire, P.E., and Wilson, B.W., 1988, "The Eigenvalue Dependence of Reduced Tilting Pad Bearing Stiffness and Damping Coefficients," ASLE Trans., **31**, pp. 411-419.

[13] White, M.F., and Chan, S.H., 1992, "The Subsynchronous Dynamic Behavior of Tilting-Pad Journal Bearings," ASME J. Tribol., **114**, pp. 167-173.

[14] Brockett, T.S., and Barrett, L.E., 1993, "Exact Dynamic Reduction of Tilting-Pad Bearing Models for Stability Analyses," STLE Trib. Trans., **36**, pp. 581-588.

[15] Ha, H., and Yang, S., 1999, "Excitation Frequency Effects on the Stiffness and Damping Coefficients of a Five-Pad Tilting Pad Journal Bearing," ASME J. Tribol., **121**, pp. 517-522.

[16] Wygant, K. D., 2001 "The Influence of Negative Preload and Nonsynchronous Excitation on the Performance of Tilting Pad Journal Bearings," Ph.D. Dissertation, University of Virginia, Charlottesville, VA.

[17] Ikeda, K., Hirano, T., Yamashita, T., Mikami, M., and Sakakida, H., 2004, "An Experimental Study of Static and Dynamic Characteristics of a 580mm (22.8in) Diameter Direct Lubrication Tilting Pad Journal Bearing," *ASME/STLE International Joint Tribology Conference*, October 24-27, Long Beach, CA.

[18] Rodriguez, L., and Childs, D., 2006, "Frequency Dependency of Measured and Predicted Rotordynamic Coefficients for Load-on-Pad Flexible-Pivot Tilting-Pad Bearing," ASME J. Tribol., **128** (2), pp. 388-395.

[19] Al-Ghasem, A., and Childs, D., 2006, "Measurements Versus Predictions for a High-Speed Flexure-Pivot Tilting-Pad Bearing (Load-Between-Pad Configuration)," ASME J. Eng. Gas Turbines Power, **128** (4), pp. 896-906.

[20] Hensley, E. J., and Childs, D., 2008, "Measurements versus Predictions for the Rotordynamic Characteristics of a Flexure Pivot-Pad Tilting Pad Bearing in an LBP Condition at Higher Unit Loads," *Proceedings of ASME Turbo Expo 2008,* Paper GT2008-50069, June 9-13, Berlin, Germany.

[21] Childs, D., and Hale, K., 1994, "A Test Apparatus and Facility to Identify the Rotordynamic Coefficients of High-Speed Hydrostatic Bearings," ASME J. of Trib., **116**, pp. 337-344.

[22] Dmochowski, W., 2006, "Dynamic Properties of Tilting-Pad Journal Bearings: Experimental and Theoretical Investigation of Frequency Effects Due to Pivot Flexibility," *ASME Turbo Expo 2006: Power for Land, Sea and Air*. Barcelona, Spain.

[23] Carter, C., and Childs, D., 2008 "Measurements versus Predictions for the Rotordynamic Characteristics of a 5-Pad, Rocker-Pivot, Tilting-Pad Bearing in Load Between Pad Configuration," *Proceedings of ASME Turbo Expo 2008*, Paper GT2008-50069, June 9-13, Berlin, Germany.

[24] Carter, C., 2007, "Measured and Predicted Rotordynamic Coefficients and Static Performance of a Rocker-Pivot, Tilt Pad Bearing in Load-on-Pad and Load-Between-Pad Configurations," M.S. thesis, Texas A&M University, College Station, TX.

[25] Childs, D., and Harris, J., 2009, "Static Performance Characteristics and Rotordynamic Coefficients for a Four-Pad Ball-in-Socket Tilting Pad Journal Bearing," ASME J. Eng. Gas Turbines Power, **131**, 062502.

[26] Schmeid, J., Fedorov, A., and Grigoriev, B., 2010, "Non-Synchronous Tilting Pad Bearing Characteristics," *Proceedings of the 10th IFToMM International Conference on Rotordynamics,* September 12-15, Seoul, Korea.

[27] Delgado, A., Ertas, B., Drexel M., Naldi, L., and Vannini, G., 2010, "A Component Level Test Rig for Dynamic Characterization of Oil Lubricated Bearings Using Different Input Excitations," *Proceedings of ISROMAC Thirteenth International*

Symposium on Transport Phenomena and Dynamics of Rotating Machinery, April 4-9, Honolulu, Hawaii.

[28] Kaul, A., 1999, “Design and Development of a Test Setup for the Experimental Determination of the Rotordynamic and Leakage Characteristics of Annular Bushing Oil Seals,” M.S. thesis, Texas A&M University, College Station, TX.

[29] Delgado, A., Ertas, B., Drexel M., Naldi, L., and Vannini, G., 2010, “Identification and Prediction of Force Coefficients in a Five-Pad and Four-Pad Tilting Pad Bearing for Load-on-Pad and Load-Between-Pad Configurations,” *Proceedings of ASME Turbo Expo 2010*, Paper GT2010-23802, June 14-18, Glasgow, UK.

[30] Nicholas, J.C., 2003, “Tilting Pad Journal Bearings with Spray-Bar Blockers and By-Pass Cooling for High Speed, High Load Applications,” *Proceedings of the 32nd Turbomachinery Symposium*, Houston, TX, pp. 27-37.

[31] Glienicke, J., 1966, “Experimental Investigation of Stiffness and Damping Coefficients of Turbine Bearings and Their Application to Instability Predictions,” Proceedings of the International Mech. E., **181** (3B), pp. 116-129.

[32] Ball, J. H., and Byrne, T.R., 1998, “Tilting Pad Hydrodynamic Bearing for Rotating Machinery”, Patent Number 5,795,076, Orion Corporation, Grafton, Wisconsin.

[33] Rouvas, C., and Childs, D., 1993, “A parameter Identification Method for the Rotordynamic Coefficients of a High Reynolds Number Hydrostatic Bearing,” ASME J. of Vibration and Acoustics, **115**, pp. 264-270.

[34] San Andres, L. A., 1995, “Bulk-Flow Analysis of Flexure and Tilting Pad Fluid Film Bearings,” TRC-B&C-3-95. Turbomachinery Laboratory, Texas A&M University, College Station, TX.

[35] Szeri, A., 1987, “Some Extensions of the Lubrication Theory of Osborne Reynolds,” ASME J. Tribol., **109**, pp. 21-36.

[36] Reinhardt, E., and Lund, L., 1975, “The Influence of Fluid Inertia on the Dynamic Properties of Journal Bearings,” ASME J. of Lubrication Technology, **97**, pp. 159-167.

[37] Rodriguez, L., 2004, “Experimental Frequency-Dependent Rotordynamic Coefficients for a Load-on-Pad, High Speed, Flexible-Pivot Tilting-Pad Bearing,” M.S. thesis, Texas A&M University, College Station, TX.

APPENDIX A: MEASURED TEST CONDITIONS

Table 10. 50% offset measured test conditions, Reynolds numbers, and estimated power loss.

NOMINAL TEST CONDITIONS					*MEASURED TEST CONDITIONS*					*MEASURED VALUES*					*CALCULATED VALUES*									
Running Speed	**Unit Load**		**Flowrate**		**Running Speed**	**Unit Load**		**Flowrate**		**P_{in}**	**P_{in}**	**T_{in}**	**T_{out}**	**$T_{in-out,\ ave}$**	**ρ_{in}**	**ρ_{out}**	**$c_{p,in}$**	**$c_{p,out}$**	**μ_{ave}**	**μ_{Tout}**	**Sommerfeld Number [-]**	**Reynolds Number [-]**	**Squeeze Reynolds Number [-]**	**Estimated Power Loss [kW]**
[rpm]	**[kPa]**	**[Psi]**	**[gpm]**	**[m^3/s]**	**[rpm]**	**[kPa]**	**[Psi]**	**[gpm]**	**[m^3/s]**	**[psi]**	**[kPa]**	**[°C]**	**[°C]**	**[°C]**	**[kg/m^3]**	**[kg/m^3]**	**[J/kg-K]**	**[J/kg-K]**	**[Pa-s]**	**[Pa-s]**				
7000	0	0	5.5	3.5E-04	7006	11	2	5.4	3.4E-04	19.0	131	44.0	58.6	51.3	854.2	844.5	1962	2015	0.0183	0.0147	-	174.29	0.77	8.9
	345	50	5.5	3.5E-04	7048	367	53	5.5	3.5E-04	19.9	137	43.6	57.9	50.8	854.4	845.0	1961	2013	0.0186	0.0150	2.32	170.73	0.75	8.9
	1034	150	5.5	3.5E-04	7153	1011	147	5.4	3.4E-04	19.8	137	43.7	58.8	51.2	854.4	844.4	1961	2016	0.0183	0.0146	0.84	175.45	0.77	9.2
	1723	250	5.5	3.5E-04	7073	1713	248	5.5	3.5E-04	20.9	144	43.7	59.7	51.7	854.4	843.8	1961	2019	0.0181	0.0142	0.49	179.78	0.79	9.8
	2412	350	5.5	3.5E-04	7082	2392	347	5.5	3.5E-04	21.4	148	43.5	60.7	52.1	854.5	843.1	1960	2023	0.0178	0.0138	0.34	185.39	0.81	10.6
	3101	450	5.5	3.5E-04	7051	3082	447	5.5	3.5E-04	22.0	152	43.6	61.0	52.3	854.4	843.0	1961	2024	0.0178	0.0137	0.26	186.68	0.82	10.8
10000	0	0	5.5	3.5E-04	10054	11	2	5.5	3.5E-04	20.9	144	43.5	62.7	53.1	854.5	841.8	1960	2030	0.0173	0.0130	-	281.04	0.86	11.9
	345	50	5.5	3.5E-04	10124	334	48	5.6	3.5E-04	21.5	148	43.5	62.2	52.8	854.5	842.1	1960	2028	0.0175	0.0132	3.44	276.75	0.85	11.7
	1034	150	5.5	3.5E-04	10071	1017	148	5.6	3.5E-04	22.1	152	43.7	62.3	53.0	854.4	842.1	1961	2028	0.0174	0.0131	1.12	277.21	0.85	11.6
	1723	250	5.5	3.5E-04	10076	1698	246	5.5	3.5E-04	22.5	155	43.6	64.4	54.0	854.5	840.7	1961	2036	0.0169	0.0123	0.65	295.17	0.91	12.9
	2412	350	5.5	3.5E-04	10087	2379	345	5.6	3.5E-04	23.3	160	43.7	65.1	54.4	854.4	840.2	1961	2039	0.0166	0.0121	0.46	301.55	0.93	13.4
	3101	450	5.5	3.5E-04	10118	3083	447	5.5	3.5E-04	24.1	166	43.7	65.9	54.8	854.3	839.7	1961	2042	0.0164	0.0118	0.35	308.52	0.95	13.9
13000	0	0	8.0	5.0E-04	13170	7	1	7.9	5.0E-04	37.1	256	43.8	66.5	55.2	854.3	839.3	1962	2044	0.0163	0.0116	-	407.77	0.96	20.3
	345	50	8.0	5.0E-04	13088	357	52	7.9	5.0E-04	37.2	256	44.0	65.3	54.6	854.2	840.1	1962	2039	0.0166	0.0120	3.94	393.54	0.93	19.1
	1034	150	8.0	5.0E-04	13151	1004	146	7.9	5.0E-04	37.5	259	43.7	64.7	54.2	854.4	840.5	1961	2037	0.0168	0.0122	1.43	387.10	0.92	18.8
	1723	250	8.0	5.0E-04	13104	1718	249	7.9	5.0E-04	38.1	263	43.7	64.6	54.1	854.4	840.6	1961	2037	0.0168	0.0123	0.83	385.49	0.91	18.7
	2412	350	8.0	5.0E-04	13113	2405	349	7.9	5.0E-04	38.8	268	43.8	65.2	54.5	854.3	840.2	1961	2039	0.0166	0.0121	0.59	392.19	0.93	19.1
	3101	450	8.0	5.0E-04	13115	3105	450	7.9	5.0E-04	39.3	271	43.5	65.5	54.5	854.5	840.0	1960	2040	0.0166	0.0120	0.46	395.55	0.94	19.5
16000	0	0	10.0	6.3E-04	16006	-7	-1	9.9	6.2E-04	52.7	363	44.2	69.6	56.9	854.1	837.2	1963	2055	0.0155	0.0105	-	549.80	1.06	28.5
	345	50	10.0	6.3E-04	15813	349	51	9.9	6.2E-04	52.8	364	43.5	68.6	56.1	854.5	837.9	1960	2051	0.0159	0.0109	4.66	533.42	1.03	28.0
	1034	150	10.0	6.3E-04	15874	1017	147	9.9	6.2E-04	53.4	368	43.6	68.3	55.9	854.4	838.1	1961	2050	0.0159	0.0110	1.61	528.85	1.02	27.5
	1723	250	10.0	6.3E-04	16305	1722	250	9.9	6.2E-04	54.0	372	43.6	69.3	56.4	854.4	837.5	1961	2054	0.0157	0.0107	0.96	544.22	1.05	28.7
	2412	350	10.0	6.3E-04	16002	2413	350	9.9	6.2E-04	54.4	375	43.4	68.8	56.1	854.6	837.7	1960	2052	0.0158	0.0108	0.68	537.63	1.03	28.5
	3101	450	10.0	6.3E-04	15946	3102	450	9.9	6.2E-04	55.1	380	43.5	69.8	56.7	854.5	837.1	1960	2056	0.0156	0.0105	0.52	552.81	1.06	29.4

Table 11. 60% offset measured test conditions, Reynolds numbers, and estimated power loss.

NOMINAL TEST CONDITIONS					*MEASURED TEST CONDITIONS*					*MEASURED VALUES*					*CALCULATED VALUES*									
Running Speed	**Unit Load**		**Flowrate**		**Running Speed**	**Unit Load**		**Flowrate**		**P_{in}**	**P_{in}**	**T_{in}**	**T_{out}**	**$T_{in\text{-}out,\ ave}$**	**ρ_{in}**	**ρ_{out}**	**$c_{p,in}$**	**$c_{p,out}$**	**μ_{ave}**	**μ_{Tout}**	**Sommerfeld Number [-]**	**Reynolds Number [-]**	**Squeeze Reynolds Number [-]**	**Estimated Power Loss [kW]**
[rpm]	**[kPa]**	**[Psi]**	**[gpm]**	**[m^3/s]**	**[rpm]**	**[kPa]**	**[Psi]**	**[gpm]**	**[m^3/s]**	**[psi]**	**[kPa]**	**[°C]**	**[°C]**	**[°C]**	**[kg/m^3]**	**[kg/m^3]**	**[J/kg-K]**	**[J/kg-K]**	**[Pa-s]**	**[Pa-s]**				
7000	0	0	5.5	3.5E-04	7025	9	1	5.4	3.4E-04	18.8	129	43.9	54.4	49.2	854.2	847.3	1962	2000	0.0195	0.0167	-	158.48	0.72	6.4
	345	50	5.5	3.5E-04	6988	350	51	5.5	3.5E-04	19.6	135	44.0	54.5	49.3	854.1	847.2	1962	2000	0.0194	0.0166	2.39	158.75	0.72	6.4
	1034	150	5.5	3.5E-04	7066	1021	148	5.5	3.5E-04	20.0	138	43.8	54.5	49.1	854.3	847.2	1961	2000	0.0195	0.0166	0.83	158.76	0.72	6.6
	1723	250	5.5	3.5E-04	7107	1705	247	5.5	3.5E-04	20.6	142	43.8	55.0	49.4	854.3	846.9	1961	2002	0.0194	0.0164	0.50	161.34	0.73	6.9
	2412	350	5.5	3.5E-04	7062	2393	347	5.5	3.5E-04	21.2	146	43.7	55.5	49.6	854.3	846.5	1961	2004	0.0192	0.0161	0.35	163.84	0.74	7.2
	3101	450	5.5	3.5E-04	7009	3083	447	5.5	3.4E-04	21.8	150	43.7	56.4	50.0	854.4	846.0	1961	2007	0.0190	0.0157	0.27	167.78	0.76	7.7
10000	0	0	5.5	3.5E-04	10052	8	1	5.4	3.4E-04	20.8	143	44.2	60.1	52.1	854.0	843.5	1963	2020	0.0178	0.0140	-	267.25	0.85	9.7
	345	50	5.5	3.5E-04	9985	329	48	5.4	3.4E-04	21.1	145	43.9	59.8	51.8	854.3	843.7	1962	2019	0.0180	0.0142	3.36	264.85	0.84	9.7
	1034	150	5.5	3.5E-04	10017	1017	148	5.4	3.4E-04	21.6	149	43.9	60.0	52.0	854.2	843.6	1962	2020	0.0179	0.0141	1.08	266.80	0.84	9.8
	1723	250	5.5	3.5E-04	10050	1708	248	5.4	3.4E-04	21.8	150	44.0	60.2	52.1	854.2	843.4	1962	2021	0.0178	0.0140	0.64	268.35	0.85	9.8
	2412	350	5.5	3.5E-04	9994	2396	347	5.4	3.4E-04	22.3	154	43.8	60.6	52.2	854.3	843.2	1961	2022	0.0178	0.0138	0.46	271.52	0.86	10.2
	3101	450	5.5	3.5E-04	10033	3085	447	5.5	3.5E-04	23.3	161	44.0	62.5	53.2	854.2	841.9	1962	2029	0.0173	0.0131	0.34	286.74	0.91	11.4
13000	0	0	8.0	5.0E-04	12993	4	1	8.1	5.1E-04	37.7	260	43.9	62.1	53.0	854.2	842.2	1962	2028	0.0174	0.0132	-	369.19	0.90	16.6
	345	50	8.0	5.0E-04	12991	352	51	8.1	5.1E-04	38.1	263	43.9	62.2	53.1	854.2	842.1	1962	2028	0.0173	0.0132	3.93	370.22	0.90	16.6
	1034	150	8.0	5.0E-04	12935	1020	148	8.1	5.1E-04	38.6	266	43.7	62.1	52.9	854.4	842.2	1961	2028	0.0174	0.0132	1.36	369.00	0.90	16.9
	1723	250	8.0	5.0E-04	12884	1722	250	8.1	5.1E-04	39.3	271	43.8	62.6	53.2	854.3	841.9	1962	2030	0.0173	0.0130	0.79	374.16	0.91	17.2
	2412	350	8.0	5.0E-04	13013	2396	348	8.1	5.1E-04	39.8	274	43.9	64.2	54.0	854.3	840.8	1962	2035	0.0168	0.0124	0.56	391.82	0.95	18.6
	3101	450	8.0	5.0E-04	12990	3100	450	8.2	5.2E-04	40.8	281	44.0	62.9	53.4	854.2	841.7	1962	2031	0.0172	0.0129	0.44	377.01	0.92	17.5
16000	0	0	10.0	6.3E-04	15986	-5	-1	10.0	6.3E-04	54.0	372	43.9	68.4	56.1	854.3	838.0	1962	2051	0.0158	0.0109	-	545.45	1.08	27.7
	345	50	10.0	6.3E-04	15994	368	53	10.0	6.3E-04	54.2	374	43.8	68.3	56.0	854.3	838.1	1961	2050	0.0159	0.0110	4.24	543.30	1.07	27.6
	1034	150	10.0	6.3E-04	16031	1021	148	10.0	6.3E-04	54.5	376	44.2	69.2	56.7	854.1	837.5	1963	2054	0.0156	0.0107	1.50	558.96	1.11	28.3
	1723	250	10.0	6.3E-04	16028	1715	249	9.9	6.3E-04	54.8	378	44.1	67.2	55.7	854.1	838.8	1962	2046	0.0160	0.0113	0.92	527.52	1.04	26.1
	2412	350	10.0	6.3E-04	16064	2402	348	9.9	6.3E-04	55.3	381	44.0	66.1	55.0	854.2	839.6	1962	2042	0.0164	0.0117	0.67	509.45	1.01	24.8
	3101	450	10.0	6.3E-04	15959	3078	446	9.9	6.3E-04	55.6	383	43.9	65.3	54.6	854.2	840.1	1962	2039	0.0166	0.0120	0.53	497.85	0.98	23.9

APPENDIX B: MEASURED ECCENTRICITY

Table 12. 50% offset measured eccentricity and attitude angle.

Running Speed [rpm]	Unit Loading [kPa]	Unit Loading [psi]	*US Customary Units*						*Metric Units*						ε_X [-]	ε_Y [-]	ε_o [-]	φ [deg]
			X_{NTS} [mils]	Y_{NTS} [mils]	X_{TS} [mils]	Y_{TS} [mils]	$e_{X,ave}$ [mils]	$e_{Y,ave}$ [mils]	X_{NTS} [μm]	Y_{NTS} [μm]	X_{TS} [μm]	Y_{TS} [μm]	$e_{X,ave}$ [μm]	$e_{Y,ave}$ [μm]				
7000	0	0	1.08	-0.61	1.07	-1.03	1.07	-0.82	27.38	-15.42	27.17	-26.04	27.27	-20.73	0.00	0.00	0.00	-
	345	50	1.15	-0.01	1.05	-0.51	1.10	-0.26	29.28	-0.14	26.80	-12.85	28.04	-6.49	0.01	0.17	0.18	3.08
	1034	150	1.19	0.76	1.07	0.22	1.13	0.49	30.15	19.22	27.14	5.55	28.65	12.39	0.02	0.41	0.41	2.37
	1723	250	1.19	1.23	1.07	0.71	1.13	0.97	30.34	31.30	27.23	18.09	28.78	24.70	0.02	0.56	0.56	1.90
	2412	350	1.24	1.55	1.10	1.00	1.17	1.27	31.59	39.29	27.89	25.36	29.74	32.32	0.03	0.65	0.65	2.66
	3101	450	1.39	1.88	1.20	1.26	1.29	1.57	35.20	47.76	30.48	31.91	32.84	39.84	0.07	0.74	0.75	5.25
10000	0	0	1.11	-0.64	1.12	-0.96	1.12	-0.80	28.09	-16.13	28.55	-24.30	28.32	-20.22	0.00	0.00	0.00	-
	345	50	1.21	-0.21	1.09	-0.66	1.15	-0.44	30.73	-5.44	27.71	-16.75	29.22	-11.10	0.01	0.11	0.11	5.61
	1034	150	1.23	0.42	1.14	0.00	1.19	0.21	31.25	10.77	29.06	-0.02	30.16	5.38	0.02	0.31	0.32	4.11
	1723	250	1.25	0.89	1.16	0.43	1.20	0.66	31.70	22.56	29.38	10.95	30.54	16.75	0.03	0.45	0.46	3.43
	2412	350	1.28	1.23	1.18	0.71	1.23	0.97	32.50	31.12	29.91	18.15	31.20	24.64	0.04	0.55	0.55	3.68
	3101	450	1.30	1.49	1.19	0.91	1.24	1.20	33.02	37.85	30.21	23.04	31.61	30.45	0.04	0.62	0.62	3.72
13000	0	0	1.07	-0.61	1.21	-0.86	1.14	-0.74	27.21	-15.49	30.64	-21.88	28.92	-18.69	0.00	0.00	0.00	-
	345	50	1.16	-0.27	1.18	-0.65	1.17	-0.46	29.39	-6.82	29.97	-16.50	29.68	-11.66	0.01	0.09	0.09	6.15
	1034	150	1.30	0.30	1.17	-0.25	1.23	0.03	32.92	7.59	29.71	-6.24	31.32	0.67	0.03	0.24	0.24	7.05
	1723	250	1.35	0.76	1.22	0.15	1.29	0.46	34.40	19.39	31.10	3.83	32.75	11.61	0.05	0.37	0.38	7.20
	2412	350	1.39	1.10	1.24	0.42	1.32	0.76	35.39	27.93	31.59	10.67	33.49	19.30	0.06	0.47	0.47	6.86
	3101	450	1.42	1.30	1.28	0.69	1.35	1.00	36.11	33.05	32.58	17.50	34.34	25.27	0.07	0.54	0.54	7.03
16000	0	0	1.06	-0.67	1.11	-1.03	1.09	-0.85	27.03	-17.08	28.21	-26.06	27.62	-21.57	0.00	0.00	0.00	-
	345	50	1.15	-0.36	1.14	-0.80	1.15	-0.58	29.20	-9.17	29.00	-20.31	29.10	-14.74	0.02	0.08	0.09	12.26
	1034	150	1.28	0.16	1.14	-0.47	1.21	-0.16	32.63	4.05	29.06	-12.02	30.84	-3.99	0.04	0.22	0.22	10.39
	1723	250	1.37	0.57	1.19	-0.12	1.28	0.23	34.87	14.50	30.15	-2.97	32.51	5.76	0.06	0.34	0.34	10.15
	2412	350	1.45	0.89	1.24	0.23	1.34	0.56	36.77	22.55	31.54	5.87	34.16	14.21	0.08	0.44	0.45	10.35
	3101	450	1.46	1.13	1.25	0.49	1.36	0.81	37.13	28.82	31.83	12.51	34.48	20.66	0.08	0.52	0.53	9.23

Table 13. 60% offset measured eccentricity and attitude angle.

Running Speed [rpm]	Unit Loading [kPa]	Unit Loading [psi]	*US Customary Units*						*Metric Units*						ε_X [-]	ε_Y [-]	ε_o [-]	φ [deg]
			X_{NTS} [mils]	Y_{NTS} [mils]	X_{TS} [mils]	Y_{TS} [mils]	$e_{X,ave}$ [mils]	$e_{Y,ave}$ [mils]	X_{NTS} [µm]	Y_{NTS} [µm]	X_{TS} [µm]	Y_{TS} [µm]	$e_{X,ave}$ [µm]	$e_{Y,ave}$ [µm]				
7000	0	0	1.47	-0.83	1.37	-1.62	1.42	-1.23	37.41	-21.19	34.86	-41.06	36.14	-31.12	0.00	0.00	0.00	-
	345	50	1.52	-0.42	1.38	-1.25	1.45	-0.83	38.60	-10.65	35.02	-31.75	36.81	-21.20	0.01	0.12	0.12	3.88
	1034	150	1.56	0.33	1.36	-0.56	1.46	-0.12	39.63	8.34	34.67	-14.35	37.15	-3.01	0.01	0.34	0.34	2.07
	1723	250	1.58	0.91	1.35	-0.03	1.46	0.44	40.03	23.06	34.25	-0.72	37.14	11.17	0.01	0.51	0.51	1.36
	2412	350	1.59	1.36	1.33	0.37	1.46	0.87	40.38	34.53	33.91	9.46	37.15	22.00	0.01	0.63	0.63	1.09
	3101	450	1.63	1.73	1.33	0.66	1.48	1.19	41.28	43.93	33.85	16.71	37.57	30.32	0.02	0.73	0.73	1.34
10000	0	0	1.43	-0.73	1.38	-1.57	1.40	-1.15	36.35	-18.52	34.98	-39.95	35.66	-29.23	0.00	0.00	0.00	-
	345	50	1.44	-0.44	1.30	-1.39	1.37	-0.91	36.50	-11.10	32.98	-35.34	34.74	-23.22	-0.01	0.07	0.07	-8.74
	1034	150	1.54	0.22	1.27	-0.88	1.41	-0.33	39.14	5.71	32.30	-22.23	35.72	-8.26	0.00	0.25	0.25	0.16
	1723	250	1.65	0.77	1.36	-0.38	1.50	0.19	41.93	19.63	34.43	-9.77	38.18	4.93	0.03	0.41	0.41	4.21
	2412	350	1.68	1.18	1.40	0.01	1.54	0.60	42.76	30.00	35.48	0.30	39.12	15.15	0.04	0.53	0.53	4.45
	3101	450	1.75	1.54	1.41	0.25	1.58	0.90	44.38	39.11	35.83	6.47	40.10	22.79	0.05	0.62	0.62	4.88
13000	0	0	1.46	-0.64	1.41	-1.60	1.43	-1.12	37.05	-16.14	35.85	-40.68	36.45	-28.41	0.00	0.00	0.00	-
	345	50	1.55	-0.33	1.37	-1.44	1.46	-0.88	39.37	-8.30	34.84	-36.50	37.10	-22.40	0.01	0.07	0.07	6.24
	1034	150	1.65	0.18	1.39	-1.02	1.52	-0.42	41.96	4.62	35.38	-25.87	38.67	-10.62	0.03	0.21	0.21	7.12
	1723	250	1.63	0.76	1.36	-0.48	1.50	0.14	41.45	19.30	34.65	-12.28	38.05	3.51	0.02	0.38	0.38	2.88
	2412	350	1.67	1.13	1.40	-0.15	1.53	0.49	42.48	28.64	35.46	-3.85	38.97	12.40	0.03	0.49	0.49	3.54
	3101	450	1.72	1.45	1.42	0.14	1.57	0.79	43.69	36.76	36.05	3.53	39.87	20.14	0.04	0.58	0.58	4.03
16000	0	0	1.30	-0.71	1.31	-1.80	1.31	-1.26	33.15	-18.06	33.18	-45.72	33.17	-31.89	0.00	0.00	0.00	-
	345	50	1.37	-0.46	1.37	-1.56	1.37	-1.01	34.68	-11.63	34.78	-39.55	34.73	-25.59	0.02	0.08	0.08	13.95
	1034	150	1.51	0.10	1.35	-1.30	1.43	-0.60	38.23	2.49	34.16	-32.97	36.20	-15.24	0.04	0.20	0.20	10.33
	1723	250	1.60	0.55	1.37	-0.95	1.49	-0.20	40.62	14.06	34.90	-24.03	37.76	-4.98	0.05	0.32	0.33	9.69
	2412	350	1.65	0.89	1.44	-0.58	1.55	0.16	42.02	22.73	36.70	-14.66	39.36	4.03	0.07	0.43	0.44	9.79
	3101	450	1.69	1.17	1.53	-0.22	1.61	0.48	42.82	29.84	38.83	-5.63	40.82	12.11	0.09	0.53	0.53	9.87

APPENDIX C: PAD METAL TEMPERATURES

Table 14. 50% offset pad metal temperatures.

Running Speed [rpm]	Unit Loading [kPa]	Unit Loading [psi]	T_{in} [°C]	T_{out} [°C]	*Pad Temperatures (°C)*																				*Uncertainties for Pad Temperatures (°C)*																			
					Pad 1 [°]					Pad 2 [°]						Pad 3 [°]					Pad 4 [°]		Pad 5 [°]		Pad 1 [°]					Pad 2 [°]						Pad 3 [°]					Pad 4 [°]		Pad 5 [°]	
					11	42	50	56	61	83	99	114	122	128	133	155	186	194	200	205	227	266	299	338	11	42	50	56	61	83	99	114	122	128	133	155	186	194	200	205	227	266	299	338
7000	0	0	44.0	58.6	53.8	60.8	62.9	62.5	64.5	54.5	59.0	62.7	65.3	64.8	66.3	52.7	59.5	61.6	60.8	62.5	54.7	63.6	53.3	62.9	0.3	0.3	0.3	0.3	0.3	0.3	0.3	0.3	0.3	0.4	0.4	0.2	0.2	0.3	0.2	0.2	0.2	0.1	0.2	0.3
	345	50	43.6	57.9	55.4	64.1	66.6	65.8	68.3	55.5	61.1	65.9	69.2	68.5	70.3	51.1	57.5	59.5	59.1	60.6	52.6	59.6	53.4	62.3	0.2	0.1	0.1	0.1	0.1	0.1	0.1	0.1	0.1	0.1	0.1	0.1	0.1	0.1	0.1	0.1	0.2	0.1	0.2	0.1
	1034	150	43.7	58.8	58.4	70.4	73.9	72.4	75.8	57.9	65.9	72.8	77.3	75.8	77.9	50.1	55.8	57.7	57.7	58.9	51.9	56.7	54.1	62.4	0.2	0.1	0.1	0.1	0.2	0.2	0.1	0.1	0.2	0.1	0.2	0.2	0.2	0.2	0.2	0.2	0.7	0.2	0.3	0.2
	1723	250	43.7	59.7	60.8	76.5	80.7	78.0	82.0	59.6	69.8	78.6	83.8	81.4	83.4	49.5	54.9	56.5	56.8	57.9	51.2	55.1	54.3	62.5	0.3	0.4	0.5	0.4	0.5	0.4	0.5	0.6	0.7	0.8	0.8	0.4	0.5	0.5	0.4	0.5	0.9	0.5	0.4	0.6
	2412	350	43.5	60.7	62.9	81.7	86.4	82.3	86.5	60.9	72.8	83.2	88.9	85.4	87.0	49.2	54.6	56.0	56.6	57.5	50.6	54.3	54.3	62.6	0.2	0.2	0.2	0.2	0.5	0.3	0.3	0.4	0.6	1.0	1.0	0.5	0.5	0.6	0.4	0.4	0.5	0.3	0.4	0.4
	3101	450	43.6	61.0	65.1	86.5	91.2	85.8	89.8	61.9	75.5	87.2	93.0	88.5	89.4	49.2	54.5	56.1	56.6	57.5	50.8	53.8	54.5	62.9	0.2	0.4	0.5	0.3	0.5	0.2	0.2	0.2	0.2	0.3	0.1	0.1	0.2	0.2	0.1	0.2	0.3	0.3	0.3	0.3
10000	0	0	43.5	62.7	57.3	66.8	69.6	69.1	71.7	58.4	64.3	69.3	72.9	72.3	74.5	56.2	65.6	68.3	67.1	69.7	58.2	70.3	56.7	69.7	0.5	0.5	0.6	0.6	0.7	0.5	0.5	0.6	0.7	0.7	0.9	0.5	0.5	0.6	0.5	0.6	0.2	0.2	0.4	0.4
	345	50	43.5	62.2	58.5	69.2	72.4	71.4	74.5	59.2	65.9	71.9	76.3	75.6	78.1	55.4	64.7	67.4	66.6	68.8	57.3	67.4	57.1	69.5	0.2	0.2	0.3	0.3	0.3	0.2	0.2	0.2	0.3	0.4	0.4	0.3	0.5	0.5	0.4	0.5	0.3	0.3	0.2	0.4
	1034	150	43.7	62.3	61.3	74.9	79.1	76.9	81.2	61.3	70.2	78.7	84.6	83.3	86.3	54.0	62.9	65.4	65.4	67.1	56.2	63.4	57.7	69.0	0.1	0.2	0.2	0.1	0.1	0.1	0.1	0.1	0.1	0.1	0.1	0.1	0.1	0.1	0.1	0.1	0.2	0.2	0.1	0.1
	1723	250	43.6	64.4	63.4	80.6	85.9	82.4	87.7	63.1	74.5	85.5	92.7	90.3	93.3	53.0	61.5	63.8	64.5	65.9	55.7	61.4	58.0	69.1	0.2	0.2	0.1	0.2	0.2	0.2	0.2	0.3	0.4	0.5	0.5	0.3	0.4	0.4	0.5	0.5	0.3	0.4	0.2	0.3
	2412	350	43.7	65.1	65.6	86.7	93.0	88.0	93.9	65.1	78.8	92.0	100.1	96.2	98.7	52.6	60.9	63.3	64.1	65.4	55.4	60.3	58.3	69.5	0.2	0.1	0.2	0.3	0.5	0.4	0.5	0.6	0.8	0.9	1.0	0.6	0.7	0.8	1.0	1.0	0.6	0.8	0.5	0.7
	3101	450	43.7	65.9	67.9	92.9	99.9	93.1	99.1	66.9	82.9	98.1	106.7	101.1	102.7	52.6	60.9	63.1	64.1	65.3	55.4	59.8	58.8	70.1	0.1	0.2	0.1	0.3	0.6	0.4	0.5	0.7	0.9	1.0	1.1	0.4	0.7	0.6	1.0	1.0	0.4	0.6	0.5	0.7
13000	0	0	43.8	66.5	60.6	73.1	76.7	74.8	78.3	61.5	69.3	75.9	80.8	79.7	82.5	58.8	70.9	74.3	72.7	75.8	61.8	77.9	59.9	77.0	0.2	0.2	0.3	0.3	0.3	0.2	0.2	0.3	0.3	0.3	0.3	0.1	0.2	0.3	0.4	0.4	0.2	0.2	0.1	0.3
	345	50	44.0	65.3	61.7	75.2	79.2	76.8	80.7	62.2	70.7	78.1	83.7	82.3	85.4	57.9	69.8	73.2	72.0	74.7	60.6	74.2	60.2	76.4	0.1	0.2	0.2	0.2	0.2	0.2	0.2	0.1	0.1	0.1	0.1	0.2	0.2	0.2	0.2	0.2	0.2	0.1	0.1	0.1
	1034	150	43.7	64.7	63.4	79.6	84.6	81.3	86.2	63.6	73.7	83.6	90.8	88.6	92.3	56.3	67.8	71.1	70.8	73.0	59.1	69.5	60.5	76.0	0.2	0.2	0.2	0.2	0.2	0.1	0.1	0.1	0.1	0.1	0.1	0.1	0.1	0.1	0.1	0.1	0.4	0.2	0.2	0.2
	1723	250	43.7	64.6	65.3	84.9	91.1	86.5	92.7	65.2	77.7	90.6	99.5	95.8	99.7	55.3	66.3	69.4	69.6	71.6	57.9	66.3	60.7	75.8	0.1	0.2	0.1	0.1	0.1	0.2	0.2	0.2	0.1	0.1	0.1	0.1	0.2	0.5	0.2	0.3	0.2	0.1	0.1	0.1
	2412	350	43.8	65.2	67.1	90.5	98.0	91.7	98.9	67.1	82.2	97.7	107.9	102.2	105.4	54.9	65.7	68.7	69.3	71.1	57.7	64.9	61.0	75.9	0.2	0.3	0.3	0.1	0.1	0.1	0.1	0.2	0.2	0.4	0.3	0.2	0.4	0.5	0.5	0.5	0.2	0.3	0.1	0.3
	3101	450	43.5	65.5	68.8	96.5	105.1	96.7	104.3	68.7	86.4	104.5	115.4	107.4	109.5	54.5	65.2	68.3	69.0	70.6	57.5	63.7	60.9	75.8	0.2	0.6	0.6	0.3	0.2	0.2	0.1	0.2	0.2	0.2	0.2	0.2	0.2	0.1	0.2	0.2	0.5	0.2	0.1	0.1
16000	0	0	44.2	69.6	61.8	75.1	79.0	76.2	81.1	62.1	70.7	78.2	83.9	82.6	86.3	61.2	74.8	78.9	76.9	80.6	63.6	80.8	61.8	81.3	0.2	0.1	0.2	0.2	0.4	0.2	0.3	0.2	0.1	0.1	0.3	0.2	0.4	0.4	0.3	0.5	0.1	0.3	0.2	0.1
	345	50	43.5	68.6	61.9	76.2	80.6	77.4	82.7	62.6	71.9	80.4	86.8	85.2	89.1	60.5	74.1	78.0	76.3	79.7	63.2	78.5	61.2	80.4	0.2	0.1	0.2	0.1	0.1	0.2	0.2	0.2	0.2	0.1	0.1	0.1	0.2	0.2	0.2	0.3	0.3	0.1	0.1	0.1
	1034	150	43.6	68.3	63.1	79.2	84.5	80.8	87.0	64.8	75.3	85.3	92.9	90.5	95.1	60.2	73.6	77.4	76.2	78.9	62.7	75.3	60.9	78.9	0.3	0.4	0.3	0.2	0.1	0.2	0.3	0.4	0.5	0.2	0.1	0.6	0.8	0.7	0.7	0.7	0.3	0.4	0.2	0.2
	1723	250	43.6	69.3	63.9	82.6	89.2	84.9	92.4	66.8	79.1	91.8	101.3	97.7	102.9	60.5	73.8	77.3	76.6	79.0	63.1	73.5	61.1	78.8	0.5	0.4	0.3	0.1	0.1	0.2	0.6	0.6	0.6	0.1	0.1	1.1	1.3	1.1	1.1	1.0	0.6	0.4	0.1	0.2
	2412	350	43.4	68.8	65.8	87.3	95.2	89.7	98.4	68.7	83.5	99.4	110.7	104.6	109.2	58.7	71.6	75.1	75.2	77.2	62.1	71.2	61.1	78.7	0.1	0.3	0.2	0.2	0.1	0.1	0.1	0.1	0.1	0.1	0.1	0.1	0.1	0.1	0.2	0.1	0.2	0.1	0.1	0.2
	3101	450	43.5	69.8	67.3	92.0	101.3	94.5	104.1	70.2	87.3	106.1	118.5	110.1	113.6	58.5	71.1	74.7	75.0	76.8	62.2	70.3	61.5	79.0	0.3	0.4	0.3	0.2	0.1	0.1	0.1	0.1	0.1	0.2	0.2	0.3	0.5	0.5	0.4	0.5	0.2	0.2	0.1	0.2

APPENDIX D: ROTORDYNAMIC COEFFICIENTS

Table 15. 50% offset experimental rotordynamic coefficients.

Running Speed [rpm]	Unit Loading [kPa]	Unit Loading [psi]	*Rotordynamic Coefficients*												*Uncertainties*											
			Stiffness [MN/m]				Damping [kN-s/m]				Added Mass [kg]				Stiffness [MN/m]				Damping [kN-s/m]				Added Mass [kg]			
			Kxx	Kxy	Kyx	Kyy	Cxx	Cxy	Cyx	Cyy	Mxx	Mxy	Myx	Myy	Kxx	Kxy	Kyx	Kyy	Cxx	Cxy	Cyx	Cyy	Mxx	Mxy	Myx	Myy
7000	0	0	117.0	4.4	27.0	142.1	185.0	24.6	16.4	194.1	4.2	5.1	9.7	1.4	4.1	2.3	1.9	4.8	7.6	2.4	4.1	5.8	3.0	1.7	1.5	3.7
	345	50	125.4	8.1	30.1	148.0	178.3	9.8	10.7	201.7	-1.0	5.9	11.0	8.0	3.4	3.7	6.6	13.8	3.1	6.1	8.4	18.6	2.6	2.9	5.3	11.1
	1034	150	162.8	22.3	39.7	239.9	179.1	2.1	5.9	218.6	-8.2	9.2	5.7	0.4	2.9	3.4	4.3	13.9	2.4	6.6	3.7	14.9	1.7	2.0	2.8	9.1
	1723	250	211.2	29.6	43.9	358.2	173.6	4.4	2.4	238.9	-9.7	15.7	5.3	-9.9	3.1	2.8	4.3	16.1	3.4	5.2	5.3	12.2	1.7	1.5	2.6	9.7
	2412	350	251.7	30.9	47.4	470.5	168.9	15.4	1.1	234.0	-10.2	17.1	5.4	-19.4	3.7	3.7	4.5	14.7	3.9	5.1	5.0	12.6	2.0	2.0	2.7	8.9
	3101	450	285.4	32.7	56.5	583.3	164.4	17.9	5.4	232.5	-11.3	17.1	8.1	-13.3	3.6	2.5	3.0	10.3	2.8	4.5	4.9	10.6	2.0	1.4	1.9	6.6
10000	0	0	157.8	-0.4	34.7	191.9	174.6	19.0	4.5	188.9	-7.9	-3.6	3.6	0.3	5.3	3.9	7.4	4.0	7.5	10.9	6.0	4.0	2.8	2.1	4.4	2.4
	345	50	164.6	6.0	38.4	189.4	185.0	29.1	-3.3	185.8	-5.0	3.2	10.2	2.2	6.5	4.6	7.0	8.8	11.0	6.7	5.5	11.2	3.7	2.6	4.5	5.6
	1034	150	193.5	16.1	53.3	258.2	162.1	11.6	-1.5	185.9	-5.8	4.0	10.4	5.1	3.0	2.8	3.1	10.7	2.0	8.5	2.5	10.5	1.8	1.7	2.0	7.2
	1723	250	232.9	28.5	59.6	356.4	160.2	3.7	-0.6	198.2	-6.1	10.0	9.6	4.2	3.1	2.8	4.1	16.2	2.9	7.3	3.0	9.6	1.7	1.5	2.5	9.8
	2412	350	271.5	35.9	65.4	462.4	157.3	8.8	-0.1	197.2	-7.1	13.6	9.5	-2.3	3.6	2.3	5.1	11.4	3.4	5.8	4.3	9.2	1.9	1.2	3.1	6.9
	3101	450	306.2	45.7	70.9	573.7	151.9	11.9	2.4	199.5	-8.6	16.0	9.8	1.3	4.2	5.8	4.3	10.1	3.1	4.9	6.2	11.8	2.4	3.3	2.7	6.3
13000	0	0	210.6	2.3	53.9	246.4	191.2	62.6	4.2	198.9	-4.9	8.5	6.4	-0.2	6.2	9.0	7.0	10.9	7.9	8.4	5.3	8.1	3.5	5.0	4.4	6.9
	345	50	217.0	6.7	63.2	257.6	171.8	50.2	-5.6	185.7	1.3	7.9	25.1	23.5	5.5	8.1	4.1	10.9	8.6	13.5	11.3	19.4	4.7	6.9	3.7	9.8
	1034	150	238.3	15.6	64.9	300.4	176.2	29.6	-7.3	193.1	-4.4	1.5	13.1	16.7	3.5	7.6	5.2	11.5	4.0	12.7	5.2	15.9	2.3	4.9	3.8	8.3
	1723	250	271.3	30.5	72.3	379.6	170.7	15.2	-5.9	202.1	-5.7	6.3	10.6	9.5	3.8	10.1	4.3	14.6	3.3	9.0	6.4	16.2	2.1	5.6	2.7	9.1
	2412	350	304.2	40.4	82.7	468.9	164.5	11.8	-3.7	198.7	-7.7	8.6	11.9	0.0	4.4	8.6	4.3	12.3	2.8	4.3	7.6	14.4	2.4	4.8	2.7	7.7
	3101	450	334.1	49.5	89.3	573.4	158.5	10.4	3.8	204.4	-9.8	7.9	13.3	2.3	4.9	12.5	4.3	14.0	2.3	3.9	9.3	20.3	2.9	7.4	2.9	9.4
16000	0	0	255.0	-1.4	72.9	295.1	153.3	45.0	6.4	178.4	-2.7	-1.0	15.4	11.3	6.6	2.5	7.5	6.8	7.6	3.5	11.7	9.8	7.5	2.9	8.5	7.7
	345	50	238.1	3.6	81.2	291.1	184.0	39.9	63.5	161.0	-13.9	1.8	42.0	7.4	25.9	2.0	25.3	2.6	31.1	5.1	51.8	5.2	32.1	2.4	31.4	3.2
	1034	150	267.6	4.2	85.5	316.8	177.8	39.9	42.5	169.8	-8.6	8.0	33.8	14.8	8.3	2.0	14.2	10.0	15.4	2.9	29.9	7.6	9.5	2.3	16.2	11.4
	1723	250	294.8	6.5	93.7	366.2	171.7	35.2	8.9	181.9	-5.0	3.0	27.8	1.9	2.8	4.4	6.1	13.8	10.5	4.0	7.6	10.8	2.5	3.9	5.4	12.2
	2412	350	322.2	24.3	100.2	452.1	157.2	32.6	-3.3	175.7	-6.9	8.7	19.7	4.3	2.3	2.4	4.9	11.7	5.0	4.4	4.0	13.1	2.3	2.5	5.1	12.1
	3101	450	345.0	31.1	107.1	533.7	156.9	31.5	3.2	183.9	-12.3	3.3	18.4	-7.7	1.8	5.3	4.2	13.0	3.9	3.5	5.0	15.7	1.6	4.7	3.8	11.5

Table 16. 60% offset experimental rotordynamic coefficients.

Running Speed [rpm]	Unit Loading [kPa]	Unit Loading [psi]	*Rotordynamic Coefficients*												*Uncertainties*											
			Stiffness [MN/m]				Damping [kN-s/m]				Added Mass [kg]				Stiffness [MN/m]				Damping [kN-s/m]				Added Mass [kg]			
			Kxx	Kxy	Kyx	Kyy	Cxx	Cxy	Cyx	Cyy	Mxx	Mxy	Myx	Myy	Kxx	Kxy	Kyx	Kyy	Cxx	Cxy	Cyx	Cyy	Mxx	Mxy	Myx	Myy
7000	0	0	172.7	9.9	46.7	197.8	187.3	40.4	26.8	197.9	-11.3	-6.5	7.0	-22.2	3.1	3.6	2.1	2.6	7.9	7.3	6.9	5.2	2.3	2.6	1.6	2.0
	345	50	175.8	15.0	48.4	192.8	177.1	30.0	9.3	183.9	-12.0	0.9	11.7	-5.3	2.7	3.1	6.4	13.1	4.6	5.0	6.6	9.7	2.1	2.5	5.3	11.0
	1034	150	199.1	28.4	54.3	240.7	175.0	16.8	7.3	194.0	-14.7	1.9	4.9	-4.5	2.6	2.1	3.1	9.9	3.4	5.9	4.2	8.7	1.6	1.3	2.1	6.9
	1723	250	227.3	44.9	65.3	314.7	173.2	12.4	8.5	212.6	-18.1	4.9	2.8	-12.0	2.8	3.6	3.5	12.4	2.4	5.4	3.6	11.4	1.6	2.1	2.3	8.1
	2412	350	258.1	54.1	70.1	394.5	170.4	7.9	3.2	217.8	-18.6	8.8	4.1	-16.5	2.9	2.9	2.7	10.7	2.5	5.1	4.6	9.3	1.5	1.6	1.6	6.4
	3101	450	286.6	54.7	71.2	476.8	165.3	12.0	5.4	226.4	-20.0	11.8	5.9	-20.0	2.7	2.2	2.5	8.1	2.5	4.6	4.8	8.4	1.5	1.2	1.6	5.1
10000	0	0	216.7	15.5	64.0	240.7	184.4	53.4	21.3	197.5	-13.3	-4.0	10.6	-18.2	4.5	5.2	2.9	5.5	5.1	9.2	5.9	8.5	3.4	3.9	2.3	4.3
	345	50	215.6	15.0	67.3	239.9	169.8	36.2	0.5	171.6	-14.2	2.4	17.0	-0.2	2.6	2.1	3.8	8.1	4.7	4.1	5.1	6.5	2.0	1.7	3.1	6.5
	1034	150	232.6	23.9	73.6	272.9	166.7	23.2	-0.5	172.5	-14.8	1.1	10.5	-0.6	2.8	3.1	2.7	10.7	1.9	6.3	2.5	6.5	1.7	1.9	1.8	7.1
	1723	250	259.5	40.7	83.8	332.7	164.2	14.4	0.7	183.1	-15.5	3.7	9.5	-2.9	3.4	4.4	2.4	11.8	2.3	7.4	3.0	7.8	1.8	2.3	1.5	7.1
	2412	350	289.5	50.6	89.0	396.4	159.1	11.9	1.5	189.8	-16.4	6.3	10.3	-9.3	4.0	2.7	2.8	9.2	2.2	5.3	2.9	6.9	2.1	1.4	1.7	5.5
	3101	450	315.0	60.4	91.9	465.5	154.0	12.7	3.7	204.6	-16.9	9.9	10.5	-17.0	3.8	4.3	2.6	14.9	2.1	5.6	3.1	12.9	2.0	2.3	1.5	8.9
13000	0	0	261.4	17.2	78.4	295.3	188.4	60.0	20.2	217.7	-11.4	8.1	6.7	-9.2	3.4	3.4	3.8	2.8	9.7	3.7	4.7	13.5	2.7	2.6	3.2	2.4
	345	50	263.2	14.3	82.6	291.8	157.8	48.0	11.6	186.4	-18.6	-5.6	10.5	-11.0	3.3	4.2	2.6	8.2	7.8	10.4	11.9	20.3	4.4	5.7	3.5	11.2
	1034	150	277.3	22.1	87.5	317.2	172.0	25.8	-3.5	170.1	-10.9	5.1	9.8	3.8	2.6	2.3	2.3	9.3	4.6	5.2	3.0	5.0	1.7	1.5	1.6	6.6
	1723	250	298.2	37.0	95.8	363.7	172.6	19.3	-5.5	180.1	-12.7	6.7	10.3	1.9	2.1	3.6	1.9	11.1	4.7	5.9	4.0	6.1	1.1	2.0	1.2	6.9
	2412	350	319.5	45.4	102.0	412.5	167.2	16.2	-3.8	185.9	-14.0	7.3	11.5	-4.4	2.3	3.1	2.4	8.7	2.9	5.7	3.3	6.1	1.3	1.7	1.5	5.4
	3101	450	342.7	57.0	107.1	480.2	160.6	13.0	-2.4	192.9	-15.1	8.4	12.5	-3.8	2.2	5.2	2.4	7.6	3.3	4.9	2.8	7.0	1.3	3.1	1.6	5.1
16000	0	0	276.6	8.4	93.4	325.3	170.3	59.9	35.1	178.3	-23.2	-6.8	17.1	-11.9	20.1	4.4	12.2	2.1	31.8	4.9	28.2	7.3	27.4	6.0	16.6	2.9
	345	50	279.7	8.8	105.5	326.7	129.7	63.0	21.1	176.4	-32.3	-4.3	13.8	-7.0	17.4	4.2	13.5	4.0	33.1	3.4	33.4	16.0	32.5	7.9	25.1	7.4
	1034	150	305.6	15.0	107.2	343.3	165.1	39.5	34.5	166.9	-22.2	-5.1	15.0	-10.4	16.7	3.6	22.9	8.8	22.6	7.6	32.2	8.1	22.7	4.9	31.1	11.9
	1723	250	320.5	23.2	106.0	380.6	159.1	35.2	7.8	169.4	-12.4	1.3	15.1	7.9	2.4	2.3	4.5	10.1	7.8	4.0	6.6	8.5	2.5	2.4	4.7	10.5
	2412	350	337.9	33.3	111.4	423.9	160.0	33.4	9.3	170.5	-14.2	2.9	15.9	5.0	2.5	2.2	4.6	7.9	6.6	3.6	4.0	6.3	2.6	2.3	4.8	8.2
	3101	450	356.4	43.2	113.2	473.9	149.0	29.5	3.0	171.1	-13.0	5.5	10.8	-0.5	1.8	2.5	3.2	7.5	3.6	3.2	3.4	6.9	1.9	2.6	3.3	7.8

APPENDIX E: EXPERIMENTAL DYNAMIC STIFFNESS

Table 17. 50% offset experimental dynamic stiffnesses at 7 krpm and zero load.

f [Hz]	VALUES [MN/m]							
	Re(Hxx)	Im(Hxx)	Re(Hxy)	Im(Hxy)	Re(Hyx)	Im(Hyx)	Re(Hyy)	Im(Hyy)
20	111.2	22.1	4.6	3.5	27.9	4.3	131.8	26.4
29	111.0	31.5	4.0	4.8	27.7	2.9	133.5	39.1
39	110.4	42.5	3.7	6.9	27.3	3.8	134.7	49.8
49	111.6	50.4	4.5	8.1	28.9	2.6	136.4	61.2
59	110.9	59.7	3.0	10.6	28.6	4.0	136.0	76.9
68	109.5	72.6	2.3	12.8	29.8	5.2	137.3	89.3
78	107.2	82.6	1.7	13.4	32.2	2.1	139.6	98.4
88	116.1	105.8	-3.6	17.5	24.0	-7.0	145.9	110.1
98	120.1	105.1	-1.6	21.7	19.1	1.0	142.0	122.1
107	117.9	115.3	1.3	24.0	18.8	3.8	140.0	133.9
117								
127	119.5	139.2	3.3	28.1	17.4	5.8	139.9	157.7
137	117.5	148.0	1.9	29.1	18.7	5.0	145.0	170.5
146	119.4	157.8	2.9	28.2	18.5	4.7	150.2	180.4
156	118.1	168.8	0.1	30.8	14.7	8.9	146.7	187.4
166	116.8	177.3	2.3	31.1	9.9	11.1	144.6	200.5
176	119.4	189.1	2.0	32.5	12.8	8.9	147.8	206.4
186	120.9	197.0	1.0	29.5	10.1	10.8	152.5	220.9
195	117.4	212.1	-3.4	31.0	10.9	13.6	150.9	227.3
205	115.1	223.1	-0.1	33.3	9.5	16.7	145.2	247.3
215	117.2	239.8	-7.4	32.6	10.4	10.9	153.8	257.7
225	113.0	246.9	-9.1	35.9	7.9	18.2	146.9	265.3
234								
244	106.8	270.5	-8.7	39.4	5.3	24.6	137.8	293.4
254	103.0	286.5	-3.6	40.0	6.2	22.6	131.7	320.2
264	95.6	308.6	-4.5	40.9	5.3	24.3	120.6	334.3
273	88.8	345.0	-22.7	47.8	-3.1	35.8	123.3	354.9
283								
293								
303								
313								

f [Hz]	UNCERTAINTIES [MN/m]							
	Re(Hxx)	Im(Hxx)	Re(Hxy)	Im(Hxy)	Re(Hyx)	Im(Hyx)	Re(Hyy)	Im(Hyy)
20	1.7	1.8	0.6	0.6	1.5	1.8	0.9	0.6
29	1.2	1.0	0.6	0.6	0.4	1.1	1.1	0.6
39	1.2	0.8	0.8	0.7	0.6	1.5	0.8	0.9
49	1.7	0.9	1.3	0.9	1.5	1.1	1.4	1.0
59	2.1	0.8	1.1	1.5	1.3	1.3	1.2	1.7
68	1.3	0.8	1.2	1.0	1.3	1.4	1.6	1.4
78	1.0	1.7	1.1	1.3	2.5	1.8	1.6	1.2
88	2.1	2.1	1.9	2.5	2.5	2.5	2.6	3.1
98	4.0	4.4	5.5	4.7	6.9	4.1	3.8	6.4
107	6.7	7.8	9.6	11.7	9.0	7.8	13.4	10.7
117								
127	6.8	10.4	17.9	13.4	10.0	9.2	18.8	17.4
137	6.4	4.4	5.2	7.5	6.3	4.9	6.1	7.1
146	5.2	3.7	6.2	4.0	5.5	4.4	6.8	5.4
156	3.1	3.5	4.7	3.5	3.8	2.6	4.1	4.8
166	2.8	3.7	4.4	2.3	3.1	2.6	3.6	3.2
176	2.0	2.4	2.8	4.1	1.7	2.3	2.6	3.3
186	1.9	2.6	3.1	3.0	1.3	1.9	2.7	2.9
195	2.0	1.2	3.7	2.6	1.3	2.3	4.5	3.6
205	1.5	1.6	3.0	1.8	1.4	1.2	2.9	2.0
215	2.1	3.0	1.7	3.5	2.1	2.8	2.5	3.7
225	1.8	2.0	3.7	3.8	1.8	1.8	3.3	2.1
234								
244	2.1	1.9	1.8	2.5	1.8	3.0	3.6	2.9
254	1.5	1.7	3.1	2.2	1.2	3.0	3.7	3.8
264	1.9	2.2	3.4	3.2	3.4	4.8	3.5	3.9
273	5.3	4.3	4.5	1.4	7.1	2.1	3.2	3.3
283								
293								
303								
313								

Table 18. 50% offset experimental dynamic stiffnesses at 7 krpm and 345 kPa.

f [Hz]	VALUES [MN/m]							
	Re(Hxx)	Im(Hxx)	Re(Hxy)	Im(Hxy)	Re(Hyx)	Im(Hyx)	Re(Hyy)	Im(Hyy)
20	123.2	26.9	6.8	4.5	35.4	2.3	147.9	21.4
29	120.2	32.6	6.7	4.6	33.8	3.3	152.5	34.1
39	123.1	43.5	5.9	7.3	31.8	2.5	145.9	44.8
49	122.3	52.9	6.7	7.9	29.6	-0.1	152.7	57.1
59	120.7	60.4	5.6	10.1	32.9	4.8	150.5	83.9
68	120.7	73.7	4.6	12.8	35.5	5.2	149.4	92.3
78	120.6	83.2	4.5	13.5	29.9	0.0	129.1	108.7
88	118.5	101.8	5.1	15.8	37.7	-1.0	162.1	125.8
98	132.3	109.6	4.0	19.8	24.8	-1.3	157.0	140.0
107	130.8	118.0	3.9	24.1	19.6	6.7	133.0	143.0
117								
127	129.6	143.3	5.0	27.4	18.8	5.4	134.3	157.2
137	131.3	152.8	7.5	27.2	25.3	4.4	152.8	188.9
146	128.8	162.2	5.2	22.7	21.0	-0.3	159.8	171.0
156	124.3	168.4	-5.7	25.6	-25.8	12.8	51.5	221.6
166	134.3	183.7	10.8	32.2	11.3	10.4	155.6	224.2
176	133.3	193.8	10.0	27.8	20.3	2.8	146.0	215.7
186	133.0	200.9	6.1	24.4	15.8	7.6	161.5	221.4
195	132.9	215.1	5.3	28.2	11.4	12.8	133.2	231.1
205	133.3	226.0	6.2	22.1	17.5	12.9	146.6	265.2
215	129.3	235.8	-0.7	18.4	14.2	2.9	138.3	254.8
225	123.8	255.1	-22.7	28.0	0.3	52.0	105.8	367.8
234								
244	124.6	271.7	-5.7	18.0	11.9	15.8	148.7	312.1
254	123.1	287.3	-8.3	18.3	13.7	12.3	138.4	320.4
264	118.2	301.0	-11.4	9.8	-0.6	1.7	110.5	306.8
273								
283								
293								
303								
313								

f [Hz]	UNCERTAINTIES [MN/m]							
	Re(Hxx)	Im(Hxx)	Re(Hxy)	Im(Hxy)	Re(Hyx)	Im(Hyx)	Re(Hyy)	Im(Hyy)
20	2.6	2.3	1.0	0.7	1.8	2.1	0.9	0.7
29	0.8	1.3	1.0	1.0	1.4	1.6	0.9	1.0
39	0.6	1.4	1.3	0.7	0.8	1.4	1.2	0.7
49	1.7	1.0	1.6	1.0	1.3	1.0	1.1	1.6
59	1.9	1.4	0.8	1.4	1.4	0.5	1.4	1.9
68	1.6	1.6	0.8	1.3	1.4	0.9	1.6	1.3
78	2.6	1.4	1.4	1.3	1.3	2.2	2.2	2.8
88	2.7	3.2	1.9	3.3	2.0	4.0	2.6	2.9
98	6.5	2.7	5.2	6.4	4.4	6.0	6.5	6.0
107	8.6	6.5	11.8	8.5	6.0	9.0	10.4	11.9
117								
127	10.3	14.3	12.1	15.2	15.0	10.3	17.3	11.7
137	6.3	5.6	6.7	6.3	7.4	6.6	7.0	9.4
146	4.9	4.2	5.7	4.0	5.0	4.7	5.2	5.1
156	4.2	3.8	4.1	4.1	5.7	6.6	5.7	8.1
166	4.8	3.0	5.1	2.9	2.7	5.3	4.7	4.5
176	2.3	2.7	3.4	4.2	3.7	2.7	4.3	4.2
186	1.2	2.4	3.0	2.8	2.1	2.0	3.7	2.1
195	2.2	1.4	3.0	2.5	2.3	1.9	4.8	3.7
205	2.2	2.4	2.6	1.2	1.7	3.3	4.2	3.5
215	2.2	2.5	1.6	3.2	3.5	2.2	3.1	3.7
225	2.2	1.8	2.7	4.3	3.4	3.8	8.8	7.6
234								
244	2.4	2.1	3.6	3.3	2.6	2.6	2.2	4.3
254	1.4	2.2	3.6	2.4	2.0	1.5	4.1	2.8
264	1.3	2.2	2.2	2.0	3.5	1.7	3.3	2.5
273								
283								
293								
303								
313								

Table 19. 50% offset experimental dynamic stiffnesses at 7 krpm and 1034 kPa.

f [Hz]	VALUES [MN/m]							
	Re(Hxx)	Im(Hxx)	Re(Hxy)	Im(Hxy)	Re(Hyx)	Im(Hyx)	Re(Hyy)	Im(Hyy)
20	158.0	22.3	16.9	3.8	44.7	-2.1	239.4	16.7
29	159.6	32.6	17.7	4.6	45.9	1.8	248.1	32.3
39	160.2	43.3	16.9	7.1	41.1	0.4	231.7	44.9
49	160.7	52.9	18.9	6.7	35.6	-1.7	241.3	58.5
59	161.1	63.3	16.8	9.7	44.5	6.3	246.1	90.9
68	160.0	74.6	15.7	10.3	48.8	6.7	238.7	100.3
78	160.4	86.0	16.0	11.3	36.6	-0.2	235.3	117.3
88	162.0	97.4	19.5	14.1	42.4	8.4	252.1	149.9
98	168.3	118.9	21.4	18.6	40.6	-2.4	240.7	167.6
107								
117								
127								
137	170.8	160.3	28.9	33.7	34.4	4.3	227.2	248.5
146	171.0	166.7	20.3	25.3	39.5	0.9	261.5	198.7
156	172.7	171.0	12.2	23.9	20.7	8.0	173.0	208.7
166	180.4	185.4	17.3	29.2	13.6	12.3	256.3	270.1
176	176.6	197.2	19.2	25.1	31.1	1.0	225.9	254.0
186	178.6	206.4	11.7	22.4	25.8	7.7	270.1	246.0
195	178.5	218.7	11.5	24.4	22.4	15.3	213.9	266.5
205	182.1	230.9	12.0	20.0	38.6	15.5	265.0	322.0
215	183.9	239.0	8.2	16.9	29.0	2.1	245.2	275.4
225	183.9	250.1	-6.0	15.4	15.0	7.4	186.9	322.0
234	186.7	259.0	8.1	21.0	26.8	13.4	271.6	313.5
244	185.2	269.9	6.3	17.6	21.7	17.6	252.9	347.1
254	180.5	282.7	-2.5	17.7	29.2	14.7	266.5	365.8
264	181.3	298.5	-4.6	11.6	37.3	4.0	264.9	350.4
273	183.0	308.7	-11.0	2.9	25.1	6.6	215.0	369.2
283	182.6	321.6	-8.8	9.5	27.7	10.5	247.7	414.1
293	181.6	333.2	-15.1	-3.9	22.1	2.2	206.2	393.4
303								
313								

f [Hz]	UNCERTAINTIES [MN/m]							
	Re(Hxx)	Im(Hxx)	Re(Hxy)	Im(Hxy)	Re(Hyx)	Im(Hyx)	Re(Hyy)	Im(Hyy)
20	1.5	1.6	1.1	1.1	2.4	3.0	0.9	1.0
29	1.6	1.6	1.5	1.8	1.7	2.4	1.4	1.5
39	1.2	0.9	1.1	1.0	1.6	2.1	0.9	0.9
49	1.3	1.3	2.1	1.0	2.6	0.9	1.7	1.5
59	1.9	2.1	1.6	1.5	3.1	2.6	2.2	2.2
68	1.6	1.3	1.3	2.1	2.5	2.1	1.2	1.5
78	2.3	2.0	1.9	1.4	3.6	2.6	3.1	1.7
88	2.7	3.4	3.3	4.1	5.2	5.1	4.4	4.4
98	7.1	5.9	6.2	7.4	9.3	7.5	6.3	10.2
107								
117								
127								
137	9.2	7.4	8.3	9.2	11.1	10.0	10.7	13.6
146	6.8	4.9	8.5	6.2	6.6	7.5	10.1	9.3
156	3.4	5.5	6.0	4.5	4.6	4.2	4.8	5.4
166	2.8	4.9	3.9	6.9	5.0	5.2	8.6	4.9
176	4.0	2.8	5.6	5.6	2.6	4.6	3.5	7.9
186	2.3	2.3	3.5	3.0	2.5	2.8	5.8	3.3
195	2.4	1.6	3.1	4.4	2.7	2.2	4.5	3.0
205	2.6	1.4	3.6	2.3	2.3	2.3	5.3	3.1
215	2.2	2.9	2.9	3.4	3.2	2.7	2.9	3.9
225	2.2	1.8	2.8	3.0	2.8	1.8	2.6	3.3
234	2.5	5.1	7.0	7.3	3.8	6.2	9.5	8.6
244	3.1	2.6	7.6	7.7	4.2	2.9	10.5	12.8
254	1.5	1.4	3.4	3.0	2.4	1.8	6.4	4.6
264	1.3	1.3	2.5	2.2	1.9	1.4	4.3	5.1
273	0.8	1.2	1.9	1.6	1.1	1.2	3.2	3.5
283	1.2	1.3	1.5	2.8	1.0	1.0	3.6	3.3
293	1.2	1.2	2.1	1.5	0.8	1.1	2.3	3.2
303								
313								

Table 20. 50% offset experimental dynamic stiffnesses at 7 krpm and 1723 kPa.

f [Hz]	VALUES [MN/m]							
	Re(Hxx)	Im(Hxx)	Re(Hxy)	Im(Hxy)	Re(Hyx)	Im(Hyx)	Re(Hyy)	Im(Hyy)
20	204.6	22.8	28.2	3.4	49.5	-0.8	357.0	18.8
29	204.9	32.8	26.7	4.3	51.5	3.5	370.6	33.6
39	207.2	44.9	27.9	6.6	45.5	-0.2	350.6	45.4
49	207.6	53.7	27.7	5.5	38.6	0.3	360.1	62.7
59	207.4	62.6	25.9	6.0	49.7	8.4	365.1	93.9
68	206.8	74.4	24.8	7.1	57.1	8.5	359.2	101.9
78	209.2	85.5	22.2	6.1	39.3	1.0	355.9	121.9
88	211.8	96.2	23.3	9.3	46.5	11.7	380.0	151.1
98	211.7	110.6	24.4	10.1	50.5	8.2	356.2	172.3
107	224.2	125.9	33.9	14.4	24.6	19.5	342.5	179.8
117								
127								
137	223.2	161.1	16.5	15.2	34.1	9.2	368.4	241.9
146	221.4	162.8	15.4	19.9	46.1	4.2	384.9	204.6
156	222.7	167.2	12.4	15.4	28.0	13.3	302.6	231.2
166	232.2	180.5	16.2	18.5	17.2	17.5	378.5	286.0
176	227.8	193.2	16.2	20.7	33.5	3.6	362.1	262.0
186	230.4	201.5	9.2	23.4	30.5	11.3	394.7	257.6
195	230.2	211.7	10.7	22.1	30.7	18.9	348.3	283.3
205	232.0	224.9	3.8	20.9	39.1	13.1	390.4	334.8
215	238.5	230.8	4.1	15.2	36.2	10.0	388.3	301.5
225	237.0	242.4	-9.6	13.0	23.0	11.0	315.0	322.0
234	230.6	245.7	-11.6	30.7	48.4	24.7	449.1	337.3
244	235.7	257.9	-7.3	17.9	31.8	24.1	402.8	376.5
254	235.6	272.7	-14.2	25.1	31.6	17.2	407.0	420.8
264	237.2	289.3	-9.6	17.7	38.2	5.5	398.0	384.3
273	239.5	298.2	-18.9	16.2	28.8	8.5	398.1	412.6
283	239.9	310.1	-12.3	14.9	26.0	13.2	401.3	449.5
293	239.7	321.6	-21.4	7.1	23.7	7.7	386.9	437.9
303	240.4	340.4	-39.8	-10.5	20.9	-10.8	299.3	443.8
313	240.0	353.6	-24.4	9.1	28.8	-2.9	429.4	457.6

f [Hz]	UNCERTAINTIES [MN/m]							
	Re(Hxx)	Im(Hxx)	Re(Hxy)	Im(Hxy)	Re(Hyx)	Im(Hyx)	Re(Hyy)	Im(Hyy)
20	2.9	3.2	1.1	2.1	2.6	5.7	3.1	2.2
29	2.1	3.1	2.4	1.4	2.2	4.0	3.8	2.4
39	1.6	1.6	1.7	1.8	2.8	3.1	3.1	2.4
49	3.1	1.2	3.1	2.4	3.0	1.9	4.4	3.2
59	2.2	2.9	3.2	3.4	4.5	3.9	3.7	6.2
68	2.3	2.9	2.0	1.9	3.2	3.2	2.9	3.9
78	6.8	2.5	3.0	2.8	6.2	5.5	7.7	3.9
88	6.4	3.8	7.2	4.7	6.5	10.0	8.3	12.1
98	10.2	10.1	8.8	11.3	18.6	11.2	11.2	20.3
107	17.7	9.6	23.0	24.2	14.6	24.6	42.3	26.6
117								
127								
137	14.2	10.4	9.4	15.7	15.5	23.0	23.1	16.0
146	8.2	5.3	13.0	6.8	7.5	13.9	12.3	16.6
156	7.8	4.0	8.9	6.7	4.7	10.0	7.5	7.9
166	4.3	5.3	8.4	5.1	7.2	9.1	7.8	12.4
176	4.0	5.7	4.3	8.1	8.0	3.3	8.1	6.4
186	3.1	2.7	6.3	3.7	6.3	2.8	6.0	5.5
195	2.5	1.7	4.9	5.0	4.2	2.5	4.3	5.7
205	2.6	1.7	4.5	2.7	1.8	3.8	5.3	5.2
215	4.4	4.2	3.1	4.2	6.0	3.4	6.0	4.9
225	3.2	1.7	4.0	3.8	3.1	2.9	6.4	5.8
234	4.7	6.7	29.5	28.0	7.8	12.7	51.9	59.4
244	3.2	2.7	8.3	5.8	6.5	5.2	11.7	8.0
254	1.6	1.1	6.4	5.4	3.3	3.3	8.0	8.6
264	1.7	1.2	3.9	5.0	3.0	2.1	5.5	4.5
273	1.0	1.3	3.0	3.5	1.3	2.5	5.4	4.4
283	1.6	1.1	2.9	4.4	2.6	2.4	3.9	2.6
293	1.3	1.3	3.1	1.5	1.7	2.7	3.2	3.1
303	1.8	1.2	1.5	4.6	2.2	2.5	11.4	9.2
313	1.4	1.0	1.8	2.7	2.6	2.2	4.5	2.7

Table 21. 50% offset experimental dynamic stiffnesses at 7 krpm and 2412 kPa.

f [Hz]	VALUES [MN/m]							
	Re(Hxx)	Im(Hxx)	Re(Hxy)	Im(Hxy)	Re(Hyx)	Im(Hyx)	Re(Hyy)	Im(Hyy)
20	243.2	23.0	31.3	1.6	50.4	0.1	470.1	24.1
29	244.5	31.9	30.9	2.2	54.4	6.4	484.9	37.6
39	246.1	44.5	30.0	3.2	48.9	3.3	471.1	53.1
49	247.1	53.2	29.4	3.0	41.7	3.8	477.8	69.4
59	248.0	63.3	30.4	5.3	51.8	12.3	477.2	93.0
68	245.9	74.6	26.7	6.2	61.0	11.2	476.5	104.4
78	249.1	84.4	21.7	5.0	43.2	7.9	479.5	125.6
88	253.4	94.9	26.0	7.2	46.5	19.5	484.6	163.4
98	250.6	107.7	28.1	10.2	56.1	18.7	474.8	175.5
107	266.9	129.7	42.1	17.8	22.4	24.3	463.0	199.8
117								
127								
137	266.5	160.5	15.8	20.8	30.5	15.0	481.1	246.7
146	263.5	160.3	10.9	22.4	50.1	11.5	511.5	205.7
156	265.0	163.3	9.4	21.6	35.4	17.3	428.3	233.2
166	275.5	176.3	15.7	24.6	24.3	24.7	508.8	282.5
176	270.3	186.7	13.7	21.1	38.1	11.8	477.8	269.5
186	273.1	195.3	5.9	28.3	37.7	17.8	514.8	258.9
195	272.9	206.2	6.1	27.4	38.5	22.9	466.3	293.1
205	278.6	213.6	5.1	22.6	45.4	19.8	516.3	336.0
215	274.0	224.1	-8.0	23.5	41.4	10.7	501.6	305.8
225	278.1	236.3	-12.0	26.6	27.5	13.5	464.4	316.4
234	272.5	244.7	-23.1	49.1	54.7	18.0	591.6	323.3
244	277.8	253.1	-12.6	28.9	36.5	23.3	532.5	376.5
254	277.9	266.2	-11.4	33.0	36.7	18.4	524.0	387.7
264	279.2	281.8	-13.5	30.5	39.8	8.6	528.2	392.9
273	281.5	290.2	-21.4	23.0	30.7	11.8	508.8	407.6
283	281.5	303.0	-14.5	30.2	28.5	15.8	541.7	447.7
293	281.2	314.9	-24.8	18.8	25.3	10.7	517.7	439.8
303	282.5	333.4	-34.3	8.2	22.2	-6.8	481.8	429.2
313	282.5	348.2	-26.1	30.6	28.6	2.4	601.5	488.1

f [Hz]	UNCERTAINTIES [MN/m]							
	Re(Hxx)	Im(Hxx)	Re(Hxy)	Im(Hxy)	Re(Hyx)	Im(Hyx)	Re(Hyy)	Im(Hyy)
20	4.4	3.7	2.3	3.9	7.4	8.5	3.0	4.5
29	2.1	2.4	4.2	3.9	4.2	5.9	5.3	4.6
39	1.4	2.2	3.8	3.6	4.0	6.4	4.6	5.3
49	2.2	2.0	4.0	3.4	6.8	1.4	7.9	5.2
59	3.7	5.5	4.8	4.5	4.5	9.9	8.1	10.4
68	2.3	3.4	1.9	3.4	5.5	6.5	6.6	5.4
78	5.9	3.7	5.1	4.4	11.8	5.5	10.2	7.3
88	6.6	4.9	8.9	9.9	13.1	12.4	18.1	14.9
98	10.6	12.3	17.8	13.4	26.0	17.6	27.4	35.9
107	20.7	14.8	42.1	37.7	28.6	30.2	59.2	71.5
117								
127								
137	17.6	11.8	25.9	16.6	20.7	26.8	27.8	44.9
146	9.5	10.1	14.1	21.4	15.7	13.8	32.6	24.3
156	5.3	8.6	12.9	10.3	9.9	10.2	18.4	16.1
166	5.5	8.0	9.6	12.9	11.7	9.0	21.1	13.7
176	5.6	4.5	12.1	7.4	8.2	6.7	12.7	16.5
186	3.3	3.2	9.6	6.3	5.8	4.3	14.3	8.3
195	4.5	1.7	4.4	7.3	3.8	3.5	9.7	7.8
205	2.3	3.1	7.3	9.2	2.3	2.8	11.7	5.5
215	4.4	2.2	9.5	6.7	4.1	3.9	5.5	11.0
225	3.3	3.0	6.7	9.1	4.3	3.5	9.7	8.1
234	9.1	7.1	40.4	18.8	15.9	11.1	73.8	37.9
244	2.5	4.1	8.3	5.8	6.2	7.2	20.9	10.1
254	1.2	2.5	5.1	5.6	3.7	4.0	6.8	12.2
264	2.2	1.5	4.3	5.3	3.9	2.1	9.8	6.2
273	0.9	2.1	2.4	5.1	1.6	1.9	5.0	6.8
283	1.8	1.5	3.7	3.3	2.5	1.9	5.1	5.8
293	0.9	2.0	3.2	1.8	1.5	2.1	6.8	2.7
303	1.3	2.0	3.9	2.6	1.8	1.3	6.3	3.8
313	0.7	1.9	1.8	3.8	2.4	1.9	4.1	4.2

Table 22. 50% offset experimental dynamic stiffnesses at 7 krpm and 3101 kPa.

f [Hz]	VALUES [MN/m]							
	Re(Hxx)	Im(Hxx)	Re(Hxy)	Im(Hxy)	Re(Hyx)	Im(Hyx)	Re(Hyy)	Im(Hyy)
20	277.7	22.2	32.2	2.7	56.5	0.7	581.7	21.7
29	278.5	31.6	31.8	3.5	58.8	6.0	593.3	34.4
39	281.3	43.7	31.4	5.1	53.7	5.0	578.0	49.9
49	282.1	52.5	31.0	4.6	47.0	4.5	587.5	62.6
59	282.7	62.0	31.1	7.1	56.4	12.1	588.2	89.1
68	280.9	72.3	29.0	7.8	65.4	12.7	583.6	99.3
78	284.7	82.3	24.8	8.8	49.3	9.6	583.2	117.1
88	288.0	92.2	28.2	11.2	52.6	18.5	601.1	150.6
98	286.9	101.0	31.8	14.7	61.3	20.2	585.4	169.7
107								
117								
127								
137	301.8	146.8	23.0	23.9	50.5	12.9	589.2	240.4
146	298.6	153.4	17.9	23.4	57.1	13.1	616.2	207.6
156	301.6	158.8	11.5	25.9	44.5	21.3	541.0	232.8
166	309.5	171.2	18.9	30.2	31.9	28.1	619.9	272.4
176	306.1	181.4	15.7	27.2	45.2	16.2	589.5	264.9
186	308.5	189.2	8.0	29.7	44.2	22.9	613.4	258.7
195	307.3	200.9	5.6	31.5	45.2	24.9	575.6	289.8
205	311.1	210.4	4.8	29.6	46.9	20.2	613.0	320.6
215	312.4	214.5	-6.4	24.6	48.0	17.4	601.3	295.4
225	312.8	229.3	-6.7	34.9	35.4	17.6	600.8	316.1
234								
244	312.9	246.4	-10.5	37.1	41.3	26.3	639.2	359.9
254	312.5	259.8	-7.4	38.1	39.5	21.6	630.6	372.0
264	314.2	274.7	-12.8	35.4	40.3	12.6	628.5	385.8
273	316.4	283.1	-19.9	26.8	31.3	15.4	609.2	395.2
283	316.9	296.2	-9.8	39.3	31.1	21.2	664.7	439.1
293	316.6	307.8	-24.5	23.2	25.7	14.1	619.7	428.2
303	318.2	325.6	-35.5	19.6	23.0	-0.6	600.9	433.2
313								

f [Hz]	UNCERTAINTIES [MN/m]							
	Re(Hxx)	Im(Hxx)	Re(Hxy)	Im(Hxy)	Re(Hyx)	Im(Hyx)	Re(Hyy)	Im(Hyy)
20	6.2	5.5	1.6	3.3	8.4	6.9	5.0	5.4
29	4.4	6.3	5.1	3.9	3.5	5.5	6.8	7.0
39	3.5	3.0	6.2	6.4	3.8	6.8	6.8	8.5
49	4.3	2.5	7.1	3.9	6.7	3.0	8.8	8.7
59	3.9	7.1	6.3	10.6	8.7	10.4	14.0	14.2
68	3.4	5.1	5.2	6.5	7.4	6.7	11.3	7.7
78	8.8	4.1	10.7	5.4	13.0	10.6	14.0	15.8
88	10.5	6.8	12.1	17.8	15.7	18.4	31.8	25.2
98	15.3	14.9	21.5	35.6	34.3	23.0	64.0	40.5
107								
117								
127								
137	17.4	12.7	36.6	25.1	22.2	35.9	62.1	67.6
146	11.5	9.3	21.0	31.1	15.5	21.2	54.8	52.7
156	7.2	7.3	13.9	16.9	12.2	15.1	41.7	19.0
166	5.5	6.5	10.9	16.9	14.0	12.7	30.0	36.8
176	4.4	5.9	16.0	13.3	11.9	8.6	30.3	25.7
186	4.0	3.5	11.2	10.7	9.2	5.3	29.1	10.9
195	3.7	3.5	8.1	11.8	6.4	5.7	9.5	23.3
205	2.2	3.2	6.1	5.8	4.0	5.6	21.0	13.3
215	4.1	3.1	9.5	8.1	7.9	5.7	19.0	14.9
225	3.9	2.6	9.6	7.0	7.4	5.4	20.1	9.4
234								
244	2.9	4.1	12.7	4.8	9.1	5.3	24.4	21.8
254	1.7	2.2	2.4	10.2	5.0	2.2	13.8	16.9
264	2.1	1.0	8.0	3.6	3.6	3.0	14.9	12.8
273	0.8	1.8	2.9	6.9	2.1	2.8	8.1	11.7
283	1.5	0.7	6.1	4.2	2.4	2.2	9.1	9.4
293	0.9	1.3	4.8	2.5	1.6	2.5	9.8	6.2
303	1.3	0.7	4.0	1.5	2.5	0.6	6.6	7.1
313								

Table 23. 50% offset experimental dynamic stiffnesses at 10 krpm and zero load.

f [Hz]	VALUES [MN/m]							
	Re(Hxx)	Im(Hxx)	Re(Hxy)	Im(Hxy)	Re(Hyx)	Im(Hyx)	Re(Hyy)	Im(Hyy)
20	158.0	21.7	5.6	4.6	42.5	2.8	185.7	24.1
29	158.6	30.2	5.4	6.0	42.3	3.6	185.9	35.0
39	157.3	39.1	4.8	8.3	43.3	2.8	188.4	46.6
49	158.2	47.4	4.1	10.3	44.1	2.7	188.7	57.0
59	157.8	56.5	2.7	12.2	43.7	3.4	187.8	69.1
68	154.1	67.0	2.5	14.7	45.6	3.1	190.0	81.8
78	149.8	79.8	2.1	15.3	51.3	-2.2	191.5	93.8
88	167.9	98.3	-1.0	21.0	34.3	-8.3	194.9	101.9
98	168.0	106.6	0.5	24.7	32.3	5.3	195.4	112.2
107	162.4	108.4	2.3	26.3	34.1	2.5	193.4	123.4
117	165.7	120.3	1.3	29.3	33.6	1.3	195.9	134.2
127	163.5	131.2	1.7	31.8	33.2	2.2	193.5	144.3
137	175.1	147.7	2.8	40.9	33.0	15.8	190.9	162.7
146	175.0	168.7	-5.3	44.5	17.5	19.5	191.2	164.3
156								
166								
176								
186	159.2	229.0	-10.6	69.6	-21.1	3.1	171.9	205.1
195	156.4	217.0	-6.3	61.1	6.3	-5.7	197.1	215.6
205	167.0	205.6	1.3	50.7	28.1	2.7	195.3	230.9
215	177.9	238.8	0.1	63.7	17.3	2.8	201.8	247.2
225	161.0	242.3	1.3	60.7	19.6	10.6	203.6	256.1
234	160.8	254.3	1.9	52.2	13.5	6.6	194.8	273.9
244	175.9	269.6	6.5	58.0	17.7	16.9	195.4	285.8
254	166.1	287.8	4.9	51.7	10.7	25.1	192.5	303.2
264	191.7	322.7	29.0	54.1	27.3	34.9	198.8	316.6
273	208.6	286.5	20.2	39.6	42.1	5.0	205.2	325.5
283	184.5	299.9	14.9	30.9	33.1	9.4	192.7	325.2
293	185.4	316.2	13.3	30.8	32.7	9.8	186.4	349.9
303	186.5	314.9	16.4	20.1	31.6	-0.9	183.4	364.9
313	181.0	325.1	8.4	9.4	36.9	-9.3	169.8	379.7

f [Hz]	UNCERTAINTIES [MN/m]							
	Re(Hxx)	Im(Hxx)	Re(Hxy)	Im(Hxy)	Re(Hyx)	Im(Hyx)	Re(Hyy)	Im(Hyy)
20	2.5	2.1	1.1	1.0	2.5	3.3	2.3	1.6
29	2.2	1.6	0.5	1.0	2.6	2.1	2.2	0.9
39	1.6	2.2	1.2	2.2	1.8	2.3	1.6	1.3
49	1.4	1.2	1.1	1.2	2.1	1.6	2.5	2.0
59	1.8	2.4	0.4	2.2	2.0	1.6	2.2	2.2
68	1.9	1.2	1.3	1.4	1.6	2.3	1.5	2.1
78	1.9	1.9	1.5	2.0	2.0	2.2	2.6	2.0
88	2.4	3.5	1.6	3.2	2.1	2.7	2.1	2.7
98	3.2	2.9	3.0	2.6	3.0	2.4	2.9	3.9
107	2.3	1.5	3.4	2.7	2.1	1.6	3.0	2.9
117	3.3	2.8	3.2	4.0	2.8	4.1	3.6	4.8
127	2.0	2.3	3.9	6.8	3.2	2.2	5.3	5.9
137	2.3	6.1	5.6	6.6	5.7	4.9	5.9	6.7
146	5.1	8.6	10.2	10.8	9.1	6.6	13.8	9.5
156								
166								
176								
186	6.0	10.7	11.8	23.6	13.6	5.2	27.3	11.6
195	3.2	3.8	7.9	12.4	8.0	4.1	17.6	6.6
205	1.8	1.9	6.7	5.3	2.7	1.6	4.8	6.2
215	4.2	4.5	4.6	7.8	5.0	4.7	5.9	7.7
225	2.5	1.9	6.5	3.8	1.6	3.5	4.9	5.6
234	1.5	1.5	4.3	3.4	3.0	1.5	4.8	3.9
244	3.1	2.3	3.5	3.6	2.5	7.8	4.7	4.4
254	2.6	4.8	4.3	4.4	4.1	11.3	4.6	5.2
264	7.9	4.9	5.2	6.8	13.8	18.1	9.7	7.2
273	2.3	2.0	3.7	3.7	9.8	11.1	6.3	8.0
283	1.6	3.4	4.0	5.1	9.9	2.1	8.8	4.3
293	2.9	2.0	4.2	3.4	10.7	3.3	7.6	5.1
303	3.2	4.5	2.5	4.9	8.2	5.9	6.7	5.4
313	3.0	2.9	2.9	2.8	2.9	11.4	4.5	11.5

Table 24. 50% offset experimental dynamic stiffnesses at 10 krpm and 345 kPa.

f [Hz]	VALUES [MN/m]							
	Re(Hxx)	Im(Hxx)	Re(Hxy)	Im(Hxy)	Re(Hyx)	Im(Hyx)	Re(Hyy)	Im(Hyy)
20	166.2	27.6	5.6	5.3	48.0	3.9	191.7	21.2
29	161.8	32.9	5.5	5.8	44.9	4.2	194.7	32.7
39	166.0	40.6	4.8	7.5	45.2	2.6	191.8	41.7
49	163.7	47.7	4.3	8.3	43.0	1.2	193.9	53.4
59	163.0	57.0	4.3	12.5	44.3	2.3	194.9	72.7
68	163.3	69.3	3.0	14.3	46.4	4.2	192.5	81.4
78	161.6	78.0	2.1	15.9	36.1	-1.1	166.9	105.6
88	163.7	104.9	0.1	17.7	47.6	-14.3	203.4	110.9
98	172.1	105.6	2.0	20.7	33.4	1.8	200.2	122.2
107	172.2	107.5	3.2	26.0	34.7	4.6	186.6	132.1
117	173.2	121.3	3.7	28.1	32.9	2.1	198.5	143.7
127	173.5	135.3	7.2	31.6	30.7	4.6	185.4	153.2
137	180.9	150.6	10.2	37.8	27.2	14.8	189.9	176.3
146	181.7	172.2	22.6	35.3	13.5	12.1	196.2	185.1
156								
166								
176								
186	154.7	217.0	11.0	67.2	-7.1	-16.6	168.4	224.1
195	172.9	209.6	3.1	46.5	13.3	-0.7	173.9	222.0
205	169.6	212.0	1.5	42.7	21.4	-6.0	180.1	239.0
215	169.5	229.2	-5.2	37.9	7.7	-8.2	164.2	237.2
225								
234	170.6	241.0	-4.1	45.0	22.9	-4.2	204.4	271.1
244	169.0	252.8	-7.1	36.7	12.7	-3.5	189.7	276.4
254	168.0	268.0	-9.5	43.1	3.6	-3.2	167.1	284.3
264	163.6	284.7	-11.7	27.5	-18.3	4.8	134.8	267.5
273								
283								
293	188.7	360.6	0.6	60.5	20.7	15.8	196.8	377.1
303	163.7	390.7	-21.6	73.7	0.5	-12.6	181.0	343.5
313	221.5	356.6	14.6	56.2	31.7	-5.2	218.5	406.8

f [Hz]	UNCERTAINTIES [MN/m]							
	Re(Hxx)	Im(Hxx)	Re(Hxy)	Im(Hxy)	Re(Hyx)	Im(Hyx)	Re(Hyy)	Im(Hyy)
20	3.4	4.2	0.8	0.9	1.8	2.4	1.1	1.2
29	1.5	2.3	1.5	1.4	2.1	1.8	1.5	1.0
39	1.9	2.1	1.0	1.4	2.8	1.9	1.4	1.0
49	2.5	1.4	2.0	1.5	2.0	1.1	1.6	1.1
59	2.1	2.4	0.8	2.1	2.4	2.3	1.4	1.7
68	1.4	1.4	0.9	2.1	1.6	1.2	0.8	1.6
78	2.1	2.1	1.7	0.9	3.2	2.2	2.2	2.7
88	2.6	3.7	1.4	2.6	2.6	1.1	1.4	3.5
98	2.9	2.8	3.1	4.3	3.4	1.7	3.3	2.8
107	2.8	2.0	3.5	3.4	2.4	2.0	3.0	3.5
117	3.7	3.8	4.2	4.4	3.0	2.6	3.9	3.7
127	1.7	3.3	6.3	7.6	4.3	2.3	7.8	8.1
137	3.8	3.5	7.8	4.7	3.8	4.5	6.3	6.2
146	7.2	6.9	10.3	12.7	8.1	7.3	11.6	12.2
156								
166								
176								
186	7.6	8.3	14.2	14.9	8.1	8.7	17.6	16.1
195	6.3	3.4	8.7	11.8	4.1	6.5	11.1	11.5
205	2.9	3.0	5.6	5.3	3.4	1.7	8.2	5.3
215	4.2	2.7	2.7	5.4	2.9	3.2	4.5	6.8
225								
234	2.1	1.1	4.4	3.2	1.4	1.3	3.9	5.6
244	1.5	1.8	2.5	3.8	3.1	2.2	3.3	4.6
254	1.7	2.2	4.7	2.8	4.5	2.6	4.0	5.2
264	1.3	3.2	3.1	2.5	4.5	6.2	2.7	3.5
273								
283								
293	8.7	3.6	4.4	1.6	10.2	13.1	10.2	7.0
303	8.5	9.3	5.5	8.3	5.4	6.1	7.7	4.2
313	5.0	6.6	4.3	4.7	8.6	17.5	15.6	7.0

Table 25. 50% offset experimental dynamic stiffnesses at 10 krpm and 1034 kPa.

f [Hz]	VALUES [MN/m]							
	Re(Hxx)	Im(Hxx)	Re(Hxy)	Im(Hxy)	Re(Hyx)	Im(Hyx)	Re(Hyy)	Im(Hyy)
20	189.6	19.8	13.9	3.0	54.9	-3.8	254.9	16.4
29	190.4	29.0	14.9	4.9	57.9	1.0	263.3	30.0
39	189.6	39.1	13.6	7.3	52.6	-1.7	250.6	39.6
49	190.3	48.3	15.8	8.1	48.5	-2.1	257.9	53.9
59	191.0	58.5	12.7	11.6	57.5	3.9	262.1	78.4
68	189.9	69.0	12.4	13.2	60.0	2.1	255.4	87.9
78	189.3	78.1	11.9	15.1	52.1	-1.1	251.0	103.6
88	187.6	89.1	13.3	17.6	59.0	1.4	267.9	127.8
98	202.9	106.8	12.0	18.3	47.1	-5.8	260.5	138.5
107	198.7	107.2	10.6	24.2	40.1	6.4	241.9	141.7
117	199.3	117.7	14.2	26.6	38.3	-2.8	256.5	158.7
127	198.8	131.2	14.1	28.5	42.8	2.5	236.3	163.5
137	203.5	141.8	16.8	29.1	46.9	1.1	257.2	204.4
146	203.2	154.1	21.3	37.7	46.4	-4.3	266.1	183.1
156								
166								
176								
186	205.3	196.4	24.0	55.3	28.6	-0.3	257.5	237.4
195	208.4	203.2	15.0	46.8	31.3	6.0	224.7	244.1
205	210.6	206.7	15.1	38.1	42.1	-0.2	271.2	275.1
215	210.5	219.5	12.8	37.1	32.0	-3.3	247.8	245.9
225	208.8	227.8	-1.0	31.9	21.9	0.1	201.4	287.8
234	209.0	237.1	8.5	32.5	35.3	-0.3	285.1	275.0
244	208.9	246.5	7.1	30.7	28.5	2.7	267.5	301.6
254	207.3	257.0	6.4	30.7	29.3	0.7	274.0	309.7
264	208.4	269.8	6.2	23.6	31.4	-7.4	266.9	297.0
273	208.0	277.6	-1.7	16.3	21.0	-5.2	217.1	313.9
283	205.9	287.9	3.9	20.6	23.8	-1.4	253.4	346.4
293	202.8	298.4	-2.2	6.4	18.4	-6.6	201.9	332.4
303								
313								

f [Hz]	UNCERTAINTIES [MN/m]							
	Re(Hxx)	Im(Hxx)	Re(Hxy)	Im(Hxy)	Re(Hyx)	Im(Hyx)	Re(Hyy)	Im(Hyy)
20	3.6	3.7	0.7	1.9	11.1	3.3	1.3	1.8
29	2.3	2.1	2.5	1.5	4.2	2.0	2.5	1.2
39	2.4	3.7	1.6	1.6	1.9	3.4	1.6	2.1
49	3.4	3.1	2.0	2.1	3.2	2.8	2.9	1.8
59	2.4	3.2	2.1	2.9	3.0	3.3	2.1	3.3
68	1.8	2.7	2.5	2.1	2.3	1.7	1.7	1.9
78	3.3	2.1	2.9	2.0	1.7	1.5	3.2	1.9
88	3.5	3.6	2.5	3.2	2.2	3.2	2.1	4.1
98	2.8	4.9	4.6	4.8	5.2	4.4	2.9	4.9
107	2.9	1.6	4.7	2.6	3.1	2.8	5.1	2.6
117	3.2	5.7	4.3	5.6	2.5	4.4	7.0	5.2
127	2.8	2.6	7.1	8.2	3.5	2.3	6.0	8.3
137	6.4	3.7	5.9	6.9	3.8	7.6	9.7	8.1
146	9.5	5.5	11.6	11.7	6.3	11.2	10.1	14.6
156								
166								
176								
186	5.5	12.8	16.2	20.7	18.1	5.0	20.1	23.9
195	3.8	6.2	9.8	8.8	8.0	3.2	10.9	13.4
205	4.2	2.2	7.3	6.8	2.0	5.8	9.8	10.2
215	2.3	3.7	4.8	7.1	7.5	3.0	7.2	6.3
225	3.2	2.8	5.3	4.9	2.7	3.4	8.3	6.5
234	1.8	2.2	5.4	4.7	3.8	1.6	4.6	4.9
244	2.2	1.4	2.7	4.6	1.7	2.7	5.6	4.5
254	1.8	1.6	4.0	3.2	1.7	2.8	4.9	4.4
264	1.5	1.6	2.4	4.6	3.9	1.2	3.9	3.1
273	1.0	1.3	3.4	2.6	1.0	1.7	3.3	3.4
283	1.0	1.5	1.8	3.2	1.9	1.4	4.9	2.4
293	1.0	1.5	1.5	1.9	1.4	1.7	2.8	3.3
303								
313								

Table 26. 50% offset experimental dynamic stiffnesses at 10 krpm and 1723 kPa.

f [Hz]	VALUES [MN/m]							
	Re(Hxx)	Im(Hxx)	Re(Hxy)	Im(Hxy)	Re(Hyx)	Im(Hyx)	Re(Hyy)	Im(Hyy)
20	226.9	18.7	25.9	2.5	64.6	-5.3	346.1	17.1
29	227.6	29.4	26.8	4.2	67.1	1.4	358.1	29.9
39	229.8	39.4	26.7	7.6	60.4	-0.9	341.4	43.0
49	228.5	48.5	26.4	8.1	54.8	-2.8	348.5	57.7
59	229.0	57.0	25.1	9.7	64.5	4.8	354.6	84.6
68	228.6	68.4	24.7	11.7	72.6	2.3	350.5	91.7
78	229.2	76.8	22.7	11.0	57.6	-0.1	344.7	109.4
88	229.5	86.6	24.9	14.4	64.1	3.9	370.4	132.3
98	234.9	107.4	24.6	12.1	62.5	-3.2	355.2	156.1
107	239.6	106.4	23.8	20.5	46.1	6.6	335.7	146.3
117	239.1	118.5	22.4	19.5	40.9	-2.7	356.9	171.6
127	238.5	129.7	23.5	23.8	50.6	4.0	337.7	159.9
137	246.1	141.7	22.9	23.5	52.1	2.9	361.7	210.7
146	242.3	155.7	21.1	27.8	50.7	-0.1	370.5	180.3
156								
166								
176								
186	246.7	200.8	23.2	39.2	22.1	7.7	369.5	228.6
195	250.1	201.4	19.6	35.9	37.1	11.2	332.7	244.5
205	249.1	201.4	11.8	22.3	47.8	2.6	372.5	281.8
215	250.9	216.8	14.3	27.6	39.9	-0.7	359.2	254.9
225	250.8	225.2	0.5	22.2	27.4	3.0	279.6	279.7
234	250.3	233.3	11.8	33.5	44.9	1.9	401.8	284.1
244	251.5	241.9	6.7	25.3	36.8	7.1	370.4	314.0
254	249.3	251.4	4.8	28.9	38.2	3.1	393.2	350.3
264	251.3	266.1	4.2	20.8	40.1	-3.5	363.0	326.5
273	252.4	272.6	-2.3	15.7	29.7	-1.6	351.1	338.0
283	250.8	282.6	4.3	17.1	30.2	4.1	363.5	377.3
293	248.4	292.7	-4.1	7.2	27.4	-0.7	335.8	366.0
303	247.3	309.1	-25.9	-10.3	26.1	-9.7	228.5	389.4
313	245.0	321.2	-8.8	3.0	30.1	-6.0	360.0	384.9

f [Hz]	UNCERTAINTIES [MN/m]							
	Re(Hxx)	Im(Hxx)	Re(Hxy)	Im(Hxy)	Re(Hyx)	Im(Hyx)	Re(Hyy)	Im(Hyy)
20	6.8	8.9	2.2	2.7	4.9	4.9	2.3	1.7
29	3.6	4.9	2.8	4.1	3.3	4.1	2.0	3.2
39	4.0	2.5	3.1	2.4	3.1	2.8	2.6	2.7
49	3.7	2.2	3.1	3.0	3.3	1.9	4.1	4.3
59	2.8	3.9	3.4	3.8	2.0	3.8	5.4	2.2
68	2.4	3.4	3.2	2.1	3.2	2.6	3.7	3.2
78	3.1	4.5	3.9	2.1	3.8	3.3	4.0	3.1
88	2.0	3.0	3.9	5.0	3.0	3.4	4.6	6.8
98	6.2	3.6	6.3	5.2	6.0	5.8	4.9	6.6
107	2.4	3.6	6.2	5.2	3.7	2.8	7.7	3.7
117	4.0	3.9	4.9	9.2	5.4	6.1	5.3	8.3
127	3.2	4.1	8.1	9.0	4.9	4.4	9.8	15.1
137	7.0	4.9	10.5	8.1	6.4	9.2	13.1	12.4
146	10.4	11.6	16.9	15.7	13.5	11.7	19.7	20.0
156								
166								
176								
186	8.8	16.8	16.5	17.5	24.0	11.5	24.3	26.1
195	5.5	5.8	10.6	11.9	8.7	6.2	12.7	15.8
205	4.3	5.1	9.2	7.0	4.3	5.1	12.8	11.3
215	3.5	5.3	8.8	8.8	7.0	5.6	9.6	9.1
225	3.8	2.0	5.2	3.7	3.3	4.3	6.3	6.6
234	1.6	3.5	8.0	6.5	3.4	3.2	6.9	9.4
244	1.7	2.7	5.6	6.2	2.0	4.0	6.4	5.2
254	1.3	2.2	3.6	5.7	2.4	4.2	8.1	8.0
264	2.2	2.0	4.7	4.9	2.8	1.9	5.3	4.7
273	1.6	1.6	3.6	5.2	1.4	2.0	5.2	4.6
283	1.0	1.5	3.5	3.6	1.7	1.6	3.3	4.6
293	1.2	0.9	2.5	1.8	1.6	1.1	3.2	3.1
303	0.8	1.4	2.2	3.1	1.3	3.3	16.3	4.5
313	1.4	1.1	1.7	2.3	1.8	1.8	3.4	3.1

Table 27. 50% offset experimental dynamic stiffnesses at 10 krpm and 2412 kPa.

f [Hz]	VALUES [MN/m]							
	Re(Hxx)	Im(Hxx)	Re(Hxy)	Im(Hxy)	Re(Hyx)	Im(Hyx)	Re(Hyy)	Im(Hyy)
20	265.1	19.3	35.1	0.3	72.1	-3.4	455.4	21.9
29	265.4	28.5	32.9	3.5	73.6	5.1	468.3	34.2
39	267.2	40.7	32.0	6.2	65.6	0.7	455.2	47.1
49	268.7	48.1	33.7	5.3	60.4	1.1	461.6	63.4
59	269.1	55.9	34.4	7.3	69.2	7.0	461.0	84.2
68	264.8	67.1	31.1	8.8	79.3	3.4	462.1	93.9
78	268.5	75.1	27.2	8.6	65.0	3.6	463.3	112.0
88	270.5	86.2	30.7	11.2	67.9	10.9	469.4	143.4
98	265.4	101.8	33.1	10.7	79.0	6.9	462.7	150.9
107	280.2	107.3	30.3	18.4	51.6	8.5	448.6	148.6
117	278.8	118.6	26.7	15.3	42.7	-0.2	469.8	173.0
127	278.3	128.2	30.5	22.2	56.3	9.4	444.1	163.4
137	288.8	141.5	27.8	19.6	55.4	12.8	471.6	213.4
146	285.1	154.6	26.1	26.8	55.5	9.8	489.9	188.2
156								
166								
176								
186	290.3	203.6	26.8	40.2	18.9	23.0	476.7	236.2
195	291.5	195.9	24.5	29.9	41.8	19.9	442.1	255.5
205	285.8	197.4	10.6	21.7	54.8	5.9	486.0	280.9
215	290.8	213.6	11.0	28.6	45.4	6.8	463.6	262.6
225	291.5	221.1	3.4	23.3	34.6	7.8	425.5	267.6
234	290.0	228.8	10.4	33.1	52.1	7.3	511.5	290.1
244	292.1	236.6	2.6	24.2	44.4	12.6	482.7	316.6
254	290.7	246.9	2.0	27.2	45.7	8.3	474.6	327.3
264	291.8	261.6	-0.8	23.2	45.7	1.2	476.8	330.2
273	293.8	267.9	-8.6	17.6	37.4	2.8	450.5	344.3
283	292.5	277.9	-1.0	22.1	36.8	7.6	484.3	379.1
293	289.7	288.5	-11.7	11.0	34.0	2.5	453.4	371.8
303	289.5	304.4	-21.9	1.0	30.7	-8.6	408.4	363.8
313	288.2	316.8	-15.0	18.8	37.4	-1.7	518.8	420.4

f [Hz]	UNCERTAINTIES [MN/m]							
	Re(Hxx)	Im(Hxx)	Re(Hxy)	Im(Hxy)	Re(Hyx)	Im(Hyx)	Re(Hyy)	Im(Hyy)
20	5.6	8.0	3.2	2.0	5.7	6.4	3.4	2.8
29	5.2	3.6	2.4	4.6	5.7	5.6	3.4	5.0
39	4.0	6.1	3.6	2.9	2.2	5.6	4.4	4.8
49	2.3	3.0	4.4	4.3	3.0	2.9	7.0	3.5
59	3.0	5.0	3.5	4.4	6.4	4.9	4.5	2.8
68	3.1	2.2	4.8	3.7	3.3	3.9	4.2	5.7
78	5.1	4.0	4.6	5.2	6.2	2.1	3.1	3.0
88	6.3	5.2	4.5	4.7	6.5	5.3	6.3	7.2
98	5.4	4.1	6.3	7.4	7.8	6.1	9.3	7.9
107	4.1	2.7	9.9	6.8	6.3	3.8	8.1	7.4
117	7.4	5.1	6.5	9.0	12.5	10.1	9.9	13.9
127	4.7	6.8	14.8	19.1	6.1	8.0	13.8	20.8
137	9.9	7.1	15.0	11.0	11.7	13.1	18.4	17.4
146	13.7	9.4	27.3	22.8	17.8	19.6	25.6	38.1
156								
166								
176								
186	14.8	16.3	19.5	25.1	23.8	20.4	40.1	29.6
195	7.6	7.7	15.1	14.2	12.2	11.6	17.7	28.2
205	5.3	4.5	10.2	11.2	6.2	7.1	13.5	16.3
215	7.0	5.4	10.7	8.7	9.0	8.3	16.9	12.5
225	3.9	4.0	7.6	6.8	4.1	6.1	10.2	7.6
234	3.8	2.0	5.2	7.2	4.4	4.5	10.4	13.0
244	3.2	2.6	4.7	6.3	2.6	4.3	9.7	7.7
254	2.4	2.5	4.2	7.8	3.1	3.0	7.8	8.7
264	3.0	1.8	4.5	5.1	3.8	1.6	7.3	7.1
273	1.7	1.8	2.9	5.9	2.1	2.5	4.2	7.2
283	2.0	1.6	2.7	4.5	2.6	1.6	5.4	6.5
293	1.5	1.5	3.5	2.7	1.0	2.5	5.3	3.9
303	1.5	1.9	2.8	2.3	1.9	2.0	4.6	4.9
313	1.1	2.3	3.4	3.5	2.4	2.5	3.6	5.1

Table 28. 50% offset experimental dynamic stiffnesses at 10 krpm and 3101 kPa.

f [Hz]	VALUES [MN/m]							
	Re(Hxx)	Im(Hxx)	Re(Hxy)	Im(Hxy)	Re(Hyx)	Im(Hyx)	Re(Hyy)	Im(Hyy)
20	299.1	18.6	39.5	1.6	77.7	-3.8	567.2	18.7
29	300.4	27.3	39.6	3.4	78.4	5.0	579.5	30.7
39	300.1	40.5	38.1	6.6	69.1	2.1	562.2	43.1
49	302.5	47.5	38.2	7.3	66.0	3.5	570.3	55.2
59	302.1	56.1	37.5	7.7	74.2	8.8	571.3	77.4
68	299.3	67.0	37.1	9.5	83.6	6.2	570.2	87.2
78	302.4	74.8	34.4	9.5	69.2	5.8	567.6	104.2
88	306.5	85.4	36.0	12.1	72.1	13.6	585.1	128.7
98	303.0	97.2	35.5	11.5	81.9	17.3	574.0	137.6
107	315.2	110.9	35.3	21.6	56.3	10.4	554.0	147.0
117	316.2	117.3	34.1	19.4	43.0	7.0	573.1	161.6
127	315.1	127.3	43.9	23.3	60.7	17.1	554.3	174.2
137	329.1	140.1	41.9	22.4	59.4	27.8	578.3	217.1
146	326.9	156.9	65.3	30.2	53.0	29.9	607.9	239.1
156								
166								
176								
186								
195	331.3	194.9	43.8	31.6	46.1	32.4	552.7	283.4
205	325.0	192.3	21.9	22.9	56.9	16.3	582.9	285.9
215	328.2	210.3	23.3	28.1	49.4	17.1	562.9	273.3
225	329.6	216.2	13.2	29.3	43.4	14.8	560.5	271.1
234	327.0	223.7	16.9	37.0	58.7	13.7	624.3	300.4
244	328.5	231.0	3.8	28.6	50.4	17.3	583.7	309.9
254	327.3	240.9	4.1	28.6	50.7	12.0	577.2	318.9
264	328.9	255.5	1.1	25.9	49.0	5.5	576.3	327.4
273	331.3	261.3	-10.1	21.3	41.5	7.4	547.9	337.0
283	330.2	271.4	0.0	28.6	43.4	12.7	600.2	376.5
293	326.6	281.3	-14.9	15.1	37.5	5.9	554.9	367.5
303	327.9	296.9	-24.3	12.3	34.9	-5.4	532.9	373.0
313								

f [Hz]	UNCERTAINTIES [MN/m]							
	Re(Hxx)	Im(Hxx)	Re(Hxy)	Im(Hxy)	Re(Hyx)	Im(Hyx)	Re(Hyy)	Im(Hyy)
20	4.3	7.1	4.2	4.6	8.0	5.2	1.8	3.4
29	5.5	4.6	5.2	3.5	5.5	5.1	5.7	4.0
39	5.1	4.3	5.6	3.1	5.4	4.2	6.8	6.8
49	6.1	2.6	4.7	6.6	5.5	2.4	6.7	5.0
59	5.3	5.1	7.1	5.1	5.1	5.6	8.3	8.1
68	3.0	2.9	3.5	5.6	4.1	3.6	6.6	4.4
78	4.3	3.0	6.0	5.4	6.8	4.5	7.3	5.3
88	5.8	4.8	5.7	6.9	7.0	5.9	9.4	9.9
98	4.8	5.8	6.2	10.0	9.4	6.5	9.7	15.4
107	5.4	3.5	10.4	6.7	9.0	4.1	15.8	12.6
117	5.8	4.3	10.4	3.7	9.4	7.0	13.9	18.3
127	4.0	6.0	20.2	18.0	8.5	8.2	32.0	27.6
137	10.8	10.4	22.6	13.2	15.3	16.6	25.6	38.1
146	16.2	8.5	28.1	31.0	22.2	25.5	62.4	51.4
156								
166								
176								
186								
195	10.1	5.4	19.7	22.7	10.4	14.4	33.5	37.3
205	5.1	6.4	15.7	12.4	8.8	7.1	25.6	20.1
215	7.5	4.9	14.4	11.4	8.1	10.3	19.5	18.7
225	5.1	3.7	12.0	9.8	4.5	6.9	14.6	13.2
234	4.0	2.7	10.5	10.1	4.8	5.8	13.4	16.6
244	2.5	4.9	10.5	5.5	5.0	4.1	11.6	10.8
254	2.0	2.9	7.7	10.6	3.5	2.3	11.1	12.2
264	3.2	2.3	8.3	7.5	3.8	2.6	8.8	10.0
273	1.4	1.3	5.4	6.9	2.0	2.2	6.2	8.6
283	1.5	1.7	5.9	5.9	2.0	2.0	6.2	8.7
293	1.9	2.0	6.3	4.7	2.2	1.8	7.2	4.7
303	1.7	1.3	3.9	4.4	3.0	1.6	4.4	5.3
313								

Table 29. 50% offset experimental dynamic stiffnesses at 13 krpm and zero load.

f [Hz]	VALUES [MN/m]							
	Re(Hxx)	Im(Hxx)	Re(Hxy)	Im(Hxy)	Re(Hyx)	Im(Hyx)	Re(Hyy)	Im(Hyy)
20	209.5	21.0	5.2	4.3	61.6	3.8	246.7	24.4
29	210.4	31.2	3.9	6.2	61.6	1.3	247.8	35.2
39	210.3	40.3	2.8	9.4	63.4	1.4	249.1	45.0
49	208.8	46.1	3.2	10.3	62.9	0.3	249.9	55.4
59	209.6	54.4	4.1	14.5	63.4	2.2	251.7	69.9
68	205.9	65.5	2.4	15.9	64.9	-0.6	253.2	79.7
78	197.5	82.6	-0.2	16.0	71.7	-8.6	255.2	90.3
88	220.1	97.5	-3.2	23.3	47.9	-4.8	257.6	99.5
98	221.5	99.7	-2.4	30.9	49.9	-1.6	253.0	111.0
107	215.0	104.4	3.9	32.9	52.7	-2.7	254.7	122.7
117	213.5	117.5	3.8	33.0	49.0	-0.7	256.2	134.6
127	217.0	130.0	3.2	37.0	49.1	-1.4	254.5	149.5
137	217.6	142.9	-1.8	38.9	46.7	1.9	253.5	154.8
146	220.1	154.7	1.9	43.0	38.6	4.5	255.1	172.1
156	217.7	163.5	-11.3	46.9	39.1	5.3	249.0	168.8
166	216.7	178.5	-6.4	52.0	30.6	9.3	246.4	188.7
176	215.5	193.8	-6.5	85.2	26.1	2.8	212.4	205.3
186	234.5	210.0	-8.5	102.9	19.9	24.4	199.2	223.1
195								
205								
215								
225								
234								
244								
254	217.7	262.2	-55.8	98.8	27.3	12.2	200.6	271.6
264	197.2	286.9	-49.5	96.0	18.8	-1.3	201.3	313.4
273	199.0	303.6	-50.8	80.9	16.0	15.6	233.7	327.1
283	220.4	341.5	-42.7	125.1	40.2	14.6	254.3	357.3
293	230.4	339.0	-14.0	94.3	36.9	5.1	271.7	367.2
303	241.8	372.6	-6.4	115.1	43.2	8.0	271.5	397.6
313	251.9	380.5	13.9	100.9	64.7	-14.5	286.9	392.2

f [Hz]	UNCERTAINTIES [MN/m]							
	Re(Hxx)	Im(Hxx)	Re(Hxy)	Im(Hxy)	Re(Hyx)	Im(Hyx)	Re(Hyy)	Im(Hyy)
20	3.1	3.5	1.9	2.0	3.8	3.6	2.6	2.4
29	2.4	3.3	1.7	1.6	3.9	3.6	3.6	1.8
39	1.5	3.3	1.1	2.1	3.2	3.1	3.0	2.4
49	3.0	2.2	2.3	3.1	2.3	1.4	3.8	1.9
59	2.6	3.6	3.5	2.8	5.4	3.1	3.2	3.3
68	2.7	2.9	1.7	1.5	2.0	1.2	2.2	1.5
78	3.6	1.5	3.1	3.2	3.5	3.2	2.7	2.5
88	1.9	3.8	4.1	2.9	3.8	3.8	3.5	3.9
98	3.4	4.8	2.5	3.2	4.7	4.6	3.2	4.1
107	2.3	3.1	4.5	5.6	2.4	3.8	5.6	4.9
117	4.2	4.6	3.7	4.4	3.0	5.1	4.9	5.3
127	3.0	3.1	3.7	6.5	4.5	2.2	7.3	4.4
137	4.7	4.4	3.3	3.4	3.9	8.0	3.7	2.8
146	3.1	3.0	4.5	3.9	6.7	4.0	5.4	4.7
156	4.5	4.9	6.0	6.1	4.2	5.8	5.2	5.6
166	4.8	4.7	5.3	5.3	4.3	7.0	6.0	7.8
176	4.6	5.9	7.2	9.9	5.7	7.9	8.3	6.3
186	4.6	4.6	7.8	4.7	4.6	5.1	6.1	7.2
195								
205								
215								
225								
234								
244								
254	4.1	8.5	9.5	4.5	9.6	4.1	7.3	9.1
264	4.8	3.8	8.8	5.1	3.7	3.6	7.3	12.7
273	5.5	4.1	6.6	9.7	6.3	7.7	8.6	5.3
283	5.1	12.8	14.0	14.5	5.9	8.6	12.6	10.3
293	6.2	9.4	5.8	9.0	8.6	4.6	9.6	6.4
303	5.8	9.1	6.3	10.8	5.7	7.2	7.0	9.7
313	7.0	8.7	7.9	7.8	4.9	7.9	4.6	7.3

Table 30. 50% offset experimental dynamic stiffnesses at 13 krpm and 345 kPa.

f [Hz]	VALUES [MN/m]							
	Re(Hxx)	Im(Hxx)	Re(Hxy)	Im(Hxy)	Re(Hyx)	Im(Hyx)	Re(Hyy)	Im(Hyy)
20	216.4	24.4	7.0	3.9	64.7	0.6	249.8	21.2
29	211.6	32.4	5.7	4.4	63.6	1.4	253.2	32.8
39	213.0	39.5	4.3	7.6	62.5	0.2	249.1	42.4
49	211.5	46.3	4.6	8.9	61.2	-0.3	251.7	54.2
59	209.3	53.8	3.6	11.9	62.4	0.1	252.3	71.1
68	210.2	66.0	2.8	14.9	61.6	-0.7	250.4	79.0
78	204.7	76.2	-0.8	18.0	58.4	1.6	229.4	114.1
88	215.9	105.9	-2.0	20.0	58.0	-17.3	262.0	108.6
98	224.9	99.8	-1.4	29.2	51.9	-1.3	256.2	117.9
107	216.1	105.5	0.8	28.4	52.0	-0.8	250.2	127.2
117	214.8	117.3	5.0	30.8	46.8	-2.2	255.2	138.5
127	219.8	129.5	1.7	33.5	48.1	-2.7	245.9	147.6
137	220.8	139.3	0.9	34.6	49.6	-0.1	252.8	161.0
146	222.1	151.7	3.9	34.6	39.9	-0.1	250.9	163.5
156	214.4	168.7	-20.8	49.8	24.7	31.7	193.7	253.8
166	221.7	175.4	0.7	47.9	41.6	5.6	262.7	200.1
176	221.4	191.0	18.0	61.3	31.2	0.8	242.0	221.4
186	234.0	203.5	8.7	70.9	29.6	11.9	235.2	225.7
195	235.9	236.3	27.5	105.0	8.7	18.8	199.5	266.3
205								
215								
225								
234								
244	202.4	264.1	1.1	50.0	5.1	-22.1	242.1	299.3
254	209.7	255.3	-47.7	84.7	18.4	-19.4	180.8	267.9
264	199.2	276.2	-20.5	52.0	-13.1	-18.6	168.6	283.1
273								
283								
293								
303								
313								

f [Hz]	UNCERTAINTIES [MN/m]							
	Re(Hxx)	Im(Hxx)	Re(Hxy)	Im(Hxy)	Re(Hyx)	Im(Hyx)	Re(Hyy)	Im(Hyy)
20	4.4	5.7	0.9	1.4	3.7	4.3	2.8	1.3
29	2.6	3.1	1.9	1.9	2.4	2.5	3.1	2.0
39	3.8	2.5	2.1	2.3	3.4	2.5	2.6	1.1
49	3.8	2.4	2.6	1.7	3.6	2.1	3.4	2.5
59	3.1	2.5	3.0	2.8	3.5	3.4	3.2	3.3
68	2.9	1.6	2.7	1.8	2.5	1.6	2.5	2.7
78	3.0	2.0	2.7	1.8	3.2	2.5	5.7	4.6
88	3.0	4.6	2.8	3.5	1.8	2.3	2.1	2.9
98	3.8	3.4	4.5	3.7	3.3	2.8	3.1	4.9
107	3.3	2.8	4.1	4.5	2.6	1.6	4.5	5.5
117	3.5	4.8	3.7	5.3	2.5	3.8	4.6	4.9
127	2.3	3.3	3.6	7.0	2.5	2.1	5.4	4.4
137	3.2	3.7	2.5	3.5	3.9	4.8	3.0	3.6
146	2.1	2.2	4.3	3.1	2.5	2.7	4.4	3.1
156	3.2	3.2	6.0	3.3	6.4	9.3	13.5	7.9
166	5.8	4.0	6.6	5.3	5.5	5.8	6.8	8.5
176	6.0	6.0	8.8	7.9	5.4	5.8	6.6	11.0
186	5.1	5.4	7.3	8.5	4.7	4.1	8.4	5.8
195	9.2	9.7	14.7	16.1	11.3	9.2	14.3	17.3
205								
215								
225								
234								
244	6.4	5.8	9.7	11.4	6.6	7.4	11.2	12.9
254	2.7	2.7	10.8	7.3	3.9	3.2	5.9	7.1
264	3.2	4.9	4.1	5.3	6.2	4.6	5.3	6.7
273								
283								
293								
303								
313								

Table 31. 50% offset experimental dynamic stiffnesses at 13 krpm and 1034 kPa.

f [Hz]	VALUES [MN/m]							
	Re(Hxx)	Im(Hxx)	Re(Hxy)	Im(Hxy)	Re(Hyx)	Im(Hyx)	Re(Hyy)	Im(Hyy)
20	236.0	20.7	15.3	2.9	69.3	-1.3	293.4	18.5
29	234.6	30.6	14.5	3.8	72.3	0.6	300.9	31.2
39	235.4	38.9	12.3	7.6	67.1	-1.7	291.0	39.9
49	235.3	47.3	13.6	8.1	64.8	-2.9	295.4	53.5
59	235.1	56.7	11.7	10.6	72.1	1.9	301.9	73.3
68	233.3	67.3	10.8	13.4	70.6	-1.6	293.7	82.8
78	232.0	76.5	9.0	15.2	68.5	0.0	288.1	97.5
88	226.4	91.1	11.4	17.5	75.6	-2.3	308.5	118.5
98	252.6	103.7	8.2	27.2	60.7	-4.4	299.6	130.3
107	242.6	106.3	8.6	25.3	56.0	2.0	289.8	133.3
117	241.3	117.9	14.0	28.0	50.3	-2.5	296.3	152.3
127	243.8	129.0	13.2	29.1	58.0	-2.5	286.7	158.6
137	248.3	139.3	11.8	30.9	61.5	-0.5	299.6	184.7
146	246.4	153.0	14.7	26.6	51.4	-6.8	313.4	161.2
156	247.0	156.5	3.7	31.6	40.5	6.9	222.2	192.3
166	246.9	170.7	10.0	37.3	36.3	3.2	309.4	215.5
176	242.7	195.1	28.4	50.8	30.1	-4.3	280.7	243.2
186	257.1	201.9	31.5	50.3	35.1	11.1	306.0	238.6
195	251.2	221.3	50.9	86.1	24.3	10.6	241.2	292.4
205								
215								
225								
234								
244	252.2	273.2	33.4	85.4	20.9	2.2	258.8	342.6
254	249.3	269.9	27.2	70.0	37.3	-8.5	275.1	334.5
264	251.0	284.6	18.3	51.5	35.0	-16.6	274.0	305.5
273	247.3	291.8	-6.1	32.5	29.7	-16.1	226.8	305.3
283	247.2	305.7	0.6	35.9	35.1	-16.8	283.4	336.3
293	246.8	319.5	-17.0	20.2	32.7	-19.1	206.6	314.7
303								
313								

f [Hz]	UNCERTAINTIES [MN/m]							
	Re(Hxx)	Im(Hxx)	Re(Hxy)	Im(Hxy)	Re(Hyx)	Im(Hyx)	Re(Hyy)	Im(Hyy)
20	6.3	3.7	1.5	2.4	6.1	4.3	2.4	1.9
29	3.1	3.0	2.2	1.6	3.0	3.6	2.7	2.2
39	2.9	1.8	3.0	2.5	4.1	2.5	1.9	2.5
49	2.0	2.8	3.0	4.8	2.9	2.0	4.4	2.5
59	3.5	3.1	4.2	2.5	3.4	2.4	3.7	3.0
68	2.0	2.2	3.2	2.5	2.3	2.0	3.6	2.1
78	4.3	3.4	3.5	2.5	5.3	2.9	4.2	2.4
88	2.9	3.9	4.1	5.1	2.3	3.0	3.8	4.3
98	5.8	3.4	4.7	6.8	3.3	4.1	3.6	6.2
107	3.8	3.7	3.1	3.0	4.0	3.1	5.6	4.1
117	5.3	2.0	5.2	4.6	3.3	3.9	6.3	6.5
127	2.7	2.5	5.7	3.6	1.5	3.1	8.0	7.4
137	1.7	2.3	4.5	4.0	2.8	4.1	5.8	3.8
146	4.1	3.7	7.8	6.1	4.2	5.9	10.1	7.1
156	4.6	3.3	5.3	3.9	3.6	3.8	4.9	7.6
166	3.6	4.5	6.8	6.8	3.9	3.6	8.5	6.7
176	3.2	5.3	7.9	11.9	7.2	7.4	13.2	14.1
186	4.1	3.9	12.5	14.5	5.8	4.9	13.1	16.9
195	4.9	8.1	16.1	15.2	7.1	6.9	19.8	20.9
205								
215								
225								
234								
244	6.4	5.3	15.4	16.3	6.1	7.0	16.1	17.3
254	3.2	5.0	14.3	13.3	4.0	4.5	16.2	12.9
264	4.6	2.8	8.7	10.2	2.6	3.1	8.6	8.5
273	2.0	1.4	5.3	5.8	1.9	2.2	5.4	4.2
283	2.9	2.3	3.9	5.8	2.0	1.1	4.6	5.1
293	2.1	1.4	3.9	3.3	1.7	1.8	4.5	3.2
303								
313								

Table 32. 50% offset experimental dynamic stiffnesses at 13 krpm and 1723 kPa.

f [Hz]	VALUES [MN/m]							
	Re(Hxx)	Im(Hxx)	Re(Hxy)	Im(Hxy)	Re(Hyx)	Im(Hyx)	Re(Hyy)	Im(Hyy)
20	267.3	18.3	25.8	2.5	75.3	-4.1	366.8	19.0
29	265.0	31.3	25.1	5.4	82.5	0.0	380.1	28.4
39	267.1	39.7	25.0	6.8	73.9	-2.9	365.1	43.2
49	266.4	47.7	25.2	7.9	71.6	-3.0	373.1	56.3
59	267.7	56.2	24.8	10.8	78.8	4.4	377.2	75.5
68	264.7	66.9	21.3	13.1	82.2	-1.0	372.1	84.7
78	263.8	75.7	18.0	13.6	73.7	1.4	367.4	103.4
88	264.2	86.4	20.7	17.5	79.7	2.1	392.5	125.2
98	282.8	109.0	24.1	21.9	75.8	-6.8	375.8	145.4
107	276.9	105.6	21.9	25.2	59.7	4.4	361.0	139.7
117	273.8	115.8	24.3	20.4	57.6	-4.3	381.6	161.4
127	276.3	125.8	21.3	23.9	66.5	-1.6	362.6	153.6
137	280.8	137.0	21.7	30.4	68.3	-2.5	381.3	195.4
146	279.9	147.7	22.0	20.4	66.2	-6.8	402.2	166.5
156	283.3	152.0	15.1	26.3	53.6	8.1	319.8	198.1
166	281.6	163.9	20.2	31.7	44.9	7.3	386.0	234.5
176	280.4	189.1	40.6	37.8	41.8	2.0	372.0	246.8
186	292.8	192.8	45.0	37.2	49.3	17.4	404.8	249.9
195	292.4	210.5	76.4	56.5	42.2	21.1	355.6	315.9
205								
215								
225								
234								
244	294.7	260.4	52.9	58.3	36.2	12.4	375.2	361.6
254	287.3	261.2	34.6	57.2	46.2	-1.2	389.8	375.1
264	290.3	277.2	28.4	44.1	48.2	-8.1	367.8	340.4
273	286.2	284.3	4.3	30.6	37.8	-11.7	355.5	326.6
283	286.2	296.5	7.8	34.5	40.9	-7.9	381.4	364.3
293	286.7	309.5	-5.2	24.2	38.8	-12.9	341.8	345.2
303	285.1	322.0	-30.4	2.3	42.4	-19.8	233.6	360.5
313	283.0	336.0	-10.5	19.3	43.9	-25.7	370.8	364.8

f [Hz]	UNCERTAINTIES [MN/m]							
	Re(Hxx)	Im(Hxx)	Re(Hxy)	Im(Hxy)	Re(Hyx)	Im(Hyx)	Re(Hyy)	Im(Hyy)
20	4.3	5.6	2.8	1.9	5.9	6.2	2.9	2.7
29	2.3	3.0	3.2	2.2	2.7	2.9	4.0	3.0
39	3.9	3.1	3.1	2.4	2.5	5.4	2.1	3.6
49	3.1	2.1	3.2	3.2	3.5	2.6	4.4	3.7
59	2.1	3.2	4.7	4.3	5.9	5.4	4.4	5.2
68	3.7	1.6	3.2	2.4	4.0	4.2	3.2	3.6
78	4.5	3.3	3.5	2.0	3.9	4.4	2.3	4.2
88	4.5	5.1	5.4	5.8	4.2	3.2	5.9	5.3
98	7.3	5.7	3.9	5.1	6.3	6.6	4.6	7.8
107	3.7	3.3	5.1	8.3	4.7	4.4	9.2	7.4
117	5.5	5.4	7.6	7.1	6.6	4.9	9.2	8.1
127	2.5	3.5	7.2	9.7	5.4	5.3	10.6	7.7
137	8.3	5.6	6.8	5.0	6.8	6.3	7.6	6.8
146	4.6	7.1	11.1	7.2	7.0	5.1	7.3	8.6
156	5.0	5.4	6.9	4.9	6.1	4.0	3.7	7.9
166	6.8	4.8	5.7	11.0	6.3	8.3	16.4	7.4
176	6.2	11.4	13.9	10.6	11.0	10.4	11.8	15.9
186	7.6	8.0	15.3	11.1	10.2	11.8	10.3	20.5
195	8.7	15.1	16.3	24.0	16.9	15.4	36.3	15.9
205								
215								
225								
234								
244	11.4	9.1	22.3	17.8	10.1	14.0	15.9	28.6
254	4.9	6.9	15.5	11.0	8.1	7.6	17.5	17.7
264	5.2	5.1	9.1	10.7	6.3	5.5	13.6	10.6
273	2.8	2.0	5.4	6.5	2.5	3.5	8.1	4.0
283	3.1	2.6	6.2	8.8	3.4	3.3	7.6	6.6
293	2.0	2.7	5.3	1.9	1.6	2.2	3.5	5.1
303	2.0	2.8	2.0	4.8	1.4	2.8	9.9	6.1
313	1.8	2.5	2.1	3.1	1.5	1.6	3.5	3.1

Table 33. 50% offset experimental dynamic stiffnesses at 13 krpm and 2412 kPa.

f [Hz]	VALUES [MN/m]							
	Re(Hxx)	Im(Hxx)	Re(Hxy)	Im(Hxy)	Re(Hyx)	Im(Hyx)	Re(Hyy)	Im(Hyy)
20	299.5	20.0	37.8	1.9	84.0	-2.8	455.9	20.4
29	297.2	30.6	34.6	3.5	91.0	2.8	472.3	33.2
39	299.0	39.0	35.0	5.5	81.8	-0.4	458.0	46.6
49	298.0	47.8	35.5	4.2	77.1	-0.1	463.3	60.2
59	301.0	57.8	36.4	10.6	86.7	6.7	466.0	76.2
68	299.1	67.0	32.9	12.1	91.2	2.0	464.0	86.6
78	299.3	75.1	28.0	10.2	80.1	1.7	464.2	105.0
88	301.0	86.0	31.1	13.2	83.0	8.1	472.9	134.7
98	296.9	106.1	34.7	17.5	102.6	-0.9	465.7	146.0
107	311.7	106.0	32.3	23.5	68.7	4.5	456.5	140.3
117	311.8	114.0	30.9	16.9	65.2	0.7	474.9	161.8
127	310.6	123.9	32.2	21.3	74.5	1.9	448.9	152.9
137	314.6	136.2	28.9	22.2	75.3	-1.1	475.8	193.9
146	315.4	144.7	25.2	17.1	78.2	-5.3	505.7	160.1
156	320.2	150.3	25.9	25.8	62.6	10.6	420.4	194.7
166	319.4	159.2	31.5	28.6	52.2	14.9	486.7	233.9
176	322.1	182.2	45.3	21.4	50.7	13.3	474.3	249.2
186	330.4	182.2	46.6	21.1	65.2	21.7	515.7	236.7
195	331.9	198.7	75.6	24.1	59.7	30.4	480.2	305.0
205								
215								
225								
234								
244	335.9	251.1	52.1	30.5	48.6	25.2	497.3	359.8
254	325.6	254.1	34.6	36.1	54.4	3.8	477.0	343.6
264	327.3	268.8	31.4	30.1	54.8	-1.6	481.6	338.7
273	323.9	276.9	4.0	23.4	45.3	-6.3	447.9	333.3
283	324.5	289.0	11.4	31.8	46.1	-1.7	485.8	363.3
293	324.8	300.4	-3.8	21.3	43.6	-7.7	445.4	349.0
303	324.0	313.4	-18.1	10.0	41.3	-20.1	398.2	338.9
313	323.1	327.4	-7.9	27.3	46.1	-19.8	507.3	390.8

f [Hz]	UNCERTAINTIES [MN/m]							
	Re(Hxx)	Im(Hxx)	Re(Hxy)	Im(Hxy)	Re(Hyx)	Im(Hyx)	Re(Hyy)	Im(Hyy)
20	4.5	7.0	2.5	2.6	9.7	7.9	3.6	2.5
29	4.1	3.9	4.4	3.6	4.4	4.1	4.2	2.6
39	4.4	2.6	4.7	4.8	4.9	6.1	5.1	5.5
49	3.3	3.5	3.2	4.0	5.1	4.0	3.5	3.1
59	7.5	7.6	4.1	8.8	5.3	6.7	4.5	7.3
68	4.3	6.7	4.3	3.5	2.7	4.5	2.2	3.3
78	3.2	4.7	5.8	3.2	6.3	4.6	3.9	5.4
88	4.1	4.3	8.3	8.3	6.1	4.2	5.6	5.9
98	6.1	5.5	4.3	9.0	5.1	6.0	6.1	11.6
107	5.3	3.9	12.1	6.9	5.5	3.6	8.4	8.5
117	6.7	4.0	8.3	9.2	7.2	7.7	6.7	5.9
127	3.7	3.6	7.6	11.0	4.8	6.7	13.5	12.0
137	7.1	5.7	8.6	7.1	8.6	5.6	8.6	7.7
146	4.7	3.9	8.2	13.2	7.3	5.8	9.8	9.3
156	5.4	7.9	5.7	8.8	8.7	3.6	9.7	11.9
166	2.7	8.4	14.4	12.9	11.9	8.9	12.7	13.4
176	9.1	6.4	14.1	25.5	6.4	16.3	23.0	18.9
186	8.6	8.1	17.0	19.7	8.3	12.9	25.8	26.5
195	12.4	8.1	32.8	23.9	11.7	17.6	34.5	41.0
205								
215								
225								
234								
244	7.3	11.1	21.8	23.1	13.8	9.7	36.6	25.6
254	3.9	5.3	14.8	15.5	8.1	7.5	17.1	27.0
264	5.3	3.8	10.0	14.3	7.2	3.8	20.1	17.3
273	2.3	3.9	9.7	9.3	3.7	1.9	8.3	16.1
283	2.7	2.8	8.7	10.0	3.9	2.6	12.1	12.1
293	2.7	3.8	6.4	5.2	3.2	1.7	8.6	5.7
303	1.9	2.4	3.6	3.6	1.8	1.8	4.0	3.6
313	1.9	2.9	3.2	2.7	2.8	2.1	3.5	6.1

Table 34. 50% offset experimental dynamic stiffnesses at 13 krpm and 3101 kPa.

f [Hz]	VALUES [MN/m]							
	Re(Hxx)	Im(Hxx)	Re(Hxy)	Im(Hxy)	Re(Hyx)	Im(Hyx)	Re(Hyy)	Im(Hyy)
20	327.9	19.4	43.8	1.1	90.5	-6.6	557.7	19.0
29	328.5	29.4	41.7	2.9	95.7	3.7	573.7	31.0
39	328.7	39.8	40.9	3.2	88.3	0.0	559.5	45.4
49	328.7	48.2	41.2	3.6	84.7	1.9	565.3	53.8
59	330.6	57.2	44.1	7.5	92.6	8.2	568.0	75.6
68	328.0	65.5	41.0	9.8	97.7	1.3	563.3	83.9
78	329.5	75.1	36.1	9.7	85.0	2.9	561.5	98.0
88	332.3	84.1	38.1	10.2	89.2	9.5	581.6	125.7
98	330.0	95.2	41.4	17.7	106.0	10.9	566.3	140.2
107	342.8	106.9	40.9	19.0	71.9	3.2	554.7	135.4
117	341.2	112.9	40.6	11.6	70.1	2.6	576.1	154.4
127	341.4	123.3	40.4	16.0	81.0	5.1	551.9	148.9
137	346.6	134.0	39.0	22.3	80.6	2.8	571.8	184.9
146	345.9	143.5	32.6	13.2	81.6	2.3	600.7	147.4
156	350.3	148.6	35.7	20.2	70.5	12.6	521.5	190.1
166	351.2	157.9	39.2	27.6	59.0	19.6	587.1	224.3
176	356.1	181.7	62.7	19.2	52.9	21.9	585.1	259.2
186	365.2	177.5	68.1	10.2	76.2	31.0	630.8	248.8
195	370.9	197.1	107.8	13.0	65.7	47.3	607.0	340.4
205								
215								
225								
234								
244	369.6	244.4	70.0	21.6	55.3	35.1	617.3	376.0
254	358.2	246.9	49.4	28.0	58.9	9.5	583.9	345.6
264	360.8	260.2	42.7	22.9	59.3	4.6	582.8	344.3
273	357.0	268.6	8.2	18.4	48.5	0.8	536.6	323.3
283	357.9	281.0	15.8	29.9	50.8	4.9	592.0	354.1
293	358.2	291.5	-5.4	19.2	45.5	-0.3	533.9	344.1
303	358.5	304.2	-19.4	13.2	43.3	-13.9	507.0	344.5
313								

f [Hz]	UNCERTAINTIES [MN/m]							
	Re(Hxx)	Im(Hxx)	Re(Hxy)	Im(Hxy)	Re(Hyx)	Im(Hyx)	Re(Hyy)	Im(Hyy)
20	6.0	5.9	4.3	3.1	7.9	7.5	4.2	2.4
29	5.0	6.5	6.1	4.1	5.9	8.7	5.2	5.1
39	4.1	7.1	4.5	5.2	4.8	4.7	5.4	4.0
49	5.5	3.2	4.6	4.9	3.7	4.3	5.7	8.2
59	5.7	6.5	5.7	5.2	8.5	4.5	7.4	6.2
68	3.8	4.3	5.9	3.3	3.8	5.6	4.0	4.6
78	4.5	3.2	6.3	4.7	6.0	5.5	4.3	5.5
88	7.3	4.5	8.9	6.1	7.3	5.9	6.6	7.4
98	4.6	3.3	8.4	11.7	5.8	9.1	7.1	11.3
107	4.7	5.3	8.8	10.2	6.2	3.6	9.9	7.7
117	6.6	4.8	15.2	12.2	6.0	6.2	7.3	12.7
127	5.3	6.0	15.1	10.1	4.3	6.1	9.8	17.2
137	8.7	4.8	9.5	10.6	9.2	9.1	16.1	7.6
146	9.8	5.6	8.9	11.5	10.9	10.4	12.5	15.0
156	7.6	7.8	10.1	14.7	10.4	4.0	13.2	10.6
166	7.1	11.2	10.8	12.6	12.2	7.8	14.5	18.2
176	7.1	12.3	15.2	14.7	10.5	19.9	25.1	21.6
186	7.9	11.6	19.5	19.0	15.4	14.9	25.8	25.4
195	15.4	16.9	42.4	34.0	21.5	28.7	51.7	56.3
205								
215								
225								
234								
244	10.7	14.7	27.1	31.5	20.4	16.0	46.5	35.5
254	6.7	8.1	23.6	15.7	12.0	8.7	21.6	32.5
264	4.6	6.2	12.8	13.3	9.5	6.0	23.0	18.4
273	3.2	3.5	11.0	7.8	5.2	3.6	6.2	17.2
283	4.2	4.3	7.2	6.0	5.4	4.4	11.3	11.8
293	2.5	2.6	3.5	4.8	3.4	3.9	7.8	4.7
303	2.7	3.1	3.0	3.2	3.1	1.8	6.6	2.9
313								

Table 35. 50% offset experimental dynamic stiffnesses at 16 krpm and zero load.

f [Hz]	VALUES [MN/m]							
	Re(Hxx)	Im(Hxx)	Re(Hxy)	Im(Hxy)	Re(Hyx)	Im(Hyx)	Re(Hyy)	Im(Hyy)
20	256.5	13.9	2.4	1.9	72.2	3.7	290.3	19.6
29	258.7	23.3	1.3	5.1	72.5	-6.7	291.9	29.7
39	253.0	37.0	-0.1	8.3	74.5	2.2	291.2	39.4
49	255.0	37.8	-0.4	10.6	75.0	6.9	292.0	49.2
59	267.8	47.3	-0.4	15.6	78.7	-17.5	293.3	58.2
68	251.2	51.2	-2.4	16.0	70.2	4.7	287.9	71.3
78	233.1	68.6	0.5	18.6	80.6	2.1	290.7	89.4
88	270.0	80.0	-3.8	22.0	52.9	-8.9	295.4	90.9
98	267.1	83.7	-2.6	28.1	61.3	-13.7	298.0	98.8
107	260.4	86.1	-0.2	30.5	71.4	2.8	290.4	106.1
117	248.8	90.7	-0.1	30.0	62.1	-0.7	291.9	114.7
127	250.7	110.9	-2.0	33.0	54.2	-18.7	287.6	131.5
137	252.3	121.3	-2.5	36.2	66.8	7.5	284.8	144.5
146	261.5	142.2	-3.8	35.9	61.3	-2.2	288.2	146.9
156	254.4	135.6	-5.6	41.3	46.3	-5.7	270.9	182.3
166	250.1	149.3	-0.2	41.8	45.4	-0.8	300.5	180.3
176	266.0	161.2	-4.7	47.0	70.6	4.2	290.2	185.1
186	259.0	175.3	2.8	43.7	65.1	1.3	297.4	191.9
195	242.5	174.3	-8.2	52.5	23.9	-14.3	271.7	202.9
205	259.8	203.4	7.6	51.3	41.9	23.4	285.8	227.8
215	275.4	197.3	6.7	67.4	64.1	12.7	246.5	257.6
225								
234								
244								
254								
264								
273								
283								
293								
303								
313								

f [Hz]	UNCERTAINTIES [MN/m]							
	Re(Hxx)	Im(Hxx)	Re(Hxy)	Im(Hxy)	Re(Hyx)	Im(Hyx)	Re(Hyy)	Im(Hyy)
20	8.9	15.0	4.2	2.9	16.1	15.8	3.5	5.0
29	22.8	9.5	3.8	3.9	13.7	18.3	3.6	3.4
39	9.5	16.0	3.0	2.7	10.2	18.4	2.9	4.6
49	14.8	10.9	3.5	3.1	18.9	15.8	3.7	3.9
59	8.5	9.6	4.5	5.9	16.7	15.5	3.0	4.7
68	12.4	10.5	3.2	4.4	19.3	12.7	4.5	4.8
78	25.2	9.6	3.6	4.2	21.1	22.9	4.0	2.8
88	22.2	18.6	4.7	2.1	14.0	18.3	5.4	5.5
98	9.4	19.6	4.1	6.1	16.0	20.8	6.1	7.6
107	21.6	17.2	7.8	7.2	24.8	25.2	8.0	3.7
117	26.8	27.1	6.6	6.1	24.2	26.0	5.7	7.3
127	13.3	13.3	7.9	6.3	15.4	17.0	5.8	6.5
137	27.3	14.0	6.4	4.1	20.9	17.3	8.3	7.4
146	24.1	23.3	6.2	3.2	31.4	24.6	8.0	7.5
156	8.3	17.3	8.0	5.5	10.1	14.6	7.8	6.4
166	13.9	19.8	3.6	6.4	23.3	22.0	7.1	9.8
176	29.8	17.4	9.4	8.9	28.5	26.8	11.8	6.2
186	21.0	14.6	7.0	9.7	31.4	27.6	6.5	8.8
195	26.5	16.0	6.6	11.9	24.5	19.9	8.2	11.1
205	29.3	31.5	12.5	12.3	24.0	42.4	17.5	17.6
215	13.6	22.2	13.7	17.2	22.6	22.8	14.5	23.1
225								
234								
244								
254								
264								
273								
283								
293								
303								
313								

Table 36. 50% offset experimental dynamic stiffnesses at 16 krpm and 345 kPa.

f [Hz]	VALUES [MN/m]							
	Re(Hxx)	Im(Hxx)	Re(Hxy)	Im(Hxy)	Re(Hyx)	Im(Hyx)	Re(Hyy)	Im(Hyy)
20	244.9	18.7	5.4	3.1	79.4	3.4	288.6	20.1
29	242.5	25.7	3.9	5.9	79.5	5.8	288.8	29.4
39	249.6	44.0	3.8	8.7	78.8	-7.5	289.3	37.6
49	247.2	45.2	2.8	12.0	74.4	-3.0	290.1	46.2
59	253.2	68.8	2.7	15.9	87.3	-20.3	290.7	58.1
68	240.8	42.2	5.0	17.6	65.9	15.8	289.9	66.0
78	203.1	89.8	2.1	15.4	104.1	-6.6	291.7	78.7
88	236.6	69.5	0.1	22.9	64.5	22.1	292.0	83.1
98	267.6	85.0	1.3	27.7	70.6	2.3	292.4	91.3
107	238.8	95.0	1.0	29.9	55.9	24.2	285.9	103.1
117	201.9	65.5	3.0	24.1	43.0	50.5	281.5	111.1
127	258.3	102.8	6.9	33.2	68.0	-16.5	290.9	122.4
137	229.2	132.8	3.3	34.0	45.5	62.9	283.9	135.9
146	273.6	205.3	-2.3	46.2	17.4	41.9	284.6	142.2
156	239.7	162.3	1.9	38.9	31.0	11.4	287.1	149.4
166	264.5	221.7	1.6	42.4	-13.9	109.5	278.3	161.1
176	289.0	194.7	9.6	42.7	83.3	107.4	286.1	181.8
186	294.1	180.0	0.0	47.4	77.3	49.6	283.0	185.5
195	142.1	227.0	0.5	37.4	-81.6	-63.6	285.4	192.2
205	318.2	213.1	-2.8	54.4	69.8	117.6	270.8	214.8
215								
225								
234								
244								
254								
264								
273								
283								
293								
303								
313								

f [Hz]	UNCERTAINTIES [MN/m]							
	Re(Hxx)	Im(Hxx)	Re(Hxy)	Im(Hxy)	Re(Hyx)	Im(Hyx)	Re(Hyy)	Im(Hyy)
20	9.4	9.3	1.4	1.5	7.5	9.6	2.4	1.2
29	5.6	3.8	1.2	2.9	5.7	7.4	1.7	1.5
39	6.1	7.7	1.3	1.3	9.0	8.9	2.0	2.3
49	9.7	9.9	1.7	2.7	6.8	8.9	2.1	2.8
59	6.9	11.0	2.2	3.4	9.2	6.6	4.0	2.6
68	7.8	5.3	1.3	1.6	6.4	5.0	1.9	1.8
78	10.9	9.0	1.5	1.7	8.8	5.5	2.0	2.5
88	7.3	11.8	2.3	2.5	6.4	12.6	2.5	2.7
98	7.8	8.5	3.4	3.4	6.2	6.0	3.3	4.5
107	9.8	13.6	3.9	2.2	10.9	8.2	4.4	5.0
117	18.3	12.1	3.3	3.0	11.1	13.7	6.3	4.7
127	7.0	7.8	6.3	6.7	5.3	6.7	4.1	4.0
137	14.4	12.5	3.0	4.4	17.4	12.5	3.5	3.9
146	17.1	30.9	4.4	8.6	19.2	14.1	6.6	4.0
156	14.9	10.2	7.0	4.6	7.2	12.0	5.3	3.9
166	39.3	20.4	6.2	4.8	22.7	22.7	7.9	7.6
176	26.6	17.8	8.3	6.5	32.8	11.4	7.0	4.4
186	9.8	11.0	4.3	3.6	9.0	8.4	3.6	5.5
195	29.4	28.1	10.8	5.8	33.0	34.3	9.5	12.3
205	9.9	4.9	6.0	6.5	7.8	10.8	5.1	7.6
215								
225								
234								
244								
254								
264								
273								
283								
293								
303								
313								

Table 37. 50% offset experimental dynamic stiffnesses at 16 krpm and 1034 kPa.

f [Hz]	VALUES [MN/m]							
	Re(Hxx)	Im(Hxx)	Re(Hxy)	Im(Hxy)	Re(Hyx)	Im(Hyx)	Re(Hyy)	Im(Hyy)
20	272.8	16.1	8.7	2.2	81.4	-2.8	311.6	17.7
29	272.6	23.5	4.7	3.0	79.3	-10.9	318.7	29.6
39	272.5	33.2	3.9	6.9	87.9	-5.2	313.1	39.6
49	269.4	43.2	3.7	9.5	73.1	4.9	314.4	50.5
59	275.9	44.0	2.5	13.8	100.2	-20.5	320.6	60.6
68	266.3	56.6	2.1	15.2	71.1	6.4	311.9	69.2
78	258.1	72.4	-1.0	17.6	101.1	21.6	302.4	89.8
88	262.2	77.6	2.2	20.7	90.7	24.8	320.0	96.9
98	291.0	75.5	-1.9	25.7	63.9	-18.4	320.8	102.1
107	273.9	95.2	1.1	28.6	60.0	10.5	309.7	113.9
117	255.8	93.4	-0.6	29.6	50.9	65.4	308.1	125.4
127	269.8	103.6	-0.1	32.1	69.2	-26.3	308.1	135.2
137	265.1	129.7	0.9	36.6	50.4	12.9	310.4	154.1
146	289.4	150.3	-0.4	38.4	70.7	15.9	317.4	150.1
156	271.5	149.1	-11.7	39.2	44.9	15.2	254.6	184.2
166	254.7	182.7	-5.4	40.3	5.4	17.5	320.7	172.4
176	289.6	182.3	-3.3	45.2	59.6	83.6	289.5	195.6
186	286.3	161.2	-1.3	39.9	91.6	-0.6	321.0	188.8
195	257.8	206.9	-11.7	43.4	-2.5	7.4	286.5	196.9
205	283.1	218.8	-8.7	47.6	29.6	44.3	302.5	221.1
215	303.4	248.6	-9.4	52.2	34.6	76.8	278.4	226.2
225								
234								
244								
254								
264								
273								
283								
293								
303								
313								

f [Hz]	UNCERTAINTIES [MN/m]							
	Re(Hxx)	Im(Hxx)	Re(Hxy)	Im(Hxy)	Re(Hyx)	Im(Hyx)	Re(Hyy)	Im(Hyy)
20	8.4	9.1	3.7	3.5	12.2	12.3	3.7	3.8
29	10.8	14.6	1.8	3.3	13.9	10.5	3.5	5.5
39	10.7	9.0	2.6	3.4	13.8	11.9	4.5	3.6
49	7.9	10.1	1.8	3.0	10.0	11.3	3.9	4.1
59	11.0	15.0	5.1	4.3	9.0	19.0	3.9	4.4
68	7.2	5.9	3.0	5.3	10.9	7.5	3.4	4.2
78	12.9	17.5	2.8	1.9	20.1	18.7	4.0	4.7
88	12.3	12.2	3.3	3.4	13.1	18.6	3.6	6.1
98	12.7	16.5	4.5	3.7	11.9	15.3	4.8	5.9
107	6.4	6.2	3.5	2.8	11.7	12.4	5.2	6.9
117	30.3	27.0	4.5	6.1	57.2	20.0	3.3	8.1
127	8.1	9.4	6.4	7.1	10.1	9.6	11.0	9.1
137	14.8	12.4	5.5	5.7	13.4	29.7	7.8	7.2
146	19.9	19.4	4.9	9.2	20.6	29.5	10.6	11.0
156	11.2	12.6	5.3	6.8	10.7	14.4	7.6	11.3
166	15.5	35.7	8.7	9.3	35.3	46.5	12.6	18.0
176	27.0	13.2	5.4	5.0	28.2	65.7	8.6	9.0
186	11.0	11.5	7.2	7.0	16.8	16.8	13.6	17.6
195	14.3	34.2	7.0	8.7	57.2	26.0	11.8	10.2
205	16.6	21.6	9.7	8.0	19.8	42.0	13.6	25.1
215	18.4	44.9	14.8	13.4	41.3	67.3	28.8	16.7
225								
234								
244								
254								
264								
273								
283								
293								
303								
313								

Table 38. 50% offset experimental dynamic stiffnesses at 16 krpm and 1723 kPa.

f [Hz]	VALUES [MN/m]							
	Re(Hxx)	Im(Hxx)	Re(Hxy)	Im(Hxy)	Re(Hyx)	Im(Hyx)	Re(Hyy)	Im(Hyy)
20	297.0	13.1	15.3	0.1	90.8	-2.7	364.5	17.2
29	296.2	26.8	13.5	3.3	94.1	-1.0	372.9	28.7
39	297.7	33.1	10.7	3.7	86.8	-2.3	362.1	40.5
49	295.5	41.8	10.4	6.7	84.5	-2.7	367.1	51.8
59	295.3	48.3	8.3	10.5	92.9	-3.1	374.5	69.2
68	293.3	57.8	6.5	12.1	90.9	-2.2	367.1	74.8
78	293.9	66.8	3.8	15.7	89.5	-1.8	357.9	90.6
88	289.5	75.7	6.5	19.6	93.0	-1.2	382.9	104.3
98	305.5	100.8	1.7	21.3	78.6	-22.9	371.0	118.3
107	301.0	94.8	2.9	28.2	71.6	-0.1	354.6	124.0
117	295.4	101.3	2.1	29.8	76.0	-7.8	369.2	137.9
127	296.3	110.5	1.3	31.1	82.2	-10.3	355.8	135.5
137	298.0	126.3	4.4	37.5	68.6	-4.7	365.7	173.5
146	306.1	135.4	5.3	33.1	76.9	-7.4	383.8	154.9
156	297.3	140.4	-7.5	33.1	59.6	-4.7	319.4	169.1
166	297.6	152.3	0.6	37.2	58.8	-0.2	387.2	198.7
176	300.2	163.7	-0.4	41.4	63.1	1.0	354.2	194.4
186	301.0	172.2	-2.2	44.7	69.4	-2.0	379.1	189.7
195	298.0	187.5	-3.7	40.0	57.6	2.2	349.9	208.3
205	300.1	197.5	-6.0	47.7	60.9	-0.1	362.2	241.6
215	300.4	227.0	-2.1	45.1	41.0	3.2	360.0	220.3
225	297.1	235.1	-8.7	48.8	25.5	-6.7	299.7	273.4
234	314.0	240.4	13.8	47.4	53.5	11.1	409.1	260.3
244	313.9	281.7	17.7	41.4	3.3	28.6	380.4	296.5
254								
264								
273								
283								
293								
303								
313								

f [Hz]	UNCERTAINTIES [MN/m]							
	Re(Hxx)	Im(Hxx)	Re(Hxy)	Im(Hxy)	Re(Hyx)	Im(Hyx)	Re(Hyy)	Im(Hyy)
20	3.7	4.5	1.4	1.7	6.1	5.7	2.3	1.7
29	3.4	4.4	2.5	1.6	4.3	2.5	2.2	2.1
39	3.4	3.6	3.0	1.8	2.6	3.6	2.6	3.9
49	2.0	2.1	3.1	2.3	2.6	2.7	2.7	3.5
59	1.7	2.6	2.7	2.9	4.0	7.2	3.6	5.2
68	3.0	2.4	1.7	1.5	3.7	2.0	2.5	2.3
78	5.2	3.7	2.4	1.7	5.1	2.9	2.9	2.9
88	3.0	2.7	4.0	3.3	4.2	3.2	4.0	3.3
98	5.4	4.9	4.0	5.3	4.5	5.3	3.8	4.2
107	3.6	3.8	5.2	4.0	4.6	3.3	2.7	4.4
117	4.4	3.6	5.6	4.9	8.2	3.3	5.4	7.0
127	3.2	2.7	6.3	5.2	3.0	4.3	4.6	4.5
137	4.5	2.8	6.4	5.4	8.2	5.0	7.8	6.6
146	3.1	3.6	4.3	5.7	6.0	4.4	5.7	5.6
156	2.8	2.7	5.4	4.6	4.7	3.6	2.5	4.2
166	3.5	3.9	3.3	3.8	4.3	6.4	7.4	6.0
176	4.7	2.4	5.8	4.2	2.2	6.8	6.3	5.5
186	3.6	4.1	3.8	4.1	5.2	6.0	4.3	4.5
195	3.9	4.8	8.7	4.9	5.1	6.3	8.1	8.1
205	2.5	2.5	6.1	5.1	6.6	3.9	5.6	8.9
215	7.9	7.2	10.6	7.6	10.4	10.6	11.9	13.7
225	4.0	6.3	12.3	7.7	10.3	7.9	10.1	15.7
234	6.4	6.0	24.6	6.2	6.9	9.4	22.4	24.4
244	6.9	17.6	40.8	18.6	21.1	13.0	39.3	42.3
254								
264								
273								
283								
293								
303								
313								

Table 39. 50% offset experimental dynamic stiffnesses at 16 krpm and 2412 kPa.

f [Hz]	VALUES [MN/m]							
	Re(Hxx)	Im(Hxx)	Re(Hxy)	Im(Hxy)	Re(Hyx)	Im(Hyx)	Re(Hyy)	Im(Hyy)
20	324.5	16.9	30.7	-1.0	93.5	-3.3	442.9	19.0
29	323.2	28.5	27.9	2.5	103.0	2.1	455.0	30.6
39	324.1	33.6	24.4	2.8	94.7	-4.1	441.8	42.9
49	322.8	42.9	23.7	5.8	91.8	-1.5	448.5	58.5
59	322.9	51.1	25.4	9.8	97.8	1.3	450.8	73.6
68	321.6	59.2	21.6	11.0	103.0	-0.5	448.6	80.8
78	322.9	69.3	17.0	12.2	98.0	-0.5	448.9	99.6
88	322.7	77.6	21.2	16.9	99.5	1.9	460.8	119.2
98	313.7	88.9	19.3	19.9	108.8	-4.4	450.0	131.3
107	331.4	99.0	15.4	25.1	79.0	-1.7	439.5	129.6
117	326.0	105.5	20.6	27.7	82.9	-6.0	456.3	153.0
127	326.0	114.7	14.9	32.5	90.8	-10.3	437.4	136.0
137	327.5	128.5	18.5	30.1	81.0	-10.6	456.9	181.6
146	334.8	137.6	18.3	32.0	89.8	-12.7	478.0	160.1
156	330.1	143.2	10.3	31.4	74.0	-3.6	411.2	176.2
166	328.6	151.7	18.9	29.6	73.0	-0.5	479.1	205.9
176	331.3	162.1	16.6	32.3	76.5	-5.1	448.8	202.3
186	332.8	171.3	12.0	38.8	80.7	-4.8	471.3	193.2
195	329.7	184.6	9.9	31.7	74.5	-2.3	439.8	213.5
205	332.3	196.1	6.8	41.1	77.3	-3.3	464.6	247.7
215	335.6	216.4	5.8	44.2	64.6	-3.3	439.5	227.8
225	335.1	225.8	14.4	35.2	49.0	-4.3	406.8	257.7
234								
244								
254								
264								
273								
283								
293								
303								
313								

f [Hz]	UNCERTAINTIES [MN/m]							
	Re(Hxx)	Im(Hxx)	Re(Hxy)	Im(Hxy)	Re(Hyx)	Im(Hyx)	Re(Hyy)	Im(Hyy)
20	6.4	5.8	2.1	1.8	4.0	7.5	2.3	1.5
29	3.6	2.5	3.9	2.4	4.3	3.1	2.1	2.5
39	2.3	3.2	2.2	3.8	4.5	4.8	3.4	5.1
49	3.6	2.7	4.8	2.8	3.6	3.1	4.0	4.8
59	6.0	5.4	4.0	3.8	6.6	3.0	3.2	5.7
68	2.9	2.5	2.6	3.9	3.2	3.9	3.6	4.1
78	4.7	4.3	2.5	5.5	3.0	4.3	3.5	5.1
88	5.5	3.0	2.7	3.6	4.9	5.2	6.9	6.5
98	4.2	4.5	5.7	6.2	4.0	4.3	8.8	8.0
107	3.8	2.1	6.0	5.3	3.3	2.5	4.8	6.2
117	3.6	4.2	6.3	3.4	4.6	3.9	4.4	6.6
127	3.4	2.0	8.6	7.5	3.5	3.7	8.3	10.5
137	5.8	5.9	6.5	6.7	4.2	6.5	5.6	7.2
146	4.6	2.7	7.0	9.9	6.2	3.8	10.1	6.3
156	5.9	2.4	7.7	7.8	4.1	3.4	7.9	6.0
166	6.5	4.3	8.4	8.4	4.9	6.2	8.4	7.0
176	3.2	4.6	7.7	8.5	3.0	7.8	6.9	9.3
186	1.5	4.6	7.7	6.6	3.9	5.8	8.0	6.7
195	3.3	3.8	7.9	7.8	5.4	4.1	10.6	8.9
205	4.2	4.2	5.7	9.8	5.3	3.7	9.8	7.5
215	4.9	7.0	10.8	8.5	6.7	5.8	8.8	13.3
225	4.8	6.8	7.6	13.9	7.7	5.8	13.9	11.5
234								
244								
254								
264								
273								
283								
293								
303								
313								

Table 40. 50% offset experimental dynamic stiffnesses at 16 krpm and 3101 kPa.

f [Hz]	VALUES [MN/m]							
	Re(Hxx)	Im(Hxx)	Re(Hxy)	Im(Hxy)	Re(Hyx)	Im(Hyx)	Re(Hyy)	Im(Hyy)
20	346.6	20.8	39.0	-0.9	106.1	-1.2	532.1	20.4
29	347.9	28.1	38.1	0.5	112.3	0.4	543.9	32.5
39	347.8	34.3	31.7	0.6	104.2	-1.2	533.7	44.6
49	347.0	42.8	34.1	2.6	100.4	-1.3	537.7	58.9
59	345.4	50.1	36.6	9.1	106.1	-0.3	536.2	71.0
68	344.1	60.9	31.3	9.5	112.4	1.0	535.7	79.4
78	347.2	70.8	26.2	11.2	104.5	-2.2	536.8	97.0
88	348.1	77.8	32.3	14.1	107.7	2.4	555.1	118.9
98	343.9	87.7	30.0	20.7	110.2	4.1	537.5	124.4
107	356.3	106.4	27.2	26.9	84.5	-6.8	523.1	125.1
117	351.6	107.1	28.1	26.3	87.7	-3.5	541.2	148.4
127	352.8	113.4	27.8	26.5	97.2	-6.9	523.6	133.8
137	352.4	129.8	26.9	28.3	89.5	-11.3	545.3	172.9
146	359.2	138.4	23.6	30.5	95.9	-7.0	565.8	154.8
156	357.1	143.8	19.9	28.8	82.4	-1.4	498.6	172.5
166	358.9	153.6	30.0	31.9	81.2	-0.9	564.1	197.4
176	360.3	165.7	25.6	29.2	82.8	-1.5	533.0	202.1
186	362.3	173.9	21.9	36.0	84.5	-2.0	550.2	185.8
195	361.6	184.7	20.4	30.9	80.8	1.5	518.5	211.4
205	361.8	193.9	13.9	34.4	81.3	-0.7	543.9	236.4
215	365.5	212.3	7.8	36.7	69.4	-1.6	517.2	217.1
225	365.0	220.8	20.5	42.7	60.1	-2.9	527.5	252.2
234	373.6	226.8	38.4	44.8	79.7	5.1	607.4	295.2
244	379.9	242.2	47.6	40.9	65.6	17.9	561.2	328.3
254								
264								
273								
283								
293								
303								
313								

f [Hz]	UNCERTAINTIES [MN/m]							
	Re(Hxx)	Im(Hxx)	Re(Hxy)	Im(Hxy)	Re(Hyx)	Im(Hyx)	Re(Hyy)	Im(Hyy)
20	8.7	6.0	4.6	3.8	5.0	8.1	3.1	2.1
29	4.9	3.1	4.6	4.0	4.9	5.1	5.0	3.8
39	4.4	2.7	6.0	4.1	4.8	7.1	4.8	6.1
49	3.8	3.8	3.9	5.3	4.1	4.5	5.1	9.4
59	4.7	6.1	5.1	6.1	8.3	7.9	9.1	6.9
68	3.4	2.4	3.5	4.4	5.6	4.9	4.5	6.8
78	6.8	4.6	4.3	4.0	6.9	6.8	5.0	5.6
88	4.1	4.6	6.1	5.7	3.0	4.2	5.4	6.4
98	5.6	5.4	5.9	7.3	5.3	2.9	9.0	11.6
107	3.1	2.7	4.5	6.8	5.1	4.8	8.8	5.1
117	7.8	6.9	6.5	7.5	9.8	8.9	12.9	17.4
127	3.1	3.8	8.6	15.8	5.3	5.5	11.7	15.6
137	5.2	6.9	12.7	9.6	9.1	5.0	13.8	12.5
146	6.7	4.3	8.3	8.2	9.9	3.7	13.1	13.8
156	4.4	5.6	7.5	10.4	5.4	5.6	8.7	10.2
166	3.8	4.3	5.4	10.8	6.5	7.0	13.3	10.2
176	7.8	6.6	14.0	10.3	6.4	8.4	10.2	15.7
186	4.3	3.5	7.3	11.5	3.9	5.7	11.7	12.2
195	4.1	4.9	10.1	11.7	4.9	6.2	10.6	10.1
205	4.5	5.6	8.3	13.4	9.2	4.5	14.8	10.5
215	7.5	6.1	14.2	14.5	6.2	12.8	11.4	18.8
225	6.7	8.3	18.2	16.0	11.5	9.7	22.2	23.9
234	6.0	6.1	25.6	21.9	9.5	10.6	35.9	38.7
244	14.6	15.3	45.5	24.8	18.2	19.0	40.3	60.1
254								
264								
273								
283								
293								
303								
313								

Table 41. 60% offset experimental dynamic stiffnesses at 7 krpm and zero load.

f [Hz]	VALUES [MN/m]							
	Re(Hxx)	Im(Hxx)	Re(Hxy)	Im(Hxy)	Re(Hyx)	Im(Hyx)	Re(Hyy)	Im(Hyy)
20	167.4	24.4	10.7	5.8	51.8	7.3	196.4	26.2
29	171.7	33.7	10.8	8.8	47.2	3.1	196.7	36.3
39	169.6	42.5	10.5	13.1	44.9	7.1	195.8	50.3
49	170.8	49.3	14.3	13.6	47.0	7.3	198.1	61.2
59	171.2	62.0	12.7	18.4	47.2	5.3	199.2	74.4
68	167.5	72.3	11.1	20.9	47.9	11.4	199.2	88.5
78	167.3	82.5	11.2	22.8	49.9	9.8	203.4	100.1
88	177.7	109.9	8.0	28.7	41.5	-7.1	209.4	111.5
98	187.2	108.9	9.2	35.1	36.3	11.4	207.1	121.0
107	179.6	111.9	16.7	36.4	40.1	14.7	207.8	135.1
117								
127	179.0	137.3	17.5	43.1	37.0	15.8	210.8	164.9
137	181.8	150.5	13.2	46.7	37.7	16.6	212.3	171.6
146	184.6	158.4	12.9	48.4	36.4	15.7	216.2	185.4
156	189.4	173.3	15.6	53.2	44.0	21.4	223.4	195.4
166	188.9	180.3	17.8	49.9	40.2	24.8	222.5	202.5
176	192.1	189.4	18.2	53.0	40.6	22.1	227.2	219.7
186	192.1	198.2	15.6	52.6	37.8	21.9	228.4	226.3
195	196.2	216.5	15.7	60.2	43.3	23.6	236.0	241.9
205	191.1	227.3	17.8	59.8	37.2	27.0	236.9	250.6
215	198.7	241.2	12.0	63.7	34.2	25.1	234.2	264.9
225	194.1	254.9	19.7	80.2	32.9	29.3	245.2	287.6
234								
244	201.9	272.2	39.6	79.8	32.6	27.9	259.0	308.8
254	199.5	293.6	43.9	42.0	25.7	35.4	261.9	297.1
264	199.3	310.4	24.5	56.4	27.2	42.9	248.3	330.5
273	194.8	348.6	18.8	73.3	24.2	72.4	253.5	359.5
283								
293								
303								
313								

f [Hz]	UNCERTAINTIES [MN/m]							
	Re(Hxx)	Im(Hxx)	Re(Hxy)	Im(Hxy)	Re(Hyx)	Im(Hyx)	Re(Hyy)	Im(Hyy)
20	2.9	5.2	0.9	1.5	3.4	7.0	1.6	1.3
29	2.9	2.1	2.1	1.9	2.6	3.4	2.1	1.7
39	2.2	1.9	2.1	1.8	3.3	2.9	2.1	1.9
49	3.2	1.6	2.6	3.3	2.6	0.8	1.5	2.8
59	2.9	2.2	3.0	3.4	1.8	2.6	3.3	2.2
68	2.3	2.6	1.4	1.9	3.2	1.9	1.6	3.1
78	3.8	2.3	4.2	2.4	3.8	2.2	2.9	2.0
88	3.4	4.6	5.3	6.3	3.8	2.8	3.6	3.2
98	8.7	5.9	6.6	4.4	7.3	5.7	5.8	9.0
107	5.1	7.5	16.0	12.5	7.7	7.6	13.4	17.5
117								
127	9.8	10.3	21.2	17.0	12.0	11.8	23.3	25.0
137	5.2	5.3	10.0	6.9	5.8	4.2	7.0	9.7
146	6.5	6.8	9.9	8.5	5.9	8.0	8.0	7.3
156	3.6	6.2	7.9	6.6	3.4	6.6	8.0	4.7
166	5.0	2.3	4.7	6.9	2.7	3.9	6.6	5.1
176	3.6	4.0	7.3	6.4	2.5	3.5	5.4	6.9
186	2.7	3.4	5.6	3.9	3.1	2.6	4.3	4.4
195	3.0	2.1	4.7	4.6	4.0	1.7	5.5	5.0
205	1.4	1.9	4.7	2.4	1.5	3.9	5.2	3.7
215	2.8	2.9	4.9	4.6	2.1	2.5	5.3	5.1
225	4.0	1.9	4.6	4.9	2.0	1.6	3.9	4.0
234								
244	2.7	1.5	5.7	6.5	2.5	2.6	5.6	5.5
254	2.2	1.0	8.1	6.8	1.7	2.0	6.9	7.0
264	3.2	3.9	5.7	4.9	2.7	4.8	5.1	4.7
273	4.2	11.7	5.7	6.0	4.4	9.1	4.4	6.4
283								
293								
303								
313								

Table 42. 60% offset experimental dynamic stiffnesses at 7 krpm and 345 kPa.

f [Hz]	VALUES [MN/m]							
	Re(Hxx)	Im(Hxx)	Re(Hxy)	Im(Hxy)	Re(Hyx)	Im(Hyx)	Re(Hyy)	Im(Hyy)
20	175.3	28.5	12.6	6.0	54.6	5.1	194.2	22.7
29	174.6	34.4	13.0	8.1	48.4	4.6	195.5	33.7
39	176.3	43.1	12.8	10.9	48.5	6.0	193.3	44.6
49	174.9	48.7	14.2	13.5	46.6	5.1	195.8	56.5
59	174.5	60.8	13.9	18.6	45.1	6.6	194.4	74.3
68	173.2	73.8	13.4	20.2	47.1	9.2	194.8	85.5
78	173.4	83.1	12.0	22.6	45.2	11.0	173.9	105.7
88	171.3	104.9	16.6	23.1	57.2	-1.7	205.1	115.0
98	188.8	112.3	10.9	30.5	35.6	11.4	207.3	126.4
107	185.4	110.5	19.4	37.2	41.2	15.7	194.9	138.3
117								
127	188.0	134.6	26.4	34.9	43.1	17.5	202.1	163.1
137	187.9	148.1	18.5	38.7	40.1	13.8	205.7	172.2
146	187.1	157.6	15.4	38.6	38.5	9.8	204.8	169.8
156	184.0	170.3	-0.6	42.0	-4.5	41.5	109.1	225.6
166	195.6	178.8	18.0	45.6	43.6	21.7	218.6	207.9
176	194.7	189.3	17.9	47.9	39.2	16.3	212.1	209.1
186	195.2	198.7	16.0	44.8	38.6	16.7	218.0	215.1
195	197.4	211.6	12.9	49.5	37.5	16.4	205.3	225.4
205	195.2	224.3	15.8	51.3	33.1	15.5	207.6	243.9
215	197.7	235.5	11.4	50.2	26.4	14.4	190.6	252.3
225								
234								
244	202.7	273.7	12.8	49.4	29.3	21.2	217.2	295.7
254	205.0	288.2	14.4	49.7	24.3	14.5	215.9	297.8
264	202.5	300.0	7.6	42.9	3.9	11.1	190.7	296.1
273								
283								
293								
303								
313								

f [Hz]	UNCERTAINTIES [MN/m]							
	Re(Hxx)	Im(Hxx)	Re(Hxy)	Im(Hxy)	Re(Hyx)	Im(Hyx)	Re(Hyy)	Im(Hyy)
20	4.9	4.4	1.7	1.6	5.1	3.4	1.2	1.6
29	2.2	3.6	2.0	2.2	3.2	2.3	1.7	1.7
39	5.1	2.5	1.3	1.6	2.2	2.0	2.1	2.3
49	3.6	2.2	3.1	2.8	3.6	2.2	2.4	2.4
59	2.0	3.1	3.2	2.9	2.5	2.4	1.5	2.5
68	3.8	4.2	2.2	2.6	2.7	3.8	2.8	2.7
78	4.2	2.9	2.7	2.4	3.7	3.2	2.5	1.8
88	7.0	5.3	5.4	5.3	5.3	4.7	4.9	5.6
98	6.5	6.8	7.1	6.3	5.5	3.4	8.6	12.3
107	9.4	4.6	18.7	17.7	6.4	8.9	22.1	16.1
117								
127	17.4	13.1	30.2	19.8	14.9	17.6	26.2	27.3
137	7.4	4.8	10.8	10.7	4.7	6.9	8.6	10.4
146	7.0	3.7	7.8	5.8	5.7	4.7	7.7	4.9
156	3.7	9.3	5.5	6.3	13.1	13.5	9.9	8.0
166	4.2	5.7	5.1	6.9	4.4	3.9	6.0	6.7
176	1.6	2.9	5.8	4.8	2.6	3.6	5.7	7.7
186	2.2	1.8	4.4	4.9	2.3	1.8	3.8	3.6
195	2.9	2.0	4.5	5.2	2.4	2.9	4.2	2.8
205	1.7	3.2	4.3	5.2	2.4	2.1	4.2	3.7
215	2.7	4.2	3.6	5.5	5.8	3.5	3.1	5.1
225								
234								
244	2.3	3.4	5.4	6.4	2.5	2.8	7.3	4.3
254	2.2	3.8	5.5	3.2	2.6	1.9	4.1	3.3
264	2.2	5.1	2.7	5.4	3.8	4.5	2.0	3.3
273								
283								
293								
303								
313								

Table 43. 60% offset experimental dynamic stiffnesses at 7 krpm and 1034 kPa.

f [Hz]	VALUES [MN/m]							
	Re(Hxx)	Im(Hxx)	Re(Hxy)	Im(Hxy)	Re(Hyx)	Im(Hyx)	Re(Hyy)	Im(Hyy)
20	193.6	25.4	24.8	5.2	57.0	2.9	238.3	19.7
29	198.2	31.5	26.2	6.9	56.4	2.8	242.8	32.5
39	196.8	42.5	25.3	10.8	55.8	2.4	235.5	43.9
49	196.2	51.7	27.2	13.6	52.7	3.2	241.9	55.7
59	198.8	63.6	27.3	17.1	55.9	9.0	241.9	81.9
68	194.2	74.0	26.1	18.7	60.1	11.3	239.4	91.3
78	197.1	84.3	25.6	21.3	52.0	9.6	235.5	104.5
88	198.9	94.6	28.3	26.4	59.4	13.9	254.2	122.2
98	210.6	120.5	27.1	25.7	51.1	4.4	247.5	144.4
107	211.9	119.3	28.5	32.0	43.0	22.5	231.1	146.7
117								
127	214.1	152.0	30.3	36.2	41.1	26.2	233.4	164.8
137	216.9	160.7	31.3	36.6	43.8	19.6	250.0	193.3
146	210.6	163.8	28.2	36.2	55.1	12.6	262.4	177.2
156	215.5	169.7	23.8	37.8	39.6	17.6	199.2	193.1
166	225.2	179.4	33.9	42.5	49.5	21.8	263.6	229.9
176	219.9	190.3	28.5	41.9	50.5	16.5	245.8	224.8
186	221.2	201.6	28.5	40.6	51.8	17.6	273.4	221.9
195	224.6	212.5	29.0	45.1	49.7	17.4	244.7	232.5
205	223.2	221.4	29.3	39.5	52.6	17.4	267.3	267.1
215	226.6	234.5	24.5	38.9	47.7	13.2	258.2	249.7
225	227.9	246.3	15.0	42.1	31.1	18.5	199.3	294.9
234								
244	234.8	266.4	25.4	41.1	45.3	22.8	258.7	309.4
254	237.3	280.4	27.2	39.2	47.4	22.0	274.5	319.7
264	238.2	293.3	25.2	36.3	48.6	11.0	271.0	317.5
273	240.7	302.5	18.5	29.6	34.3	12.6	238.0	322.0
283	241.2	314.9	23.3	40.8	42.5	19.3	270.2	367.5
293	244.2	327.4	16.8	25.0	32.8	12.1	228.8	354.1
303								
313								

f [Hz]	UNCERTAINTIES [MN/m]							
	Re(Hxx)	Im(Hxx)	Re(Hxy)	Im(Hxy)	Re(Hyx)	Im(Hyx)	Re(Hyy)	Im(Hyy)
20	4.5	4.5	1.6	1.8	3.9	3.8	1.3	1.4
29	2.2	3.8	2.3	2.0	2.9	4.5	2.4	2.0
39	2.5	3.9	3.4	2.5	3.3	2.3	1.3	1.7
49	2.1	4.1	3.4	2.7	2.7	3.0	2.6	2.0
59	2.4	4.2	3.8	1.8	1.7	5.6	3.3	3.7
68	2.9	2.8	2.3	2.0	4.7	3.3	3.5	2.9
78	2.6	3.5	2.7	3.5	3.8	4.3	2.6	3.8
88	3.7	4.5	6.2	6.0	4.3	5.0	5.8	5.6
98	5.4	7.6	7.9	10.3	8.9	5.9	8.6	10.8
107	12.6	9.2	22.7	15.2	12.0	11.4	19.8	21.5
117								
127	15.9	17.1	22.7	20.4	17.1	18.9	30.5	18.5
137	9.0	10.9	10.2	10.8	11.3	9.8	11.7	11.5
146	8.0	7.6	9.5	7.5	8.1	5.4	10.1	10.9
156	3.3	5.2	7.4	6.0	3.7	4.3	5.8	7.6
166	3.4	4.3	6.7	8.6	3.1	4.1	7.5	6.1
176	4.5	3.5	6.4	8.6	4.3	5.2	3.7	7.4
186	3.1	2.7	5.5	2.2	3.0	2.1	5.1	3.3
195	3.2	2.9	6.1	7.2	3.1	3.0	4.2	4.6
205	1.9	2.6	4.1	5.0	2.2	2.9	3.9	5.1
215	4.0	3.0	5.6	4.9	3.3	3.3	3.1	4.4
225	2.9	2.9	5.6	4.2	1.9	2.1	7.1	6.2
234								
244	3.6	3.9	5.4	5.4	3.0	3.1	3.0	3.1
254	2.9	2.4	5.5	5.0	2.2	2.1	3.5	2.8
264	2.7	1.9	3.9	3.2	1.4	1.8	2.7	4.1
273	1.3	1.8	2.1	2.4	1.1	0.7	2.5	3.6
283	1.6	1.2	2.8	4.8	0.8	1.3	3.1	4.1
293	1.4	1.8	2.5	2.1	1.1	1.0	1.9	3.0
303								
313								

Table 44. 60% offset experimental dynamic stiffnesses at 7 krpm and 1723 kPa.

f [Hz]	VALUES [MN/m]							
	Re(Hxx)	Im(Hxx)	Re(Hxy)	Im(Hxy)	Re(Hyx)	Im(Hyx)	Re(Hyy)	Im(Hyy)
20	225.2	23.6	39.6	5.8	64.6	2.9	311.8	21.0
29	226.2	32.9	40.1	7.2	65.3	6.5	318.7	34.1
39	225.0	44.5	39.5	9.8	64.0	3.3	308.2	45.8
49	226.7	52.9	41.6	12.4	58.8	4.4	315.5	57.8
59	228.0	62.9	40.7	14.8	64.2	11.6	318.5	86.6
68	223.5	74.9	39.9	16.5	71.3	13.0	315.3	95.6
78	226.7	85.3	39.9	18.9	61.4	10.4	309.9	108.6
88	231.4	94.5	44.3	21.9	67.7	18.6	336.6	135.2
98	230.1	111.9	49.6	27.1	73.2	13.7	320.0	158.4
107								
117								
127								
137	251.0	160.4	56.5	37.2	55.0	22.6	327.3	224.5
146	245.1	164.2	47.2	34.7	72.0	14.0	340.7	192.4
156	247.9	169.8	39.4	34.3	53.1	21.5	276.3	207.9
166	258.4	179.1	49.4	37.3	55.9	25.9	341.1	246.9
176	253.9	189.4	44.6	35.2	61.5	17.9	326.2	235.7
186	255.3	199.6	40.1	34.9	61.7	20.3	348.8	232.4
195	257.4	210.7	39.9	36.4	61.7	22.4	316.9	253.3
205	257.2	221.0	37.8	32.1	66.8	19.5	344.6	285.3
215	262.7	233.3	35.4	31.5	60.5	14.5	340.0	267.6
225	265.6	245.3	27.7	31.8	46.6	18.0	275.1	282.9
234	262.7	254.8	21.8	27.2	74.6	22.1	396.1	332.7
244	271.2	262.8	32.7	31.1	60.9	25.2	358.5	332.5
254	273.0	277.1	35.0	35.6	57.2	24.7	359.8	362.9
264	275.1	291.4	32.8	29.7	63.2	14.2	347.7	342.0
273	279.3	299.5	26.8	25.6	53.1	15.4	338.6	359.9
283	281.1	311.8	34.3	33.3	56.0	22.5	359.2	401.5
293	283.0	323.4	25.4	19.6	51.4	15.2	337.3	386.7
303								
313								

f [Hz]	UNCERTAINTIES [MN/m]							
	Re(Hxx)	Im(Hxx)	Re(Hxy)	Im(Hxy)	Re(Hyx)	Im(Hyx)	Re(Hyy)	Im(Hyy)
20	6.1	7.8	2.6	3.5	3.2	3.8	1.0	2.3
29	3.8	2.5	3.5	2.0	3.8	2.7	2.9	1.8
39	3.2	3.6	3.4	3.1	1.8	3.1	1.8	2.8
49	3.3	1.8	4.5	2.7	4.1	2.1	4.5	2.8
59	4.5	3.5	4.0	6.6	4.5	3.1	2.8	4.0
68	3.1	3.9	3.0	4.1	4.3	3.4	2.2	3.6
78	6.4	4.2	4.9	3.2	4.9	4.2	4.2	5.5
88	5.5	4.2	8.7	8.1	7.1	6.2	8.1	8.3
98	11.0	8.9	8.9	16.6	11.9	8.6	16.7	14.0
107								
117								
127								
137	15.8	8.3	16.0	16.6	12.0	16.8	22.2	17.5
146	10.0	4.9	12.6	8.1	6.4	11.7	14.3	17.4
156	4.3	5.6	5.9	9.0	5.8	5.6	11.5	4.3
166	2.8	5.7	6.1	9.8	7.2	4.8	7.3	11.0
176	3.3	3.9	7.8	9.6	5.1	2.8	12.6	9.3
186	3.1	3.0	6.2	7.0	3.9	3.6	6.1	6.1
195	3.7	2.5	6.9	5.2	3.2	2.6	5.8	7.0
205	2.8	2.3	5.3	6.2	3.1	3.6	7.2	4.3
215	4.1	3.1	6.0	4.7	2.9	2.7	6.5	6.8
225	4.5	2.5	6.5	4.5	3.4	2.5	7.8	3.6
234	8.9	11.1	15.6	23.1	13.2	13.8	18.8	29.4
244	4.1	4.1	6.7	6.1	4.2	4.4	7.8	7.8
254	2.6	1.8	6.0	5.9	2.1	2.3	6.8	5.6
264	2.8	1.9	3.5	4.4	1.9	1.9	2.7	5.4
273	0.8	1.5	2.9	3.7	1.2	1.8	5.1	4.7
283	1.7	1.3	4.0	4.5	1.6	1.4	3.8	3.4
293	1.2	1.4	3.1	1.9	0.6	1.5	3.1	1.9
303								
313								

Table 45. 60% offset experimental dynamic stiffnesses at 7 krpm and 2412 kPa.

f [Hz]	VALUES [MN/m]							
	Re(Hxx)	Im(Hxx)	Re(Hxy)	Im(Hxy)	Re(Hyx)	Im(Hyx)	Re(Hyy)	Im(Hyy)
20	254.8	23.3	49.8	4.6	67.4	3.4	394.2	21.9
29	256.2	32.4	50.1	7.1	69.0	7.6	401.3	35.1
39	255.2	44.9	49.7	9.7	67.4	4.0	390.3	47.7
49	257.2	53.0	49.7	10.2	62.1	5.6	398.0	60.2
59	257.1	62.8	49.2	10.2	67.8	11.3	400.0	87.4
68	253.5	72.1	48.7	12.6	75.4	13.8	397.3	96.6
78	258.8	83.4	48.0	14.6	65.7	11.8	393.0	111.0
88	261.8	93.7	50.8	16.3	68.8	19.0	406.8	139.7
98	261.2	104.8	57.3	19.8	77.4	17.6	403.4	156.0
107								
117								
127								
137	278.9	152.3	56.1	24.4	64.6	16.1	410.0	219.1
146	273.2	158.3	48.4	27.7	77.4	10.1	429.0	194.7
156	281.1	164.8	47.1	25.9	60.4	24.1	367.3	217.3
166	290.8	173.7	54.3	27.2	58.9	27.4	432.5	254.2
176	285.4	184.8	49.8	28.4	65.9	18.6	412.2	244.5
186	288.0	194.3	43.5	30.1	66.3	21.2	435.2	241.1
195	290.8	204.6	45.2	29.2	65.3	22.6	402.7	263.4
205	289.6	214.1	37.6	25.7	70.5	18.6	432.6	291.5
215	294.5	226.8	33.2	29.7	64.6	16.3	419.7	280.8
225	300.2	239.3	35.4	32.2	54.0	17.8	389.4	289.1
234								
244	306.1	255.3	36.9	33.6	63.8	24.5	449.2	340.4
254	307.3	268.4	31.8	28.0	63.0	22.2	438.1	363.0
264	309.5	284.4	30.6	26.1	64.6	11.8	442.0	356.0
273	313.7	291.7	23.2	21.7	56.7	15.4	433.4	379.9
283	316.5	303.3	35.3	25.6	57.8	20.0	466.2	414.6
293	318.5	314.6	21.6	13.8	52.7	13.9	443.0	406.3
303	318.0	330.6	12.7	6.1	45.8	0.5	405.1	392.0
313	322.3	343.8	20.2	20.1	57.4	6.4	507.8	438.6

f [Hz]	UNCERTAINTIES [MN/m]							
	Re(Hxx)	Im(Hxx)	Re(Hxy)	Im(Hxy)	Re(Hyx)	Im(Hyx)	Re(Hyy)	Im(Hyy)
20	6.0	6.5	2.7	2.4	5.3	7.6	3.3	3.3
29	2.7	2.6	4.2	4.2	3.1	3.4	4.7	4.8
39	1.8	4.8	4.1	2.9	2.2	5.7	4.9	5.4
49	4.3	3.6	5.0	4.3	5.9	3.3	7.7	4.6
59	4.3	3.3	4.6	4.8	4.3	5.3	6.4	9.6
68	4.8	4.1	4.9	3.1	4.5	5.3	6.7	5.4
78	5.9	3.9	5.3	3.5	8.3	4.7	7.5	3.1
88	5.5	4.9	12.3	6.5	10.3	7.0	11.3	16.9
98	9.2	9.3	18.5	10.0	18.0	10.7	13.8	31.1
107								
117								
127								
137	12.4	13.7	19.4	23.7	18.7	16.4	26.5	27.3
146	8.5	12.9	20.9	13.9	13.8	14.7	15.6	19.2
156	4.8	8.8	12.0	5.1	7.6	9.1	9.6	15.6
166	5.3	4.1	16.7	11.5	6.1	6.6	14.4	13.6
176	4.5	4.4	11.4	9.7	6.3	4.5	12.4	14.0
186	3.3	2.8	10.3	6.2	4.5	2.7	9.2	10.1
195	4.3	2.8	6.2	10.5	3.3	2.8	6.3	7.4
205	2.6	4.6	6.7	5.1	2.4	3.2	9.4	8.4
215	6.1	4.3	8.2	7.9	5.4	4.0	10.4	6.1
225	4.3	3.9	10.4	5.4	3.6	4.8	10.3	6.9
234								
244	1.6	2.4	11.6	6.7	3.6	4.1	13.1	10.3
254	2.0	2.2	4.1	5.2	2.3	2.3	7.0	6.8
264	2.1	2.4	6.8	5.1	2.3	1.6	5.7	4.5
273	1.7	1.7	3.8	7.0	1.0	1.5	4.4	5.8
283	1.4	1.2	5.3	4.8	1.6	0.9	4.8	2.9
293	1.3	1.3	5.8	1.9	1.5	1.6	4.1	3.6
303	1.5	1.2	1.8	3.1	1.4	1.2	2.5	2.3
313	1.5	2.1	2.4	3.6	2.0	1.3	3.2	3.4

Table 46. 60% offset experimental dynamic stiffnesses at 7 krpm and 3101 kPa.

f [Hz]	VALUES [MN/m]							
	Re(Hxx)	Im(Hxx)	Re(Hxy)	Im(Hxy)	Re(Hyx)	Im(Hyx)	Re(Hyy)	Im(Hyy)
20	282.1	22.1	53.4	3.6	68.5	1.3	475.1	22.0
29	285.0	29.5	52.6	4.8	69.7	7.4	483.5	36.8
39	284.0	44.2	53.2	8.1	68.8	4.8	472.3	47.9
49	286.6	51.8	54.5	8.6	60.9	7.6	477.6	62.7
59	288.2	62.0	52.8	8.9	68.0	12.8	481.8	86.9
68	284.3	70.5	51.4	10.9	76.3	14.3	479.6	98.1
78	288.9	82.2	49.5	12.2	66.6	12.7	474.7	111.2
88	290.4	90.8	50.1	14.7	68.1	18.4	491.2	140.5
98	290.1	101.1	53.3	14.5	73.2	19.4	488.5	149.3
107								
117								
127								
137	306.4	147.0	44.8	18.8	66.7	15.0	489.0	210.8
146	301.3	153.0	42.7	23.5	74.6	8.9	513.6	194.6
156	311.8	157.2	40.7	22.1	63.5	25.7	456.1	221.7
166	320.1	170.2	46.1	28.4	58.2	29.9	514.2	256.7
176	316.6	179.5	45.8	25.2	65.5	19.9	497.1	252.0
186	316.9	188.8	36.3	25.7	65.6	23.3	518.9	247.6
195	320.2	198.6	39.9	28.3	65.6	23.8	484.5	274.5
205	321.3	208.3	33.5	27.5	70.0	21.4	516.1	303.2
215	326.2	220.3	28.9	28.0	62.7	17.6	502.1	284.0
225	330.8	232.7	36.1	36.2	57.3	18.2	512.0	304.9
234								
244	335.6	247.9	29.9	31.0	60.7	25.6	538.4	351.8
254	338.3	261.0	27.6	30.4	60.0	22.2	540.2	366.8
264	340.1	277.8	22.3	30.5	59.8	13.5	540.1	374.7
273	344.4	283.9	16.9	20.6	51.0	16.4	526.6	382.6
283	347.3	296.7	26.1	29.1	53.0	22.2	571.7	429.6
293	350.1	306.7	12.4	14.4	46.0	14.9	536.2	415.4
303	351.1	323.6	3.2	13.7	41.7	2.2	524.8	416.9
313								

f [Hz]	UNCERTAINTIES [MN/m]							
	Re(Hxx)	Im(Hxx)	Re(Hxy)	Im(Hxy)	Re(Hyx)	Im(Hyx)	Re(Hyy)	Im(Hyy)
20	3.3	6.0	3.3	1.7	5.0	6.6	2.8	2.0
29	4.8	5.0	2.6	3.2	4.7	7.2	4.8	2.6
39	5.1	2.9	3.5	2.3	3.9	4.7	3.7	5.0
49	4.8	3.2	5.1	4.1	4.6	3.5	5.5	3.5
59	4.7	3.5	6.8	6.0	5.3	7.6	6.3	7.3
68	4.3	5.0	4.9	3.9	4.1	6.6	7.0	6.1
78	6.2	5.2	4.7	4.2	8.3	7.7	10.2	5.2
88	7.0	8.1	9.4	8.6	12.7	10.4	13.9	13.0
98	12.2	11.1	17.4	9.7	19.1	19.6	21.4	30.0
107								
117								
127								
137	15.4	17.0	20.6	16.1	24.1	21.5	18.7	27.8
146	9.3	14.8	10.2	13.9	12.9	18.4	21.7	17.0
156	6.4	8.8	14.1	8.2	7.5	11.0	11.9	12.6
166	5.8	5.5	10.1	10.1	6.9	7.2	12.2	10.0
176	5.8	3.5	9.7	11.3	7.4	4.0	9.0	8.6
186	4.7	5.0	8.5	5.4	6.0	3.1	7.6	6.1
195	4.7	2.6	6.1	8.7	4.6	3.5	6.0	7.4
205	1.6	3.5	7.5	5.8	3.3	4.9	6.9	6.9
215	4.6	4.8	10.0	8.6	4.2	5.3	7.8	8.6
225	3.7	4.4	11.2	6.4	2.3	7.9	13.8	7.9
234								
244	5.0	1.8	6.1	7.2	7.4	5.3	9.5	9.4
254	3.6	1.5	7.3	4.6	3.3	3.3	6.5	4.5
264	3.3	2.1	5.9	4.4	4.0	2.5	5.8	5.6
273	1.9	1.6	5.6	4.9	1.9	2.1	4.2	5.7
283	2.2	0.7	3.6	3.5	1.8	2.0	4.1	5.6
293	1.6	1.3	3.8	3.3	1.6	1.7	4.0	2.3
303	2.0	1.3	4.0	1.9	1.4	1.2	2.3	2.9
313								

Table 47. 60% offset experimental dynamic stiffnesses at 10 krpm and zero.

f [Hz]	VALUES [MN/m]							
	Re(Hxx)	Im(Hxx)	Re(Hxy)	Im(Hxy)	Re(Hyx)	Im(Hyx)	Re(Hyy)	Im(Hyy)
20	212.5	19.8	14.4	4.1	63.3	11.5	243.1	22.8
29	216.9	27.9	14.6	9.7	65.8	9.9	242.8	34.7
39	214.9	36.8	12.7	12.3	66.1	5.3	243.2	45.2
49	213.8	43.6	18.4	16.1	67.4	5.8	245.6	53.8
59	214.2	56.6	17.3	17.8	61.3	4.2	244.9	65.9
68	209.8	66.9	16.9	21.1	65.7	3.9	244.6	78.2
78	206.4	80.5	12.4	20.4	72.1	6.7	247.6	93.9
88	228.0	102.0	10.8	27.7	51.9	-3.8	251.9	101.4
98	230.5	107.0	12.1	33.1	51.4	11.6	253.2	112.2
107	222.3	105.2	14.5	35.6	56.8	11.4	249.6	122.8
117	223.9	122.4	15.8	39.5	58.9	9.1	252.4	133.5
127	222.9	133.7	22.7	42.9	55.7	11.6	256.9	155.0
137	239.6	144.8	28.0	54.0	59.9	20.7	254.8	172.0
146	239.9	153.4	25.1	68.3	55.3	25.1	242.4	188.4
156								
166								
176								
186	247.0	206.2	40.7	85.7	38.6	34.0	237.5	252.6
195	246.1	214.4	29.9	66.0	47.1	24.3	272.1	252.1
205	233.9	218.1	18.3	76.4	46.1	19.6	256.3	247.7
215	243.4	244.5	-1.8	78.4	44.1	26.0	260.1	245.4
225	237.5	248.4	18.7	94.0	46.4	22.8	279.6	284.0
234	242.9	258.6	27.9	83.5	42.2	24.0	284.9	293.8
244	244.4	270.4	16.9	80.0	36.8	25.8	287.9	288.2
254	246.2	285.6	34.4	58.2	36.1	35.4	303.1	292.7
264	250.5	311.9	27.1	71.6	41.3	50.2	296.0	327.3
273								
283								
293								
303								
313								

f [Hz]	UNCERTAINTIES [MN/m]							
	Re(Hxx)	Im(Hxx)	Re(Hxy)	Im(Hxy)	Re(Hyx)	Im(Hyx)	Re(Hyy)	Im(Hyy)
20	6.9	9.1	2.8	4.2	7.5	7.0	2.5	4.3
29	5.0	5.4	3.0	3.6	6.2	3.7	5.2	4.7
39	7.8	7.3	4.3	4.5	3.3	4.8	2.4	2.7
49	5.3	4.6	4.1	5.0	5.5	6.1	4.0	5.6
59	4.5	4.4	6.0	5.0	6.4	3.9	3.6	4.3
68	4.7	5.1	2.4	4.2	3.9	5.3	4.7	3.4
78	6.7	3.9	4.9	2.5	5.1	5.2	3.8	4.2
88	3.9	6.5	3.9	7.3	4.5	6.0	4.5	7.3
98	6.3	3.9	9.8	3.6	6.1	5.5	4.6	4.6
107	4.5	3.8	8.5	8.8	4.0	3.8	5.5	6.1
117	7.0	6.8	4.9	6.9	7.2	5.2	4.1	7.6
127	6.3	5.7	11.1	10.8	4.6	5.6	6.7	13.4
137	8.4	9.1	10.4	10.7	8.0	8.4	7.8	9.8
146	16.1	14.3	20.1	15.3	12.3	13.0	12.1	16.4
156								
166								
176								
186	9.3	11.9	23.3	28.1	12.4	10.8	23.2	31.6
195	7.7	5.3	9.7	14.7	5.3	8.7	12.5	15.3
205	4.5	2.9	6.4	8.9	5.5	4.8	9.3	6.8
215	6.5	6.0	3.6	10.0	7.0	5.8	10.1	7.1
225	3.1	1.7	9.4	6.9	4.7	4.0	10.0	7.7
234	3.8	2.7	6.3	5.2	3.2	3.3	7.6	7.1
244	4.0	3.4	8.3	8.0	5.0	3.5	4.4	8.6
254	4.4	3.0	4.4	11.3	4.5	4.0	7.9	8.5
264	4.0	4.9	7.2	7.8	8.0	7.8	8.8	11.7
273								
283								
293								
303								
313								

Table 48. 60% offset experimental dynamic stiffnesses at 10 krpm and 345 kPa.

f [Hz]	VALUES [MN/m]							
	Re(Hxx)	Im(Hxx)	Re(Hxy)	Im(Hxy)	Re(Hyx)	Im(Hyx)	Re(Hyy)	Im(Hyy)
20	215.1	27.7	13.8	4.9	67.0	13.9	238.3	21.6
29	215.5	28.3	14.3	8.9	64.4	11.9	239.7	32.4
39	216.9	37.7	13.6	12.7	69.3	4.7	238.1	40.3
49	210.3	47.3	14.6	15.6	67.2	0.8	236.7	50.8
59	215.1	54.3	15.5	17.3	61.3	0.9	237.4	64.9
68	211.9	69.1	13.3	18.9	64.5	6.1	234.9	76.2
78	211.0	78.7	11.0	22.7	57.4	8.0	211.3	107.9
88	221.5	107.6	12.6	23.4	65.3	-15.3	249.0	108.4
98	229.2	104.0	11.0	30.6	51.1	8.7	246.7	111.5
107	223.2	104.9	14.4	36.8	57.4	10.5	240.9	122.9
117	223.5	119.1	14.1	37.7	59.8	5.9	244.9	132.5
127	225.4	132.0	11.0	40.1	57.6	6.9	240.3	141.3
137	232.2	141.5	17.8	42.4	56.8	8.3	247.0	156.1
146	231.6	146.9	15.5	43.5	53.8	7.2	241.2	158.8
156								
166								
176	239.0	186.9	21.1	49.3	47.5	15.0	250.6	195.1
186	236.9	194.5	14.9	49.6	49.1	9.6	254.5	201.4
195	241.7	200.9	13.7	52.9	47.9	7.2	243.1	210.0
205	237.4	211.9	12.5	49.8	44.1	6.4	242.3	225.6
215	242.4	224.2	5.2	53.1	30.1	4.1	221.2	227.6
225								
234	243.7	248.6	12.3	63.6	41.9	6.3	264.9	265.1
244	248.0	259.5	10.0	62.1	32.6	6.7	256.3	281.2
254	252.0	272.2	10.0	61.8	26.1	4.9	240.8	279.0
264	248.6	284.4	0.8	51.8	0.1	4.5	203.8	274.3
273								
283								
293								
303								
313								

f [Hz]	UNCERTAINTIES [MN/m]							
	Re(Hxx)	Im(Hxx)	Re(Hxy)	Im(Hxy)	Re(Hyx)	Im(Hyx)	Re(Hyy)	Im(Hyy)
20	6.8	6.8	2.4	3.3	6.6	5.8	2.8	2.7
29	7.7	3.9	2.4	4.0	4.1	6.4	4.1	2.9
39	5.6	6.6	5.4	3.1	3.8	8.1	3.4	4.2
49	5.5	5.1	4.4	6.0	3.4	3.6	3.6	4.5
59	4.5	4.9	4.2	3.5	5.8	4.0	4.4	3.0
68	3.1	3.8	4.8	3.5	4.0	3.6	2.3	3.9
78	3.4	6.8	4.8	4.4	4.4	4.4	4.3	5.1
88	5.5	8.9	8.3	4.8	6.9	5.5	6.6	5.7
98	6.8	6.4	4.9	8.3	5.2	4.2	7.2	9.6
107	5.9	4.3	6.3	8.9	3.0	6.0	9.4	9.2
117	8.3	6.5	7.8	10.8	7.6	10.6	5.4	10.6
127	6.6	7.3	7.9	10.9	7.0	4.1	7.5	11.7
137	12.0	4.4	10.1	13.8	7.5	12.0	9.6	8.6
146	16.4	10.1	16.1	11.0	15.0	17.2	6.6	17.6
156								
166								
176	22.2	16.7	28.3	35.5	16.0	23.0	31.3	30.9
186	14.5	11.8	15.8	12.1	10.9	10.5	10.9	19.5
195	6.2	7.7	9.3	9.2	7.8	5.1	8.6	12.6
205	5.4	5.1	10.6	6.1	3.9	5.5	5.1	8.5
215	4.5	4.0	4.7	5.5	5.7	5.7	8.6	8.2
225								
234	3.2	1.8	6.8	5.5	2.2	2.5	7.5	5.2
244	3.9	2.8	5.1	7.9	2.6	3.4	5.5	6.7
254	2.7	2.8	6.8	7.1	2.4	2.1	4.9	2.8
264	3.3	2.5	3.9	4.7	3.3	2.7	4.2	5.6
273								
283								
293								
303								
313								

Table 49. 60% offset experimental dynamic stiffnesses at 10 krpm and 1034 kPa.

f [Hz]	VALUES [MN/m]							
	Re(Hxx)	Im(Hxx)	Re(Hxy)	Im(Hxy)	Re(Hyx)	Im(Hyx)	Re(Hyy)	Im(Hyy)
20	234.5	20.1	21.3	4.2	74.6	1.1	270.2	19.0
29	236.2	26.1	21.2	9.4	73.3	7.2	274.2	28.5
39	229.4	37.0	20.9	11.9	75.1	1.9	265.8	40.0
49	230.2	48.1	24.1	15.1	71.5	-2.0	270.3	50.0
59	230.4	57.5	20.8	15.5	72.6	3.5	272.1	69.3
68	228.1	72.7	21.1	19.1	75.4	4.8	269.6	78.7
78	231.4	77.8	19.8	23.0	69.4	5.6	262.4	92.2
88	226.7	88.1	22.1	26.7	78.0	6.8	280.9	109.1
98	247.3	107.8	18.1	28.4	60.3	1.3	280.9	123.0
107	240.8	106.4	20.9	33.7	61.7	12.3	263.0	127.5
117	241.6	122.5	24.0	36.8	65.0	2.6	274.3	141.7
127	240.5	131.0	22.9	39.6	67.4	7.2	266.4	149.6
137	251.5	140.4	28.8	45.5	65.9	9.9	279.1	172.9
146	249.3	154.4	32.0	45.9	70.3	4.4	283.1	169.8
156								
166								
176								
186	256.4	193.5	35.1	51.5	57.0	8.1	290.4	212.3
195	258.0	199.8	24.9	51.3	59.4	9.3	265.8	222.5
205	259.6	209.7	29.8	50.1	61.9	5.3	287.9	242.8
215	263.7	222.9	23.3	50.9	54.1	2.6	275.9	229.1
225	264.0	233.5	12.7	49.3	38.8	7.2	210.2	252.3
234	266.7	241.7	25.4	53.2	57.3	4.2	308.6	261.3
244	269.6	250.9	24.3	52.9	51.0	6.0	296.5	278.9
254	271.3	263.7	24.7	49.1	50.0	3.8	298.4	285.2
264	272.8	277.3	21.0	44.3	49.5	-2.9	288.7	279.7
273	275.2	283.5	14.1	39.7	37.8	1.6	250.3	290.0
283	275.7	293.5	19.5	47.7	42.3	3.9	291.2	320.0
293	274.9	306.2	10.8	33.8	34.5	1.3	239.3	309.2
303								
313								

f [Hz]	UNCERTAINTIES [MN/m]							
	Re(Hxx)	Im(Hxx)	Re(Hxy)	Im(Hxy)	Re(Hyx)	Im(Hyx)	Re(Hyy)	Im(Hyy)
20	8.4	5.1	4.2	4.0	6.2	3.2	3.9	2.4
29	6.8	6.9	3.6	5.4	5.0	3.1	4.1	3.9
39	6.9	4.6	3.9	3.8	5.5	4.0	3.0	4.4
49	6.8	5.5	7.6	5.6	5.7	3.9	4.6	4.2
59	6.1	6.9	5.0	5.2	5.5	5.7	2.3	4.6
68	7.2	7.4	6.8	4.7	3.8	2.7	3.4	2.9
78	6.7	5.1	8.3	5.0	4.1	5.1	3.6	3.9
88	8.9	6.2	9.2	7.7	6.0	3.5	4.5	4.3
98	5.5	12.0	12.7	13.4	4.9	2.4	4.9	7.7
107	9.0	5.9	11.9	13.2	4.5	4.5	7.0	6.7
117	8.4	6.3	9.1	11.1	6.3	4.2	9.4	6.7
127	6.4	7.9	10.6	15.1	5.2	5.8	5.7	13.1
137	9.7	7.7	12.5	13.2	7.6	6.6	13.7	5.4
146	17.7	7.0	15.0	15.1	6.8	12.7	7.3	23.0
156								
166								
176								
186	4.9	9.8	13.1	19.3	8.7	7.4	16.7	16.4
195	3.5	4.9	13.3	10.1	4.7	2.8	6.3	18.2
205	5.4	5.6	11.4	12.0	4.4	4.1	7.6	11.1
215	4.3	6.2	7.2	12.7	6.3	3.8	9.6	7.9
225	5.2	3.8	7.3	10.2	1.7	1.1	6.5	3.3
234	2.5	5.1	6.2	7.4	2.7	2.0	8.0	7.7
244	5.3	3.4	6.6	8.9	1.4	3.2	5.6	3.2
254	4.3	2.5	7.8	6.1	2.9	2.7	4.4	6.0
264	2.5	3.1	4.3	4.6	3.2	2.6	5.2	4.9
273	1.9	3.3	4.2	3.5	0.7	1.5	2.6	4.3
283	2.5	2.3	3.6	3.5	1.5	1.7	5.1	4.2
293	1.7	1.6	3.1	3.3	1.4	0.9	2.1	3.3
303								
313								

Table 50. 60% offset experimental dynamic stiffnesses at 10 krpm and 1723 kPa.

f [Hz]	VALUES [MN/m]							
	Re(Hxx)	Im(Hxx)	Re(Hxy)	Im(Hxy)	Re(Hyx)	Im(Hyx)	Re(Hyy)	Im(Hyy)
20	255.4	21.7	32.7	4.5	83.9	-1.7	329.7	18.1
29	259.2	27.2	35.9	8.5	86.3	4.8	332.2	29.4
39	255.7	38.7	35.9	10.4	82.6	-1.2	326.0	41.7
49	257.6	53.6	38.6	16.8	78.5	-1.0	329.5	52.6
59	255.3	60.7	34.6	17.9	81.7	5.2	330.8	74.5
68	254.5	72.0	34.9	16.6	86.9	3.3	329.6	83.1
78	257.3	80.7	33.7	20.9	78.2	3.8	322.9	93.6
88	261.5	87.3	35.4	25.2	83.1	6.9	343.6	114.6
98	258.6	113.7	37.1	19.3	89.0	-6.2	334.0	133.9
107	269.5	110.1	35.2	32.5	70.0	9.8	319.9	134.7
117	272.1	122.6	34.6	33.0	71.8	2.0	334.2	153.6
127	270.3	131.3	42.3	40.1	78.3	6.4	325.1	153.6
137	281.7	141.1	47.1	42.8	78.1	7.6	341.1	187.2
146	277.7	150.5	49.5	43.3	83.0	2.0	350.1	180.3
156								
166								
176								
186	288.1	191.9	57.9	53.5	68.3	11.3	350.9	232.4
195	290.5	198.7	43.5	46.6	69.7	9.7	328.6	232.7
205	286.8	208.5	40.6	44.7	71.7	5.0	350.0	254.4
215	294.5	219.8	37.7	48.0	66.6	4.9	345.9	245.8
225	297.4	230.2	31.4	44.5	53.4	6.6	290.2	254.3
234	297.0	239.4	38.8	47.0	68.8	6.0	380.9	276.1
244	299.0	248.7	33.9	44.3	61.4	8.6	358.0	287.8
254	302.2	260.3	33.6	46.8	59.4	9.0	358.4	325.3
264	305.1	274.4	31.7	38.6	62.4	0.6	350.6	302.5
273	308.2	281.2	26.5	37.2	52.2	2.2	340.8	317.3
283	309.0	291.0	33.1	41.5	53.9	8.9	362.5	348.1
293	309.1	302.2	25.0	30.1	50.8	3.3	337.4	337.2
303	304.5	316.2	9.0	14.0	44.0	-4.9	259.1	326.9
313	306.8	331.2	21.1	28.0	53.0	-4.2	370.7	359.9

f [Hz]	UNCERTAINTIES [MN/m]							
	Re(Hxx)	Im(Hxx)	Re(Hxy)	Im(Hxy)	Re(Hyx)	Im(Hyx)	Re(Hyy)	Im(Hyy)
20	14.8	10.3	4.2	6.0	6.3	10.5	4.2	4.7
29	9.5	5.6	5.5	6.5	4.5	5.0	4.6	3.7
39	8.1	7.0	7.5	7.2	4.9	4.8	4.3	4.2
49	10.6	10.8	4.4	6.9	7.9	5.4	7.2	4.9
59	5.1	9.1	10.2	10.1	6.9	3.8	5.4	5.0
68	10.7	11.6	7.5	4.5	3.6	5.5	3.0	4.3
78	8.5	7.8	9.2	5.1	7.5	4.4	5.4	2.6
88	13.5	9.4	10.8	14.0	5.3	3.3	5.4	6.6
98	17.0	10.0	13.1	14.9	7.0	5.9	8.3	6.7
107	8.6	7.7	10.6	13.2	4.5	5.8	11.0	8.2
117	14.1	9.3	11.1	10.2	7.2	5.4	3.8	9.9
127	9.8	10.9	20.5	15.5	7.9	7.9	15.7	18.9
137	10.3	15.4	13.9	15.4	6.1	9.6	12.4	13.8
146	18.8	16.1	21.7	11.8	15.1	14.2	20.2	19.0
156								
166								
176								
186	13.7	9.9	32.6	20.3	15.4	12.2	19.3	27.9
195	6.1	8.2	13.0	21.9	10.5	7.1	17.0	10.3
205	5.0	7.6	15.1	9.6	4.4	6.5	8.2	10.1
215	7.9	8.0	13.6	16.0	6.6	5.9	8.0	12.8
225	6.6	2.1	7.4	6.4	3.5	3.7	6.1	7.4
234	5.7	3.4	10.6	13.1	4.6	3.2	5.8	9.7
244	5.4	4.4	10.9	8.1	3.5	4.2	5.3	8.7
254	4.2	3.3	5.9	8.9	2.9	2.7	4.6	7.1
264	3.6	4.2	7.0	7.2	4.8	1.5	5.8	7.3
273	2.1	2.3	8.0	5.7	1.3	2.1	3.3	6.2
283	1.9	2.2	4.8	5.8	1.5	1.4	4.8	5.7
293	1.9	2.5	5.9	6.1	1.7	2.4	3.2	3.5
303	2.8	2.0	2.8	3.1	2.6	1.4	2.3	6.7
313	2.4	2.6	3.2	4.4	1.6	1.2	2.1	3.0

Table 51. 60% offset experimental dynamic stiffnesses at 10 krpm and 2412 kPa.

f [Hz]	VALUES [MN/m]							
	Re(Hxx)	Im(Hxx)	Re(Hxy)	Im(Hxy)	Re(Hyx)	Im(Hyx)	Re(Hyy)	Im(Hyy)
20	281.7	23.9	43.6	4.0	90.0	-2.4	396.7	19.1
29	291.2	28.4	46.5	5.8	92.4	5.5	401.1	31.7
39	285.1	39.5	47.3	10.7	89.0	-1.2	392.2	41.9
49	286.8	49.1	49.5	11.7	85.0	-2.0	397.6	51.8
59	285.4	59.9	47.3	14.2	90.3	3.9	399.3	77.1
68	282.9	70.4	44.3	15.5	95.0	3.7	398.4	85.5
78	291.1	77.1	43.4	19.8	85.7	2.3	392.8	98.2
88	289.6	85.9	46.4	17.3	85.8	9.1	401.2	120.5
98	285.5	103.7	54.2	19.2	98.1	7.6	401.5	130.8
107	299.3	104.9	47.9	26.8	76.6	9.8	387.0	138.0
117	303.8	119.1	48.9	27.7	74.6	3.1	404.3	155.3
127	301.9	129.8	48.5	30.9	79.0	6.6	390.0	150.7
137	316.9	140.2	48.8	32.3	80.4	10.7	406.4	181.2
146	310.8	148.7	51.6	29.7	82.6	4.6	416.4	172.0
156								
166								
176								
186	316.0	198.6	44.1	35.8	62.3	13.4	424.9	212.2
195	322.0	196.9	47.0	36.7	72.4	13.5	396.9	233.5
205	318.9	204.1	42.8	34.5	77.5	5.3	421.3	255.5
215	328.0	217.1	40.3	38.7	68.3	4.4	408.3	246.2
225	330.8	227.4	41.5	39.2	60.1	6.3	384.1	255.8
234	329.0	233.1	42.7	41.9	71.9	5.6	453.6	280.9
244	332.9	241.4	39.8	34.4	65.6	10.5	433.6	297.3
254	334.3	251.9	37.8	35.2	64.3	8.3	421.2	311.1
264	335.8	267.4	34.2	31.7	63.4	2.1	421.8	313.0
273	338.3	272.4	26.9	27.7	56.4	5.4	408.8	326.1
283	340.7	282.8	36.1	33.6	57.8	10.9	441.7	360.7
293	342.1	291.4	26.8	21.1	53.2	6.1	415.3	351.6
303	338.6	305.5	16.0	14.6	47.6	-4.4	377.6	339.2
313	339.6	318.4	21.6	28.9	56.8	1.5	472.8	392.6

f [Hz]	UNCERTAINTIES [MN/m]							
	Re(Hxx)	Im(Hxx)	Re(Hxy)	Im(Hxy)	Re(Hyx)	Im(Hyx)	Re(Hyy)	Im(Hyy)
20	12.1	8.7	7.1	5.0	6.3	3.0	4.0	3.3
29	12.3	11.0	9.4	9.0	5.7	6.0	2.3	3.6
39	13.7	12.0	4.4	9.3	2.6	6.0	6.0	5.2
49	11.0	8.2	19.3	10.3	5.5	5.5	9.0	5.7
59	9.8	11.6	13.4	4.1	7.0	5.6	7.5	9.8
68	11.2	11.6	7.8	7.9	8.8	5.2	6.2	4.0
78	9.4	16.9	8.1	10.1	1.7	5.4	5.2	7.0
88	14.4	14.1	12.7	18.0	7.3	7.8	8.4	4.8
98	16.8	10.7	16.7	20.2	9.0	5.6	11.1	7.3
107	17.0	11.9	17.3	16.2	2.9	3.7	11.6	5.6
117	18.6	19.6	24.3	19.9	5.9	8.7	7.6	16.5
127	7.7	11.1	16.1	31.4	9.0	7.4	18.0	15.5
137	12.1	19.1	20.3	14.3	9.3	17.3	12.1	23.5
146	14.1	22.5	23.7	30.8	15.6	21.4	26.7	26.1
156								
166								
176								
186	11.9	12.6	32.2	20.2	14.9	7.4	24.4	23.7
195	8.1	6.2	13.5	24.5	10.1	6.7	19.5	14.2
205	5.5	6.5	12.6	12.8	3.5	6.5	12.2	14.1
215	6.9	10.5	14.3	18.1	6.4	4.1	11.9	12.2
225	5.2	4.6	17.1	11.7	3.6	5.9	8.7	11.8
234	2.4	7.6	10.0	15.5	4.3	3.6	5.6	7.6
244	5.0	3.8	12.2	10.9	3.3	3.8	6.3	10.1
254	6.3	3.6	10.0	13.6	3.8	4.0	5.5	10.8
264	7.2	5.1	11.3	6.6	4.8	2.9	8.0	7.2
273	2.1	3.2	8.0	7.9	2.5	2.1	7.9	6.4
283	2.3	3.0	3.9	6.9	2.8	2.2	6.5	3.2
293	2.4	2.7	5.6	4.9	1.6	2.3	5.4	4.6
303	2.8	2.8	4.3	5.0	1.8	0.9	4.2	2.7
313	1.7	4.0	4.8	4.2	2.3	2.5	4.4	3.2

Table 52. 60% offset experimental dynamic stiffnesses at 10 krpm and 3101 kPa.

f [Hz]	VALUES [MN/m]							
	Re(Hxx)	Im(Hxx)	Re(Hxy)	Im(Hxy)	Re(Hyx)	Im(Hyx)	Re(Hyy)	Im(Hyy)
20	306.3	26.0	53.7	2.9	94.4	-1.8	467.9	20.1
29	318.9	26.4	55.1	6.4	94.1	6.3	475.7	31.8
39	309.8	42.4	51.7	9.5	91.3	-1.7	465.1	43.4
49	306.2	51.3	49.4	11.6	87.8	-1.2	473.0	51.7
59	311.2	60.4	55.5	11.2	93.1	2.3	474.0	76.8
68	311.7	69.1	52.7	15.0	96.1	4.1	470.8	84.3
78	313.1	78.0	49.6	15.2	86.5	3.7	465.0	96.8
88	320.4	88.5	57.6	23.3	89.5	10.1	483.1	118.5
98	315.6	91.1	54.7	19.2	97.3	11.7	473.7	128.4
107	326.8	110.8	53.1	26.1	78.8	5.1	462.3	140.9
117	328.6	116.0	59.0	24.6	75.6	3.8	471.6	155.3
127	327.8	128.3	67.0	26.8	82.7	8.1	460.5	159.5
137	341.6	137.2	60.1	25.3	83.5	11.2	480.7	191.2
146	334.9	145.8	63.1	30.0	91.4	-0.7	499.6	187.6
156								
166								
176								
186	341.6	187.8	61.8	31.4	70.9	15.8	499.2	239.1
195	345.9	194.3	52.9	32.5	73.8	13.7	470.5	244.9
205	343.3	200.2	46.7	30.3	77.5	10.3	492.8	267.8
215	356.5	210.1	49.0	34.1	73.9	5.8	481.2	255.1
225	358.2	218.0	46.3	32.4	65.7	7.2	485.1	263.3
234	354.5	228.6	46.8	39.6	74.8	7.7	543.6	301.5
244	358.0	232.4	38.0	30.8	68.0	13.1	505.1	302.8
254	360.3	246.4	30.3	25.7	65.6	9.7	501.3	313.1
264	363.0	259.9	30.3	27.7	64.0	4.0	500.0	317.1
273	364.7	265.1	23.8	20.9	56.2	7.7	476.8	327.5
283	367.8	276.7	36.1	32.5	60.0	14.1	528.9	372.2
293	369.3	284.8	20.7	18.0	52.8	7.7	489.1	360.0
303	367.4	298.5	11.0	13.6	49.9	-2.8	469.2	359.0
313	367.9	313.0	19.7	56.8	60.3	11.3	644.8	481.4

f [Hz]	UNCERTAINTIES [MN/m]							
	Re(Hxx)	Im(Hxx)	Re(Hxy)	Im(Hxy)	Re(Hyx)	Im(Hyx)	Re(Hyy)	Im(Hyy)
20	14.1	16.3	8.2	5.9	9.2	7.4	2.4	3.2
29	13.6	10.6	4.7	8.2	5.0	6.7	4.6	6.1
39	12.7	9.7	12.7	10.1	3.1	6.6	3.9	5.1
49	8.9	12.3	13.8	14.6	5.4	4.4	6.0	8.6
59	15.0	12.6	13.0	18.6	7.7	8.3	7.7	8.5
68	7.1	15.5	10.3	15.8	5.3	5.6	3.5	6.4
78	15.9	10.8	8.4	10.6	4.8	6.7	7.9	6.9
88	15.0	17.7	9.4	19.5	9.8	8.0	9.2	10.4
98	20.8	14.2	30.9	18.0	7.6	8.9	12.3	17.4
107	10.9	8.0	21.8	25.8	9.4	7.8	19.7	12.9
117	15.2	8.9	16.6	21.3	9.7	9.7	20.7	15.3
127	15.4	12.7	31.7	23.0	8.9	12.0	20.3	27.6
137	24.3	26.0	28.7	39.1	17.9	23.5	29.0	23.8
146	26.0	23.4	48.5	24.6	25.1	32.8	32.0	52.2
156								
166								
176								
186	17.2	22.7	36.0	33.8	26.9	20.1	45.1	43.6
195	10.4	11.4	27.9	19.0	15.5	12.0	22.2	32.3
205	10.6	7.6	16.1	16.9	8.2	11.2	17.0	18.4
215	8.5	12.4	20.6	22.1	9.6	9.0	18.6	15.7
225	7.5	7.2	12.3	18.1	3.8	8.2	12.7	13.4
234	6.5	4.2	11.2	14.5	7.3	6.1	14.1	19.2
244	6.0	6.5	11.9	16.2	4.8	5.3	11.8	7.9
254	6.0	5.3	13.3	11.0	5.4	2.8	6.4	10.4
264	6.3	4.5	11.4	9.2	4.5	4.2	7.4	8.9
273	3.5	3.3	12.0	9.2	2.7	2.2	8.0	7.8
283	2.9	2.6	7.8	10.1	3.2	2.2	10.7	8.9
293	2.7	2.4	9.5	6.3	2.0	2.2	6.2	5.9
303	3.5	2.4	6.2	6.1	2.7	1.9	4.0	5.6
313	3.0	2.4	7.3	7.7	5.2	2.4	17.5	11.7

Table 53. 60% offset experimental dynamic stiffnesses at 13 krpm and zero load.

f [Hz]	VALUES [MN/m]							
	Re(Hxx)	Im(Hxx)	Re(Hxy)	Im(Hxy)	Re(Hyx)	Im(Hyx)	Re(Hyy)	Im(Hyy)
20	255.5	24.1	13.9	3.3	79.5	4.5	290.4	25.8
29	259.7	31.0	13.4	8.2	81.4	3.6	291.5	35.1
39	258.0	42.6	13.6	11.9	80.0	5.5	294.4	44.0
49	261.3	48.2	14.4	15.1	81.9	4.1	295.1	50.2
59	258.7	58.9	14.1	22.3	82.6	4.6	292.9	67.3
68	257.9	70.0	15.6	22.1	84.7	5.6	294.2	79.4
78	253.2	85.6	14.8	25.1	91.9	1.0	296.3	87.0
88	275.4	95.0	10.4	30.0	68.5	-4.5	304.4	99.3
98	281.0	96.6	13.3	36.9	66.1	3.9	302.6	109.5
107	269.1	103.3	17.6	40.5	74.9	7.6	304.2	120.5
117	268.6	117.8	15.7	39.1	71.5	7.8	301.6	130.3
127	268.6	127.9	12.2	41.5	69.8	8.4	302.9	146.0
137	271.5	143.0	11.6	45.2	71.1	8.0	305.7	151.9
146	272.2	153.9	10.3	46.2	69.7	11.0	310.7	165.8
156	273.5	158.5	8.5	55.4	71.2	6.8	306.7	174.3
166	276.6	171.3	9.1	58.5	69.5	11.1	302.5	185.6
176	277.6	181.1	18.1	66.0	63.0	11.4	304.2	204.9
186	281.5	191.8	19.2	68.2	64.6	15.2	304.9	221.6
195								
205								
215								
225								
234								
244	284.8	280.4	7.6	81.9	51.0	23.8	314.7	316.7
254	287.2	289.3	-13.3	92.2	60.8	30.7	310.0	322.7
264	296.0	324.3	-14.6	109.6	72.4	34.9	313.7	377.9
273	290.7	325.4	-7.3	94.8	66.1	38.7	335.4	378.7
283								
293								
303								
313								

f [Hz]	UNCERTAINTIES [MN/m]							
	Re(Hxx)	Im(Hxx)	Re(Hxy)	Im(Hxy)	Re(Hyx)	Im(Hyx)	Re(Hyy)	Im(Hyy)
20	6.8	6.0	2.6	2.0	8.4	8.8	4.0	2.5
29	4.2	5.1	3.4	4.5	4.6	6.1	3.0	3.2
39	5.2	7.8	3.6	3.7	4.9	5.7	4.0	3.7
49	6.8	5.9	2.7	5.2	6.0	4.9	5.9	4.3
59	5.3	9.4	3.3	5.1	8.2	6.3	3.9	5.6
68	7.0	6.6	6.5	4.6	4.0	6.1	4.1	5.8
78	4.3	7.1	5.3	3.7	5.6	7.3	4.6	4.6
88	9.9	6.4	6.6	9.2	5.4	5.8	9.0	6.9
98	8.2	6.0	7.9	8.0	7.0	7.2	8.4	6.8
107	6.3	3.0	2.8	7.7	4.5	5.0	11.5	8.0
117	9.7	6.9	8.9	9.4	6.4	6.6	10.9	8.6
127	7.7	8.6	10.5	11.1	7.9	3.0	14.0	10.7
137	8.3	9.7	5.6	9.1	2.0	9.8	6.1	7.8
146	6.8	10.8	10.7	9.8	6.9	9.4	6.2	5.4
156	10.2	9.3	15.9	11.0	6.4	7.3	12.4	10.0
166	4.7	5.5	10.8	6.9	6.1	6.9	9.9	8.4
176	9.5	5.1	23.5	26.0	10.0	9.3	18.9	31.2
186	6.9	4.9	21.4	31.5	6.4	7.1	17.1	34.0
195								
205								
215								
225								
234								
244	12.3	13.0	33.3	41.0	15.0	6.9	37.5	49.0
254	6.7	4.9	19.5	16.7	6.0	7.6	28.7	15.1
264	15.7	15.2	13.6	25.6	13.0	9.5	18.8	20.5
273	7.2	8.1	10.3	9.6	13.9	5.7	11.6	12.2
283								
293								
303								
313								

Table 54. 60% offset experimental dynamic stiffnesses at 13 krpm and 345 kPa.

f [Hz]	VALUES [MN/m]							
	Re(Hxx)	Im(Hxx)	Re(Hxy)	Im(Hxy)	Re(Hyx)	Im(Hyx)	Re(Hyy)	Im(Hyy)
20	264.0	26.1	19.7	3.9	85.7	3.8	295.4	23.7
29	263.3	33.8	17.1	7.0	84.4	3.5	294.5	31.7
39	265.3	43.3	19.6	10.3	82.5	2.6	296.2	40.6
49	264.1	44.4	16.2	9.9	81.0	2.7	294.7	47.3
59	263.3	54.5	15.8	17.8	83.9	2.5	295.7	62.9
68	263.8	69.8	15.0	21.7	84.1	4.8	290.2	73.4
78	260.1	79.0	12.8	25.6	82.6	9.9	283.2	109.1
88	272.6	108.5	13.8	22.4	81.3	-20.8	302.1	103.9
98	284.2	98.9	12.5	34.5	71.2	1.2	302.8	107.4
107	273.5	100.4	19.3	35.2	73.0	6.1	296.1	118.2
117	271.4	118.3	16.8	34.6	74.4	3.8	303.3	127.8
127	272.3	127.9	15.9	43.4	73.5	4.4	297.7	138.4
137	275.2	139.4	15.7	41.8	74.1	3.3	299.2	149.4
146	280.3	148.9	16.2	43.0	70.3	7.6	295.8	159.2
156	279.1	162.5	2.8	63.6	71.4	32.8	263.6	234.5
166	287.5	166.4	16.9	55.1	73.9	9.8	310.7	185.7
176	280.2	177.9	29.3	50.6	66.9	4.8	315.3	198.7
186	289.6	189.6	22.8	62.1	68.1	12.1	302.7	209.7
195	292.3	193.0	32.7	35.1	74.6	13.0	324.5	218.0
205								
215								
225								
234								
244								
254								
264								
273								
283								
293								
303								
313								

f [Hz]	UNCERTAINTIES [MN/m]							
	Re(Hxx)	Im(Hxx)	Re(Hxy)	Im(Hxy)	Re(Hyx)	Im(Hyx)	Re(Hyy)	Im(Hyy)
20	7.1	7.8	2.7	2.2	8.9	10.7	2.5	3.5
29	6.7	4.4	3.0	3.6	3.8	6.2	4.9	3.6
39	3.5	5.0	3.0	3.6	2.8	6.4	3.6	4.1
49	6.9	4.1	6.4	3.4	7.5	5.2	3.2	6.1
59	8.3	3.6	4.3	7.1	5.5	7.6	7.4	5.5
68	6.6	4.5	3.5	2.6	5.4	3.2	3.6	4.9
78	4.4	7.1	5.4	5.4	3.9	6.9	5.8	5.4
88	3.7	3.0	4.4	6.9	8.0	4.1	4.9	9.2
98	5.6	5.8	7.4	7.4	8.5	6.5	7.3	7.1
107	5.7	4.2	6.6	8.7	5.3	5.9	8.7	8.2
117	6.4	3.7	9.7	7.8	4.4	6.6	11.1	4.6
127	5.1	7.0	9.3	11.9	4.6	5.9	8.0	6.9
137	7.0	5.7	4.4	10.5	6.1	6.4	7.7	5.6
146	12.1	9.6	9.2	4.8	10.2	4.5	9.5	7.0
156	5.5	6.0	7.0	8.0	7.8	10.4	11.3	17.8
166	6.2	8.0	10.8	10.9	8.3	6.2	12.1	11.8
176	7.6	5.1	15.7	12.5	7.0	8.2	13.5	19.4
186	7.2	6.5	13.3	20.1	7.3	6.8	10.9	20.8
195	8.4	12.5	43.2	24.2	17.4	7.3	42.4	30.0
205								
215								
225								
234								
244								
254								
264								
273								
283								
293								
303								
313								

Table 55. 60% offset experimental dynamic stiffnesses at 13 krpm and 1034 kPa.

f [Hz]	VALUES [MN/m]							
	Re(Hxx)	Im(Hxx)	Re(Hxy)	Im(Hxy)	Re(Hyx)	Im(Hyx)	Re(Hyy)	Im(Hyy)
20	275.6	18.7	20.6	4.5	86.6	-0.5	312.4	19.3
29	274.7	29.9	20.2	8.3	90.4	2.4	316.1	30.4
39	275.4	42.1	20.0	10.8	87.0	1.1	312.4	39.4
49	278.2	47.4	19.7	13.3	86.9	2.4	316.3	49.4
59	277.8	54.4	20.3	17.6	89.6	4.2	315.5	64.0
68	271.6	70.9	18.2	20.5	87.1	2.7	311.2	73.3
78	273.1	76.5	18.6	22.5	87.0	5.0	303.6	87.4
88	274.5	86.0	22.4	26.7	95.8	1.9	324.6	100.5
98	294.8	103.7	17.1	26.6	75.8	-6.4	323.5	112.4
107	285.2	101.8	20.3	35.3	76.5	7.4	310.9	116.4
117	284.2	116.2	19.2	33.6	77.5	1.0	318.5	129.5
127	280.8	125.1	17.7	38.2	80.7	3.3	310.2	140.2
137	290.0	136.5	20.4	38.5	83.0	4.3	319.7	155.0
146	289.7	148.2	16.9	43.1	80.6	-0.9	320.0	150.8
156	288.8	155.9	11.4	44.7	68.5	8.2	262.9	176.0
166	297.7	160.6	25.4	45.8	76.6	2.3	332.4	184.1
176	292.7	173.2	23.3	45.6	75.0	1.9	319.7	191.8
186	296.2	185.4	21.1	46.8	73.1	2.9	328.7	187.9
195	295.2	191.2	20.9	43.9	72.4	3.6	313.0	206.9
205								
215								
225								
234	298.5	244.2	13.8	52.4	69.8	3.2	336.0	255.1
244	303.2	254.2	12.8	54.7	67.3	5.2	326.1	272.0
254	303.6	267.2	8.9	56.1	66.9	0.7	324.8	283.3
264	307.0	281.7	6.2	48.6	64.5	-6.3	312.1	272.8
273	307.4	293.4	1.4	44.0	52.5	-5.8	275.8	283.1
283	311.3	306.8	8.5	55.8	60.0	-5.0	322.4	314.8
293	311.6	320.0	-2.3	39.3	50.1	-9.3	263.6	305.2
303								
313								

f [Hz]	UNCERTAINTIES [MN/m]							
	Re(Hxx)	Im(Hxx)	Re(Hxy)	Im(Hxy)	Re(Hyx)	Im(Hyx)	Re(Hyy)	Im(Hyy)
20	5.9	7.3	1.6	2.3	6.6	9.7	2.4	2.7
29	6.4	5.3	2.6	3.7	6.6	4.0	4.9	3.9
39	5.1	3.0	2.7	3.4	3.6	4.5	3.3	2.7
49	2.6	3.6	3.7	6.6	3.9	5.0	3.9	4.3
59	6.9	4.9	5.2	4.5	6.7	5.9	5.8	5.8
68	4.9	6.9	3.2	3.8	3.2	6.0	3.0	4.0
78	4.3	6.2	2.7	2.7	4.9	4.7	5.2	3.8
88	5.2	5.6	6.2	7.3	7.9	7.1	8.9	9.1
98	11.1	9.0	10.6	6.3	7.2	6.5	4.5	8.2
107	7.3	7.3	12.3	9.2	3.3	5.2	8.7	8.1
117	6.6	5.8	6.6	7.6	5.0	5.1	4.9	7.6
127	5.4	7.8	12.1	12.0	3.4	6.8	14.4	5.9
137	12.0	8.5	9.4	9.0	12.5	7.7	10.7	9.7
146	10.2	7.3	11.6	5.9	9.6	8.8	8.4	12.2
156	7.7	7.3	8.8	5.4	7.7	5.1	5.8	8.5
166	7.6	5.8	13.7	10.4	10.6	9.3	13.6	6.9
176	9.3	7.9	8.2	17.1	8.7	5.8	11.4	15.4
186	13.1	10.6	13.0	10.9	8.1	10.8	10.7	16.0
195	9.7	10.8	15.8	16.2	11.7	9.7	21.8	16.0
205								
215								
225								
234	12.1	9.7	18.7	16.8	11.2	9.5	18.0	18.0
244	7.7	7.0	11.5	15.8	5.3	8.4	13.4	12.2
254	6.5	4.0	11.0	5.9	4.5	5.1	12.1	9.6
264	5.5	7.1	6.1	8.8	3.2	2.1	7.4	9.7
273	2.7	4.5	5.4	7.2	2.6	3.1	6.4	5.6
283	3.3	4.9	6.8	7.1	2.7	2.8	5.7	4.8
293	2.0	6.4	4.3	4.3	2.3	1.6	3.9	4.0
303								
313								

Table 56. 60% offset experimental dynamic stiffnesses at 13 krpm and 1723 kPa.

f [Hz]	VALUES [MN/m]							
	Re(Hxx)	Im(Hxx)	Re(Hxy)	Im(Hxy)	Re(Hyx)	Im(Hyx)	Re(Hyy)	Im(Hyy)
20	293.6	21.7	34.5	2.8	95.3	-3.0	359.3	19.5
29	294.7	27.9	34.1	4.7	99.1	1.4	364.7	28.9
39	297.9	44.3	32.4	10.3	97.1	-1.4	358.5	40.0
49	300.3	47.3	34.6	12.0	94.6	1.0	361.4	48.5
59	296.5	52.9	34.9	14.3	95.8	4.5	362.2	68.3
68	294.6	68.9	32.3	18.4	98.7	1.0	358.6	75.4
78	296.6	75.1	32.4	18.8	93.3	0.5	349.9	87.9
88	297.7	85.1	34.4	25.3	98.4	2.9	373.8	107.3
98	307.7	114.7	30.1	16.4	95.6	-16.5	365.6	124.6
107	309.7	102.1	33.0	30.9	82.4	7.7	352.6	123.7
117	307.5	113.9	34.1	28.0	83.4	1.4	364.0	139.2
127	302.9	125.2	28.2	37.5	89.2	2.7	354.1	138.4
137	310.3	135.9	32.7	31.1	88.8	2.1	366.4	168.4
146	309.2	149.0	26.0	35.9	90.2	-4.1	370.6	158.2
156	313.6	154.4	28.6	40.3	78.0	5.1	320.2	177.0
166	321.4	160.7	38.5	40.8	83.1	2.0	382.8	194.8
176	316.1	172.9	38.3	43.3	80.0	0.3	365.6	199.3
186	318.6	184.5	33.0	40.1	80.4	2.5	379.4	196.1
195	321.4	193.4	45.0	40.6	79.6	4.4	361.0	220.6
205								
215								
225								
234	325.1	243.4	31.4	51.0	76.7	1.3	395.8	271.5
244	329.1	251.5	26.1	45.2	73.1	3.1	376.8	280.5
254	330.1	265.7	20.3	48.7	69.7	0.7	362.7	310.5
264	334.0	281.4	17.8	43.8	73.0	-6.4	366.5	293.9
273	335.5	290.5	12.6	42.9	62.9	-7.4	350.8	307.5
283	339.4	302.9	19.8	50.9	65.0	-4.5	381.4	335.0
293	341.2	315.1	11.2	38.7	60.2	-9.1	351.9	326.8
303	339.7	327.8	-4.4	21.9	53.4	-15.9	271.8	320.0
313	343.3	343.4	10.6	35.9	61.0	-19.3	384.9	352.0

f [Hz]	UNCERTAINTIES [MN/m]							
	Re(Hxx)	Im(Hxx)	Re(Hxy)	Im(Hxy)	Re(Hyx)	Im(Hyx)	Re(Hyy)	Im(Hyy)
20	7.3	9.4	1.9	2.3	7.8	4.5	2.2	2.9
29	5.5	7.8	3.4	3.1	6.0	7.2	2.8	2.5
39	4.9	3.7	3.8	4.2	4.3	6.1	2.6	4.1
49	5.5	4.0	7.0	6.3	5.8	5.3	4.9	3.7
59	10.5	8.0	7.3	4.8	6.0	6.9	6.4	7.4
68	5.3	5.4	5.2	5.1	5.2	5.1	1.8	4.0
78	6.6	6.3	5.6	6.1	3.9	6.9	4.1	4.7
88	7.0	7.7	8.5	8.4	6.0	7.9	5.4	5.1
98	11.5	6.0	11.4	6.6	11.4	9.0	10.1	9.3
107	7.2	8.2	10.9	7.8	4.7	3.6	5.6	9.6
117	6.2	7.5	8.6	6.9	8.0	8.5	9.8	9.6
127	6.2	7.5	15.6	15.7	5.1	7.1	6.1	8.1
137	7.1	6.5	9.3	6.0	8.0	7.7	9.9	8.5
146	7.8	9.0	14.7	7.5	8.3	8.5	9.1	9.1
156	8.3	8.4	8.2	10.6	5.9	6.7	13.0	8.6
166	9.1	8.5	18.5	13.2	9.6	9.9	11.8	17.0
176	9.6	9.3	13.2	17.2	7.3	8.3	15.3	17.7
186	6.9	10.5	13.6	18.0	6.2	11.3	15.3	9.5
195	8.2	8.4	30.8	19.6	8.6	9.1	24.5	32.5
205								
215								
225								
234	11.8	10.9	26.8	21.4	12.2	11.5	14.4	25.4
244	4.3	6.3	15.2	11.2	4.8	7.4	14.2	14.3
254	4.0	4.8	10.6	14.5	3.2	5.0	11.5	8.9
264	4.7	6.2	6.2	6.9	4.2	4.4	9.2	8.4
273	2.2	3.3	6.9	7.8	1.6	3.9	7.1	9.7
283	2.8	2.3	5.0	4.5	2.9	2.1	5.5	9.4
293	2.2	4.2	8.2	5.7	1.9	1.8	5.3	4.7
303	2.1	2.9	2.8	3.6	2.1	2.1	3.0	5.9
313	2.6	2.2	1.9	3.4	1.9	1.7	4.3	4.1

Table 57. 60% offset experimental dynamic stiffnesses at 13 krpm and 2412 kPa.

f [Hz]	VALUES [MN/m]							
	Re(Hxx)	Im(Hxx)	Re(Hxy)	Im(Hxy)	Re(Hyx)	Im(Hyx)	Re(Hyy)	Im(Hyy)
20	319.2	22.0	46.5	2.2	100.7	-2.6	412.1	19.5
29	317.5	27.8	43.5	3.0	105.7	2.3	419.4	29.6
39	318.4	44.0	42.9	9.0	102.4	-3.9	409.2	38.9
49	321.8	47.0	44.2	12.1	97.8	-0.3	415.0	48.3
59	318.1	57.1	40.8	14.9	103.4	3.6	417.4	70.4
68	316.4	65.9	42.4	16.1	105.3	0.9	413.0	76.9
78	317.7	72.8	39.6	19.0	98.9	0.1	405.7	90.3
88	321.8	83.6	43.1	20.6	99.5	3.6	415.7	112.0
98	318.5	101.2	44.5	25.8	114.1	-1.1	416.4	124.3
107	334.0	102.8	41.1	31.4	88.2	4.8	406.4	127.4
117	328.8	112.4	43.0	24.6	90.5	0.6	420.5	141.2
127	328.5	120.8	39.7	29.5	93.7	2.7	403.7	141.6
137	328.9	137.4	35.1	29.5	91.7	2.1	415.2	169.6
146	329.8	149.8	32.0	31.0	95.5	-2.5	431.8	158.3
156	337.2	151.7	34.2	35.9	88.1	5.1	380.5	177.0
166	343.3	163.9	43.0	42.2	84.9	3.7	432.2	202.0
176	338.2	175.7	39.0	38.3	81.9	0.0	415.1	203.9
186	345.1	184.0	42.6	36.7	85.0	6.4	434.9	205.5
195	347.3	194.3	44.1	45.9	80.9	7.1	405.8	224.5
205								
215								
225								
234	349.3	242.3	43.9	49.9	74.2	4.8	452.0	286.0
244	353.0	247.2	30.3	39.6	74.3	6.8	431.8	286.1
254	351.2	259.1	27.7	39.7	74.3	-1.3	424.6	300.5
264	359.3	274.8	28.0	38.3	75.1	-2.8	423.8	304.5
273	360.9	283.6	16.8	35.8	67.2	-4.8	410.8	315.3
283	366.0	292.8	29.5	40.7	68.6	-1.5	446.0	346.1
293	368.3	303.6	16.5	31.2	61.7	-6.6	415.3	334.7
303	364.9	315.8	6.0	20.0	56.6	-16.3	376.1	324.8
313	368.5	329.9	15.5	34.7	63.8	-12.6	466.8	374.4

f [Hz]	UNCERTAINTIES [MN/m]							
	Re(Hxx)	Im(Hxx)	Re(Hxy)	Im(Hxy)	Re(Hyx)	Im(Hyx)	Re(Hyy)	Im(Hyy)
20	11.1	11.4	3.4	3.5	7.9	6.1	2.9	2.4
29	9.2	5.8	4.3	4.3	7.0	7.7	3.0	3.0
39	7.1	8.9	6.1	5.8	5.1	6.7	6.3	4.7
49	11.1	5.8	9.2	6.9	5.5	5.6	5.5	5.7
59	7.5	7.7	7.0	11.1	4.6	8.5	4.9	6.2
68	7.6	8.8	4.1	4.4	5.9	6.7	4.4	6.7
78	6.4	6.5	5.8	4.1	6.4	8.3	3.0	6.5
88	9.0	11.0	9.6	9.5	8.4	7.3	9.8	7.2
98	14.4	8.0	18.1	13.2	8.1	7.9	7.9	10.8
107	4.9	6.0	11.4	16.1	6.7	4.6	7.1	6.2
117	11.6	7.1	6.1	13.3	10.2	9.5	9.5	10.6
127	8.3	4.8	9.0	15.6	3.0	4.3	12.7	12.9
137	7.4	12.1	11.6	9.1	9.0	6.7	12.7	8.6
146	5.4	5.8	8.7	19.7	13.2	7.6	9.0	11.5
156	7.7	9.3	12.7	10.7	6.7	8.8	7.9	15.5
166	8.3	13.9	19.7	15.3	9.6	10.2	12.8	15.7
176	10.0	9.2	21.9	14.5	8.8	9.9	14.3	19.6
186	10.0	13.6	19.6	18.1	7.9	12.0	19.5	19.8
195	11.4	10.0	33.3	22.2	9.3	14.9	31.4	31.0
205								
215								
225								
234	12.6	14.5	35.5	32.6	15.7	20.2	32.3	51.1
244	4.4	9.0	15.9	16.2	8.3	6.9	16.8	17.5
254	7.3	4.4	9.8	10.6	5.7	6.0	14.8	18.2
264	4.8	5.7	8.2	14.6	5.1	5.3	8.3	15.3
273	4.9	4.2	9.9	7.5	3.5	2.5	6.8	9.6
283	2.9	3.4	8.2	10.3	4.0	3.3	11.9	9.8
293	2.9	5.3	6.3	3.0	4.2	2.3	6.3	5.2
303	4.0	2.9	4.4	4.0	2.0	1.9	5.1	3.1
313	2.7	3.0	6.0	6.9	2.3	2.9	4.5	9.7

Table 58. 60% offset experimental dynamic stiffnesses at 13 krpm and 3101 kPa.

f [Hz]	VALUES [MN/m]							
	Re(Hxx)	Im(Hxx)	Re(Hxy)	Im(Hxy)	Re(Hyx)	Im(Hyx)	Re(Hyy)	Im(Hyy)
20	341.5	24.1	54.7	3.1	107.3	-3.6	476.8	19.1
29	339.9	27.4	52.0	2.9	108.5	2.3	484.0	30.4
39	341.4	42.0	51.6	7.1	105.2	-3.1	474.9	40.8
49	340.7	45.2	52.1	9.0	100.9	0.2	480.4	47.4
59	341.8	54.1	50.1	13.7	107.0	2.3	483.1	71.4
68	340.5	66.1	51.7	15.7	114.3	0.4	478.3	79.6
78	343.8	73.1	50.2	14.5	102.3	0.9	472.2	90.9
88	346.4	84.0	54.0	21.3	105.3	4.6	492.1	113.4
98	344.9	92.9	57.2	21.4	111.9	4.5	480.4	123.1
107	357.4	104.2	53.4	22.8	92.9	0.7	472.1	133.4
117	354.1	108.7	55.5	19.4	92.1	-0.2	487.6	145.0
127	352.4	118.2	49.8	16.9	97.6	2.0	475.7	148.3
137	356.4	133.0	46.6	26.2	97.4	-0.1	482.2	169.7
146	352.6	144.0	43.3	24.2	103.7	-5.2	499.9	158.7
156	359.0	148.0	40.0	30.8	88.7	2.6	445.9	179.0
166	369.3	157.3	53.1	36.4	88.2	6.7	497.9	208.9
176	365.5	168.8	57.7	33.2	91.5	1.5	485.8	218.2
186	368.9	176.8	60.7	31.4	90.4	3.4	506.7	221.7
195	369.0	186.4	67.9	36.8	88.2	5.0	481.4	252.5
205								
215								
225								
234								
244	378.2	234.4	52.1	33.0	81.3	4.1	505.0	310.6
254	376.9	249.9	41.4	29.5	76.8	-0.2	499.7	310.0
264	383.0	266.7	40.4	31.6	77.2	-3.5	496.7	320.4
273	385.9	276.2	23.6	23.2	67.4	-2.7	474.7	315.1
283	392.3	286.5	32.3	35.2	70.8	0.0	526.4	355.0
293	394.0	295.2	17.9	24.6	62.8	-4.4	481.9	344.1
303	392.2	308.1	7.8	20.1	58.0	-13.3	464.2	344.2
313								

f [Hz]	UNCERTAINTIES [MN/m]							
	Re(Hxx)	Im(Hxx)	Re(Hxy)	Im(Hxy)	Re(Hyx)	Im(Hyx)	Re(Hyy)	Im(Hyy)
20	6.3	8.4	4.9	4.8	4.8	12.6	2.6	5.3
29	6.0	5.6	5.0	5.9	6.2	6.3	7.2	5.5
39	6.4	8.2	6.3	7.5	6.1	5.4	5.2	5.0
49	7.9	4.7	7.4	10.9	6.6	5.5	6.1	5.6
59	7.9	13.2	9.1	10.4	8.4	6.1	8.7	8.1
68	5.6	6.8	4.2	8.8	5.2	5.7	5.7	4.3
78	8.0	6.8	7.0	3.6	6.7	4.9	4.6	4.3
88	12.3	10.6	10.5	7.3	9.9	8.3	9.1	8.7
98	12.7	9.1	9.6	11.2	7.6	8.5	9.3	12.5
107	8.2	5.5	9.2	10.9	6.8	6.1	13.5	11.8
117	8.8	6.0	12.2	11.7	10.5	6.4	14.4	13.0
127	8.7	7.6	21.9	11.9	8.1	9.4	18.8	16.1
137	11.6	11.7	12.9	10.4	12.3	10.3	14.6	12.9
146	17.7	14.5	15.7	13.7	11.1	8.5	10.1	13.0
156	7.1	8.8	12.6	16.4	8.6	13.1	12.8	11.3
166	8.3	6.0	15.8	15.2	10.8	13.7	13.7	12.8
176	11.4	12.9	16.8	17.2	12.8	15.3	21.3	23.7
186	12.7	8.6	21.3	22.6	14.0	15.1	30.1	31.4
195	19.9	17.5	46.2	23.7	23.8	19.1	40.4	53.3
205								
215								
225								
234								
244	9.7	10.9	23.7	22.7	11.5	19.3	32.6	34.2
254	9.9	6.1	21.4	16.2	7.3	11.3	21.7	24.9
264	8.6	8.4	17.3	10.4	9.7	5.4	20.2	23.0
273	4.2	4.8	12.2	14.6	3.8	3.6	9.1	12.9
283	5.4	3.4	11.0	13.2	6.4	2.9	10.7	13.5
293	3.4	4.8	5.8	9.1	2.9	3.4	9.6	6.3
303	3.9	2.5	7.5	3.9	2.0	3.4	5.5	7.0
313								

Table 59. 60% offset experimental dynamic stiffnesses at 16 krpm and zero load.

f [Hz]	VALUES [MN/m]							
	Re(Hxx)	Im(Hxx)	Re(Hxy)	Im(Hxy)	Re(Hyx)	Im(Hyx)	Re(Hyy)	Im(Hyy)
20	290.5	24.6	14.6	4.1	86.0	-0.9	322.4	23.4
29	290.0	25.6	13.4	6.8	84.7	8.3	323.5	32.7
39	276.8	49.2	13.2	9.9	94.7	2.7	325.8	41.7
49	264.8	63.8	9.4	10.8	104.0	-0.2	328.0	48.2
59	299.0	64.2	11.2	14.7	103.1	-10.7	328.3	57.4
68	282.8	46.9	9.8	20.5	92.5	3.3	325.1	66.3
78	258.9	115.1	10.1	19.4	104.0	-8.6	323.9	85.2
88	277.3	91.9	0.2	30.9	77.4	25.4	330.5	92.9
98	313.4	107.6	4.8	32.1	89.8	6.1	333.9	101.1
107	269.6	94.2	7.8	39.3	78.9	24.4	330.1	114.8
117	285.6	80.6	13.2	34.2	80.3	-1.8	335.5	120.8
127	280.6	116.0	17.5	43.2	77.6	7.3	336.0	134.9
137	234.3	148.2	9.0	39.5	48.5	51.0	334.5	142.7
146	368.8	200.2	11.7	57.8	105.1	35.5	334.5	158.2
156	293.8	137.2	10.2	54.7	84.9	-11.0	339.4	165.0
166	262.5	160.1	11.6	54.0	42.5	-2.5	334.9	175.3
176	317.3	218.1	29.3	65.0	72.6	80.7	344.0	204.0
186	328.7	179.2	9.0	62.2	104.8	18.3	336.6	201.3
195	310.1	232.1	28.1	67.5	58.3	38.3	342.3	224.3
205								
215								
225								
234								
244								
254								
264								
273								
283								
293								
303								
313								

f [Hz]	UNCERTAINTIES [MN/m]							
	Re(Hxx)	Im(Hxx)	Re(Hxy)	Im(Hxy)	Re(Hyx)	Im(Hyx)	Re(Hyy)	Im(Hyy)
20	14.2	17.0	6.7	8.6	19.4	16.3	6.4	4.8
29	12.3	14.2	5.0	4.3	17.2	9.1	5.5	2.9
39	19.4	11.7	5.0	6.1	10.4	10.8	4.1	3.7
49	21.8	23.0	3.0	5.8	8.5	24.0	5.0	5.8
59	27.9	26.8	6.1	7.4	19.1	16.8	5.6	6.7
68	25.2	14.1	3.9	7.9	15.6	18.7	9.1	4.5
78	15.1	22.1	5.3	6.1	16.0	12.7	3.3	5.6
88	36.6	29.2	5.8	7.7	22.8	29.1	8.5	7.8
98	11.8	11.7	11.3	9.2	8.7	11.0	6.7	7.1
107	25.2	24.7	10.6	14.3	14.1	25.2	11.7	8.9
117	27.1	28.2	9.2	11.6	39.1	23.7	8.5	11.1
127	20.0	10.8	12.6	10.0	27.9	20.3	9.8	12.5
137	74.0	43.8	12.3	9.0	48.1	82.4	13.4	7.0
146	73.9	59.4	14.1	18.7	38.3	22.4	14.3	9.1
156	14.7	19.0	10.8	16.2	12.9	14.1	12.0	12.5
166	33.3	15.5	11.8	6.3	37.3	19.6	9.3	13.4
176	46.0	33.9	16.9	20.5	41.4	55.6	15.1	16.7
186	16.9	10.3	14.4	9.2	13.8	8.2	13.6	8.5
195	20.8	73.2	13.8	17.7	35.1	57.9	18.0	10.7
205								
215								
225								
234								
244								
254								
264								
273								
283								
293								
303								
313								

Table 60. 60% offset experimental dynamic stiffnesses at 16 krpm and 345 kPa.

f [Hz]	VALUES [MN/m]							
	Re(Hxx)	Im(Hxx)	Re(Hxy)	Im(Hxy)	Re(Hyx)	Im(Hyx)	Re(Hyy)	Im(Hyy)
20	289.4	23.8	12.2	4.4	82.9	0.4	321.6	23.9
29	292.9	20.4	15.8	6.2	90.7	3.4	327.6	30.4
39	289.1	57.5	13.3	11.0	112.1	-7.0	327.0	41.1
49	281.6	72.8	12.5	12.3	125.6	-15.8	328.6	50.1
59	306.5	74.7	8.6	14.5	108.9	-15.3	327.4	57.8
68	283.1	55.0	8.6	19.1	93.8	25.7	318.6	69.4
78	269.1	118.9	11.2	25.9	136.9	-14.8	329.5	96.0
88	287.8	97.1	1.1	31.2	105.6	22.8	337.5	100.1
98	325.5	108.2	6.2	35.2	91.9	-10.0	335.0	104.8
107	256.1	118.2	0.9	38.7	113.1	41.6	332.1	121.9
117	289.4	85.2	9.7	38.2	77.1	24.2	333.1	122.7
127	268.1	136.9	16.1	45.2	87.5	30.5	329.7	127.7
137								
146								
156	292.7	134.2	9.1	56.3	75.2	5.9	324.2	193.1
166								
176								
186	359.3	167.9	21.9	68.2	101.7	1.2	339.0	194.1
195								
205								
215								
225								
234								
244								
254								
264								
273								
283								
293								
303								
313								

f [Hz]	UNCERTAINTIES [MN/m]							
	Re(Hxx)	Im(Hxx)	Re(Hxy)	Im(Hxy)	Re(Hyx)	Im(Hyx)	Re(Hyy)	Im(Hyy)
20	18.9	14.7	5.3	4.2	14.3	17.4	5.8	4.5
29	11.6	13.6	5.2	4.7	6.3	12.8	3.8	3.9
39	20.0	25.8	5.6	3.6	18.0	12.3	6.6	5.0
49	27.2	13.8	6.6	5.4	16.5	16.6	5.0	7.9
59	18.0	27.7	5.4	6.8	21.0	28.3	4.4	3.1
68	26.1	29.2	6.5	6.1	23.2	26.8	5.1	5.3
78	26.1	20.6	7.8	6.1	26.0	21.5	10.5	9.7
88	27.3	20.1	11.5	5.9	28.0	22.0	7.2	8.6
98	25.3	20.3	12.7	11.8	17.6	18.0	11.2	6.9
107	47.7	30.9	12.6	11.9	63.8	47.0	15.9	8.8
117	26.2	34.4	9.1	6.6	51.8	47.5	14.3	13.9
127	44.2	35.7	12.0	10.5	45.4	36.4	9.6	6.2
137								
146								
156	17.1	17.6	11.8	9.3	14.3	23.0	12.1	14.8
166								
176								
186	8.7	15.2	13.8	18.2	12.2	7.9	8.1	12.6
195								
205								
215								
225								
234								
244								
254								
264								
273								
283								
293								
303								
313								

Table 61. 60% offset experimental dynamic stiffnesses at 16 krpm and 1034 kPa.

f [Hz]	VALUES [MN/m]							
	Re(Hxx)	Im(Hxx)	Re(Hxy)	Im(Hxy)	Re(Hyx)	Im(Hyx)	Re(Hyy)	Im(Hyy)
20	308.7	15.3	19.4	1.5	101.8	-5.3	341.7	21.6
29	304.4	33.7	18.9	7.8	92.4	6.2	346.7	32.2
39	306.6	43.4	17.6	9.3	112.9	0.8	342.5	38.8
49	307.2	55.3	16.7	10.3	117.6	8.5	346.5	52.3
59	322.0	49.9	17.0	11.5	116.1	-21.8	349.1	57.4
68	299.2	57.1	12.7	17.0	74.7	14.0	337.5	64.6
78	301.7	82.2	15.4	23.9	113.4	25.2	331.4	89.7
88	295.9	104.4	18.6	22.4	136.1	30.6	351.2	99.2
98	330.8	96.5	8.7	32.2	98.1	2.8	355.3	108.0
107	310.3	99.3	14.5	37.2	72.4	17.6	349.6	115.8
117	307.9	97.8	16.5	31.2	86.8	8.2	351.1	127.1
127	315.1	107.0	17.3	35.3	106.2	-6.4	358.5	130.6
137	309.1	160.6	12.1	39.0	71.6	72.3	348.0	145.2
146	403.9	180.0	24.8	50.4	165.3	43.2	361.8	161.9
156	306.4	146.5	13.5	40.5	65.2	2.2	313.9	178.7
166	306.9	165.9	21.5	37.0	62.4	14.0	372.9	165.6
176	345.0	191.4	32.9	35.5	94.0	79.4	365.4	184.1
186	349.2	158.1	15.8	47.3	152.5	-5.0	357.9	188.2
195	316.3	222.5	25.4	42.8	35.6	39.3	353.7	204.6
205								
215								
225								
234								
244								
254								
264								
273								
283								
293								
303								
313								

f [Hz]	UNCERTAINTIES [MN/m]							
	Re(Hxx)	Im(Hxx)	Re(Hxy)	Im(Hxy)	Re(Hyx)	Im(Hyx)	Re(Hyy)	Im(Hyy)
20	18.5	7.9	4.7	3.8	12.8	13.5	4.7	6.8
29	10.8	8.8	3.7	2.6	10.4	16.7	3.1	5.5
39	11.0	17.1	2.0	4.6	12.9	11.1	3.8	5.0
49	11.3	12.6	5.4	3.9	22.2	10.6	5.2	5.3
59	14.2	20.0	5.8	7.5	23.3	11.3	6.0	7.0
68	19.4	18.4	6.0	6.7	30.5	25.8	6.6	5.2
78	26.7	15.9	4.8	4.6	22.0	14.6	4.5	4.7
88	17.6	22.1	5.5	4.6	21.1	18.8	4.7	7.6
98	9.2	15.7	7.8	7.4	20.8	16.5	9.9	6.3
107	15.2	12.0	8.4	7.0	22.1	14.4	10.7	6.0
117	27.1	17.4	7.3	6.6	30.6	23.6	10.5	10.8
127	14.7	16.1	10.2	10.7	19.1	17.8	11.7	8.4
137	21.8	26.2	9.6	8.7	30.9	15.1	9.9	7.1
146	63.1	75.0	19.2	15.2	40.5	70.4	11.6	12.8
156	11.6	13.0	6.9	8.0	15.8	8.9	11.6	11.4
166	12.6	5.8	12.9	8.9	20.2	19.0	12.0	8.4
176	18.2	14.2	12.2	14.4	19.6	18.1	8.2	13.2
186	8.8	11.6	12.9	5.2	21.0	16.3	13.4	6.5
195	17.5	28.3	11.7	10.7	21.7	20.1	12.6	12.3
205								
215								
225								
234								
244								
254								
264								
273								
283								
293								
303								
313								

Table 62. 60% offset experimental dynamic stiffnesses at 16 krpm and 1723 kPa.

f [Hz]	VALUES [MN/m]							
	Re(Hxx)	Im(Hxx)	Re(Hxy)	Im(Hxy)	Re(Hyx)	Im(Hyx)	Re(Hyy)	Im(Hyy)
20	319.0	17.6	27.1	3.4	100.1	1.7	373.8	19.0
29	317.6	29.1	26.5	5.0	105.6	2.4	378.6	30.2
39	319.1	36.2	23.9	6.7	102.7	0.3	372.9	37.5
49	319.9	45.3	22.4	9.0	103.4	4.0	376.7	50.6
59	324.0	54.2	21.6	13.2	106.2	5.0	379.6	63.4
68	318.8	63.1	20.3	18.3	105.1	5.1	373.3	68.6
78	322.3	69.7	19.8	21.2	103.7	4.8	363.3	83.0
88	323.2	79.7	25.0	25.1	113.3	9.7	390.2	99.8
98	328.4	112.2	19.6	24.1	100.9	-17.6	382.8	120.0
107	330.6	97.3	21.9	33.1	90.9	8.2	372.6	118.4
117	326.5	109.8	23.4	31.0	93.3	1.0	383.2	130.2
127	328.0	114.5	21.4	32.4	100.0	-2.5	377.2	130.4
137	335.0	129.2	24.6	38.2	90.7	7.8	384.6	152.5
146	340.6	136.3	25.5	37.8	101.4	2.6	391.1	148.4
156	330.9	143.7	15.2	37.6	80.4	5.0	339.8	157.9
166	332.5	156.7	26.2	36.7	84.6	10.4	398.2	177.9
176	336.1	165.2	25.8	37.6	89.8	7.7	377.4	180.3
186	336.5	173.6	16.9	39.7	97.8	5.9	383.7	183.5
195	335.2	188.7	16.4	39.4	85.5	10.6	370.0	198.5
205	342.0	203.3	17.0	48.5	88.9	13.6	376.4	226.7
215	346.4	224.9	24.0	51.8	80.3	16.8	374.6	225.7
225	339.2	229.4	25.0	46.6	62.3	6.1	325.0	255.5
234								
244								
254								
264								
273								
283								
293								
303								
313								

f [Hz]	UNCERTAINTIES [MN/m]							
	Re(Hxx)	Im(Hxx)	Re(Hxy)	Im(Hxy)	Re(Hyx)	Im(Hyx)	Re(Hyy)	Im(Hyy)
20	6.9	7.7	2.1	2.8	8.6	5.4	1.4	3.0
29	4.4	4.6	2.8	3.2	5.5	5.9	2.5	4.2
39	7.9	4.9	1.6	3.4	3.1	5.3	1.9	1.7
49	5.0	5.1	3.2	3.5	4.8	7.8	4.4	4.5
59	7.7	7.3	3.5	4.3	7.6	5.5	3.9	4.1
68	5.4	3.6	3.5	3.4	4.3	5.2	3.8	2.7
78	5.5	4.6	3.2	3.8	5.3	6.4	4.9	4.2
88	5.6	6.4	5.8	4.7	6.9	10.4	4.0	6.0
98	5.4	4.6	6.7	6.3	7.1	6.7	7.6	5.3
107	4.4	5.0	6.8	7.1	6.9	6.4	10.6	5.4
117	6.8	15.1	7.0	6.9	6.9	8.4	7.2	7.7
127	5.4	5.4	6.7	5.7	5.3	8.5	7.9	10.5
137	8.3	7.0	6.3	7.2	12.0	6.7	7.3	6.8
146	7.4	7.0	12.7	9.3	5.9	10.6	8.1	6.0
156	6.0	4.6	4.8	8.9	8.0	8.7	4.9	9.5
166	8.3	7.8	6.7	6.8	9.2	6.6	8.2	5.9
176	6.3	5.6	8.0	6.3	5.8	6.7	5.8	7.3
186	6.7	6.2	9.5	8.2	6.6	10.2	5.9	6.9
195	4.9	4.3	8.1	6.1	3.4	7.1	11.6	5.4
205	3.4	3.4	6.9	10.7	6.1	3.5	7.7	6.3
215	7.7	6.1	9.5	10.7	8.6	8.9	6.4	6.8
225	8.1	6.9	9.5	5.2	11.1	6.4	7.2	10.9
234								
244								
254								
264								
273								
283								
293								
303								
313								

Table 63. 60% offset experimental dynamic stiffnesses at 16 krpm and 2412 kPa.

f [Hz]	VALUES [MN/m]							
	Re(Hxx)	Im(Hxx)	Re(Hxy)	Im(Hxy)	Re(Hyx)	Im(Hyx)	Re(Hyy)	Im(Hyy)
20	335.9	19.9	36.2	3.0	104.0	0.9	418.1	17.2
29	335.0	27.8	36.1	5.9	111.2	2.5	423.7	29.5
39	337.3	36.9	33.5	5.7	106.9	0.1	415.1	39.2
49	339.8	46.2	32.9	8.6	107.6	3.5	421.6	51.1
59	341.1	51.5	31.6	11.7	110.2	5.3	423.3	66.8
68	336.4	64.6	28.3	16.3	111.2	3.1	420.3	71.0
78	342.5	70.1	29.5	18.9	108.9	5.0	412.2	84.9
88	342.4	80.4	32.2	25.0	113.2	7.8	428.3	102.0
98	338.2	88.2	34.8	26.3	116.1	7.0	425.5	112.4
107	350.6	100.8	31.4	28.9	94.9	3.3	416.6	118.9
117	344.7	109.0	35.0	30.7	101.5	-3.5	431.0	132.1
127	346.0	114.8	30.0	30.2	103.5	1.1	418.6	131.7
137	352.9	130.2	31.1	32.2	92.5	9.9	425.2	152.2
146	360.8	137.8	33.7	34.7	106.5	9.1	436.7	151.9
156	348.9	145.2	23.9	32.6	85.3	3.2	392.5	160.4
166	355.9	154.1	34.2	34.8	91.3	9.3	443.6	183.8
176	354.2	164.9	33.0	39.6	96.4	12.5	423.3	189.1
186	359.4	174.3	28.4	40.3	102.6	8.7	432.0	188.2
195	357.0	188.2	26.2	37.1	89.5	14.8	414.0	201.9
205	360.7	202.1	23.6	43.6	94.1	16.1	422.9	229.6
215	364.4	228.6	26.6	49.9	76.7	15.0	407.7	227.3
225	361.4	228.4	33.9	43.5	69.5	7.8	392.3	245.9
234								
244								
254								
264								
273								
283								
293								
303								
313								

f [Hz]	UNCERTAINTIES [MN/m]							
	Re(Hxx)	Im(Hxx)	Re(Hxy)	Im(Hxy)	Re(Hyx)	Im(Hyx)	Re(Hyy)	Im(Hyy)
20	5.9	7.2	3.1	1.9	6.1	12.8	3.9	3.6
29	6.9	3.9	2.4	3.4	5.9	3.6	2.8	2.5
39	6.0	4.0	2.8	3.3	5.2	7.1	3.3	3.5
49	4.6	3.2	4.7	5.6	4.9	6.8	6.3	6.0
59	7.0	6.7	4.3	4.2	8.9	9.5	6.1	6.1
68	4.1	4.5	4.2	3.5	5.0	4.5	5.0	3.6
78	4.7	6.9	1.6	4.7	4.3	3.6	4.2	4.1
88	4.4	4.9	5.0	7.4	6.4	4.7	6.8	7.5
98	6.0	8.1	5.7	7.4	7.6	9.1	8.0	10.1
107	5.1	6.1	3.9	5.4	3.7	3.7	3.6	7.8
117	6.0	7.3	7.0	7.5	7.3	7.4	8.2	8.6
127	5.3	8.8	10.7	14.7	4.5	5.4	11.6	8.2
137	8.9	6.6	6.9	8.8	11.4	8.0	6.4	5.6
146	5.2	5.8	7.8	7.7	9.2	6.0	12.4	8.1
156	6.1	5.4	5.4	7.8	7.4	5.7	4.3	6.4
166	4.5	5.4	7.5	8.7	7.9	6.5	6.7	8.9
176	5.3	5.4	6.9	12.0	6.9	9.4	8.8	13.6
186	6.2	6.4	8.2	5.2	5.6	6.3	6.4	7.2
195	7.3	4.7	8.7	8.3	4.2	6.6	5.4	12.2
205	5.8	4.5	8.6	9.7	5.6	4.8	9.2	12.5
215	7.7	10.8	11.8	11.6	6.9	7.8	7.5	7.1
225	10.6	8.9	12.3	11.6	6.1	9.4	12.5	13.6
234								
244								
254								
264								
273								
283								
293								
303								
313								

Table 64. 60% offset experimental dynamic stiffnesses at 16 krpm and 3101 kPa.

f [Hz]	VALUES [MN/m]							
	Re(Hxx)	Im(Hxx)	Re(Hxy)	Im(Hxy)	Re(Hyx)	Im(Hyx)	Re(Hyy)	Im(Hyy)
20	355.0	19.3	45.3	2.4	112.6	0.4	469.4	17.6
29	353.5	29.6	44.1	4.9	115.1	1.2	475.4	29.5
39	355.2	38.9	43.5	5.6	110.7	-0.7	465.5	38.2
49	358.0	45.4	44.3	8.2	110.3	1.1	473.2	51.2
59	361.0	54.7	42.4	12.3	114.4	3.0	477.7	67.7
68	356.1	63.1	39.1	15.5	117.5	2.6	471.9	73.7
78	359.7	70.6	40.4	16.8	108.9	3.7	464.5	87.1
88	361.1	77.5	41.5	19.1	114.5	4.9	485.5	101.8
98	358.6	86.0	39.4	25.0	116.7	4.6	476.2	114.0
107	367.5	103.3	39.8	26.6	99.0	-3.8	469.4	125.7
117	364.7	107.5	40.0	27.8	102.7	-1.1	481.4	136.6
127	364.4	115.1	40.3	29.3	105.0	-0.6	469.4	132.4
137	370.7	126.5	41.6	29.1	102.5	-1.3	479.6	157.8
146	371.3	132.9	41.7	31.8	109.5	-2.0	493.0	155.4
156	368.0	141.1	31.8	28.3	93.0	3.7	445.5	165.6
166	372.9	150.6	42.3	30.5	97.5	7.0	497.8	187.4
176	369.9	161.0	38.3	33.9	97.8	4.2	474.1	190.2
186	370.2	170.6	32.0	32.1	101.0	5.5	484.3	188.8
195	373.7	182.9	29.6	34.2	98.3	7.8	462.9	207.1
205	377.0	194.0	29.4	40.0	102.0	7.8	480.3	230.2
215	383.5	208.1	29.8	42.3	95.2	4.2	463.7	224.4
225	380.9	211.9	42.4	41.8	89.5	-0.9	474.9	245.1
234								
244								
254								
264								
273								
283								
293								
303								
313								

f [Hz]	UNCERTAINTIES [MN/m]							
	Re(Hxx)	Im(Hxx)	Re(Hxy)	Im(Hxy)	Re(Hyx)	Im(Hyx)	Re(Hyy)	Im(Hyy)
20	7.0	9.7	3.1	3.0	10.6	6.4	3.7	4.8
29	5.8	2.9	5.3	3.9	4.7	10.2	3.3	3.5
39	6.9	4.1	5.3	3.3	7.1	5.7	4.8	4.5
49	5.0	5.2	6.1	6.2	6.9	5.7	4.4	3.3
59	9.3	5.8	4.2	7.9	7.6	7.8	5.6	6.6
68	5.4	5.3	6.1	6.2	7.1	4.3	3.2	5.3
78	5.7	3.8	5.5	4.7	5.6	4.8	5.1	4.1
88	6.0	7.7	8.3	6.0	11.3	7.5	8.9	8.0
98	8.0	6.8	7.4	13.3	8.6	7.3	8.7	14.5
107	3.6	4.8	11.8	8.1	5.0	6.7	8.1	5.9
117	9.1	3.3	11.8	10.7	10.4	6.5	14.0	12.0
127	5.5	5.3	6.9	11.7	2.4	7.4	11.4	11.2
137	7.9	11.0	11.2	9.4	7.6	7.1	6.9	11.4
146	11.1	7.1	14.1	6.8	13.2	8.0	14.1	10.9
156	6.6	8.9	8.5	10.8	9.7	7.0	7.1	12.1
166	6.0	3.6	12.6	8.4	5.2	6.7	15.0	9.0
176	4.3	8.7	7.1	14.8	7.2	9.8	11.8	9.6
186	5.5	7.6	10.2	8.0	4.4	5.4	7.5	12.2
195	6.4	9.0	14.7	13.7	4.0	5.2	13.5	8.6
205	6.9	4.5	14.7	7.9	6.8	4.4	9.2	12.8
215	7.6	9.8	12.1	15.9	9.5	10.7	19.9	16.8
225	7.3	6.7	17.6	6.6	9.1	7.8	11.4	20.0
234								
244								
254								
264								
273								
283								
293								
303								
313								

APPENDIX F: ADIABATIC AND ISOTHERMAL PREDICTION MODELS

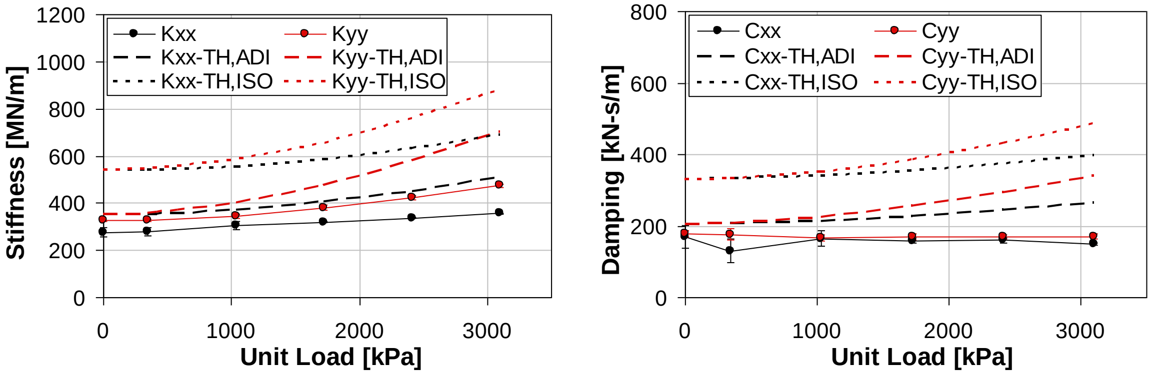

(a) **(b)**

Figure 58. Adiabatic and isothermal models for 60% offset at 16 krpm for the direct: (a) stiffness, (b) damping.

APPENDIX G: PROBE LOCATION COMPARISON

The following provides static and dynamic data comparing probe locations for the 50% offset bearing. Data was taken with a nominal inlet temperature 32.2 °C (90 °F) with a rotor speed of 13 krpm.

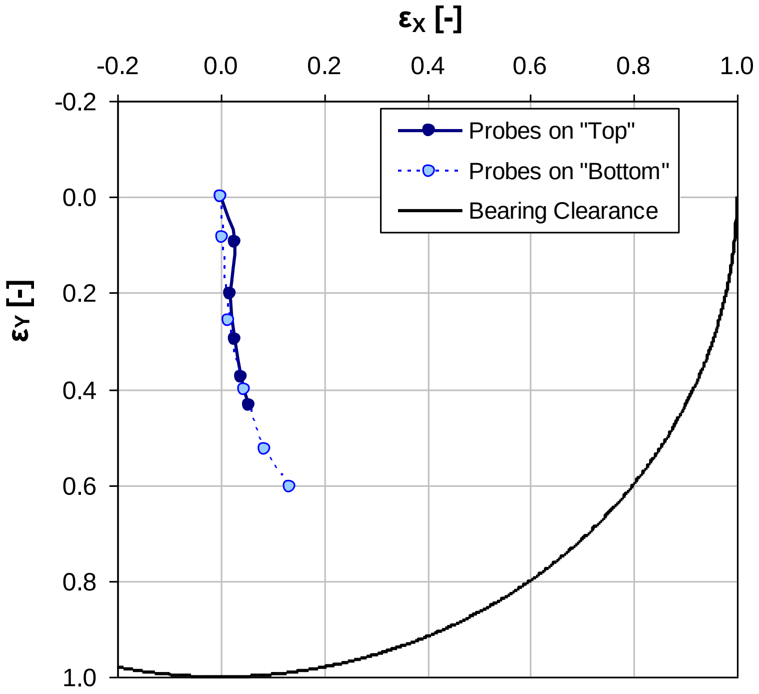

Figure 59. Bearing loci comparing top and bottom probes for the 50% offset at 13 krpm.

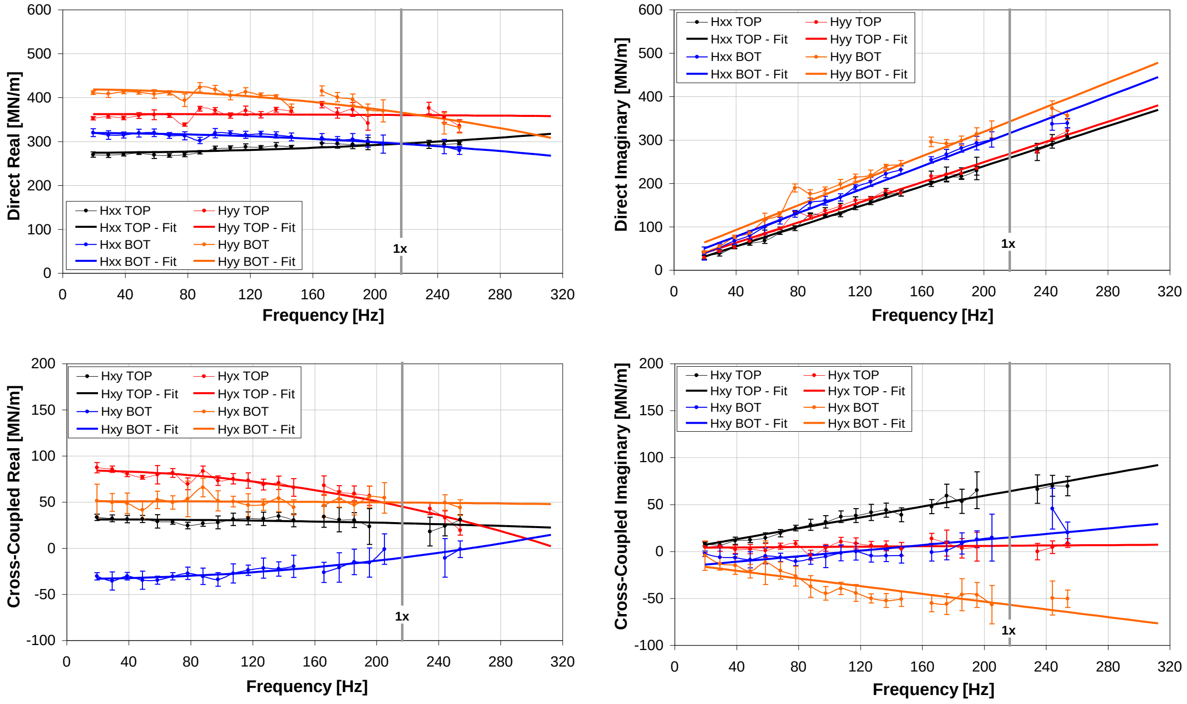

Figure 60. Dynamic stiffness comparing proximity probe location at 13 krpm and 345 kPa for the 50% offset.

VITA

Name: Chris David Kulhanek

Address: Texas A&M University
Department of Mechanical Engineering
Attn: MEEN Graduate Studies
3123 TAMU
College Station, TX 77843-3123

Email Address: cdkulhanek@gmail.com

Education: B.S., Mechanical Engineering, Texas A&M University, 2008
M.S., Mechanical Engineering, Texas A&M University, 2010